DEVELOPMENT, CHARACTERIZATION AND BIOLOGICAL EVALUATION OF POLYSACCHARIDE BASED NANOMATERIALS FOR ENHANCED DELIVERY OF CURCUMIN TO CANCER CELLS

A Thesis submitted

in partial fulfillment for the Degree of

Doctor of Philosophy

by

SARIKA P R

Department of Chemistry

INDIAN INSTITUTE OF SPACE SCIENCE AND TECHNOLOGY

THIRUVANANTHAPURAM

JULY, 2015

To my guide Dr. Nirmala Rachel James, for her guidance, support and love

To my parents for their love and care

CERTIFICATE

This is to certify that the thesis entitled **Development, characterization and biological evaluation of polysaccharide based nanomaterials for enhanced delivery of curcumin to cancer cells** submitted by **Sarika P R** to the Indian Institute of Space Science and Technology, Thiruvananthapuram, in partial fulfillment for the award of the degree of **Doctor of Philosophy** is a *bona fide* record of research work carried out by her under my supervision. The contents of this thesis, in full or in parts, have not been submitted to any other Institution or University for the award of any degree or diploma.

Dr. Nirmala Rachel James
Supervisor
Department of Chemistry

Thiruvananthapuram
July, 2015

Counter signature of HOD with seal

DECLARATION

I declare that this thesis entitled **Development, characterization and biological evaluation of polysaccharide based nanomaterials for enhanced delivery of curcumin to cancer cells** submitted in partial fulfillment of the degree of **Doctor of Philosophy** is a record of original work carried out by me under the supervision of Dr. Nirmala Rachel James, and has not formed the basis for the award of any other degree or diploma, in this or any other Institution or University. In keeping with the ethical practice in reporting scientific information, due acknowledgements have been made wherever the findings of others have been cited.

SARIKA P R

SC10D017

Thiruvananthapuram - 695 547

24-07-2015

ACKNOWLEDGEMENTS

I would like to place my sincere thanks to the Almighty for giving me an opportunity to fulfill my dream, the blessings showered to strengthen me physically, mentally, intellectually and spiritually for the successful completion of this work.

Words are incapable to formulate my deep sense and immense regards, yet I express my sincere thanks to my guide Dr. Nirmala Rachel James for her valuable guidance, support, constant encouragement and enormous care she had given throughout the entire period of my work.

I place on record, my sincere thanks to Prof. Kuruvilla Joseph, Head of the Department, for his constant support, encouragement and care. I take this opportunity to express my sincere gratitude to all the faculty members of Dept.of Chemistry for their wholehearted support and help extended to me. I am grateful to Director, IIST for my fellowship and providing me all the facilities to complete my research work.

I am also indebted to the members of the Doctoral committee for the many valuable discussions and critical comments, which helped me to understand my research area better. I am indebted to Dr. Anil kumar P R, Scientist, SCTIMST for his encouragement and practical advice. I am also thankful to him for the biological evaluation of the samples, prepared as part of the research work. I would like to acknowledge Mrs. Deepa K Raj for her help to complete the biological studies. My sincere thanks to Ms. Nishna N for her contributions to my work. I am thankful to SAIF, IIT Madras for providing their facility for SEM analysis, NIIST for TEM and temperature dependant UV-spectroscopy studies, RGCB for MALDI-TOF-MS analysis, IISER Trivandrum for NMR analysis and SCTIMST for all biological studies.

I sincerely thank all the non-teaching and technical staff of Dept. of Chemistry, especially Mr. Dilip kumar K G and Mr. Loveson Albert for their support and help.

Many friends have helped me stay sane through these difficult years. Their support and care helped me overcome setbacks and stay focused on my study. I greatly value their friendship and I deeply appreciate their belief in me. I wish to express my deepest gratitude to my friends especially Sarah Titus, Dhanya M, Kavita M K, Remyamol T, Haripadmam P C, Narasimman R, Raneesh konnoola, Cinthya Kuriakose and all other students in the department for their never ending support. Heart-felt thanks to my friends in the other department also.

Most importantly, none of this would have been possible without the love and patience of my family. I would like to express my heart-felt gratitude to my parents and brother for the unceasing encouragement, support, love and attention poured on me throughout this venture.

SARIKA P R

ABSTRACT

Chemotherapeutic drugs which are now used for the treatment of cancer have many limitations. Most of them are highly toxic, expensive and cause damage to the healthy cells. In this context, research on natural chemotherapeutic agents for cancer treatment gains great attention, since these agents can avoid many of the drawbacks of conventional drugs. Curcumin is one such natural chemotherapeutic agent derived from turmeric. Since long, curcumin is being used in Ayurvedic medicines as healing agent for a variety of diseases. Research on the therapeutic effects of curcumin on various tumors has escalated tremendously over the last few decades. Anticancer activity of curcumin is mediated through its regulation of various transcription factors, inflammatory cytokines, protein kinase and growth factors. It is effective towards many types of cancers including skin, lung, brain, pancreas etc.

Draw backs of curcumin such as low solubility, stability and fast degradation reduces the practical usage of curcumin in cancer therapy. Increasing the bioavailability of curcumin by protecting it from degradation can enhance the efficacy in cancer treatment. Developments in nanobiomaterial research pave a new way in the enhancement of therapeutic effect of curcumin. Several nanomaterials such as polymeric nanoparticles, micelles, lipid bilayers and polymer-curcumin conjugates were developed for the encapsulation and safe delivery of curcumin. This thesis deals with development of three types of nanomaterials for the delivery of curcumin to carcinoma cells. These nanomaterials are polymer-curcumin conjugates, nanogels and polyelectrolyte complex. All the three nanomaterials are prepared from polysaccharides namely pullulan, alginate and gum arabic.

Owing to their high solubility, biocompatibility and biodegradability, polysaccharides are one of the best choices for developing nanoformualtions for curcumin encapsulation followed by delivery. Biomedical applications of gum arabic, pullulan and alginate are reported, but the potential of these highly soluble polymers for curcumin delivery to carcinoma cells is not yet reported. Hence, in the present work, nanosized carriers from these polysaccharides for the safe and effective delivery of curcumin to cancer cells are developed.

Conjugation of curcumin to hydrophilic polysaccharides enhances the solubility and bioavailability of curcumin. Polymer-drug conjugates are one of the best choices to increase the solubility of curcumin. Drug molecules are covalently linked to the polymer chain in a polymer-drug conjugate. Conjugates with targeting agents show enhanced cytotoxicity than that of nontargeted conjugates. Therefore, in the present study, curcumin conjugates, based on pullulan and alginate with and without targeting groups are developed and their cytotoxicity towards the hepatocarcinoma cells is evaluated. Both galactosylated and nongalactosylated pullulan-curcumin conjugates self assemble to micelle and increase the solubility and stability of curcumin. Conjugate with targeting ligand shows enhanced uptake and toxicity towards HepG2 cells.

Alginate-curcumin conjugates are prepared to avoid the shortcomings of pullulan-curcumin conjugates. Curcumin conjugates from alginate with and without targeting group are also prepared by the same synthetic strategy used for the preparation of conjugates with pullulan. These conjugates also increase the solubility and stability of curcumin and show high negative zeta potential.

Polysaccharides containing targeting ligands in the structure itself are better choice for drug conjugation; since better toxicity may be achieved with minimum steps for the preparation. Based on this hypothesis, gum arabic-curcumin conjugate also is prepared since it contains galactose group which is identified as targeting ligand towards hepatocarcinoma cells. Gum arabic-curcumin conjugate is the best among the three systems studied. It shows the highest solubility and cytotoxicity.

Encapsulation of drugs in nanoparticles will enhance the solubility and pharmacokinetics of the drug. Nanogels and polyelectrolyte complexes based on suitable polysaccharides may act as effective carrier for curcumin delivery. Nanogels are prepared by the cross-linking of polysaccharides, namely, gum arabic and alginate with protein gelatin by inverse miniemulsion technique. In order to improve the bioavailability and therapeutic efficacy, curcumin is encapsulated in alginate aldehyde-gelatin and gum arabic aldehyde-gelatin nanogels. Physicochemical properties of both bare and curcumin loaded nanogels are analyzed by dynamic light scattering, nuclear magnetic resonance spectroscopy, thermogravimetric analysis and scanning electron microscopy. Both curcumin loaded alginate aldehyde-gelatin and gum arabic aldehyde-gelatin nanogels induce toxicity to human breast carcinoma cells. Intracellular uptake of the drug encapsulated nanogels is investigated by fluorescent imaging.

Self assembled hybrid polyelectrolyte complex nanoparticles are prepared from cationically modified gelatin and alginate by electrostatic complexation between the polymers. Cationised gelatin is prepared by the reaction of gelatin with ethylenediamine. Structural changes occurred in gelatin after modification with ethylenediamine is investigated by X-ray diffraction, nuclear magnetic resonance spectroscopy and matrix-assisted laser desorption/ionization – time of flight analysis. These polyelectrolyte complex nanoparticles can be used for the encapsulation and delivery of natural antioxidant curcumin to carcinoma cells. The cationised gelatin-alginate nanoparticles show curcumin entrapment efficiency of 69 % and also exhibit sustained release of curcumin *in vitro*. Anticancer activity of curcumin loaded cationised gelatin-alginate nanoparticles towards human breast carcinoma cells are disclosed by MTT assay. Intracellular uptake of curcumin loaded polyelectrolyte complex nanoparticle is also confirmed by fluorescent imaging.

In conclusion, solubility and stability of curcumin can be increased by conjugation to pullulan, alginate and gum arabic or encapsulation in nanogels and polyelectrolyte complex nanoparticles. Curcumin conjugates and curcumin encapsulated nanogels and polyelectrolyte complex show cytotoxicity towards hepatocarcinoma cells/human breast carcinoma cells. Hence the prepared nanomaterials could be promising candidates in cancer therapy.

TABLE OF CONTENTS

LIST OF FIGURES

Scheme

LIST OF TABLES

ABBREVIATIONS

°C	degree celsius
μg	microgram
μL	microliter
μM	micromolar
μm	micrometer
AITC	allyl isothiocyanate
Alg	alginate
Alg Ald	alginate aldehyde
Alg Ald-Gel	alginate aldehyde-gelatin
Alg-Cur	alginate-curcumin conjugate
ASGPR	asialoglycoprotein receptor
ATRP	atom-transfer radical-polymerization
amu	atomic mass unit
bw	bodyweight
cm	centimeter
cps	centipoise
CG	cationised gelatin
CHA	cholesteryl-hyaluronic acid
CLSM	confocal laser scanning microscopy
CMC	critical micelle concentration
COX-2	cyclooxygenase-2
Cur	curcumin
Cur SA	modified curcumin
Da	dalton
dBECM	decellularized brain extracellular matrix
DCC	N,N'-dicyclohexylcarbodiimide
DLS	dynamic light scattering

DMAP	dimethylaminopyridine
DMSo-d_6	dueterioted dimethyl sulfoxide
DMSO	dimethyl sulfoxide
DNA	deoxyribonucleic acid
EA	ethylenediamine
EDC	1-ethyl-3-[3-dimethylaminopropyl] carbodiimide
EE	entrapment efficiency
EPR	enhanced permeation and retention
Et_3N	triethylamine
FAO	food and agriculture organisation
FBS	fetal bovine serum
FDA	food and drug administration
FT-IR	fourier transform infrared
g	gram
GA	gum arabic
GA Ald	gum arabic aldehyde
GA Ald-Gel	gum arabic aldehyde-gelatin
GA-Cur	gum arabic-curcumin conjugate
Gel	gelatin
GPC	gel permeation chromatography
h	hour
HA	hyaluronic acid
HBMECs	human brain microvascular endothelial cells
HCl	hydrochloric acid
HepG2	human hepatocellular carcinoma cells
HHC	hexahydrocurcumin
kg	kilogram
kV	kilovolt
LA	lactobionic acid
$LANH_2$	modified lactobionic acid

$LANH_2$-Alg Ald	galactosylated alginate aldehyde
$LANH_2$-Pu Ald	galactosylated pullulan aldehyde
$LANH_2$-Alg Ald-Cur	galactosylated alginate aldehyde-curcumin conjugate
$LANH_2$-Pu Ald-Cur SA	galactosylated pullulan aldehyde-curcumin conjugate
LBL	layer by layer
LE	loading efficiency
M	molar
MALDI-TOF-MS	matrix-assisted laser desorption/ionization time of flight mass spectroscopy
MCF-7	human breast cancer cell line
MEM	minimum essential medium
mg	milligram
MHz	megahertz
min	minutes
mL	milliliter
MMPs	matrix metalloproteinases
mol	moles
MTT	3-(4,5-dimethylthiazol-2-yl)-2,5-diphenyltetrazolium bromide
mV	millivolt
Mw	milliwatt
MW	molecular weight
MWCO	molecular weight cut off
N	normal
Na_2CO_3	sodium carbonate
Na_2HCO_3	sodium bicarbonate
NaOH	sodium hydroxide
nm	nanometer
NMR	nuclear magnetic resonance
NPs	nanoparticles
ODC	ornithine decarboxylase

PBS	phosphate buffer saline
PCL	Polycaprolactone
PDLLA	poly(d,l-lactic acid)
PEC	polyelectrolyte complex
PEG	polyethyleneglycol
PET	polyethylene terephthalate
PGA	polyglycolic acid
pH	potential of hydrogen
PI	propidium iodide
PLGA	poly(lactic-co-glycolic acid)
PLLA	poly-l-lactic acid
PMMA	poly(methylmethacrylate)
poly NIPAM	poly(N-isopropylacrylamide)
Pu	pullulan
Pu Ald	pullulan aldehyde
Pu-Cur SA	pullulan-curcumin conjugate
RAFT	reversible addition−fragmentation chain-transfer
RBC	red blood cells
RBE4s	rat brain endothelial cells
REF	reticuloendothelial clearance
RGD	arginine-glycine-aspartic acid
rpm	revolutions per minute
RT	room temperature
s	seconds
SA	succinic anhydride
SEM	scanning electron microscopy
siRNA	small interfering ribonucleic acid
TEM	transmission electron microscopy
TGA	thermogravimetric analysis
THC	tetrahydrocurcumin

THF	tetrahydrofuran
TNBS	trinitrobenzenesulfonic acid
TMS	trimethylsilane
UV	ultraviolet
VEGF	vascular endothelial growth factor
v/v	volume/volume
w/v	weight/volume
WHO	world health organisation
XRD	x-ray diffraction

NOTATIONS

η	absolute zero-shear viscosity
α	alpha
β	beta
^{13}C	carbon-13
A_{380} and A_{450}	correction factors applied for uroporphyrin absorption falling in the same wavelength range.
δ	delta
D	dextrorotatory
ε	dielectric constant
U_e	electrophoretic mobility
γ	gamma
IC_{50}	half maximal inhibitory concentration
Hb	hemoglobin
$f(\kappa a)$	henry function
I_{373}	intensity at 373
I_{384}	intensity at 384
pI	isoelectric point
L	levorotatory
m/z	mass/charge
λ_{max}	maximum wavelength
E	molar absorptivity value of oxyhemoglobin at 415 nm
Mn	number average molecular weight
^{1}H	proton
κa	ratio of the particle radius to the Debye length
A_{415}	soret band based absorption of hemoglobin
θ	theta
λ	wavelength
ζ	zeta potential

NOMENCLATURE

Ca^{2+}	calcium ion
$-CH_2$	methylene
$-CH_3$	methyl
-COOH	carboxylic acid group
$-COO^-$	carboxylate ion
$-NH_2$	amino group
$-NH_3^+$	ammonium ion
-OH	hydroxyl group
$-OCH_3$	methoxy
-SH	thiol group

CHAPTER 1
INTRODUCTION

This chapter gives an introduction about the properties, limitations and drug delivery systems of curcumin. It also depicts different types of drug delivery systems developed for curcumin delivery. Scope and objectives of this thesis and organization of the chapters are also described.

Cancer therapy remains challenging, even with the development of many anticancer drugs. Delivering therapeutics to the entire region of tumor in an appropriate concentration is an intricate task and is not easy with conventional cancer therapy techniques. Anticancer drugs used in chemotherapy requires modification to increase solubility, circulation time and alteration to reduce adverse side effects and nonspecific activity (Liang et al. 2006). In addition to that, reiterated treatment with these drugs makes the tumors resistant to chemotherapeutics. In this context, identification of a naturally occurring drug which has the capability to down regulate growth and induces apoptosis in human carcinoma cells without causing any toxicity to healthy cells is crucial. Among the natural drugs, polyphenols are extensively used for decease prevention and treatment due to their antioxidant properties (Zern & Fernandez 2005). Polyphenols are present in green and black tea, peanut, dark chocolate and turmeric. Among the polyphenols found in the food components, curcumin which is present in turmeric is the most important and widely studied chemopreventive agent.

1.1 Curcumin

Curcumin (Cur) (1,7-bis[4-hydroxy-3-methoxyphenyl]-1,6-heptadiene-3,5-dione) is a natural hydrophobic polyphenol obtained from rhizome of the plant

Curcuma longa or root turmeric. It is mainly used as flavoring agent, coloring agent, spice and food preservative. For centuries, it is being used in the Ayurvedic medicines for the treatment of inflammation, open wounds, skin diseases and as a cosmetic agent for beauty care.

Curcumin constitutes three major curcuminoids namely curcumin (77 %), demethoxycurcumin (17 %) and bisdemethoxycurcumin (6 %) (Anand, Kunnumakkara, Newman, & Aggarwal 2007). It exhibits keto-enol tautomerism with prevailing keto form in neutral and acidic conditions and acts as a powerful donor of hydrogen atoms. Under alkaline conditions, enol form prevails and phenolic part of the curcumin plays main role as an electron donor (Jovanovic, Steenken, Boone, & Simic 1999).

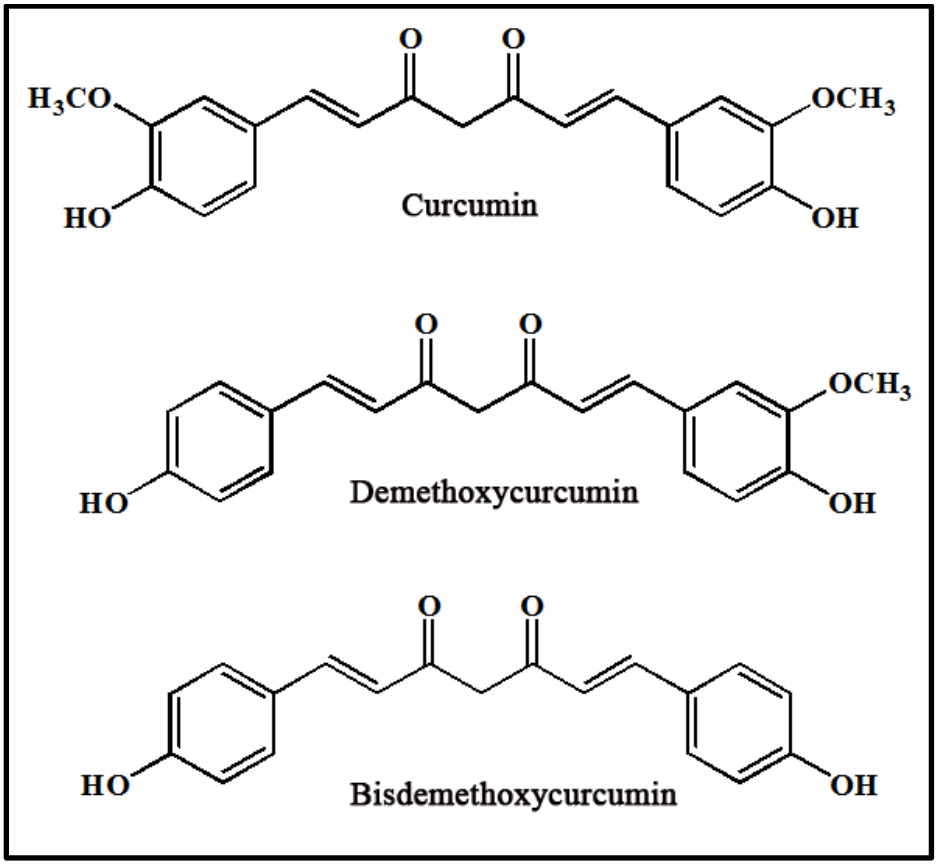

Figure 1.1 Chemical structures of curcuminoids

1.1.1 Chemical properties of curcumin

Curcumin is readily soluble in organic solvents like ethanol, chloroform, dimethyl sulfoxide, acetonitrile etc., while it is insoluble in water and ether (Aggarwal, Kumar, & Bharti 2003). Curcumin in organic solvents shows absorption maximum in the UV-visible region ranging from 408-434 nm (Inoue, Yoshimura, & Nakazawa 2001, Khopde, Indira Priyadarsini, & Mukherjee 2000, Mandeville, Froehlich, & Tajmir-Riahi 2009). Absorption maximum of curcumin varies with solvents. In polar solvents like acetone, curcumin shows absorption maximum at 420 nm, while in hydrogen bond acceptor and donor solvents, the absorption maximum is around 430–434 nm (Priyadarsini 2009).

Curcumin shows an aqueous solubility of 2.792 μg/mL (T. H. Kim et al. 2011) and partition coefficient of 3.2 μg/mL (Patel, Singh, Singh, Sheth, & Gendle 2009). Orally delivered curcumin undergoes quick metabolism in the liver, while when intraperitoneally administrated, it undergoes reduction and the degradation products show low therapeutic activity (R. Sharma, Gescher, & Steward 2005).

1.1.2 Medicinal properties

Medicinal properties of curcumin such as antioxidant, anti inflammatory, antimicrobial and anticancer effects have been explored over the past three decades (Aggarwal, Surh, & Shishodia 2007, Maheshwari, Singh, Gaddipati, & Srimal 2006). Curcumin related research gained acceleration and prominence after the discovery of its anticancer potential. Anti inflammatory and antioxidant property of curcumin is responsible for the prevention and/or treatment of cancer. It induces anticancer activity through particular pathways in different cells by blockade of cellular targets which are culpable for cancer induction, expansion and metastasis (Joe, Vijaykumar, & Lokesh 2004), suppression of cell proliferation and induction of apoptosis. In the treatment of colorectal and breast cancer models (MDA-MB-231 and BT483),

curcumin induces toxicity by impediment of NF-κB/PI3K/Src pathway and NF-κB, cyclin D1 and matrix metalloproteinases (MMPs) respectively (Q. Liu, Loo, Sze, & Tong 2009, Shakibaei et al. 2013). Curcumin down regulates many anti apoptotic factors such as cyclooxygenase-2 (COX-2) (Goel, Boland, & Chauhan 2001, Joe et al. 2004), survivin and vascular endothelial growth factor (VEGF) *via* the suppression of NF-κB activity. Curcumin shows anticancer activity in breast, prostate, bladder, neuron, lung and ovary cancer cells by inducing p53-dependent apoptosis (Aggarwal 2008, Tian et al. 2008). Recent research demonstrated that curcumin can also be used for the treatment of Parkinson's disease and Alzheimer's disease (Jagatha, Mythri, Vali, & Bharath 2008, Mourtas, Lazar, Markoutsa, Duyckaerts, & Antimisiaris 2014, Tiwari et al. 2014, F. Yang et al. 2005).

1.1.3 Toxicity and safety

In several Asian countries, people use turmeric in small daily doses as a spice. The average intake of turmeric in India is 2.0-2.5 g/day (corresponding to approx. up to 0.1 g of curcumin), and no adverse effects have been reported (Chainani-Wu 2003). The amount of curcumin present in the plasma of those who have taken high oral dose of curcumin is in nanomolar level. This is due to the extensive metabolism in intestine and liver. Because of its metabolism, high concentration of curcumin cannot be achieved in plasma and tissues after oral administration (C. Ireson et al. 2001, C. R. Ireson et al. 2002). Based on several studies, US FDA approved turmeric as safe and the acceptable daily intake of curcumin according to FAO/WHO is 0.1–3 mg/kg-bw.

For examining the adverse effects of curcumin, many studies have been performed all over the world. In one of the studies conducted in India, curcumin at a dose of 1.2–2.1 g administrated orally for 2–6 weeks to patients with rheumatoid arthritis did not cause any toxicity. Phase I clinical trial was performed in patients with severe colorectal cancer to assess the potential toxicity of orally delivered curcumin (R. A. Sharma et al. 2004). *In vitro* studies on cancer cells demonstrated

that the concentration of curcumin needed for cell death is 5-50 μM (López-Lázaro et al. 2007, López-Lázaro 2008, Syng-ai, Kumari, & Khar 2004). If curcumin was taken orally, this particular concentration would not achieve outside the gastrointestinal tract because of its intensive metabolism. All these studies (animal models or human studies) prove the safety of curcumin even at very high doses (Lao et al. 2006, Shoba et al. 1998, Yum et al. 2001). Three different phase I clinical trials indicated that oral administration of curcumin up to 12.0 g per day does not lead to any cytotoxic effect in humans (Yum et al. 2001). Therefore, based on several clinical trials to obtain the maximum therapeutic effects of curcumin, the targeted oral doses can be in between 4.0–8.0 g per day (Basnet & Skalko-Basnet 2012).

The efficacy and safety of curcumin makes it a potential candidate for treatment and prevention of a wide variety of human diseases including cancer.

1.1.4 Limitations of curcumin

Despite its therapeutic efficacy and safety, curcumin has not been widely utilized for treatment owing to its low bioavailability. The reasons for reduced bioavailability of curcumin are poor absorption, rapid metabolism and fast elimination. Curcumin undergoes glucuronidation and sulfation at various tissues after absorption. Major metabolism of curcumin is in liver and the vital billiary metabolites of curcumin are glucuronides of tetrahydrocurcumin (THC) and hexahydrocurcumin (HHC) in rats (Garcea et al. 2004, Hoehle, Pfeiffer, Sólyom, & Metzler 2006, Wahlström & Blennow 1978). Other minor biliary metabolite of curcumin is dihydroferulic acid and ferulic acid. Pharmacokinetic study of curcumin in humans demonstrated that it undergoes extensive reduction, through alcohol dehydrogenase, followed by conjugation.

Another challenge associated with curcumin, to be used as a drug for treatment of various diseases is its very low aqueous solubility. Inadequate solubility

notably curbs its availability in biological systems. Soluble fraction of curcumin lacks stability in physiological conditions. It will undergo rapid degradation first by hydrolysis, then by molecular fragmentation. The aqueous solubility of curcumin can be enhanced by increasing the pH of the solution. However, alkaline pH accelerates degradation of curcumin by hydrolysis. Curcumin undergoes 90 % decomposition within 30 min when it is incubated in 0.1 M phosphate buffer (pH 7.2) and serum-free medium, at 37 °C (Y.-J. Wang et al. 1997). Decomposition of curcumin is pH dependent and shows swift degradation at neutral-basic conditions. The major degradation product of curcumin under basic condition is trans 6-(4'-hydroxy-3'-methoxyphenyl) 2,4-dioxo-5-hexenal. Other minor degradation products are vanillin, ferulic acid and feruloyl methane. The amount of vanillin increased with incubation time (Shen & Ji 2012).

Curcumin is more stable in cell culture medium containing 10 % fetal calf serum and in human blood; less than 20 % of curcumin decomposed within 1 h and, after incubation for 8 h, about 50 % of curcumin remained (Y.-J. Wang et al. 1997).

1.1.5 Drug delivery systems

In order to improve the therapeutic efficacy, bioavailability and to overcome the aforementioned shortcomings, curcumin should be protected from degradation and metabolism. Research groups are working with this aim to investigate new approaches that could vanquish the limitations of curcumin. Nano sized drug delivery systems are the best choice to overcome the poor water solubility of lipophilic drugs. Encapsulation of hydrophobic drugs into nanoparticles would improve the solubility and hence the pharmacokinetics and biodistribution of the drugs. In addition to that, the entrapment protects the drug from degradation by hydrolysis or by enzymes present in the blood plasma (Orive, Hernández, Gascón, & Pedraz 2005).

Effective drug delivery systems such as polymeric micelles (J. H. Kim et al. 2012), liposomes (Lehtinen et al. 2012), nanogels (Chacko, Ventura, Zhuang, & Thayumanavan 2012), lipids (Das & Chaudhury 2011), microspheres (X. Yang, Chen, Han, Yang, & Duan 2010) and nanoparticles (Caldorera-Moore, Guimard, Shi, & Roy 2010) have been developed for the encapsulation and delivery of various drugs. During the last decade, research in this area has experienced an exponential raise. All these delivery systems differ in their production, structure, pharmaceutical properties and therapeutic index. Nanoparticle drug delivery systems are advantageous since they can cross the cell membranes and provide long duration in blood stream benefited from their tiny volume (Brannon-Peppas & Blanchette 2012).

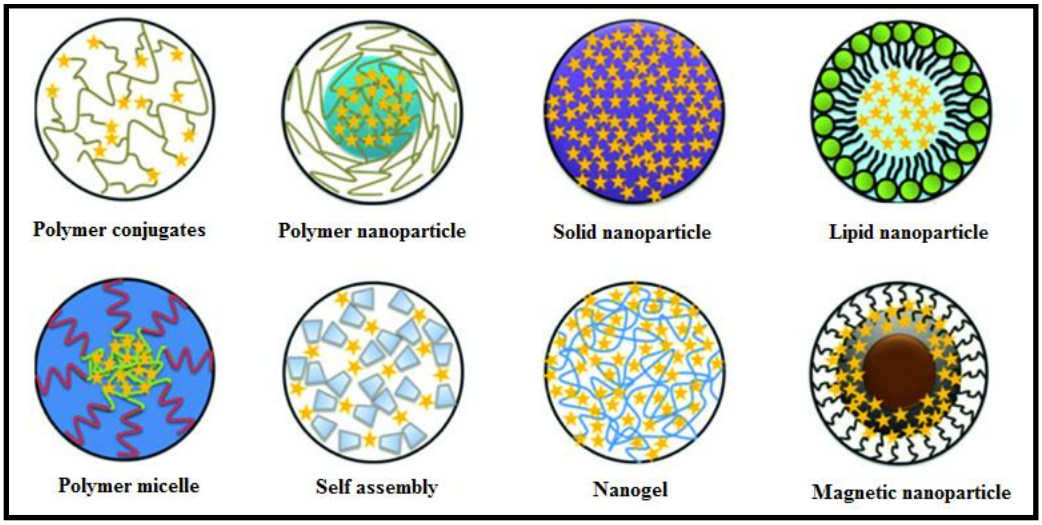

Figure 1.2 Different types of nanomaterials developed for curcumin delivery (Murali M Yallapu, Jaggi, & Chauhan 2012).

Nanogels are one of the important drug delivery systems with high loading capacity and stability. Daoud-Mahammed et al prepared cyclodextrin nanogels and studied the entrapment of two hydrophobic molecules, benzophenone and tamoxifen (Samia Daoud-Mahammed et al. 2009). Another group fabricated chondroitin sulfate based nanogels by inverse microemulsion process and utilized for doxorubicin encapsulation and delivery (Xi, Zhou, & Dai 2012). Polymer based nanoparticles were explored for curcumin encapsulation. Both synthetic and natural polymers were

used for the development of drug delivery systems. Alginate, chitosan, fibrinogen, gelatin and dextran are some of the biopolymers used for the fabrication of nanoparticles. Poly(lactic-co-glycolic acid) (PLGA) is one of the widely used synthetic polymers for nanoparticle development (Mukerjee & Vishwanatha 2009). Yallappau et al developed poly(lactic-co-glycolide) (PLGA) (biodegradable polymer) nanoparticles, in presence of poly(vinyl alcohol) and poly(L-lysine) stabilizers, using a nano-precipitation technique and utilized for curcumin delivery (Murali Mohan Yallapu, Gupta, Jaggi, & Chauhan 2010).

In the present study, three types of nanosized carriers for the safe and effective delivery of curcumin to carcinoma cells are developed. These nanomaterials are 1) Polymer-drug conjugates 2) Nanogels and 3) Polyelectrolyte complex.

1.1.5.1 Polymer-drug conjugates

Ringsdorf proposed the concept of polymer-drug conjugates in 1975 for the delivery of hydrophobic drug molecules (Ringsdorf 1975). In a polymer-drug conjugate, low molecular weight drugs are covalently conjugated to the macromolecular vectors. Polymer-drug conjugates improve the solubility of hydrophobic drugs, protect the drug from degradation and thereby increase their bioavailability (Xiao et al. 2011). Conjugate can circulate longer time than that of free drug and it provides enhanced drug accumulation in tumor tissues by enhanced permeability and retention (EPR) effect (Chau, Dang, Tan, & Langer 2006). In addition to that, the conjugate helps to achieve improved drug targeting to the tumor and reduce toxicity to healthy tissues. In early sixties, many research groups synthesized polymer-drug conjugates from polyvinylpyrrolidone and various antibiotics (Givetal, Ushakov, Panarin & Popova 1965, Shumikina, Panarin & Ushakov 1966). Design of polymer-drug conjugates needs several features such as selection of the polymer, the mode of conjugation of the drug to the polymer (either by direct or indirect conjugation) and the site of conjugation etc. Polymers should be

biodegradable and possess appropriate molecular weight for permeation and retention in solid tumors (Duncan 2006, Goodarzi, Varshochian, Kamalinia, Atyabi, & Dinarvand 2013).

Conjugation of a drug to a polymer depends upon the molecular weight, chemical structure, steric hindrance and reactivity of the drug as well as the polymer. Both the drug molecule and the polymer should possess appropriate functional groups such as –COOH, –OH, –SH or $–NH_2$ for conjugation and the resulting ester, amide or disulphide bond should be stable to prevent premature drug release during its transport through the blood stream. These types of macromolecular drug conjugates are expected to be stable in circulation and should degrade only after reaching the targeted cells or tissues.

Polymer-drug conjugates with a targeting moiety will enhance the therapeutic index of the conjugate and will give a selective and enhanced therapeutic effect than that of conjugate without targeting group. Many tumors over express particular antigens on their surface and may be identified by targeting moieties. The basic theory behind targeting of specific tumor is that the conjugate remains inactive until it reaches the specific site. Target group selectively identify the over expressed antigens on the cancer cells and these interactions may lead to the receptor mediated endocytosis into the tumor cells. A growth factor ErbB2 is over expressed in 20–30% of human breast carcinomas and two antibodies (F5 and C1) were used to target breast tumor cell line SK-BR-3. F5 linked PEG-doxorubicin conjugate showed a faster regression in tumor volume over unmodified conjugate (Nielsen et al. 2002). ASGPR (asialoglycoprotein receptor) on hepatocyte has been validated as a potential target for selective drug delivery to the liver because of its over expression on hepatocytes (Villa et al. 2013). Folate receptor is another target for drug delivery, since it is present on the surface of most of the tumors (Sudimack & Lee 2000).

Nanosized polymer-drug conjugates or prodrugs derived from biocompatible, water soluble polymers have received tremendous interest for cancer therapy (Zhan et al. 2011). Synthetic polymers and natural polymers such as proteins, antibodies, polysaccharides, polyethylene glycols and poly amino acids were used for conjugation of cytotoxic drugs.

Among different types of hydrophilic polymers, polysaccharides have gained significant attention because of their biodegradability, biocompatibility, cost effectiveness and presence of large number of reactive functional groups for further modification (Z. Liu, Jiao, Wang, Zhou, & Zhang 2008). Polysaccharides such as hyaluronic acid (Auzenne et al. 2007), dextran (Chau, Tan, & Langer 2004), chitosan (Hu, Liu, Du, & Yuan 2009) and heparin (I.-K. Park, Kim, Tran, Huh, & Lee 2010) etc are already been used for polymer-drug conjugation.

Sreenivasan and coworkers reported the efficacy of polysaccharides such as hyaluronic acid (HA) and alginate for the conjugation of curcumin, considering HA's affinity towards cell-specific surface markers such as CD44 and the hydrophilicity and biodegradability of alginate (Dey & Sreenivasan 2014, S Manju & Sreenivasan 2011a). Both of the polymer-curcumin conjugates formed micelle in aqueous solution and showed enhanced toxicity. Another curcumin conjugate was prepared from cholesteryl-hyaluronic acid. Curcumin was conjugated to cholesteryl-hyaluronic acid (CHA) nanogel through ester linkage and its capability for targeted delivery to CD44-expressing drug-resistant cancer cells was evaluated (Wei, Senanayake, Bohling, & Vinogradov 2014). In most of the curcumin-polymer conjugates, curcumin was grafted to the polymer for micelle formation (S Manju & Sreenivasan 2011b, Safavy et al. 2007, Tang et al. 2010). Yang et al reported a new strategy of conjugation of multiple curcumin molecules to the hydrophobic polymer backbone for generating more hydrophobic drug binding blocks for spontaneous micelle formation, enhanced drug loading and micelle stability. Polymer-drug conjugate with multiple drug

molecules will enhance the drug loading and hence intracellular delivery of the drug (R. Yang et al. 2012).

1.1.5.2 Nanogels

Nanogels are an important class of nanomaterials used for drug delivery applications. They are the nanoscopic counter parts of hydrogels. Hydrogels are a class of excellent and efficient biomaterials for variety of biomedical applications (Van Vlierberghe, Dubruel, & Schacht 2011). Hydrogels are three dimensional polymer networks prepared from either biopolymers or synthetic polymers by physical or chemical cross-linking. Ability to possess large amount of water without dissolving made hydrogels biocompatible and enabled diffusion of oxygen and nutrients. Even though hydrogles are excellent materials for drug delivery (Elvira, Mano, San Roman, & Reis 2002) and tissue engineering (K. Y. Lee & Mooney 2001), researchers are now focused on their nanosized counter parts, nanogels. Nanogels are hydrogels of nanometer size, formed by chemically or physically cross-linked polymers and have gained considerable attention in the field of nanomedicine and bionanotechnology.

Nanogels have properties of hydrogels and properties inherent to it because of their nanoscale size. Nanoscale size offers large surface area for multivalent bioconjugation of targeting agents like folic acid, peptides and galactose moiety which recognize receptors on cancer cells. Size can be modulated from nanometer to micrometers by changing the preparation parameters. Nanogels can reach the areas that cannot be accessed by hydrogels because of their small size. Nanogels with size between 100-200 nm are ideal for the cellular uptake since they can cross the cell membranes through endocytosis (Vinogradov, Bronich, & Kabanov 2002).

Nanogels encompass high loading efficiency for bioactive molecules such as proteins, DNA, siRNA and drugs and their release can be regulated by stimuli

responsive functional groups or by biodegradable bonds in a controlled fashion (Ayame, Morimoto, & Akiyoshi 2008, Vinogradov et al. 2002). They protect drugs and biomolecules from premature leakage into blood stream or other tissues and hence lower doses are adequate, leading to reduced side effects. In addition to the drugs and biomolecules, nanogels can incorporate magnetic nanoparticles and quantum dots for live cell imaging and photo thermal therapy (Hasegawa, Nomura, Kaul, Hirano, & Akiyoshi 2005, Jiang et al. 2013, Wu, Shen, Banerjee, & Zhou 2010).

Nanogels can be prepared from synthetic polymers like poly(*N*-vinylformamide), polyethyleneimine, poly NIPAM (poly(N-isopropylacrylamide), poly acrylamide, PMMA (poly methylmethacrylate), PGA (polyglycolic acid), PLLA (poly-l-lactide acid), PCL (polycaprolactone), PLGA (poly(D,L-lactide-co-glycolide) (Aliyar, Hamilton, Remsen, & Ravi 2005, Kuckling, Vo, Adler, Völkel, & Cölfen 2006, W. C. Lee, Li, & Chu 2006, Mimi, Ho, Siu, Wu, & Li 2012, Shi, Khondee, Linz, & Berkland 2008) and from several biopolymers. Among the biopolymers, polysaccharides are the most popular materials for the preparation of nanogels.

Natural polysaccharides like hyaluronic acid, dextran, pullulan, alginate, chitosan, mannan, chondroitin sulfate, cellulose and heparin have frequently been used for the development of nanogels. Different synthetic strategies were used for the development of nanogels including self assembly, inverse emulsion, precipitation etc. Nanogels can be used for the controlled and targeted delivery of hydrophobic and hydrophilic anticancer drugs like doxorubicin and curcumin. Biomolecules such as siRNA and peptides can be safely delivered using nanogels by active or passive targeting path ways. Delivery of the cargo from nanogels depends on the interaction of the cargo with the polymer chains.

Biodegradable, synthetic and biopolymer based nanogels were considered to be promising carriers for curcumin encapsulation and delivery (Sahu, Bora, Kasoju,

& Goswami 2008, Shaikh, Ankola, Beniwal, Singh, & Kumar 2009). Jayakumar and coworkers prepared curcumin loaded chitin and chitosan based nanogels and used for various cancer treatments including skin cancer (Mangalathillam et al. 2012, Sanoj Rejinold et al. 2011). Self assembled nanogels were prepared from hydrophobically modified dextrin and used as a nanocarrier for the formulation of lipophilic curcumin and evaluated its therapeutic efficacy in Hela cells (Gonçalves, Pereira, Schellenberg, Coutinho, & Gama 2012).

1.1.5.3 Polyelectrolyte complex

Polyelectrolytes are those polymers which contain ionisable groups in its structure. Polyelectrolytes undergo partial or complete dissociation in aqueous solutions, making the polymers charged. Polyelectrolyte complex (PEC) is formed when polyelectrolytes of opposite charges are mixed in aqueous solution. Strong electrostatic interaction between oppositely charged polymers gain in entropy due to the dissociation of counter ions to the medium and drives the PEC formation (Doi & Kokufuta 2010a). Other forces like hydrogen bonding or hydrophobic interactions also play an important role in PEC formation.

Formation of polyelectrolyte complex depends on pH of the reaction medium, temperature, the ratio of polymers/charges, molecular weight of the polymers, degree of ionization of the polymers, ionic strength and polymer charge density (Berger, Reist, Mayer, Felt, & Gurny 2004, Hamman 2010). Generation and stability of the polyelectrolyte complex (PEC) also get affected by temperature and pressure of the medium (Schmitt, Sanchez, Desobry-Banon, & Hardy 1998). The motive for the interaction between the polyelectrolytes arises from the enthalpic and entropic contribution respectively due to the association of oppositely charged groups and release of their counter ions (Doi & Kokufuta 2010a). The electrostatic interactions in a polyelectrolyte complex can be regulated by varying the ionic strength by addition

of salt (Kudlay & de la Cruz 2004), since low molecular weight ions can screen the charge density on the polymers.

PEC which are biocompatible have been investigated for drug delivery (H. Wang & Roman 2011), wound dressing (H.-J. Kim et al. 1999) and tissue engineering applications (Coimbra et al. 2011). The popularity of the PEC nanoparticle formation technique is due to its low cost, low energy requirement and effectiveness compared to common processes such as solvent evaporation, emulsification, RAFT (Reversible addition−fragmentation chain-transfer) and ATRP (*Atom-transfer radical-polymerization*) methods (Bencherif et al. 2009, Ibrahim, Bindschaedler, Doelker, Buri, & Gurny 1992, Qi, Chen, Huang, Jin, & Wang 2012). PEC formation does not involve organic solvents, cross-linking agents and elevated shear rates, (Jintapattanakit, Junyaprasert, & Kissel 2009, Lankalapalli & Kolapalli 2009) avoiding the probable toxicity and other unwanted effects of the reagents.

Proteins and some of the polysaccharides are polyelectrolytes, which can get ionized in aqueous solutions. When proteins and polysaccharides with opposite charges are mixed together in aqueous solutions, they undergo either attractive or repulsive interaction and form polyelectrolyte complex (PEC). Studies on the electrostatic interactions between proteins and polysaccharides started long ago in 1920's by Bungenberg de Jong and Kruyt as they undertook investigation on complex coacervation of gum arabic and gelatin (Bungenberg de Jong & Kruyt, 1929). Proteins carry positive charges below their isoelectric point (pI) and can interact with polysaccharides having opposite charges.

Polyelectrolyte complexes can be used as carriers for delivery of drugs (Grenha et al. 2010, Sarmento et al. 2007) and proteins (Perevyazko et al. 2012), as membranes (Smitha, Sridhar, & Khan 2004) and for coating on films and fibers. Delivery substance can be incorporated into the complex either from the solution during formation of the complex or gets assimilated into the already formed complex

on contact. The substance which has to be delivered can also be introduced into the complex by grafting chemically it to one of the polyelectrolytes and precipitates during complexation. In another method, the active substance to be delivered acts as poly ion and forms complex with the other component. The payload from the polyelectrolyte complex can be released by many methods. This includes ion exchange mechanism, slow decomplexation by charge interaction, breakdown and dissolution of the complex (Lankalapalli & Kolapalli 2009).

Polyelectrolyte complexation between polysaccharides and proteins are well established. After the studies on gum arbic and gelatin system in 1920, many research groups have studied the interaction between different polysaccharides and proteins. Fajardo et al reported the polyelectrolyte complexation between pectin–NH_2 and chondroitin sulfate (Fajardo, Lopes, Pereira, Rubira, & Muniz 2012). Nanoparticle formation by electrostatic complexation between chitosan and gellan gum was also explored by another research group (Picone & Cunha 2013).

Even though the above mentioned nanomaterials were prepared from both synthetic and natural polymers, biopolymer based materials gain much attraction owing to their superior properties. The present study focuses upon the preparation, characterization and *in vitro* biological evaluation of three different classes of the nanomaterials, namely polymer-drug conjugates, nanogels and polyelectrolyte complex prepared from polysaccharides, for the delivery of curcumin.

Following sections outline the properties and applications of various polysaccharides in drug delivery systems.

1.2 Polysaccharides

Polysaccharides are polymeric carbohydrate structures made up of repeating units of mono- or disaccharides connected together by glycosidic bonds.

Polysaccharides are widely used in the design of drug delivery systems. Depending on their monosaccharide components it can be homopolysaccharides or heteropolysaccharides. Pharmacokinetics of polysaccharides is greatly influenced by their electric charge, polydispersity, branching, extent of chemical modifications and molecular weight (Mehvar 2003). Polysaccharides are found to have abundant sources and are cost effective that made them good biomaterials for biomedical applications (Lemarchand et al. 2005, Rinaudo 2008).

Polysaccharides contain hydrophilic groups such as hydroxyl, carboxyl and amino groups responsible for providing solubility in water. Polysaccharides derived from non-mammalian and mammalian sources are widely used as biomaterials. Non-mammalian originated polysaccharide biomaterials are cellulose, chitosan, chitin, alginate, gum arabic, pullulan and dextran, whereas heparin, heparin sulfate, hyaluronic acid, chondroitin sulfate and keratan sulfate are derived from mammalian tissues.

1.2.1 Gum arabic

Gum arabic is a biocompatible, nontoxic, natural gum obtained from acacia tree. It is a branched, slightly acidic complex polysaccharide containing arabinose, rhamnose, galactose and glucuronic acid residues with a backbone consisting of 1,3 linked β-D- galactopyranosyl units. The side chains are composed of two to five 1,3 linked β-D-galactopyranosyl units, joined to the main chain by 1,6 linkages (Verbeken, Dierckx, & Dewettinck 2003). Gum arabic is an inexpensive polysaccharide which is being extensively used as stabilizing, emulsifying and thickening agent in the food industry. It is a highly water soluble polymer with broad molecular weight distribution from 260000 to 1160000 Da. Low viscous aqueous solutions of gum arabic with concentration more than 50 % can be prepared.

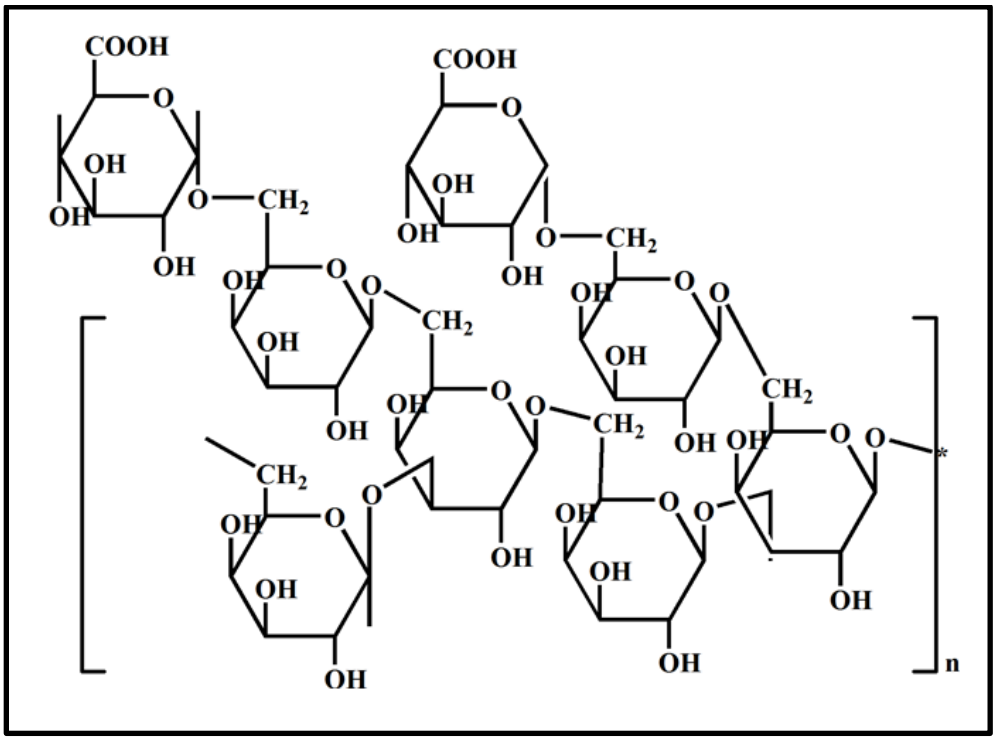

Figure 1.3 Structure of gum arabic

Three major components are present in the molecular structure of gum arabic, which includes arabinogalactan (>90 %) with a low protein content (0.5 %), arabinogalactan with a high protein content (10 %) and glycoprotein having protein content of 47.3 % (Randall, Phillips, & Williams 1989, Ray, Bird, Iacobucci, & Clark Jr 1995). Connolly et al have reported that gum arabic has a ‘‘wattle-blossom’’ type structure with a number of polysaccharide units linked to a common polypeptide chain (Connolly, Fenyo, & Vandevelde 1988).

Gum arabic is a weak anionic polyelectrolyte with carboxylic acid groups, and it is negatively charged above pH 2.2 due to the dissociation of the carboxylic acid groups above this pH. Gum arabic is widely used as food additive and for encapsulation of oils and terpenes (Bertolini, Siani, & Grosso 2001, Y. D. Kim & Morr 1996).

Biomedical applications of gum arabic include tissue engineering, drug delivery etc (Nishi, Antony, Mohanan, et al. 2007). Gum arabic and chitosan based nanoparticle systems for oral delivery of insulin (Avadi et al. 2010) have been developed. Oxidized gum arabic-primaquine microspheres were prepared by heat denaturation process in an inverse emulsion of 1:1 light paraffin oil and toluene stabilized by sorbitan sesquioleate as the surfactant (Nishi & Jayakrishnan 2004). Maltodextrin-gum arabic nanoparticles coated with lipid layers produced by spray drying were used for controlled release of epigallocatechin gallate (Gomes et al. 2010). Release properties of gum arabic microparticles were investigated with vettiver essential oil and camphor oil as models (Chang, Leung, Lin, & Hsu 2006, Prata, Zanin, Ré, & Grosso 2008). Gum arabic was also used as a surface modification agent for magnetic nano particles (Wilson Jr, Blair, Kennedy, Rivera, & Mehl 2008). Tannic acid cross-linked gelatin–gum arabic coacervate microspheres, capable of sustained release of allyl isothiocyanate (AITC) with high encapsulation efficiency, were developed for safe and efficient oral delivery of AITC (Z.-Q. Zhang, Pan, & Chung 2011). Reis et al modified gum arabic with glycidyl metharylate to prepare pH responsive hydrogels (Reis, Guilherme, Cavalcanti, Rubira, & Muniz 2006). Gum arabic was employed as a nontoxic phytochemical construct in the production of readily administrable biocompatible AuNPs for diagnostic and therapeutic applications in nanomedicine (Axiak-Bechtel et al. 2014, Gamal-Eldeen, Moustafa, El-Daly, & Katti 2014, Kattumuri et al. 2007).

1.2.2 Alginate

Alginate is a polyanionic and biodegradable polysaccharide composed of β-D-mannuronic acid (M) and α-L-guluronic acid (G) units extracted from brown algae. This linear polysaccharide is composed of consecutive G residues (GGGGGG), consecutive M residues (MMMMMM) and alternating M and G residues (GMGMGM). The ratio of guluronate to mannuronate varies depending on the source it was derived (K. Y. Lee & Mooney 2012) from. Physical properties of the

alginate depend on M/G ratio and sequence, G-block length and molecular weight. Commercially available alginate has molecular weight in the range between 32000 and 400000 g/mol. Solubility of alginate in water is low and it forms viscous solution. Viscosity increases with decrease in pH due to the protonation of carboxylate groups in alginate. The viscosity of the alginate solution depends upon the molecular weight distribution and concentration of the polymer.

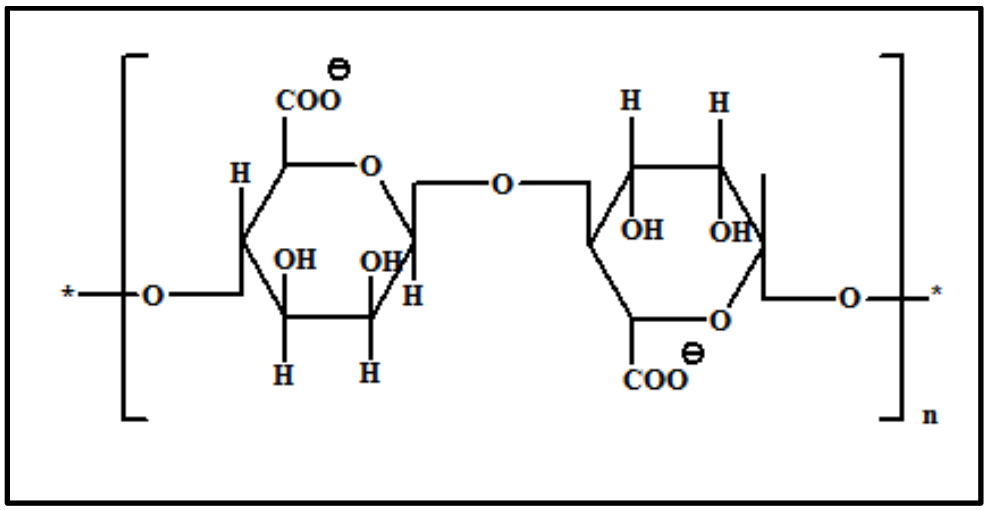

Figure 1.4 Structure of alginate

Alginate is a well established biomaterial and its applications also include thickening, gel forming and stabilizing of food formulations. Many alginate derivatives have been prepared to date by introducing hydrophobic moieties such as long alkyl chains and hydrophobic polymers to the polymer chain. These amphiphilic derivatives can self assemble to microparticles and gels in aqueous ambience. Cholesterol grafted amphiphilic conjugate could self assemble to nanoparticle with diameter of 136 nm (L. Yang, Zhang, Wen, Liang, & Zhang 2007). Poly(butyl methacrylate) modified alginate has been used for drug delivery applications (Yao, Ni, Xiong, Zhu, & Huang 2010).

Alginate based hydrogels and nanoparticles play a significant role in controlled release of bioactive molecules. In the presence of divalent cations, alginate

forms gels in aqueous medium and these gels are used for wound healing, tissue engineering and drug delivery applications. Divalent cations interact with guluronic acid blocks of alginates and forms cross-linked hydrogels, since the guluronate blocks allow high degree of coordination to the cations. One of the most commonly used divalent cation is Ca^{2+} for ionic cross-linking of sodium alginate. Covalent cross-linking is another method to prepare cross-linked gel. Physical properties like mechanical strength of the gels can be improved by covalent cross-linking (K. Y. Lee & Mooney 2012). Alginate gels have been utilized for the delivery of low molecular weight drugs, since the drugs can be easily diffused through the nanoporous (5 nm) architecture. Alginate gels were also used for the encapsulation and delivery of multiple drugs for simultaneous or sequential delivery (Bouhadir, Alsberg, & Mooney 2001). Ionically cross-linked alginate microspheres efficiently encapsulated proteins such as lysozyme and chymotrypsin (Wells & Sheardown 2007).

Another important application of alginate gel is as wound dressing. Alginate based wound dressings are more advantageous to traditional dressing (gauze) since they provide moist environment and help in wound healing. Dried alginate gel sheets absorb wound fluid to re-gel and furnish water to the dry wound, maintaining moist environment and lessen the bacterial infection. Some of the commercially available alginate gel dressings are Algicell™ (Dermal Sciences), AlgiSite M™ (Smith & Nephew), Tegagen™ (3M Healthcare), Comfeel Plus™ (Coloplast) and Sorbsan™ (UDL Laboratories) (K. Y. Lee & Mooney 2012).

Another important application of alginate based gel is as a substrate for *in vitro* tissue regeneration. RGD peptide modified alginate gels dramatically enhanced the adhesion and proliferation of myoblasts (Rowley, Madlambayan, & Mooney 1999). Alginate gels were used in cancer biology as a 3D cell culture substrate to understand the influence of a 3D microenvironment in cancer cell signaling and tumor vascularization (Fischbach et al. 2009).

Alginate–chitosan nanoparticles have been developed and used as carrier for DNA and for protein delivery exploiting the gelling property of alginate in presence of calcium chloride (Douglas & Tabrizian 2005, T. Li, Shi, Du, & Tang 2007). However, the loss of the cations and the resultant release of the components may pose problems in ionically cross-linked systems. Li et al prepared bioreducible alginate-poly(ethylenimine) nanogels through electrostatic interactions and used as an antigen delivery system (P. Li et al. 2013). Alginate can also form covalently cross-linked nanogels with hyaluronic acid in polyion complex nanoreactors (De Santis, Diociaiuti, Cametti, & Masci 2014).

Dey et al developed alginate-curcumin conjugate for enhancing solubility and stability of curcumin (Dey & Sreenivasan 2014). Alginate-daunomycin conjugates were synthesized to release the drug in the acidic environment of the endosomal and lysosomal compartments of tumor cells (Al-Shamkhani & Duncan 1995). Abu-Rabeah et al synthesized pyrrole-alginate conjugate for biosensor application (Abu-Rabeah, Polyak, Ionescu, Cosnier, & Marks 2005).

1.2.3 Pullulan

Pullulan is a linear, water soluble extracellular polysaccharide produced by polymorphic fungus Aureobasidium pullulans. It is a nonionic polysaccharide with blood compatibility, biodegradability, nontoxicity, non immunogenicity, non mutagenicity and non carcinogenicity. Its structure consists of α-1,4 linked glucose units that are included in a α-1,6 linked maltotriose unit. Pullulan and its derivatives have applications in pharmaceutical, food and biomedical field because of their biocompatibility and biodegradability. The enzyme pullulanase hydrolyses the α-1-6 linkages of pullulan and converts the polymer into maltotriose units (Leathers 2003).

Depending on the growth conditions of the fungus Aureobasidium pullulans, molecular weights of pullulan range from 10000 to 2000000 Da. Viscous aqueous

solutions of pullulan have high adhesion and film forming abilities and these films possess anti-static and elastic properties. Pullulan is an excellent material for food preservation since it carries properties like impermeability to oxygen, prevent fungal growth and possess moisture retention capacity. FDA approved it as a safe material and according to the usage and food categories, the daily intake of pullulan was limited to 10 g per day for a person (Rekha & Sharma 2007).

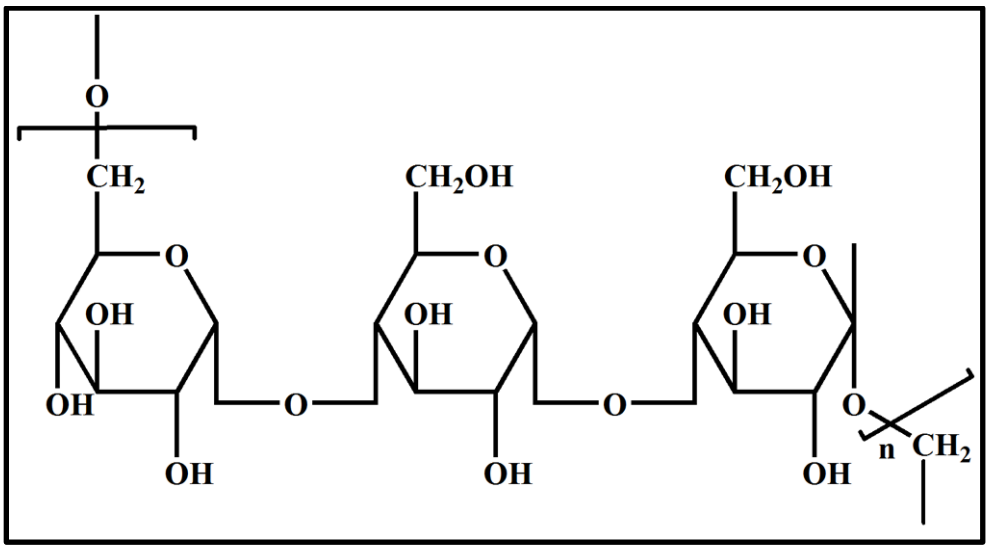

Figure 1.5 Structure of pullulan. Three glucose units in maltotriose are connected by α-1,4 glycosidic linkage

Pullulan has been extensively used for various biomedical applications owing to its excellent properties. Pullulan has been modified with hydrophobic groups and the resulting amphiphilic derivatives have applications in pharmaceutical and biomedical field (Na, Seong Lee, & Bae 2003, H.-z. Zhang et al. 2009). Self assembled nanoparticles were prepared from hydrophobically modified pullulan and used for drug/gene delivery and for cancer therapy (Ferreira, Coutinho, & Gama 2011). pH sensitive/temperature sensitive groups were attached to pullulan and the resulting derivatives were utilized for pH sensitive drug delivery (Lu et al. 2009, Seo, Lee, Jung, & Na 2012). Cholesterol modified pullulan nanoparticles were utilized for quantum dot encapsulation and these nanoparticles could be promising candidates for fluorescent imaging (Hasegawa et al. 2005).

Crescenzi et al prepared methacrylated pullulan hydrogels by reversible addition–fragmentation chain-transfer (RAFT) process and its physicochemical properties were evaluated (Crescenzi, Dentini, Bontempo, & Masci 2002). Porous scaffolds were prepared from pullulan and its efficacy for endothelial progenitor delivery for vascular disease treatment was evaluated (Lavergne et al. 2012). Pullulan based hydrogels were also used for mesenchymal stem cell delivery into high-oxidative-stress wounds (Wong et al. 2011). Carboxymethyl pullulan and cystemine based hydrogels were synthesized for gentamycin encapsulation and wound dressing (H. Li et al. 2011).

Several low molecular weight drug molecules were attached to pullulan and the resulting prodrugs were utilized for chemotherapy. The pharmacokinetics and half-life of the drug molecules were improved considerably after conjugation to pullulan. Longer half life time of the prodrug leads to passive accumulation of the prodrug in the tumor tissues. Pullulan can be used as a surface modification material for many polymers to improve their blood compatibility and bio-intertness. Hasuda et al prepared azidophenylpullulan and studied the interactions of this modified pullulan with proteins like albumin. They found that this hydrophilic azidophenylpullulan considerably reduced protein adsorption (Hasuda, Kwon, Kang, & Ito 2005).

Gupta et al prepared pullulan nanoparticles and used for the delivery of pBUDLacZ plasmid to cells (M. Gupta & Gupta 2004). Sharma and coworkers developed pullulan–polyethyleneimine conjugates suitable for liver cell gene delivery (Rekha & Sharma 2011). They also developed cationically modified pullulan and used for gene delivery applications, targeted to liver cells (Rekha & Sharma 2009). Pullulan–spermine complexes were designed for neuronal delivery of DNA (Thakor, Teng, & Tabata 2009). Blood-brain barrier protects the brain from harmful substances present in the circulation and restricts the entry of drugs or proteins from entering the brain. A novel approach for the introduction of protein to brain is gene delivery. Thomsen et al prepared pullulan-spermine complex and demonstrated its capability to

transfect immortalized human brain microvascular endothelial cells (HBMECs) and rat brain endothelial cells (RBE4s) using plasmid DNA (Thomsen, Lichota, Kim, & Moos 2011).

1.3 Gelatin

In the present work, gelatin which is a protein is used for cross-linking oxidized polysaccharides for preparation of nanogels. Gelatin is a protein obtained from partial hydrolysis of collagen and is extensively being used as gelling agent, stabilizer and thickener in food. It is also used as suspending agent, tablet binder and encapsulating agent in pharmaceutical industries. Gelatin contains carboxyl and amino groups in its structure and gets cationised by protonation of amino groups at pH below its isoelectric point. Gelatin, a versatile protein, is being utilized as a drug carrier system because of its appealing physical and chemical properties such as biocompatibility, safety and biodegradability. Biomedical applications of gelatin includes tissue engineering, gene delivery and wound dressing (Kanokpanont, Damrongsakkul, Ratanavaraporn, & Aramwit 2012, Lim et al. 2011, Tseng et al. 2008). However, poor mechanical properties may limit its potential in certain applications (Boanini, Rubini, Panzavolta, & Bigi 2010). For overcoming this limitation and to improve stability in aqueous medium and mechanical properties, gelatin is subjected to cross-linking with different cross-linking agents (Imani, Rafienia, & Hojjati Emami 2013, M. S. Kim et al. 2010).

Gelatin based biodegradable hydrogels are a promising class of scaffolds for tissue engineering applications. Kang et al prepared glutaraldehyde cross-linked gelatin scaffolds by freeze drying and utilized it for tissue engineering (Kang, Tabata, & Ikada 1999). Chitosan-gelatin scaffolds were employed for dermal tissue engineering (Huang, Onyeri, Siewe, Moshfeghian, & Madihally 2005). An injectable scaffold was prepared from gelatin and 4-arm-polypropylene oxide–polyethylene oxide for tissue regeneration (K. M. Park et al. 2012). Nanofibrous gelatin scaffolds

were utilized for tissue engineering. Liu et al prepared nanofibrous gelatin/apatite (NF-gelatin/apatite) composite scaffolds and demonstrated its efficacy in bone tissue engineering (X. Liu, Smith, Hu, & Ma 2009). Genipin cross-linked gelatin scaffolds incorporating rat decellularized brain extracellular matrix (dBECM) prepared by electrospinning was exploited as a platform for nervous tissue regeneration (Baiguera et al. 2014).

Different kinds of gelatin nanoparticles have been explored and are used for various biomedical applications (S. J. Lee, Yhee, Kim, Kwon, & Kim 2013, Ofokansi, Winter, Fricker, & Coester 2010, J. Xu, Gattacceca, & Amiji 2013). Li et al prepared EGF tumor-specific ligand modified gelatin nanoparticles and utilized for cisplatin delivery (J. K. Li, Wang, & Wu 1997, Tseng, Su, Yen, Yang, & Lin 2009). Long circulating PEGylated gelatin nanoparticles were prepared for intracellular drug delivery. PEGylation increases the circulation time of the nanoparticles thereby facilitating the internalization of the nanoparticles in tumor cells (Kaul & Amiji 2002). Balthasar et al prepared biotinylated anti-CD3 antibodies attached gelatin nanoparticles and demonstrated its ability to be used as a carrier system for the specific drug targeting to T-lymphocytes (Balthasar et al. 2005).

Complex coacervation and electrostatic interactions of gelatin with different polysaccharides such as gum arabic (Y. Yang, Anvari, Pan, & Chung 2012), sodium alginate (Yifan Li, Jia, Cheng, Pan, & Jiang 2011), κ-carrageenan (Haug, Draget, & Smidsrød 2004), pectin (L. Liu, Liu, Fishman, & Hicks 2007) and chitosan (Kołodziejska, Piotrowska, Bulge, & Tylingo 2006) have been investigated in detail by many research groups.

Cationically modified gelatin contains excess amino groups and remains protonated even at neutral pH. Cationically modified gelatin can form complex with siRNA and plasmid IGF-1 and is shown to be successful carriers for gene delivery (Matsumoto et al. 2006, Morimoto, Chono, Kosai, Seki, & Tabata 2008, X. Xu,

Capito, & Spector 2008). Cationised gelatin (CG) and hyaluronic acid (HA) layer by layer (LBL) self-assembled coatings were used to modify polyethylene terephthalate (PET) artificial ligament grafts (H. Li et al. 2012).

Oxidized polysaccharides were used for preparing cross-linked hydrogels since the external cross-linking agents induce toxicity. Oxidized dextran was cross-linked with gelatin for preparing cryogels and utilized as a tissue engineering scaffold (Inci, Kirsebom, Galaev, Mattiasson, & Piskin 2013). Biji et al prepared injectable *in situ* forming scaffolds from oxidized alginate and gelatin and the resulting hydrogels were utilized as a wound dressing material (Balakrishnan, Mohanty, Umashankar, & Jayakrishnan 2005). Another polysaccharide pectin was oxidized by sodium hypochlorite and cross-linked with gelatin (Chetouani, Elkolli, Bounekhel, & Benachour 2014).

In the current work, gelatin is utilized for cross-linking alginate aldehyde and gum arabic aldehyde for nanogel preparation. Gelatin is also modified cationically and polyelectrolyte complex is prepared by the electrostatic interaction between cationically modified gelatin and alginate.

1.4 Scope and objectives of the thesis

Therapeutic properties of curcumin include anti inflammatory, antioxidant, analgesic, antiseptic and anticancer activities. After the discovery of anticancer potential, curcumin related research has been increased tremendously. Anticancer activity of curcumin originates from its ability to inhibit the tumor cell proliferation, to reduce tumor volume and to induce apoptosis (Sa & Das 2008). Inhibition on cell proliferation is mediated by its effect on the cell cycle arrest. It has the ability to suppress to ornithine decarboxylase (ODC) that leads to the hindrance of cell proliferation. Curcumin incites apoptosis depending on the cell type through

mitochondria dependent as well as mitochondria independent mechanisms (Aggarwal et al. 2003).

Low solubility of curcumin (2.792 μg/mL) (T. H. Kim et al. 2011) is the major factor limiting the applications of curcumin. Preclinical and clinical studies in human and in rats disclosed the low bioavailability of curcumin. Different types of nanoformulations have been so far developed for encapsulation and delivery of curcumin. Bioavailability and circulation time of curcumin in blood can be increased by conjugating it with polymers, encapsulating in liposomal nanoparticles and in polymer nanogels. Both synthetic and biopolymers are utilized for preparing nanoformulations.

The scope of this work is to develop nanosized carriers from polysaccharides for the safe and effective delivery of curcumin to cancer cells.

Polymer-drug conjugates are one of the best choices to increase the solubility of curcumin. High solubility of curcumin can be achieved by conjugating it to a highly hydrophilic polysaccharide. Even though the polysaccharides gum arabic and pullulan are used in biomedical applications; their utility in conjugating curcumin is not yet explored. Taking into consideration of the high solubility of gum arabic, pullulan and alginate, curcumin conjugates are developed from these polysaccharides. Conjugates with targeting agents show better cytotoxicity than that of non-targeted conjugates (Scomparin, Salmaso, Bersani, Satchi-Fainaro, & Caliceti 2011). Hence the conjugates with and without targeting group are developed and cytotoxicity towards the cancer cells is compared. Polysaccharides which contain targeting ligands in the structure itself are better choices for drug conjugation; since this would offer elevated toxicity and reduce number of steps required for preparation. In this context, gum arabic which contains galactose moiety in its structure offers promise.

Encapsulation of drugs in nanoparticles will enhance the solubility and pharmacokinetics of the drug. Nanogels and polyelectrolyte complex are excellent carriers for drug delivery. The present study also deals with preparation and characterization of novel nanogels and polyelectrolyte complex based on the above mentioned polysaccharides. Polysaccharide based nanogels and polyelectrolyte complexes may offer better solubility for curcumin.

Hence the major aim of this thesis is to improve the solubility and bioavailability of curcumin by conjugating or encapsulating it in different nanoformulations. In order to achieve the goal, the following objectives have been set.

- Development of polymer-drug conjugates with and without targeting group from pullulan, alginate and gum arabic.
- Characterization and targeting efficiency analysis of the polymer-drug conjugates in hepatocarcinoma cells.
- Preparation of cross-linked nanogels from gum arabic and alginate for curcumin encapsulation.
- Cytotoxicity analysis of the nanogels in breast cancer cells.
- Cationic modification of gelatin for polyelectrolyte complex formation with alginate.
- Evaluation of biological activity of curcumin loaded polyelectrolyte complex.

1.5 Organization of the thesis

Chapter 1 describes the properties, potential in therapeutic applications and limitations of the drug curcumin which is selected for this study. This chapter contains illustration about the properties, limitations and applications of curcumin and

various drug delivery systems of curcumin. It also elucidates various types of nano delivery systems and different types of polysaccharides and proteins employed in delivery systems for curcumin.

Chapter 2 explains the experimental procedures adopted for the preparation and characterization of the nanomaterials such as polymer-drug conjugates, nanogels and polyelectrolyte complex developed in the present work for the delivery of curcumin.

Chapter 3 depicts polymer-drug conjugates developed for the study. Polymer-drug conjugates are prepared from three different polysaccharides; pullulan, alginate and gum arabic. The polymer-drug conjugates are characterized in detail and their anticancer activities are evaluated.

Chapter 4 explains preparation and evaluation of the nanogels developed from alginate and gum arabic by cross-linking with gelatin. The nanogels are loaded with curcumin and biological evaluation of the drug loaded nanogels are performed.

Chapter 5 describes the modification of gelatin and detailed characterization of the modified gelatin. Later, complex formation of the cationically modified gelatin with alginate is explained. The prepared polyelectrolyte complex nanoparticles are utilized for encapsulation and delivery of curcumin to cancer cells. This chapter also explains the characterization and biological evaluation of curcumin loaded polyelectrolyte complex nanoparticles.

Chapter 6 provides summary and conclusion of the thesis.

CHAPTER 2

EXPERIMENTAL

This chapter deals with details of different materials used and various synthetic strategies for the development of polymer-drug conjugates, nanogels and polyelectrolyte complex. Besides, different characterization techniques such as spectroscopy, microscopy and thermal analysis techniques used for the analysis of the samples throughout this research work are also depicted in this chapter. Biological characterizations such as hemocompatibility and cytoxicity analysis of the nanoparticle systems developed are also described here.

2.1 Materials

Alginate (Medium Viscosity Grade, viscosity of 2 % solution: 3500 cps at 25 °C), gum arabic (from acacia tree), pullulan, gelatin (Type A, Bloom 175), dimethylaminopyridine (DMAP), N,N'-dicyclohexylcarbodiimide (DCC), trinitrobenzenesulfonic acid (TNBS), 1-ethyl-3-[3-dimethylaminopropyl] carbodiimide (EDC), ethylenediamine (99.8 %), glutamine, lactobionic acid (LA), minimum essential medium (MEM), 3-(4,5-dimethylthiazol-2-yl)-2,5-diphenyltetrazolium bromide (MTT), propidium iodide (PI), sodium pyruvate and Trypsin-EDTA were obtained from Sigma Aldrich, Saint Louis, USA; Fetal Bovine Serum (FBS) is procured from Invitrogen, USA. Chloroform, cyclohexane, dimethyl sulfoxide (DMSO), disodium hydrogen phosphate, ethyl acetate, hydroxylamine hydrochloride, isopropanol, methyl orange, sodium carbonate, sodium metaperiodate, sodium bicarbonate, sodium chloride, sodium dihydrogen phosphate, sodium hydroxide, succinic anhydride (SA), sodium tetraborate decahydrate (borax, $Na_2CO_3.10H_2O$), Span 20, tetrahydrofuran (THF) and triethylamine (Et_3N) were

obtained from Merck (Mumbai, India). Curcumin was obtained as a gift from Synthite Industries Ltd Kolenchery, Kerala. Dialysis tubing (3500 and 6000-8000 MWCO) was procured from Spectrum Laboratories Inc.CA, USA.

2.2 Methods

2.2.1 Preparation of nongalactosylated and galactosylated pullulan-curcumin conjugates

2.2.1.1 Modification of curcumin (Cur-SA)

Modified curcumin (Cur-SA) was prepared by a previously reported procedure with slight modification (R. Yang et al. 2012). Curcumin (1 g, 0.0027 mol), Et_3N (1.388 mL, 0.0099 mol) and DMAP (0.4022 g, 0.0032 mol) were dissolved in THF (80 mL) in a 250 mL round bottomed flask, followed by the addition of succinic anhydride (0.6604 g, 0.0065 mol) dissolved in THF. The mixture was stirred and refluxed under nitrogen for 17 h at 50 °C. Solvent was removed under vacuum; the crude product was redissolved in ethyl acetate (60 mL) and then extracted with 1 M HCl (20 mL) to remove Et_3N. This process was repeated three times and ethyl acetate was removed under vacuum to get the product.

2.2.1.2 Preparation of nongalactosylated pullulan-curcumin conjugate (Pu-Cur SA)

Modified curcumin (Cur SA) was conjugated to pullulan (Pu) by DCC/DMAP coupling reaction. Initially, Cur-SA (0.243 g, 0.0005 mol) was dissolved in anhydrous DMSO. To this solution, DCC (0.055 g, 0.0005 mol) and DMAP (0.026 g, 0.0002 mol) were added and stirred magnetically under nitrogen at room temperature for 1 h to activate the acid groups in Cur SA. Later, pullulan (0.5 g, 0.0030 mol) was added to the reaction mixture and stirred at 60 °C for 6 h. The unreacted curcumin was

removed by dialysis (MWCO 3500) in DMSO for 1 day followed by dialysis in distilled water for 3 days. Purified dialysate was lyopilized to get non nongalactosylated pullulan-curcumin conjugate (Pu-Cur SA)). The product was kept under refrigeration.

2.2.1.3 Preparation of oxidized pullulan

Pullulan was oxidized to pullulan aldehyde (Pu Ald) based on reported procedure (Bruneel & Schacht 1993). Briefly, into 5 g (0.030 mol) of pullulan dissolved in 50 mL of distilled water, appropriate amount of sodium periodate (3.3 g, 0.015 mol) dissolved in 20 mL of water, required for 50 % oxidation was added. The reaction mixture was stirred magnetically at 20 ºC for 6 h in dark. Purification was done by dialysis using dialysis tube of MWCO 3500 for 3 days against distilled water. After purification, the dialysate was frozen and lyophilized. Oxidized pullulan (Pu Ald) was obtained in high yield of 90 %.

2.2.1.4 Modification of lactobionic acid

Lactobionic acid (LA, 5 g, 0.0129 mol) was refluxed with 30 fold excess of ethylenediamine (26.02 mL, 0.389 mol) dissolved in anhydrous DMSO at 70 °C for 2 h. The modified lactobionic acid ($LANH_2$) was precipitated with chloroform and was vacuum dried (Haensler & Schuber 1988).

2.2.1.5 Preparation of $LANH_2$-Pu Ald

$LANH_2$ was conjugated to pullulan by Schiff's base reaction between aldehyde group of Pu Ald and amino group of $LANH_2$ under basic conditions. Pu Ald (1.3 g) was dissolved in 0.1 M borax (13 mL, pH 9.4) and $LANH_2$ was (3.8 g) in water (38 mL). Both the solutions were mixed and stirred for 4 h at room temperature and then dialysed against distilled water for 1 day. The purified conjugate was lyophilized to obtain $LANH_2$-Pu Ald (galactosylated pullulan aldehyde).

2.2.1.6 Preparation of galactosylated pullulan-curcumin conjugate ($LANH_2$-Pu Ald-Cur SA)

Cur SA was conjugated to $LANH_2$-Pu Ald by DCC/DMAP coupling reaction. DCC (0.055 g, 0.0005 mol) and DMAP (0.026 g, 0.0002 mol) were added to Cur SA (0.243 g, 0.0005 mol) dissolved in anhydrous DMSO and this solution was stirred magnetically under nitrogen at room temperature for 1 h. After the activation of carboxylic acid group in Cur SA, $LANH_2$-Pu (0.5 g) dissolved in DMSO was added to the reaction mixture and stirred at 60 °C for 6 h. The product was purified by dialysis using dialysis tube of MWCO 3500 for 1 day in DMSO and 3 days in distilled water. After purification, the dialysate was lyophilized to obtain galactosylated pullulan-curcumin conjugate ($LANH_2$-Pu Ald-Cur SA).

2.2.2 Preparation of nongalactosylated and galactosylated alginate-curcumin conjugates

2.2.2.1 Preparation of nongalactosylated alginate-curcumin conjugate (Alg-Cur)

Curcumin was conjugated to alginate based on a reported procedure (Dey & Sreenivasan 2014). Alginate (0.1g, 0.0005 mol) was dispersed in anhydrous DMSO. DCC (0.103g, 0.0005 mol) and DMAP (0.0610g, 0.0005 mol) were dissolved in anhydrous DMSO, added to alginate and stirred magnetically under nitrogen for 1 h to activate acid groups in alginate. Curcumin (0.1841 g, 0.0005 mol) dissolved in DMSO was added to the reaction mixture and stirred for 6 h at 60 °C. The product was purified by dialysis using dialysis tube of MWCO 3500 and lyophilized.

2.2.2.2 Preparation of oxidized alginate

Alginate aldehyde (Alg Ald) was prepared by a previously reported procedure (Balakrishnan, Joshi, Jayakrishnan, & Banerjee 2014). Alginate (10 g, 0.0568 mol)

was dissolved in ethanol-water mixture (1:1, v/v). Sodium periodate (6.05 g, 0.028 mol required for 50 % oxidation) was added to the reaction mixture and stirred at 20 °C for 6 h in dark. Excess periodate was removed by dialysis using a dialysis tube of MWCO 3500 for 3 days against distilled water. Then the dialysate was frozen and lyophilized to obtain Alg Ald. The yield of the product was in the range of 60-65 %.

2.2.2.3 Conjugation of Alg Ald to $LANH_2$

$LANH_2$-Alg Ald was prepared by conjugation of alginate aldehyde to modified lactobionic acid ($LANH_2$) by Schiff's base reaction. Briefly, 0.5 g of Alg Ald was dissolved in 5 mL of 0.1 M borax. To this solution, 1.2 g of $LANH_2$ dissolved in water (5 mL) was added and stirred magnetically for 4 h. The solution was dialyzed to remove the unreacted $LANH_2$ using dialysis tube (MWCO 3500) for 1 day. The purified dialysate was lyophilized to obtain $LANH_2$-Alg Ald.

2.2.2.4 Preparation of galactosylated alginate-curcumin conjugate ($LANH_2$- Alg Ald-Cur)

$LANH_2$-Alg Ald-Cur was prepared by conjugating curcumin to the acid gropus of Alg-Ald by DCC/DMAP coupling reaction. Briefly, 0.5 g of $LANH_2$-Alg Ald (0.0007 mol) was dissolved in anhydrous DMSO. To this, DCC (0.144 g, 0.0007 mol) and DMAP (0.085 g, 0.0007mol) were added and stirred under nitrogen at room temperature for 1 h to activate the carboxylic acid groups in Alg Ald. Curcumin (0.25 g, 0.0007 mol) was dissolved in anhydrous DMSO and added to the reaction mixture. The reaction mixture was stirred at 60 °C for 6 h. Purification was done by dialysis using dialysis tube of MWCO 3500 for 1 day in DMSO followed by 3 days in water and then lyophilized to obtain galactosylated alginate-curcumin conjugate ($LANH_2$-Alg Ald-Cur).

2.2.3 Preparation of gum arabic-curcumin conjugate (GA-Cur)

Curcumin was conjugated to gum arabic (GA) by a previously reported procedure (S Manju & Sreenivasan 2011a) with slight modification. Briefly, 0.4 g (2.3×10^{-3} mol) of gum arabic was dispersed in anhydrous DMSO (50 mL) for 12 h by stirring magnetically. To this solution, 0.009 g of DCC (4.36×10^{-5} mol) and 0.005 g of DMAP (4.09×10^{-5} mol) were added and stirred for another 1 h at room temperature under nitrogen atmosphere to activate the carboxylic acid groups of GA. Curcumin (0.05 g, 1.35×10^{-4} mol) dissolved in DMSO (20 mL) was added to the above solution and was stirred for 6 h at 55-60 °C. After the reaction, the solution was dialyzed using dialysis tube of MWCO 3500 for 1 day in DMSO followed by 3 days in water to purify GA-Cur conjugate and then lyophilized to obtain the product.

2.2.4 Preparation of Nanogels

2.2.4.1 Preparation of alginate aldehyde

Alginate aldehyde was prepared according to the procedure reported under section **'2.2.2.2 Preparation of oxidized alginate'.** For nanogel preparation, 30 % oxidized alginate was used. For 30 % oxidation of alginate (10 g, 0.058 mol), 3.28 g of sodium periodate (0.015 mol) was used.

2.2.4.2 Preparation of alginate aldehyde-gelatin (Alg Ald-Gel) nanogel

Nanogels were prepared by an inverse miniemulsion technique with appropriate modification to a previously reported procedure (Ethirajan, Schoeller, Musyanovych, Ziener, & Landfester 2008). Typical procedure for nanogel preparation is as follows. Span 20 (0.2 g) was dissolved in 10 mL of cyclohexane and a mixture of 250 µL of alginate aldehyde (10 % solution in 0.1 M borax) and 250 µL of gelatin (10 % solution in water) were added to the solution under sonication over a

period of 5 min. The nanogel emulsion was precipitated by drop wise addition into acetone (50 mL) while stirring with a magnetic stirrer. The precipitate was collected by centrifugation (rpm 5000, for 15 min) and washed three times with water and dried under reduced pressure to obtain the nanogel powder. Nanogel samples were prepared with different weight fractions of the water phase and surfactant concentrations to investigate the impact of these factors on the size of the nanogels.

2.2.4.3 Preparation of curcumin loaded alginate aldehyde–gelatin (Alg Ald-Gel) nanogel

Curcumin was dissolved in acetone (2 mg/mL) and added to Alg Ald-Gel nanogel inverse minemulsions (10 mL) mentioned above and allowed to stir for two days. After that, drug loaded nanogels were separated by centrifugation at 5000 rpm for 10 min and washed thrice with distilled water. The nanogels were then vaccum dried.

2.2.4.4 Preparation of oxidized gum arabic

Gum arabic aldehyde (GA Ald) was prepared from gum arabic using sodium metaperiodate by periodate oxidation by previously reported procedure (Nishi, Antony, Mohanan, et al. 2007). Gum arabic (10 g, 0.058 mol) was dissolved in 100 mL distilled water and sodium periodate (1.24 g, 0.0058 mol) required for 10 % oxidation was added to it. The reaction mixture was stirred magnetically under dark at 20 ºC for 6 h. After the reaction, the mixture was purified by dialysis using dialysis tube of MWCO 6000-8000 for three days against distilled water. After purification, the dialysate was frozen and lyophilized to obtain GA Ald. The yield of the product was in the range of 80-85 %.

2.2.4.5 Preparation of gum arabic aldehyde-gelatin (GA Ald-Gel) nanogels

Gum arabic aldehyde–gelatin (GA Ald-Gel) nanogels were prepared by an inverse miniemulsion technique (Ethirajan et al. 2008). The procedure involves preparation of two separate emulsions A and B, where A contains gum arabic aldehyde nanoparticles, while B contains nanoparticles of gelatin. Later, these two emulsions were mixed and sonicated to obtain GA Ald-Gel nanogel. For both the emulsions, 6 mg of Span 20, dissolved in 5 mL of cyclohexane acted as the continuous organic phase. The procedure adopted in a typical experiment for the preparation of nanogel is as follows. For preparing inverse miniemulsion of GA Ald, a solution of GA Ald (10 %, w/v) was prepared in 0.1 M borax. This solution (250 µL) was added to the continuous organic phase and sonicated for 5 min. The second miniemulsion (B) was prepared in a similar fashion. Gelatin (5 g) was dissolved in water (10 mL) by heating at 40 °C and 250 µL of the solution was added to the continuous organic phase and sonicated for 5 min. Later, these two emulsions were mixed and sonicated again for 5 min to obtain GA Ald-Gel nanogel. The nanogel emulsion was poured drop wise into 50 mL of acetone and was stirred magnetically. The nanoparticles were isolated by centrifugation at 6000 rpm for 5 min. The collected nanoparticles were washed with acetone and water to remove the surfactant and other impurities. The centrifugate was then dried under reduced pressure to obtain the nanogel powder. Nanogels were prepared by varying the surfactant concentration and total volume of the aqueous phase.

2.2.4.6 Preparation of curcumin loaded gum arabic aldehyde-gelatin (GA Ald-Gel) nanogels

Curcumin loading was done as described in section **‘2.2.4.3’**. Curcumin dissolved in acetone (2 mg/mL) was added to GA Ald-Gel nanogel inverse minemulsions (10 mL) and allowed to stir for two days. After this, curcumin loaded

nanogels were separated by centrifugation at 5000 rpm for 10 min and washed thrice with distilled water. The nanogels were then vaccum dried.

2.2.5 Preparation of polyelectrolyte complex

2.2.5.1 Cationic modification of gelatin

Gelatin was modified using ethylenediamine according to previously reported procedure (X. Xu et al. 2008). Briefly, 5 g of gelatin was dissolved in 50 mL of 0.1 M phosphate-buffered solution (pH 5.0), to which 15.8 mL (0.2358 mol) of ethylenediamine and 2.68 g (0.017 mol) of 1-ethyl-3-(3-dimethylaminopropyl) carbodiimide were added. The pH was adjusted to 5 using 6 N hydrochloric acid and the mixture was stirred at room temperature for 18 h. The modified gelatin was purified by dialysis for 48 h in distilled water, and then lyophilized to obtain cationised gelatin (CG).

2.2.5.2 Formation of CG/Alg polyelectrolyte complex

Alginate solution (0.1 %, w/v) and 0.1 % solution (w/v) of cationised gelatin (CG) were prepared in distilled water. Polyelectrolyte complex was prepared by the addition of aqueous solutions of Alg to CG at room temperature under vigorous vortexing for 5 min. Polyelectrolyte complexes of different compositions were prepared by varying the volume of Alg and CG. Polyelectrolyte suspension was centrifuged at 15,000 rpm for 20 min to separate the nanoparticles. Separated nanoparticles were vaccum dried and used for further studies.

2.2.5.3 Preparation of curcumin loaded CG/Alg polyelectrolyte complex

Curcumin was dissolved in acetone (1 mg/mL) and 100 μL of curcumin was added to 0.1 % solution (3 mL) of CG. Complex formation was performed as mentioned above. Alginate solution (1 mL, 0.1 %) was added to the curcumin

containing CG solution (3 mL) and vortexed for 5 min. Drug loaded nanoparticles were separated by centrifugation as mentioned above and was dried under vacuum.

2.2.6 Characterization Techniques

Physicochemical properties of the prepared nanomaterials were analyzed by various spectroscopic, microscopic and thermal analysis techniques.

2.2.6.1 Fourier Transform-Infrared spectroscopy

Fourier Transform-Infrared spectroscopy was used to analyze the structural characteristics of the prepared nanomaterials. In the present study, FT-IR spectra of polysaccharide-curcumin conjugates, nanogels and polyelectrolyte complex were recorded on Perkin Elmer FT-IR spectrometer in the range of 4000 to 400 cm^{-1} with 32 scans per sample.

2.2.6.2 NMR Spectroscopy

Nuclear magnetic resonance spectroscopy is used to understand the magnetic properties of certain atomic nuclei. In the present work, NMR spectroscopy is used to analyze changes happened in molecules after modification and also used for the confirmation of curcumin conjugation/encapsulation in polysaccharide-drug conjugates, nanogels and in polyelectrolyte complex. NMR spectra of the samples were recorded using 500 MHz spectrometer (Bruker Avance DRX 500). All the spectra were recorded using TMS as internal standard and D_2O or DMSO-d_6 as solvent.

2.2.6.3 Fluorescence spectroscopy

Fluorescence spectra were used for the confirmation of curcumin conjugation to various polysaccharides and for determining CMC values of polymer-curcumin

conjugates. The spectra were recorded on an F-2500 fluorescence spectrophotometer (HITACHI, Tokyo). Samples were dissolved in water with equivalent curcumin concentration of 5 µg/mL. Curcumin was dissolved in water by sonication. The excitation wavelength was 430 nm and the emission spectra were recorded from 454 nm to 700 nm. The excitation and emission slit width were 5 nm.

2.2.6.4 Ultraviolet-visible absorption spectroscopy

In the present study, UV-visible spectroscopy is used to find out the absorbance of polysaccharide-curcumin conjugates during stability studies, to plot calibration curve for curcumin estimation, to find out the amount of released curcumin in drug release experiments and to find out the amount of curcumin conjugated or encapsulated in the various drug conjugates and curcumin loaded nanogels and polyelectrolyte complex. The spectra were recorded (Cary 100 UV-spectrophotometer, USA) at a wavelength of 430 nm.

2.2.6.5 Temperature dependant ultraviolet-visible absorption spectroscopy

The structural changes occurred in gelatin after modification was evaluated by temperature dependant UV-Spectroscopy. Absorbance spectra of gelatin and cationised gelatin were recorded on Shimadzu 3101 PC UV-VIS-NIR spectrophotometer over a temperature range of 20–65 °C. All the samples were analyzed in a quartz cuvette with 1 cm path length. Temperature was allowed to equilibrate for 5 min before acquisition of each spectrum, sufficient for equilibrium to be obtained. Samples were analyzed over the wavelength range of 200–700 nm.

2.2.6.6 Size and Zeta potential measurements

Hydrodynamic radii and zeta potential of all the prepared nanoparticles were measured by dynamic light scattering. Particle size and size distribution of the nanomaterials are often found out using a well established technique called ‘Dynamic

Light Scattering' (DLS). DLS is based on the Brownian motion of the particles. Particles in suspension or dispersion undergo continuous motion and when light hit on these particles it get scattered to different directions. Scattering intensities of the particles vary with time, since the particles are in continuous motion. Stokes-Einstein equation can be used to find out the hydrodynamic diameter of the particle. Laser light from the source hit the sample in the cuvette and the scattered light signal is collected at 173 ° (back angle) scattering angle. Refractive index and viscosity of the dispersion medium is needed to carry out the measurement.

Zeta potential measurement provides an insight to the surface charge of the particles. Particle surface charge plays main role in their stability in medium, agglomeration tendencies and interaction with biological systems. The surface charges control the interactions between particles and therefore determine the behavior of a sample suspension. During zeta potential measurements, an electrical field is applied across the sample and the motion or electrophoretic mobility of the particle is measured by the light scattering of the particles. Then the zeta potential is measured from Henry equation, Eq. (2.1)

$$Ue = \frac{2\varepsilon z f(\kappa a)}{3\eta} \qquad (2.1)$$

U_e is the electrophoretic mobility, ε is the dielectric constant, η is the absolute zero-shear viscosity, $f(\kappa a)$ is the Henry function and κa is a measure of the ratio of the particle radius to the Debye length.

Measurements were performed on Malvern Zetasizer (Nano ZS, UK) equipped with a 4 mW He/Ne laser beam operating at λ= 633 nm, which was operated at a scattering angle of 173 °. All measurements were performed at 25 °C and each value reported is the average of three series of 10 measurements. All the polysaccharide-curcumin conjugates were redispersed in deionized water at a

concentration of 1 mg/mL and their size and zeta potential were measured. Hydrodynamic radius of different combinations of Alg Ald-Gel and GA Ald-Gel nanogels in miniemulsions was measured. Size and zeta potential of bare and curcumin loaded Alg Ald-Gel and GA Ald-Gel nanogels were also measured after dispersing the dried nanogels (1 mg/mL) in water. In the case of polyelectrolyte complex nanoparticles, size and zeta potential of various combinations of CG/Alg complex were measured after preparation. Later, bare and curcumin loaded CG/Alg complex nanoparticles were redispersed in water (1 mg/2mL) and their size and zeta potential were also measured.

2.2.6.7 CHN elemental analysis

CHN elemental analysis gives an insight about the elemental composition of a material. The analysis was performed on PerkinElmer 2400 Series II CHNS/O Elemental Analyzer. Carbon, hydrogen and nitrogen contents in the samples were measured.

2.2.6.8 Scanning electron microscopy

Morphology of the prepared nanoparticles was analyzed by scanning electron microscopy. In SEM, a focused beam of electrons scan the sample and gives its images. SEM images of the samples were taken on FEI Quanta FEG 200 HR Scanning Electron Microscope (SEM) by applying an acceleration voltage of 10 kV. A drop of the prepared nanoparticle dispersion (polysaccharide-curcumin conjugates, nanogels and polyelectrolyte complex) was placed on a glass slide and allowed to air-dry at ambient temperature, sputter coated and observed by SEM. The concentration of each category of the nanoparticles is given below. The galactosylated and nongalactosylated polysaccharide-curcumin conjugates were dispersed in water (1 mg/mL) and used for the analysis. Morphology of the Alg Ald-Gel and GA Ald-Gel nanogels were analyzed in miniemulsion as well as after dispersing the dried nanogels

in water. To analyze the changes in morphology after curcumin loading, both bare and curcumin loaded Alg Ald-Gel and GA Ald-Gel nanogels were dispersed in water with a concentration of 1 mg/mL. In polyelectrolyte complex nanoparticle also, bare and curcumin loaded CG/Alg complex was dispersed in water (1mg/2mL) and images were taken.

2.2.6.9 Transmission electron microscopy

TEM images were recorded on FEI, TECNAI S twin microscope with accelerating voltage 300 kV. The concentration of samples for TEM is 1 mg/5mL. The dispersion was placed on a copper grid and air dried for 2 days before taking the images.

2.2.6.10 Thermogravimetric analysis

Thermal stability of the samples were analyzed by thermogravimetry using Thermal Analysis System (Universal V4 7A, TA Instrument). Analysis was performed in N_2(g) atmosphere with flow rate of 20 mL/min and a scanning rate of 10 °C min^{-1} from RT to 800 °C. Percentage change in the mass of the sample was recorded continuously as a function of temperature.

2.2.6.11 X-ray Diffraction technique

X-ray diffraction patterns were obtained by X-ray Diffractometer (Bruker D8 discover Small Angle X-Ray Scattering Spectrometer, Germany).

2.2.6.12 Molecular weight determination

The molecular mass analysis was performed using matrix-assisted laser desorption/ionization time-of flight mass spectrometry (MALDI-TOF-MS) (Ultrafluxtreme, Bruker) with 2,5 dihydroxy acetophenone as matrix. One micro

liter of the sample was mixed with 2 μL of matrix solution and 1 μL of the mixture was spotted onto a target plate. Measurements were made in the positive linear mode.

The molecular mass analysis was also performed using Gel permeation chromatography (GPC) (Waters HPLC System) using 0.07 M disodium hydrogen phosphate with a flow rate of 1 mL/min as mobile phase. Dextran standards of molecular weight 900000/25000 and PEG 400 were used for relative calibration.

2.2.7 Determination of isoelectric point (pI)

Isoelectric point (pI) of cationised gelatin was determined using Malvern zetasizer, Nanoseries ZEN40002/SYS. CG was introduced into a capillary cell connected to an autotitrator and titrated against 0.25 M HCl and 0.25 M NaOH. Three measurements were taken with a time span of 10 s.

2.2.8 Determination of amino groups

Amino groups in gelatin and CG were estimated by TNBS assay (Bubnis & Ofner 1992). Briefly, 11 mg of gelatin and cationised gelatin were taken in 15 mL screw caped test tube. To that, 1 mL of 4 % $NaHCO_3$ and 1 mL of 0.5 % TNBS were added and heated at 60 °C for 4 h. Then, 3 mL of 6 N HCl was added to this mixture and heated for another 2 h at 40 °C. After heating, the mixture was diluted with 5 mL water and absorbance was measured spectrophotometrically (Cary 100 UV-spectrophotometer, USA) at λ= 334 nm.

2.2.9 Aldehyde content determination

Aldehyde content in pullulan aldehyde (50 % oxidation), alginate aldehyde (30 % and 50 % oxidation) and gum arabic aldehyde (10 % oxidation) was determined by titrimetric method (Balakrishnan et al. 2005). Gum arabic aldehyde,

alginate aldehyde and pullulan aldehyde (0.1 g) were dissolved in 25 mL, 0.25 N aqueous solution of hydroxylammonium chloride. Liberated hydrochloric acid resulting from the reaction of aldehyde groups with hydroxylamine hydrochloride was titrated against 0.1 N NaOH using methyl orange (0.05 % solution, w/v) as indicator. The colour change from red to yellow was taken as endpoint. The number of moles of NaOH consumed is equivalent to the number of moles of aldehyde present in the sample.

2.2.10 Estimation of curcumin conjugated to the polysaccharides

Amount of curcumin conjugated to $LANH_2$-Pu Ald, pullulan, $LANH_2$-Alg Ald, alginate and gum arabic was estimated by plotting a standard curve using free curcumin. A stock solution of curcumin was prepared in DMSO-water mixture (1:1, v/v). From this stock solution (1 mg/mL), different concentrations of curcumin, ranging from 0.002 mg/mL to 1 mg/mL were prepared using the same DMSO-water mixture. Concentration of curcumin in the conjugate was estimated by measuring the absorption intensity at 430 nm from the standard curve.

2.2.11 Determination of critical micelle concentration

Critical micelle concentrations (CMC) of the conjugates were determined by fluorescence spectroscopy using pyrene as the fluorescence probe (Guo et al. 2013). Briefly, 5 μL of pyrene solution (6.0×10^{-5} M) in acetone was added to a series of vials proceeded by evaporation to remove acetone. Aqueous solutions of the polysaccharide-curcumin conjugates with concentrations ranging from 0.001 μg/mL to 0.5 mg/mL were added to vials and sonicated in an ultrasonic bath for 40 min to equilibrate pyrene and conjugate and then left undisturbed overnight at room temperature. The final concentration of pyrene in each vial was 6.0×10^{-7} M. For obtaining pyrene emission spectra, the slit widths for excitation and emission were set at 5 nm. The emission spectrum (F-2500 fluorescence spectrophotometer, HITACHI,

Tokyo) was recorded from 350 to 600 nm with an excitation wavelength of 334 nm. The intensity ratio (I_{373}/I_{384}) of pyrene fluorescence bands at 373 nm and 384 nm were plotted against the logarithm of the conjugate concentration; CMC were determined by taking the cross-point when extrapolating the intensity.

2.2.12 Stability analysis of curcumin conjugated to the polysaccharides

Stability of curcumin in all the polysaccharide-curcumin conjugates and free curcumin at physiological pH (pH 7.4) was analyzed by measuring their absorbance at 430 nm at varied time intervals. The samples were maintained in PBS (pH 7.4) at 37 °C. Aliquots were withdrawn at specified time intervals (1 h) and absorbance was recorded using UV-Vis Spectrophotometer (Carry100 UV–Visible spectrophotometer, Melbourne, Australia).

2.2.13 Encapsulation efficiency and loading efficiency of curcumin loaded nanogels and polyelectrolyte complex

The encapsulation efficiency and loading efficiency of curcumin loaded nanogels and polyelectrolyte complex were determined by quantifying the loaded curcumin (Murali Mohan Yallapu et al. 2010). A known quantity of the lyophilized samples were dispersed in water-acetone mixture (1:1, 4 mL) by sonication using a probe sonicator (Sonics Vibra-cell, Modal-VCX 750) at 25 % of amplitude for 5 min. The dispersion was centrifuged at 10000 rpm for 20 min and the supernatant was collected. The amount of curcumin in the supernatant was estimated spectrophotometrically from the standard curve by measuring the absorption intensity at 430 nm. Encapsulation efficiency (EE) and loading efficiency (LE) were calculated by the following equations Eq. (2.2) and (2.3)

$$\text{EE (\%)} = \frac{Total\ amount\ of\ curcumin\ within\ nanogel\ or\ PEC}{Amount\ of\ curcumin\ taken\ for\ loading} \times 100 \qquad (2.2)$$

$$\text{LE (\%)} = \frac{Total\ amount\ of curcumin\ within\ the\ nanogel\ or\ PEC}{Yield\ of\ curcumin\ loaded\ complex} \times 100 \qquad (2.3)$$

2.2.14 *In vitro* curcumin release studies from polysaccharide-curcumin conjugates, nanogels and polyelectrolyte complex

Curcumin releases from all the conjugates, nanogels and polyelectrolyte complex were performed at two different pH (7.4 and 5) for a period of 48 h. A known amount of the sample was dissolved in 3 mL of buffer of pH 5 or pH 7.4 and transferred to dialysis membrane. The membranes were immersed in the corresponding buffer (10 mL) release medium and incubated at 37 °C. Curcumin loaded nanogels (5 mg) and polyelectrolyte complex (5 mg) were placed in buffer solution (10 mL) and incubated at 37 °C. At predetermined time intervals, 3 mL of the release medium was withdrawn from the sample and replenished with fresh buffer. Released curcumin was dissolved in 1 mL of DMSO and quantified spectrophotometrically from the standard curve for curcumin.

2.2.15 Hemocompatibility studies of nanogels and polyelectrolyte complex

Blood compatibility of bare and curcumin loaded nanogels and polyelectrolyte complex were evaluated since it is an important property of biomaterials to be used for drug delivery applications (Morris & Sharma 2010). In this work, hemolysis assay was performed to rule out the possible RBC destroying effects of nanogels and PEC. Automatic hematology analyzer (Sysmex-K 4500) was used to measure the total hemoglobin in the blood samples. Briefly, anticoagulated fresh human blood (0.9 mL) was added to samples dispersed in PBS (0.1 mL). Concentration of bare and curcumin

loaded nanogels and PEC (equivalent curcumin concentration) ranged from 3.1-50 μg/mL. PBS and 0.1 % of Na_2CO_3 were used as negative (0 % hemolysis) and positive controls (100 % hemolysis) respectively. All the samples were incubated at 37 °C for 90 min. After incubation, samples were centrifuged at 4500 rpm for 15 min to obtain the plasma. Optical density of the hemoglobin in plasma was analyzed spectrophotometrically and it was calculated by the following equation Eq. (2.4)

$$PlasmaHb = \frac{2A_{415} - (A_{380} + A_{450})] \times 1000 \times dilutionfactor}{E \times 1.655} \quad (2.4)$$

Where A_{415} denotes the Soret band based absorption of hemoglobin. A_{380} and A_{450} stand for correction factors applied for uroporphyrin absorption falling in the same wavelength range. Molar absorptivity value of oxyhemoglobin at 415 nm is represented by E and is 79.46. The dilution factor for accounting the turbidity of plasma sample is 1.655. Hemolysis % was calculated by equation Eq. (2.5)

$$Hemolysis = \frac{Plasma\ \ Hb\ value\ \ of\ \ the\ sample}{Total\ \ Hb\ value\ \ of\ blood} \times 100 \quad (2.5)$$

2.2.16 Cytotoxicity studies

Cytotoxicity analysis of galactosylated and nongalactosylated polysaccharide-curcumin conjugates was performed in HepG2 cells. Activity of GA-Cur conjugate towards HepG2 cells and MCF-7 cells was compared. Anticancer efficacy of both bare and curcumin loaded nanogels and polyelectrolyte complex was analyzed in MCF-7 cells. Human Hepatocellular Carcinoma (HepG2) cells (NCCS, Pune) and MCF-7 (Human Breast Cancer Cell line) cells were procured from National Centre for Cell Science (Pune). The cells were maintained in Eagles MEM supplemented with 2 mM glutamine, sodium bicarbonate (7.5 %), 10 % Foetal Bovine Serum (FBS) and 1 % sodium pyruvate in an incubator set at 37 °C, 5 % CO_2 and >90 % relative humidity. Cells were seeded on a 96-well plate with a density of 10000 cells/well and

incubated at 37 °C for 24 h. Equal volumes (100 μL) of all the polysaccharide-curcumin conjugates (dissolved in water and mixed with equal volume of 2X concentrated culture medium to prepare test stock solutions) and free curcumin (dissolved in DMSO and mixed with equal volume of 2X concentrated culture medium) at 5 different concentrations (1.5-25 μg/mL) were added to the subconfluent cells and incubated for a period of 24 h at 37 °C. Five different concentrations of bare and curcumin loaded nanogels and CG/Alg polyelectrolyte complex were prepared by dilution with the 2X culture medium with equivalent curcumin concentration ranging from 3.1-50 μg/mL. Cells receiving normal culture medium were considered as cell control. After 24 h, the medium was removed and the cells were washed with serum free MEM. To each well, 100 μL of MTT reagent (50 μg/mL in serum free medium) was added and incubated for 2 h. MTT reagent was replaced with 100 μL isopropanol and absorbance was read at 570 nm in a multiwell plate reader (BioTek, USA). Percentage cell activity was calculated and analyzed statistically. The half maximal inhibitory concentration (IC_{50}) was found from the dose response curve prepared using Microsoft Excel software.

2.2.17 Intracellular uptake studies

Intracellular uptake studies of all the polysaccharide-drug conjugates were performed in HepG2 cells, while it was performed in MCF-7 cells in the case of curcumin loaded nanogels and polyelectrolyte complex. Uptake studies of GA-Cur conjugate were performed both in HepG2 cells and in MCF-7 cells. Concentration of polysaccharide-curcumin conjugates was taken to contain equivalent curcumin concentration of 1.5 μg/mL, while that of curcumin loaded Alg Ald-Gel and GA Ald-Gel nanogels and CG/Alg polyelectrolyte complex was 3.1 μg/mL. $LANH_2$-Pu Ald-Cur SA, Pu-Cur SA, $LANH_2$-Alg Ald-Cur, Alg-Cur, GA-Cur and free curcumin (test samples were prepared as mentioned in the previous section) were added to HepG2 cells cultured on glass cover slips at a density of $1x10^4$ cells/cm^2 and incubated for

24 h. Density of MCF-7 cells were also similar to HepG2 cells. After 24 h, the cells were washed thrice with PBS and were fixed in 70 % ethanol. The cell nuclei were counter stained with PI. The uptake was visualized by confocal laser scanning microscope (CLSM Meta 510 Carl Ziess, Germany) under multichannel sequential scanning mode using excitation wavelengths of 405 nm and 514 nm for particles and PI respectively. Cells cultured in normal medium without particles were used to adjust the background fluorescence.

CHAPTER 3
POLYMER-DRUG CONJUGATES

This chapter outlines the design, development, characterization and biological evaluation of polysaccharide-curcumin conjugates from three polysaccharides, namely pullulan, alginate and gum arabic. Polysaccharide-drug conjugates with and without targeting group is prepared and described in detail in this chapter.

3.1 Introduction

Polymer-drug conjugates are developed to enhance the anticancer efficacy of the drugs which have short half lives in blood stream and unacceptable pharmacokinetics. Conjugation of hydrophobic low molecular weight drugs to macromolecules amplifies its distribution in the body. Consequently, the polymer-drug conjugate concept is considered to be the most promising approach for improving the cytotoxicity of the drugs in tumor tissues along with less toxicity on normal cells. The main advantages of polymer-drug conjugates are, they increase the solubility, biodistribution and therapeutic efficacy of the drug. Among different macromolecules utilized for polymer-drug conjugate development, polysaccharides gained a special attention owing to their spectacular properties. Polysaccharides such as hyaluronic acid, dextran and chitosan are already being used for the conjugation of doxorubicin, paclitaxal and curcumin (Goodarzi et al. 2013).

In the present study, polymer-drug conjugates are prepared for overcoming the limitations of anticancer natural drug, curcumin and to make it available for the delicate cells. Curcumin has low solubility and hence extremely skimpy

bioavailability. In the present study, polysaccharide-curcumin conjugates are developed to ameliorate the efficacy of curcumin by conjugating it with three different polysaccharides namely pullulan, alginate and gum arabic. Drug delivery systems with the aid of targeting groups direct the curative agents in a site-specific manner to a particular cell or tissue. Targeted drug delivery is beneficial in cancer therapy since it can direct the system only towards the tumor cells evading the healthy tissue. Targeted drug delivery can be achieved in many ways and the most important approaches are based on EPR effect and tumor receptor or antigen targeting. In the present work, polysaccharide-curcumin conjugates with and without targeting group are prepared in order to understand the difference in their efficacy in drug delivery. The first section deals with the development, characterization and biological evaluation of polysaccharide-curcumin conjugates from pullulan. Pullulan-curcumin conjuguates with and without targeting group are prepared. Even though pullulan-curcumin conjugate enhanced the solubility and stability of curcumin, it has some drawbacks. To avoid these shortcomings, another drug conjugate is prepared from alginate. The last section describes the preparation of gum arabic–curcumin conjugate, in which the polysaccharide carries targeting ligand in its structure itself.

3.2 Pullulan-curcumin conjugates with and without targeting group

Application of nanomedicine in cancer treatment paves the way to new opportunities. Polymeric nanoparticles containing drug molecules qualify several preclinical trials and are approved for clinical cancer treatment. Benefits of applying nanomedicine alternative to chemotherapy encompass enhanced water solubility, diminished clearance, reduced drug resistance and improved therapeutic efficacy. Polymer-drug conjugates; a class of polymeric nanoparticle drug delivery systems offer many beneficial properties and eliminate several bottlenecks of conventional chemotherapy.

Curcumin; a well known spice with handful of medicative properties is selected as an anticancer drug in this study. Anticancer activity of curcumin originates from its ability to interact with several cellular targets NF-kb, protein kinase C and epidermal growth factor receptor tyrosine kinase (Aggarwal & Shishodia 2006, R. Sharma et al. 2005, Tomita et al. 2006). In order to overcome the draw backs of curcumin, various nanoformulations are developed for its encapsulation and protection. The development of a polymer-curcumin conjugate provides a facile strategy to enhance the therapeutic effectiveness of curcumin (Maeda, Seymour, & Miyamoto 1992). Various biopolymers and water soluble synthetic polymers have been exploited for conjugation with curcumin. Grafting of curcumin to a hydrophilic polymer is found to increase its solubility, permeability and stability ultimately leading to the enhanced biological activity. Solubility of curcumin so far achieved in aqueous medium by conjugation with a polymer is in the range of ≤ 852 μg/mL (Dey & Sreenivasan 2014, T. H. Kim et al. 2011, S Manju & Sreenivasan 2011a). Increasing the amount of conjugated curcumin would lead to enhanced therapeutic potency towards cancer cells.

The first category of polysaccharide-drug conjugate is prepared from a highly hydrophilic polysaccharide namely, pullulan. Pullulan is a water soluble linear polysaccharide produced by aureobasidium pullulans. It is made up of α-1,6 linked maltotriose unit. Pullulan has been extensively used in pharmaceutical and biomedical fields because of its biocompatibility, biodegradability, blood compatibility and presence of suitable functional groups for further modifications (Kumar, Saini, Pandit, & Ali 2012, Prajapati, Jani, & Khanda 2013, Rekha & Sharma 2007). Biomedical applications of pullulan include tissue engineering (G.-S. Lee, Park, Shin, & Kim 2011), gene delivery (M. Gupta & Gupta 2004, Rekha & Sharma 2011), drug delivery (Kazunari Akiyoshi et al. 1998, Fundueanu, Constantin, & Ascenzi 2008, Lu et al. 2009) and as a carrier for fluorescent probes like quantum dots for diagnostic bioimaging (Bae & Na 2010). Pullulan has been modified with various hydrophobic moieties such as cholesterol (W.-z. Yang et al. 2010), diethylaminoethyl

(San Juan, Hlawaty, Chaubet, Letourneur, & Feldman 2007), maleic (H. Zhang et al. 2011) and acetyl (Na, Lee, & Bae 2004) groups for producing self assembled pullulan nanoparticles. These amphiphilic pullulan nanomaterials were used for various pharmaceutical applications such as gene delivery and drug delivery (Kazunari Akiyoshi et al. 1998, Hirakura, Nomura, Aoyama, & Akiyoshi 2004, Na & Bae 2002, Na et al. 2004).

Though pullulan has been used for preparing several drug conjugates, suitability of this highly water soluble polysaccharide for curcumin conjugation is not yet attempted. The aim of the present study is to prepare pullulan-curcumin conjugates for targeted delivery of curcumin to hepatocarcinoma cells. Targeted conjugates show enhanced efficacy when compared to nontargeted polymer drug conjugates (Scomparin et al. 2011). Target ligand containing conjugates also reduce toxicity towards normal cells. Hence, we designed pullulan-curcumin conjugates with and without targeting ligand (galactosyl group) to compare the enhancement in cytotoxicity offered by the targeting group. Hepatocytes bear asialoglycoprotein receptor (ASGPR), which has been validated as a potential target for selective drug delivery to the liver cells. Galactosylated conjugates have already been used for the targeted drug delivery to hepatocarcinoma cells *via* asialoglycoprotein mediated endocytosis (Duan et al. 2011, Zheng et al. 2012, Zhou et al. 2013). Hepatic receptive ligands used for targeted drug delivery include neogalactosyllipid (Haensler & Schuber 1988), mannose, fructose (Scomparin et al. 2011) and lactose (Hayashi et al. 2012, M. Zhang et al. 2013). Galactose-terminal molecules are recognized selectively by ASGPR present on the sinusoidal surface of the hepatocytes and transport them to lysosomes inside the liver cell (Yan Li, Huang, Diakur, & Wiebe 2008). In this study, galactose moiety has been attached to pullulan for augmented accumulation of curcumin in hepatocytes and for elevated cytotoxicity.

Pullulan is made up of maltotriose units and it doesn't have acid functional groups for curcumin conjugation. Hence, in the present work, curcumin is initially

modified with succinic anhydride to introduce carboxylic acid functionality required for conjugation to pullulan. In order to prepare conjugate without targeting group (Pu-Cur SA), modified curcumin (Cur-SA) is directly conjugated to $–CH_2OH$ group of pullulan. The development of conjugate with targeting group ($LANH_2$-Pu Ald-Cur SA) involves several steps that include oxidation of pullulan, modification of the targeting ligand, grafting of the modified targeting ligand to pullulan aldehyde and finally conjugation of modified curcumin to pullulan. Both conjugates could self assemble to micelle in water with spherical morphology and showed enhancement in stability of curcumin in physiological pH. Compared to Pu-Cur SA, $LANH_2$-Pu Ald-Cur SA exhibits higher toxicity and internalization towards HepG2 cells. This indicates the enhanced uptake of $LANH_2$-Pu Ald-Cur SA conjugate *via* ASGPR mediated endocytosis into HepG2 cells.

3.2.1 Results and discussions

3.2.1.1 Preparation and characterization of galactosylated and nongalactosylated pullulan-curcumin conjugates

The main limitation that restricts curcumin's use as a potent anticancer agent is its low bioavailability due to the low solubility and instability in physiological pH. Conjugation of curcumin to a highly water soluble polymer may increase its solubility (Dey & Sreenivasan 2014, S Manju & Sreenivasan 2011a) to an extent. In this study, pullulan is selected for the preparation of drug conjugate, because of its high hydrophilicity. Grafting of curcumin to a hydrophilic polymer endows salient features such as easy dispersibility in aqueous medium, significantly higher stability in physiological pH and enhanced intracellular uptake leading to improved therapeutic efficacy as already mentioned. Zhang et al reported the synthesis of folate-decorated maleilated pullulan–doxorubicin conjugate which is effective in ovarian carcinoma A2780 cells than free doxorubicin (Scomparin et al. 2011, H. Zhang et al. 2011).

Amphiphilic pullulan conjugates with pH sensitivity have also been reported for the delivery of doxorubicin (Lu et al. 2009).

In the present study, galactosylated pullulan-curcumin conjugate **(**$LANH_2$-Pu Ald-Cur SA) is prepared for hepatocyte targeted delivery of curcumin. Non galactosylated conjugate (Pu-Cur SA) is also prepared to compare the toxicity towards HepG2 cells. Steps involved in the preparation of $LANH_2$-Pu Ald-Cur SA and Pu-Cur SA are given below. In the first step of the preparation of $LANH_2$-Pu Ald-Cur SA, vicinal diols present in pullulan are oxidized to introduce aldehyde functionality (Scheme 3.1).

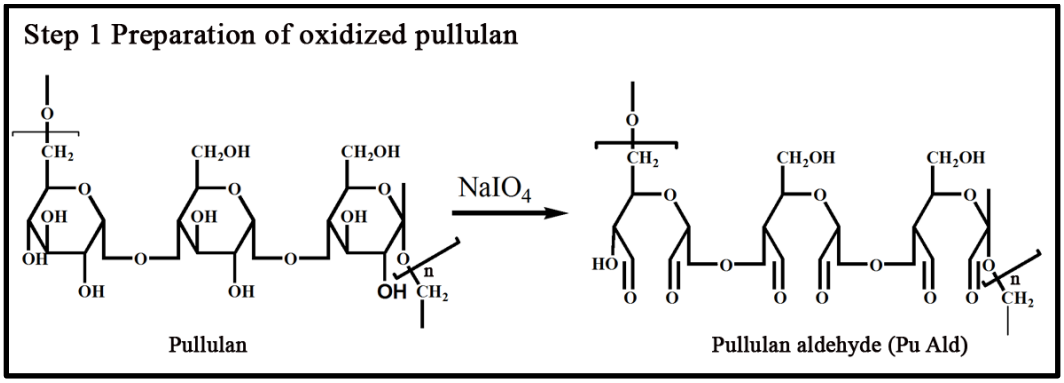

Scheme 3.1 Preparation of pullulan aldehyde by the oxidation of pullulan using sodium periodate

The presence of aldehyde in oxidized pullulan (Pu Ald) is confirmed by FT-IR spectroscopy (Figure 3.1). A characteristic aldehyde peak is seen at 1747 cm^{-1} in the spectrum of pullulan aldehyde (Figure 3.1b) which is absent in the spectrum of pullulan (Figure 3.1a).

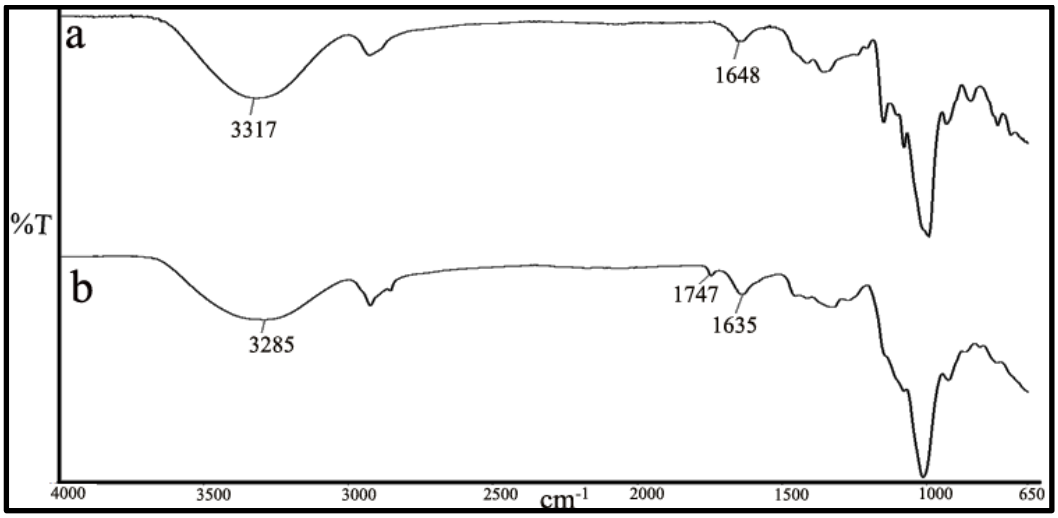

Figure 3.1 FT-IR spectra of pullulan (a) and pullulan aldehyde (b)

Amount of aldehyde produced after oxidation (50 %) is estimated by tirtimetry and is found to be 7.4×10^{-3} mol/g. Aldehyde content will decrease with decrease in percentage of oxidation. Oxidized pullulan (10 % and 20 %) contains 3×10^{-3} mol/g and 5×10^{-3} mol/g of aldehydes respectively. In order to get maximum number of aldehyde groups for $LANH_2$ conjugation, pullulan with 50 % oxidation is selected for further studies.

In this work, galactose containing lactobionic acid (LA) is selected as the targeting ligand. Lactobionic acid can be directly attached to the hydroxyl groups of pullulan without any modification. If LA is attached to pullulan in this way, there is a possibility of steric hindrance during Cur SA conjugation. In order to avoid steric hindrance, LA is modified to $LANH_2$ and conjugated to pullulan aldehyde. Hence the second step in the conjugate preparation is modification of LA (Scheme 3.2). LA is modified with ethylenediamine (EA) to introduce amino groups required for Schiff's base reaction with pullulan aldehyde (Pu Ald).

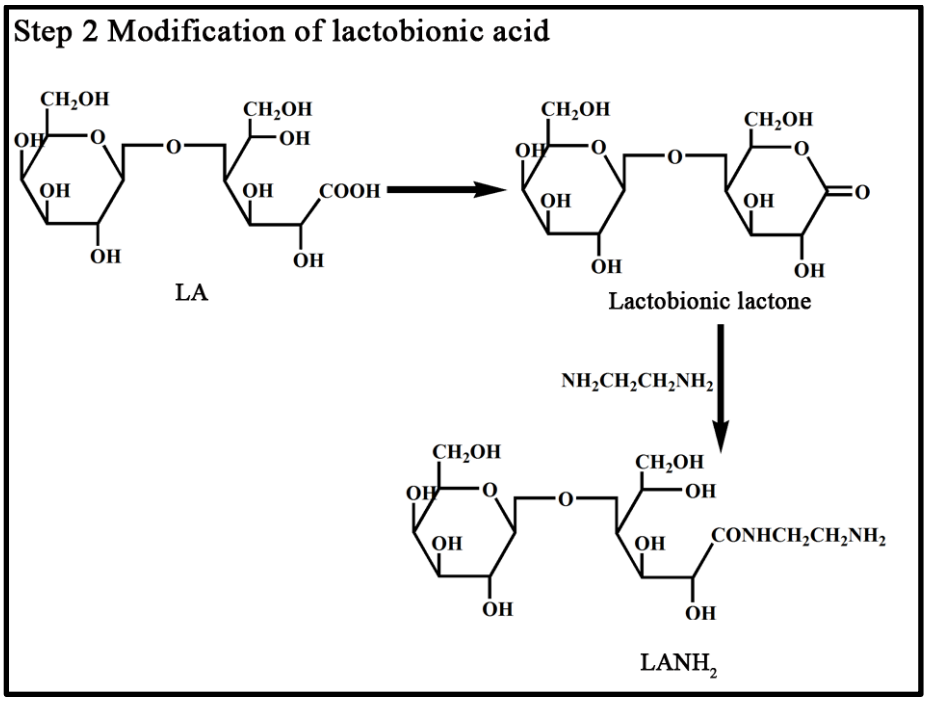

Scheme 3.2 Modification of LA with ethylenediamine

Modified lactobionic acid is characterized by FT-IR spectroscopy (Figure 3.2).

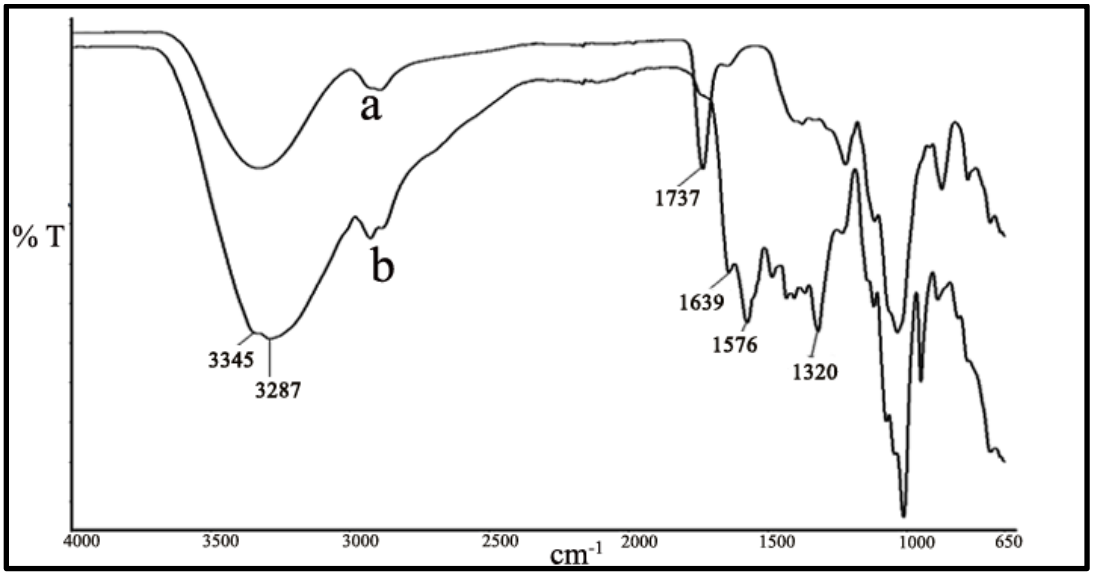

Figure 3.2 FT-IR spectra of LA (a) and $LANH_2$ (b)

In the FT-IR spectrum of lactobionic acid, (Figure 3.2a) gluconic acid carbonyl peak is seen at 1737 cm^{-1} and it is vanished in the spectrum of $LANH_2$. Besides, new amide I and amide II bands at 1639 cm^{-1} and 1574 cm^{-1} respectively are observed in the IR spectrum of $LANH_2$ (Figure 3.2b) indicating the successful conversion of LA to $LANH_2$. Additionally, peaks at 3345 cm^{-1} and 3287 cm^{-1} correspond to –OH stretching and –NH stretching of primary amine respectively.

Chemical shift values in ^{13}C NMR spectrum are similar for $LANH_2$ (Figure 3.3b) and LA (Figure 3.3a) except the peaks seen at 39–41 ppm in the spectrum of $LANH_2$, corresponding to the -CH_2 groups introduced as a result of reaction with EA.

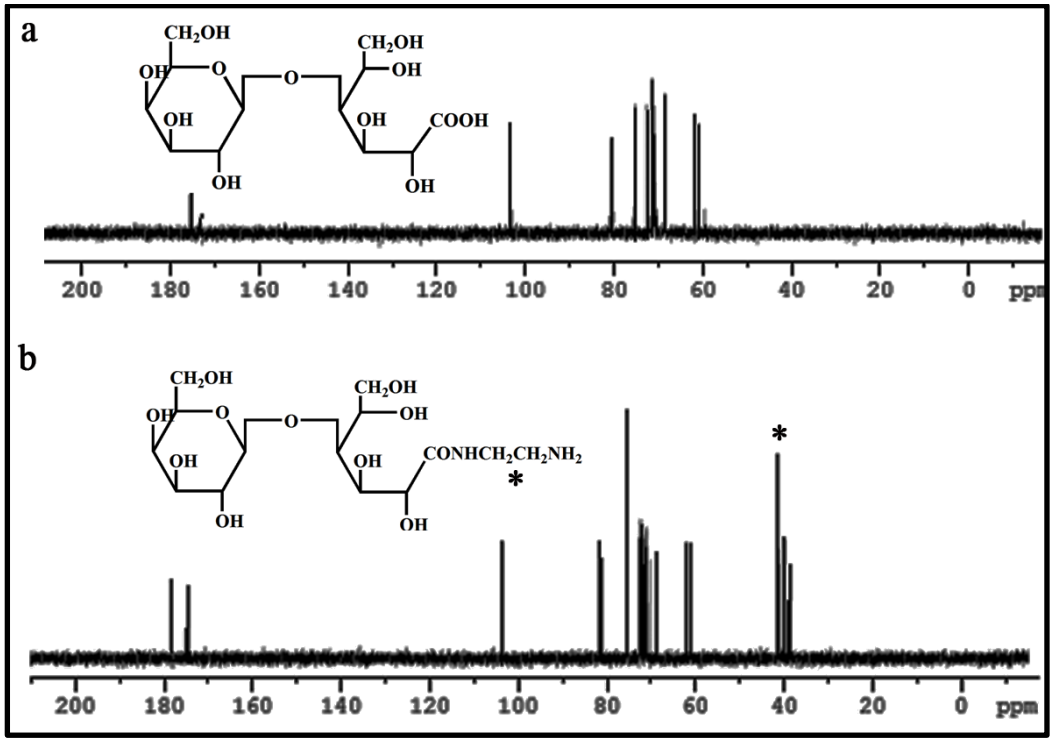

Figure 3.3 ^{13}C NMR spectra of LA (a) and $LANH_2$ (b)

Followed by the modification, $LANH_2$ is attached to Pu Ald by Schiff's base reaction between aldehyde and amino groups of Pu Ald and $LANH_2$ respectively (Scheme 3.3). The Schiff's base, $LANH_2$-Pu Ald is stable at neutral pH, while it will

break at acidic pH leading to the rupture of the micelle and enhanced curcumin release.

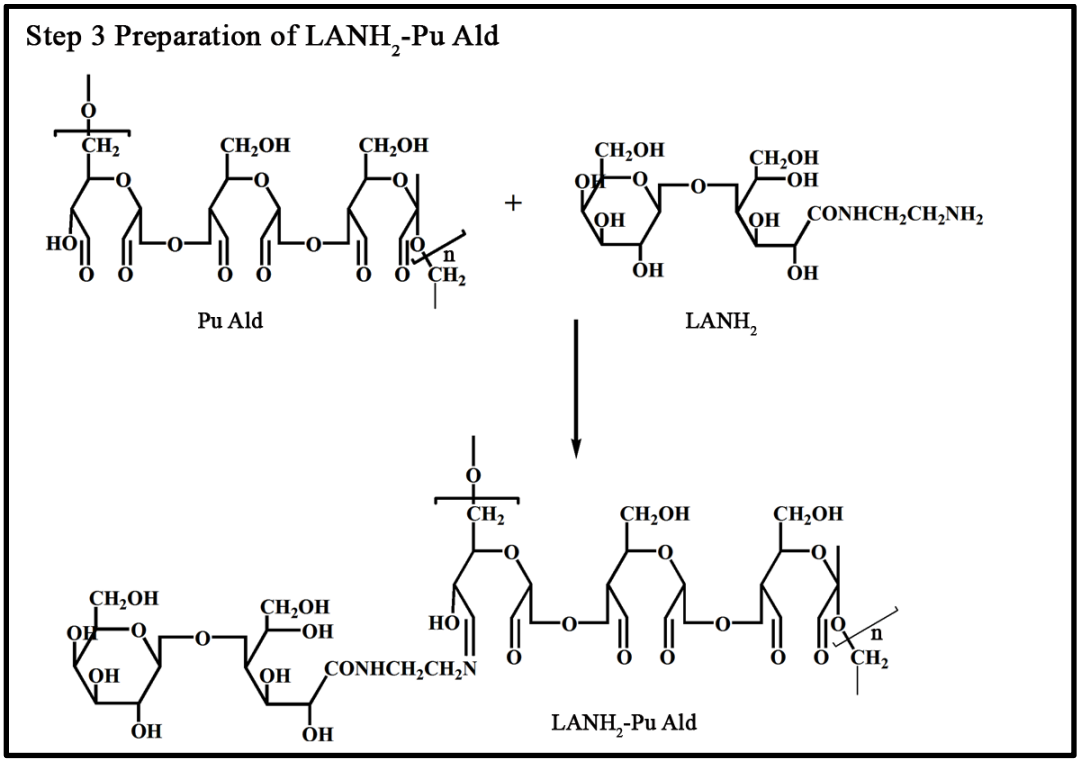

Scheme 3.3 Preparation of $LANH_2$-Pu Ald by Schiff's base reaction between $LANH_2$ and Pu Ald

Conjugation of $LANH_2$ to Pu Ald (galactosylation) is confirmed by CHN elemental analysis. Galactosylation resulted in an increase of 5.8 % in nitrogen content. Percentage of aldehyde groups remaining in Pu Ald after $LANH_2$ conjugation is also calculated by titrimetry. It is found that 40 % of the aldehyde groups are reacted with $LANH_2$. FT-IR spectrum of $LANH_2$-Pu Ald (Figure 3.5b) also indicates successful conjugation of $LANH_2$ to Pu Ald. Aldehyde peak at 1747 cm^{-1} of pullulan aldehyde is not observed in the IR spectrum of $LANH_2$-Pu Ald (Figure 3.5b), indicating the reaction between pullulan aldehyde and $LANH_2$.

Phenolic hydroxyl group of the curcumin is modified with succinic anhydride (SA) to introduce acid functional groups facilitating the conjugation of curcumin to pullulan. Synthetic route for this modification is given below (Scheme 3.4).

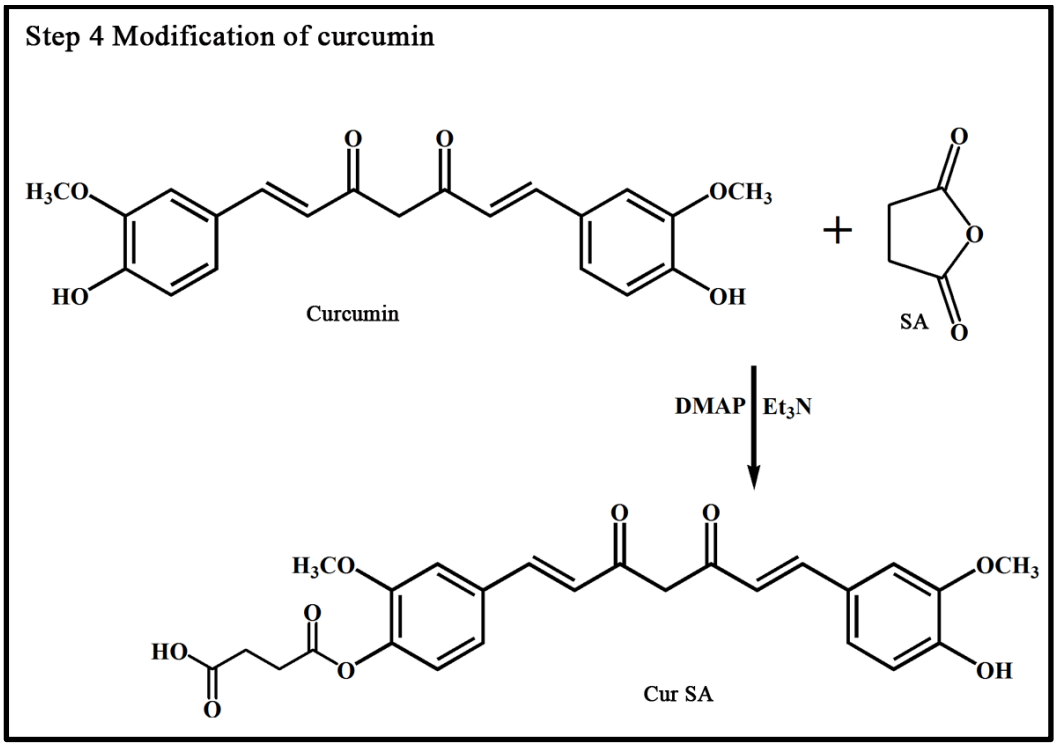

Scheme 3.4 Modification of curcumin with succinic anhydride

FT-IR spectra of curcumin (Figure 3.4a) and modified curcumin (Cur SA, Figure 3.4b) are shown in Figure. 3.4. The spectrum of curcumin (Figure. 3.4a) shows –OH peak at 3511 cm^{-1} which is broadened after modification, due to the introduction of acid hydroxyl group. In addition to this, new acid and ester carbonyl peaks are observed at 1768 cm^{-1} and 1708 cm^{-1} respectively.

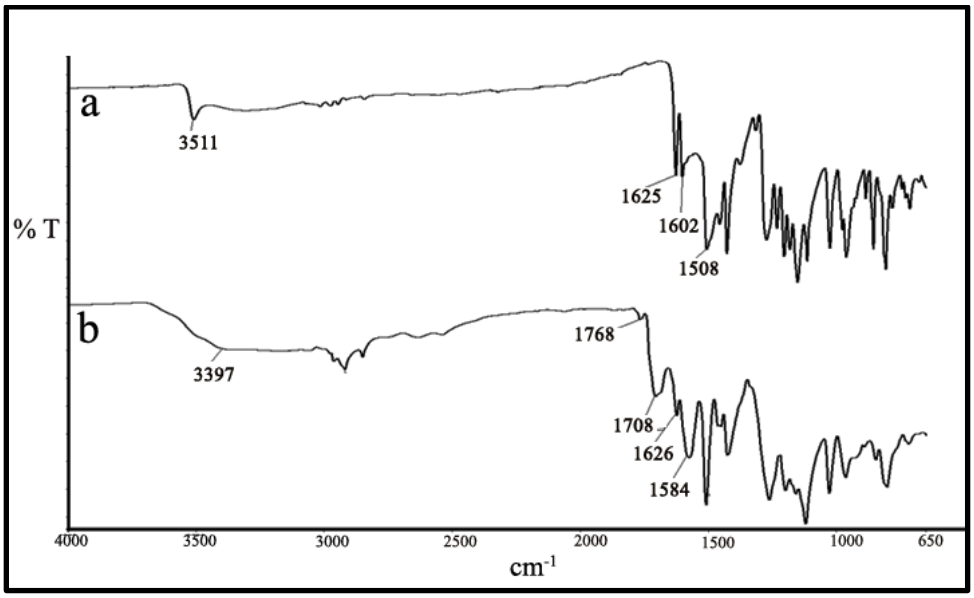

Figure 3.4 FT-IR spectra of curcumin (a) and Cur SA (b)

In the final step, Cur SA is conjugated to galactosylated pullulan ($LANH_2$-Pu Ald) by DCC/DMAP coupling reaction (Scheme 3.5).

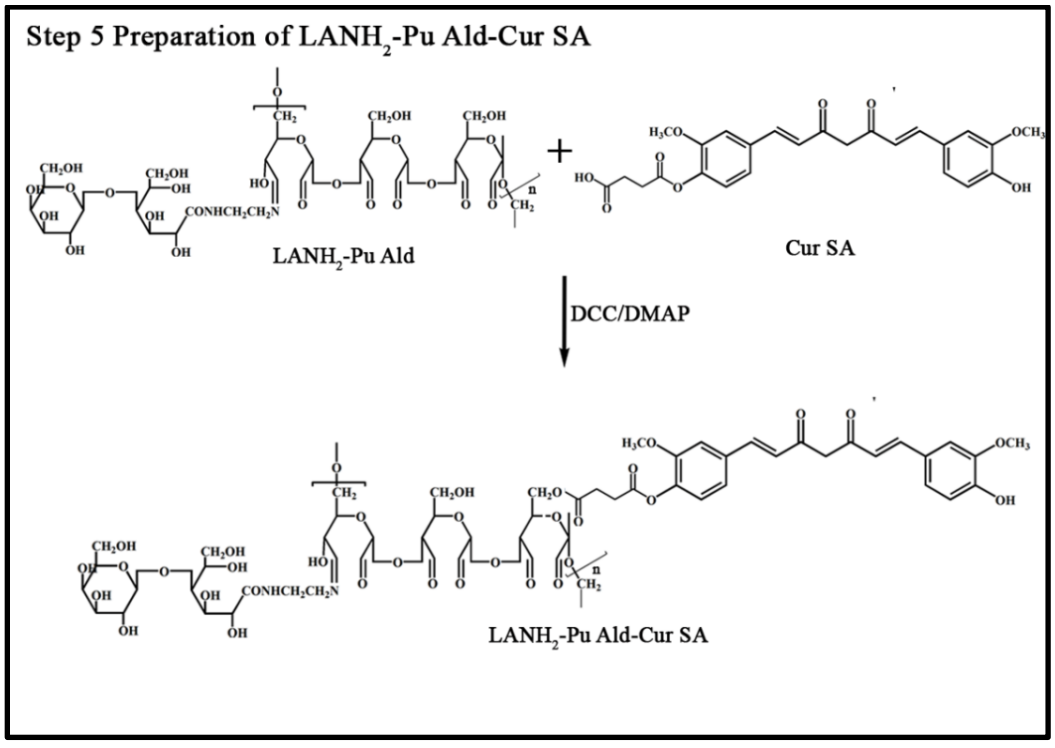

Scheme 3.5 Preparation of $LANH_2$-Pu Ald-Cur SA

Modified curcumin is directly conjugated to pullulan by DCC/DMAP coupling reaction through an ester linkage to prepare nongalactosylated pullulan-curcumin conjugate (Pu-Cur SA, Scheme 3.6).

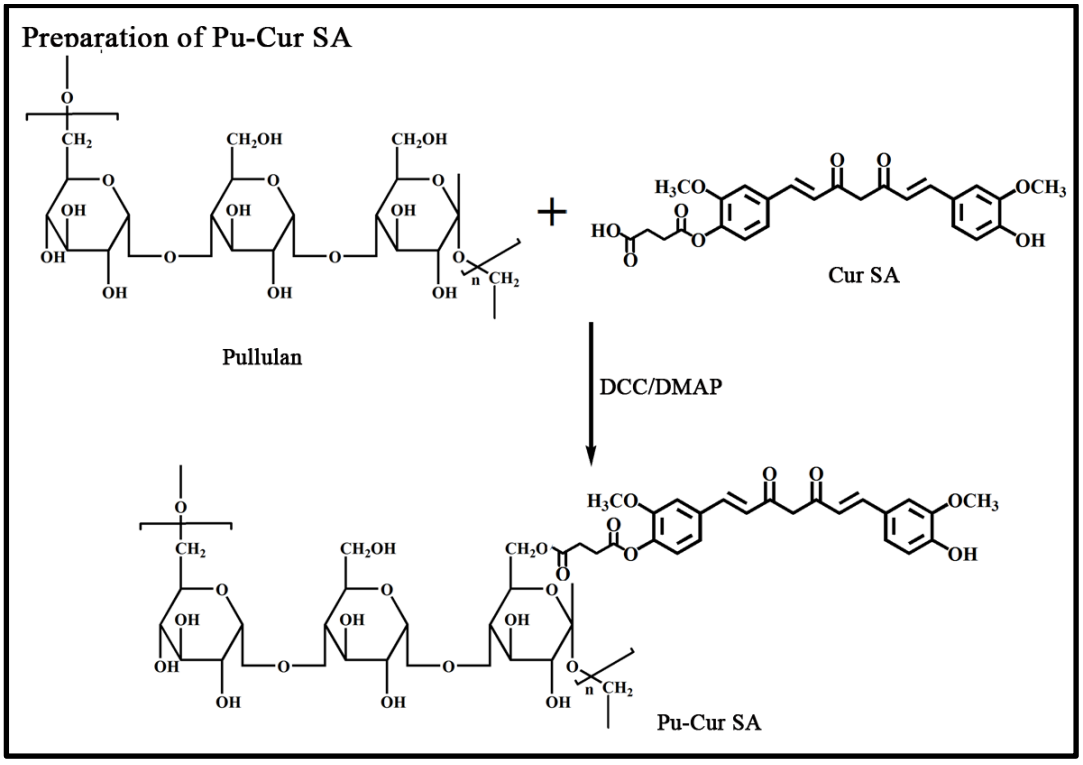

Scheme 3.6 Preparation of Pu-Cur SA

Figure 3.5 represents IR spectra of Pu-Cur SA, $LANH_2$-Pu Ald and $LANH_2$-Pu Ald-Cur SA. In the FT-IR spectrum of Pu-Cur SA (Figure 3.5a), the peak at 1747 cm^{-1} corresponds to the ester carbonyl bond formed between acid groups of Cur SA and hydroxyl group of pullulan. Peaks at 1654 and 1628 cm^{-1} correspond to keto (-C=O) stretching of curcumin. Peaks at 1515 and 1581 cm^{-1} correspond to C-C stretching of aromatic ring of Cur SA in Pu-Cur SA. Figure 3.5c represents IR spectrum of $LANH_2$-Pu Ald-Cur SA and the peak at 1739 cm^{-1} corresponds to the ester carbonyl formed between Cur SA and $LANH_2$-Pu Ald. Peak at 1629 and 1579 cm^{-1} correspond to keto -C=O stretching of curcumin. Curcumin conjugation is again proved by the presence of C-C stretching of aromatic ring at 1513 cm^{-1}.

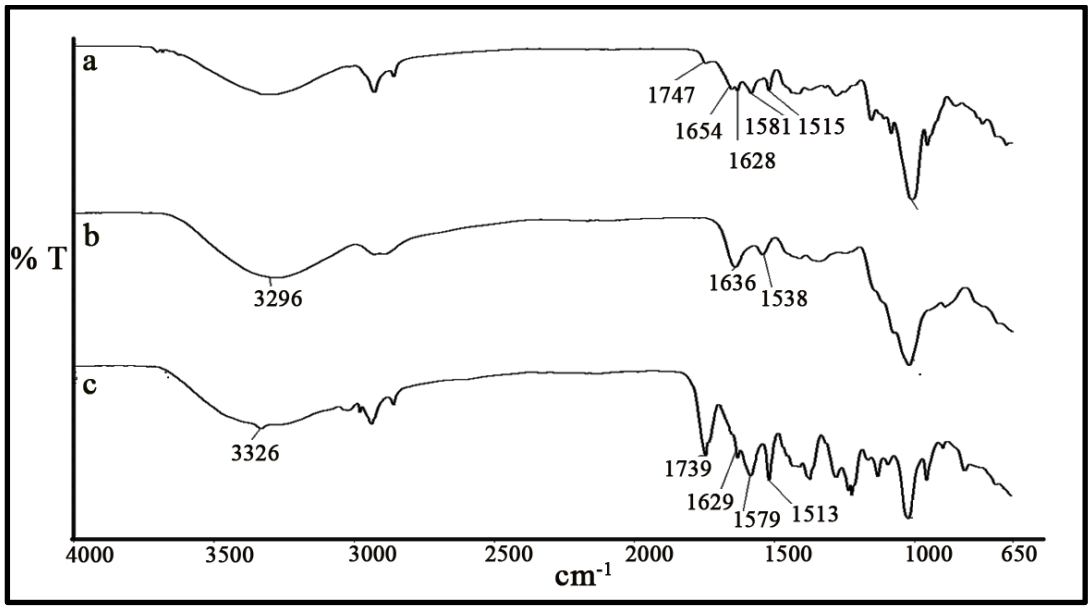

Figure 3.5 FT-IR spectra of Pu-Cur SA (a), $LANH_2$-Pu Ald (b) and $LANH_2$-Pu Ald-Cur SA (c)

Molecular weights (Mn) of pullulan, Pu-Cur SA and $LANH_2$-Pu Ald-Cur SA are measured using GPC analysis and found to be 47849, 38919 and 29000 Da respectively. The reduction in molecular weight of pullulan after the modification can be due to chain cleavages occurred during the reaction.

^1H NMR spectra of curcumin, Pu-Cur SA and $LANH_2$-Pu Ald-Cur SA are shown in Figure 3.6. In the spectrum of $LANH_2$-Pu Ald–Cur SA (Figure 3.6c), characteristic curcumin (Figure 3.6a) peak is seen in the region between 6.5–8 ppm. In addition to that, distinctive singlet $–CH_2$ proton peak of succinic group is seen at 2 and 2.5 ppm. In the spectrum of Pu–Cur SA (Figure 3.6b) also, characteristic $-CH_2$ protons of succinyl group and curcumin peaks are present.

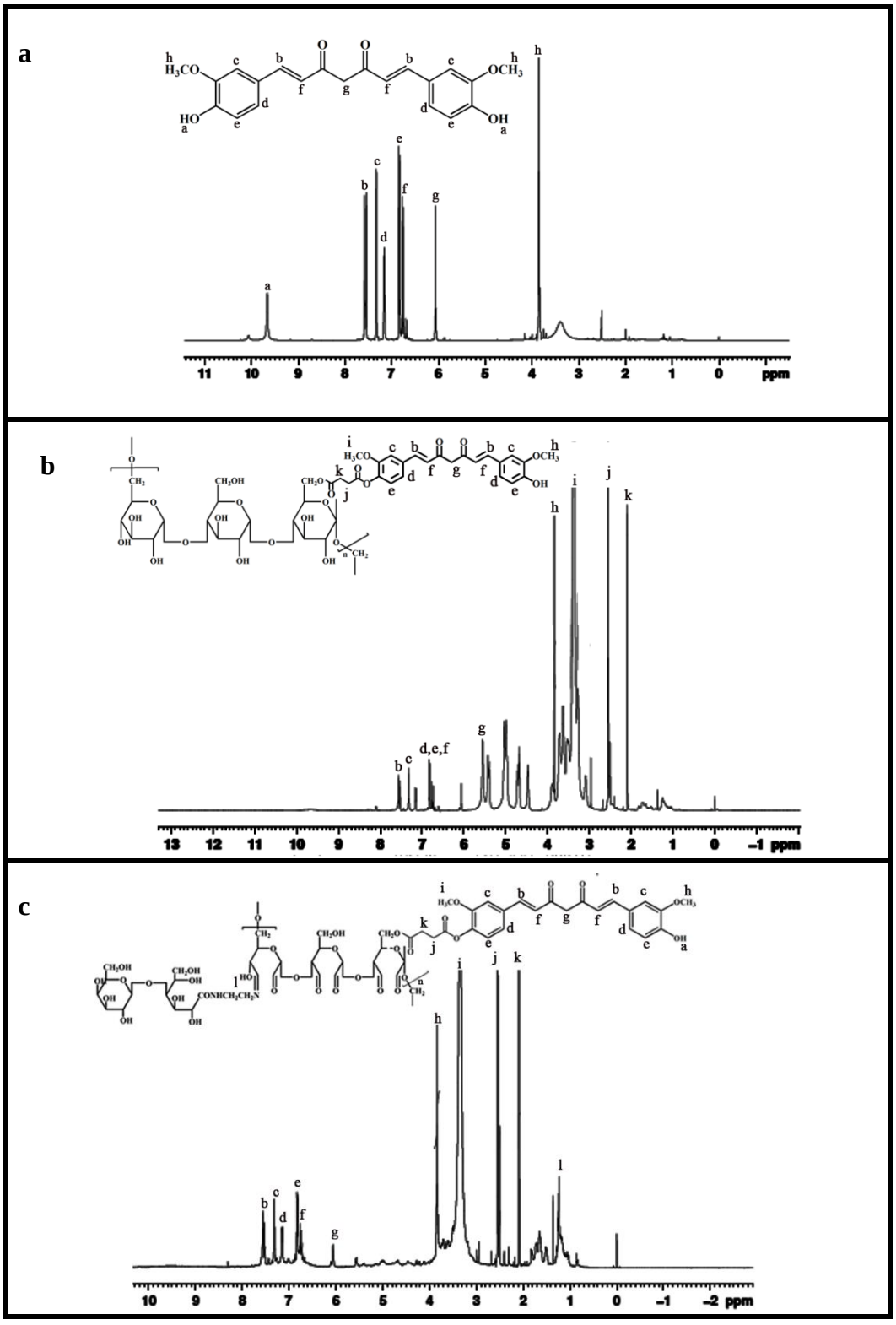

Figure 3.6 ^{1}H NMR spectra of curcumin (a), Pu-Cur SA (b) and $LANH_2$-Pu Ald-Cur SA (c)

Self assembled nano micelle formation of amphiphilic polymers have been reported in the literature (Endres, Beck-Broichsitter, Samsonova, Renette, & Kissel 2011, Guo et al. 2013, S. H. Lee, Mok, Lee, & Park 2011). Amphiphilic $LANH_2$-Pu Ald-Cur SA and Pu-Cur SA prepared in the present study, readily form micelle with hydrophobic core, resulting from the aquaphobic union of curcumin and hydrophilic shell of pullulan. Because of the hydrophobic and hydrophilic interactions, these polymer drug conjugates can easily self assemble into micelle in aqueous environment. $LANH_2$-Pu Ald-Cur SA and Pu-Cur SA conjugate micelle exhibit unimodal distribution with hydrodynamic diameter in the range of 355 ± 9 nm and 363 ± 10 nm respectively. The size of the micelle plays a vital role in the accumulation of conjugates in tumor cells. Tumor vasculature cut off determines the diffusion and accumulation of nanoparticles inside the tumor and it varies between tumors. Normally, the vasculature cut off is in the range of 200-800 nm. Therefore polymer-drug conjugate with small size can easily enter into the tumor through enhanced permeability and retention (EPR) effect.

Scanning electron microscopy is performed to investigate the morphology and nanosize of the conjugates. In the representative SEM images, Pu-Cur SA (Figure 3.7a) and $LANH_2$-Pu Ald-Cur SA (Figure 3.7b) conjugates show size in the range of 320 ± 10 nm and 290 ± 16 nm respectively with spherical morphology. This is not in agreement with the size obtained from DLS measurements. However, the difference in size observed in these two techniques is owing to the changes occurred during processing. DLS measurement is performed in aqueous medium, thus the size obtained is the hydrodynamic diameter and it is higher than that of the size measured by SEM. The zeta potential of Pu-Cur SA is -15 mV and in $LANH_2$-Pu Ald-Cur SA, it is reduced to -10 mV. The negative zeta potential must have originated from the presence of unreacted succinic acid groups on the conjugated curcumin molecules of which, both the phenolic hydroxyl groups reacted with succinic anhydride. The residual negative charge of the system also indicates the absence of cross-linking reaction between Pu and Cur SA.

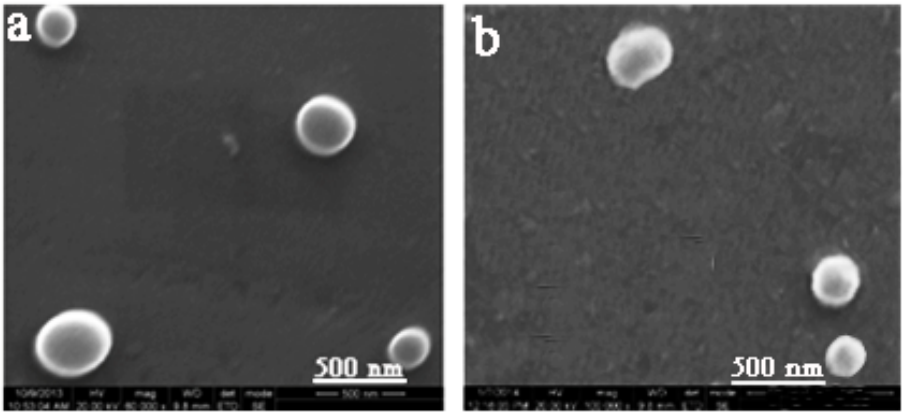

Figure 3.7 SEM images of Pu-Cur SA (a) and $LANH_2$-Pu Ald-Cur SA (b)

Self assembly of $LANH_2$-Pu Ald-Cur SA and Pu-Cur SA is again confirmed by analyzing CMC using fluorescent probe pyrene. Fluorescence characteristics of pyrene depend on the properties of the solubilising medium and it exhibits different fluorescence behavior in micellar and nonmicellar solutions. Pyrene is hydrophobic and shows less fluorescence emission below CMC of micelle. $LANH_2$-Pu Ald-Cur SA and Pu-Cur SA form micelles in aqueous medium and pyrene prefers to occupy the inner hydrophobic core of these micelles leading to alterations in emission pattern of the conjugate. Pyrene's intensity ratio between the first peak (373 nm) and the third peak (384 nm) depends on the polarity of the medium (Yinsong, Lingrong, Jian, & Zhang 2007). Intensity ratio I_{373}/I_{384} is decreased with increase in conjugate concentration and is plotted against logarithm of Pu-Cur SA (Figure 3.8), $LANH_2$-Pu Ald-Cur SA (Figure 3.9) conjugate concentration. CMC is achieved from the cross-over point in the low concentration region. From the plot of intensity ratios (I_{373}/ I_{384}), the CMC values of $LANH_2$-Pu Ald-Cur SA and Pu-Cur SA are estimated to be 0.027 mg/mL and 0.031 mg/mL respectively. Low CMC values are beneficial for prolonged circulation time and tumor targeting (C. Yu et al. 2013).

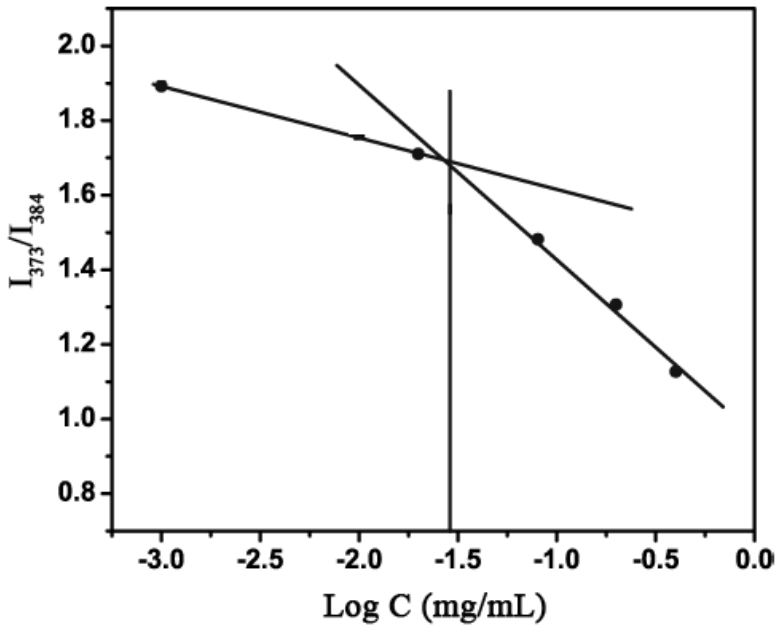

Figure 3.8 Plot of intensity ratio I_{373}/I_{384} of pyrene as a function of logarithm of concentration of Pu-Cur SA

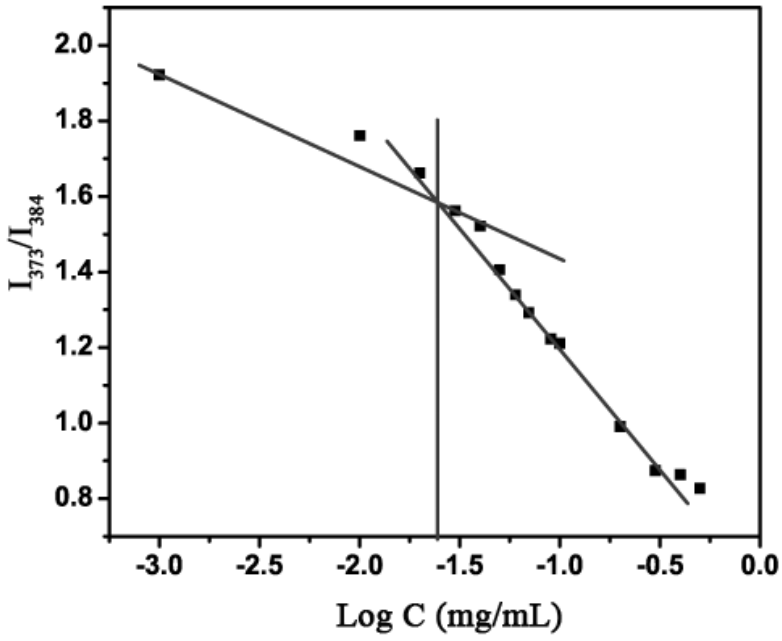

Figure 3.9 Plot of intensity ratio I_{373}/I_{384} of pyrene as a function of logarithm of concentration of $LANH_2$-Pu Ald-Cur SA

Changes occurred in the fluorescent properties of curcumin after conjugating to $LANH_2$-Pu Ald and pullulan is monitored by fluorescence emission spectroscopy. A red shift of 53 nm and 40 nm are observed in the emission spectrum of $LANH_2$-Pu Ald-Cur SA (Figure 3.10c) and Pu-Cur SA (Figure 3.10b) conjugate respectively compared to pure curcumin (Figure 3.10a). The red shift demonstrates the successful conjugation of curcumin to $LANH_2$-Pu Ald and pullulan (S Manju & Sreenivasan 2011a).

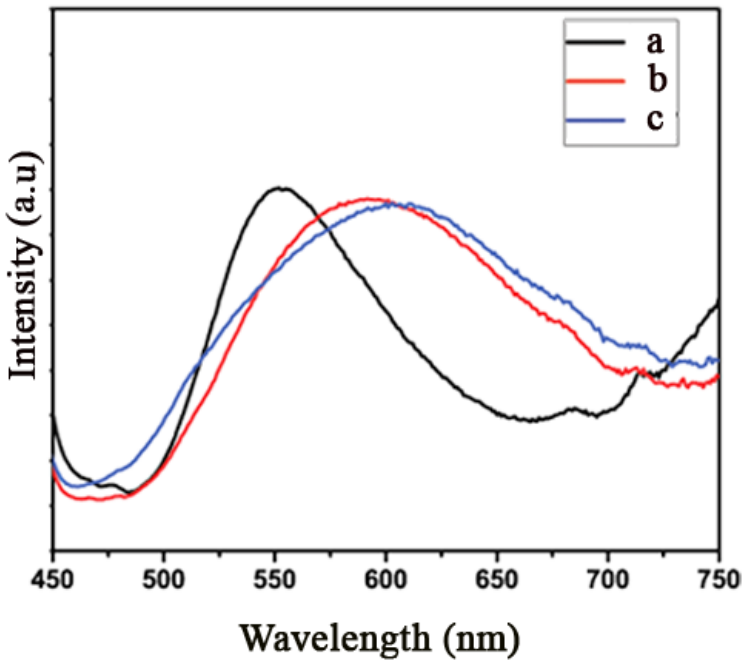

Figure 3.10 Emission spectra of curcumin (a), Pu-Cur SA (b) and $LANH_2$-Pu Ald-Cur SA (c)

The main disadvantage that restricts curcumin's use as an anticancer drug is its less solubility in aqueous medium. Bare curcumin displays an aqueous solubility of 2.792 μg/mL (S Manju & Sreenivasan 2011a, Thomsen et al. 2011) and it is deficient to provide anticancer activity. To improve the solubility, curcumin is conjugated to $LANH_2$-Pu Ald and pullulan. The amount of curcumin present in the conjugates are estimated from the standard curcumin curve and found that 1 mg of the $LANH_2$-Pu Ald-Cur SA and Pu-Cur SA conjugate contain 22 μg and 35 μg of curcumin respectively. More than 25 mg of both of the conjugates could be

solubilised in 1 mL of water. Thus, 550 μg/mL of curcumin could be solubilised in the case of $LANH_2$-Pu Ald-Cur SA which corresponds to 200-fold increase in the solubility of curcumin. With Pu-Cur SA, 875 μg/mL of curcumin could be solubilised giving rise to 314-fold increase in solubility. Thus, significantly higher solubility than that of bare curcumin is achieved by conjugating it to $LANH_2$-Pu Ald and pullulan.

3.2.1.2 Stability studies of $LANH_2$-Pu Ald-Cur SA and Pu-Cur SA conjugates

The main aim of conjugation of curcumin to hydrophilic polysaccharide is to increase its stability in physiological pH. Curcumin (Figure 3.11c) undergoes complete degradation and metabolism under these conditions within 30 min (S Manju & Sreenivasan 2011a). The changes occurred in stability of curcumin after conjugation to pullulan is evaluated by monitoring the reduction in absorbance of $LANH_2$-Pu Ald-Cur SA (Figure 3.10b) and Pu-Cur SA (Figure 3.10a) dissolved in PBS of physiological pH. The increment in stability after conjugation is owing to the micellar structure, since it is present in the inner corona of the micelle which is protected from outer hydrophilic acquaintance. Only a slight change in the absorbance is observed even after 5 h of incubation at 37 °C in PBS (pH 7.4), while free curcumin degraded completely within 30 min under the same condition. It has been reported that grafting of curcumin to polysaccharides through esterification can increase its stability to a great extent (Wichitnithad, Nimmannit, Callery, & Rojsitthisak 2011, R. Yang et al. 2012).

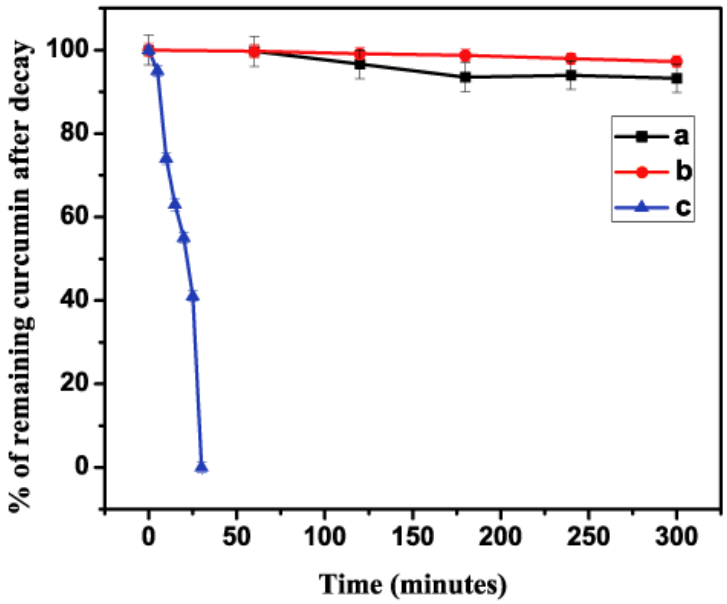

Figure 3.11 Stability studies of Pu-Cur SA (a), $LANH_2$-Pu Ald-Cur SA (b) and free curcumin (c) in PBS at 37 °C. Data shown are mean value±standard deviation (SD) (n=3, ∗$p<0.05$). There is no statistically significant difference between the absorbance obtained over the entire time period in $LANH_2$-Pu Ald-Cur SA and Pu-Cur SA

3.2.1.3 *In vitro* curcumin release studies

In vitro release of curcumin is examined at pH 5 and 7.4 for 48 h. Curcumin release pattern of $LANH_2$-Pu Ald-Cur SA and Pu-Cur SA are shown in Figure 3.12. The release of curcumin from the conjugates is higher at acidic pH and is relatively slower at pH 7.4. The faster release of curcumin at acidic pH is attributed to the easy breakage of ester linkages at this pH. In $LANH_2$-Pu Ald-Cur SA, the Schiff's base formed between $LANH_2$ and Pu Ald is sensitive to acidic pH (Xin & Yuan 2012) leading to the fastest curcumin release among the conditions studied. It can also be seen that at both pH, compared to the release pattern of Pu-Cur SA, $LANH_2$-Pu Ald-Cur SA shows higher curcumin release. This is attributed to the greater extent of rupture of $LANH_2$-Pu Ald-Cur SA conjugate due to the presence of more hydrolysable groups as explained above.

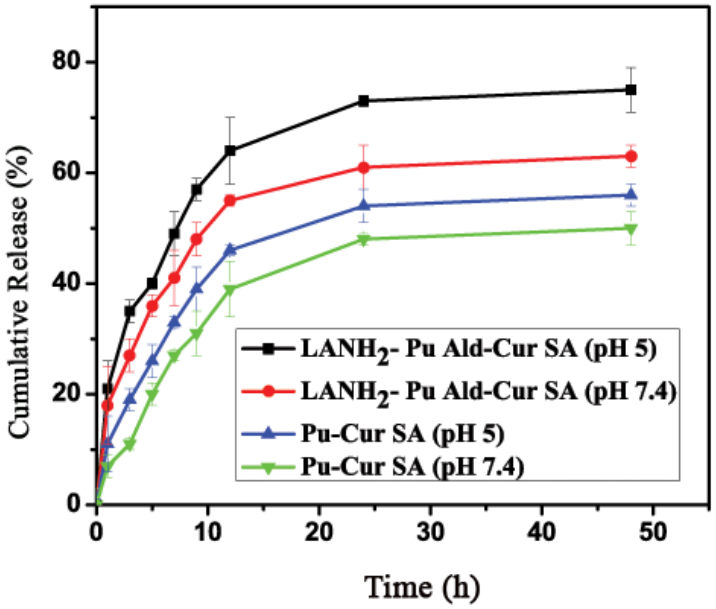

Figure 3.12 *In vitro* curcumin release patterns from $LANH_2$-Pu Ald-Cur SA and Pu-Cur SA at pH 5 and 7.4

3.2.1.4 Cytotoxicity studies

The cytotoxicity of galactosylated and nongalactosylated pullulan curcumin conjugate in HepG2 cells is compared by MTT assay (Figure 3.13). HepG2 cells are exposed to both conjugates and curcumin at different equivalent curcumin concentrations varying from 1.5 to 25 μg/mL for 24 h. The toxicity of the conjugate is found to be dose dependant. It can also be observed that, at all the tested concentrations, $LANH_2$-Pu Ald-Cur SA shows elevated toxicity to HepG2 cells compared to Pu-Cur SA. IC_{50} value of Pu-Cur SA conjugate is 11.7 μg/mL which is significantly greater than IC_{50} value of free curcumin (5.6 μg/mL). Since curcumin is dissolved in DMSO, its bioavailability to cells are more and might have reached the cells by endocytosis. It can be seen that the anticancer activity of pullulan-curcumin conjugate has been enhanced significantly after galactosylation. This might have resulted from the increased uptake of $LANH_2$-Pu Ald-Cur SA *via* ASGPR mediated endocytosis (Craparo, Triolo, Pitarresi, Giammona, & Cavallaro 2013, R. Yang et al.

2011). IC_{50} values are decreased to 4.8 μg/mL after galactosylation and it is lower than that of IC_{50} of free curcumin. Toxicity analysis of $LANH_2$-Pu Ald is also provided to prove the activity of conjugated curcumin. $LANH_2$-Pu Ald is nontoxic to HepG2 cells in all the equivalent concentrations. These results demonstrate that at a same equivalent curcumin dose range, $LANH_2$-Pu Ald-Cur SA conjugate is more effective than that of the nongalactosylated Pu-Cur SA and proves the ability of galactose moiety to induce elevated toxicity to HepG2 cells.

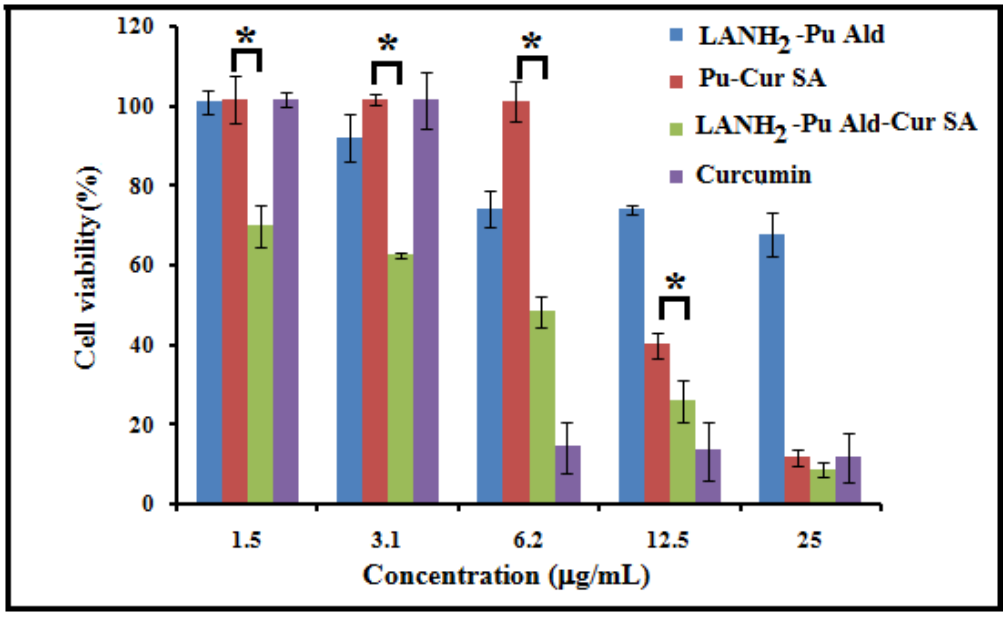

Figure 3.13 Cytotoxicity analysis of Pu-Cur SA, $LANH_2$-Pu Ald, $LANH_2$-Pu Ald-Cur SA and free curcumin. $LANH_2$-Pu Ald-Cur SA conjugate shows enhanced toxicity to HepG2 cells than Pu-Cur SA. Data shown are mean value ± SD (n =3, $*p < 0.05$)

3.2.1.5 Intracellular uptake studies

Cell uptake of $LANH_2$-Pu Ald-Cur SA and Pu-Cur SA is performed in HepG2 for a period of 24 h to evaluate the role of the ASGPR in internalization. The green fluorescence properties of curcumin allow qualitative analysis of biodistribution of the conjugates in HepG2 by confocal laser scanning microscopy (CLSM). Images of uptake studies of conjugates and free curcumin are shown in Figure 3.14. The

fluorescent intensity of curcumin is very less in HepG2 (Figure 3.14, row 1) compared to Pu-Cur SA (Figure 3.14, row 2) and $LANH_2$-Pu Ald-Cur SA (Figure 3.14, row 3). Low fluorescence intensity of curcumin can be due to its rapid metabolism in HepG2 cells. As expected, $LANH_2$-Pu Ald-Cur SA conjugate exhibits stronger fluorescence intensity in HepG2 cells than Pu-Cur SA. Thus galactosylation enhances cellular internalization and accumulation in HepG2 *via* ASGPR mediated pathway.

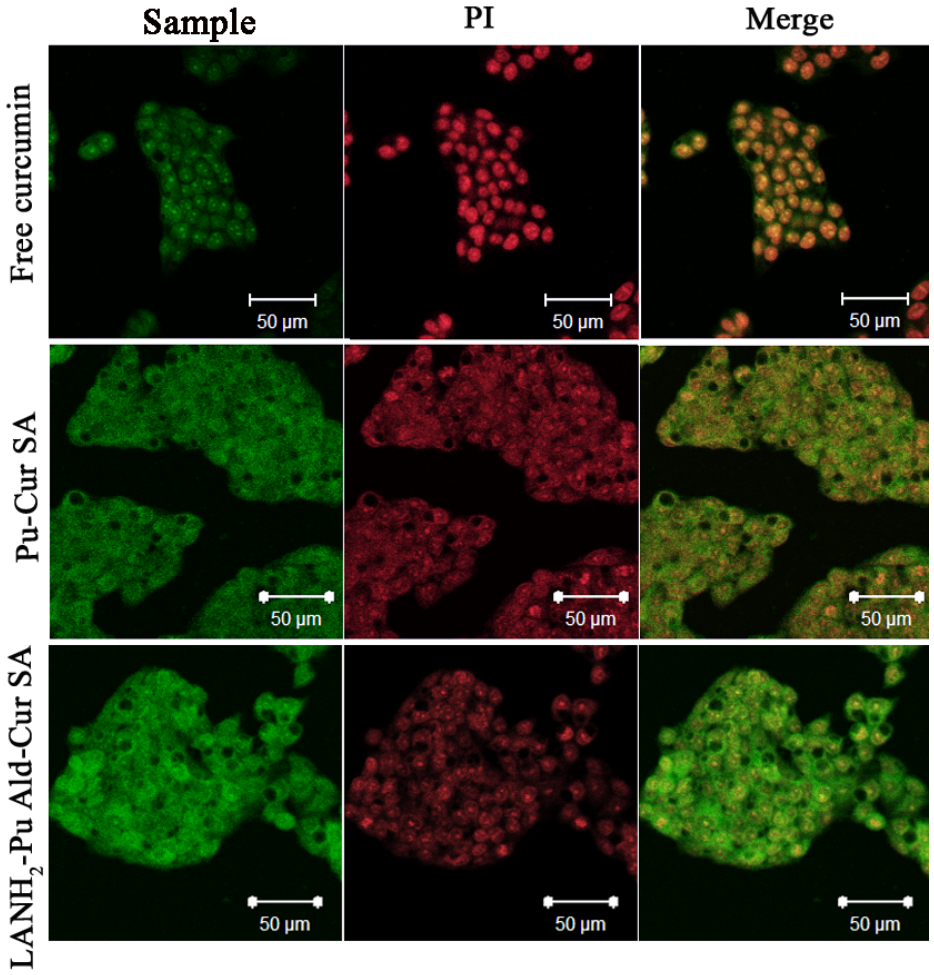

Figure 3.14 Intracellular uptake studies of free curcumin (row 1), Pu-Cur SA (row 2) and $LANH_2$-Pu Ald-Cur SA (row 3) by HepG2 cells observed under CLSM. Signal from curcumin (column 1) and PI (column 2) were separately obtained and merged (column 3)

It can be concluded that, by conjugating curcumin to pullulan, the solubility and stability of curcumin could be increased significantly. In Pu-Cur SA conjugate, the toxicity towards HepG2 cells is due to the elevated solubility and stability of the conjugated curcumin. In $LANH_2$-Pu Ald-Cur SA, targeting group plays a role in enhancing toxicity in addition to the effect due to the increased solubility and toxicity achieved for curcumin, by conjugation.

3.3 Alginate-curcumin conjugates with and without targeting group

The pullulan-curcumin conjugates described in the previous section increase the solubility and stability of curcumin to a great extent and the conjugate with the targeting group induces enhanced toxicity to HepG2 cells. However, the conjugate micelles show very low zeta potential since pullulan is a neutral polysaccharide. This may have implication on the tendency of the conjugate micelles for aggregation. Moreover, curcumin has to be modified for conjugating to pullulan. It would be advantageous, if the polysaccharide contains appropriate functional groups for curcumin conjugation. Hence, alginate which is a highly anionic polysaccharide with high zeta potential is selected for curcumin conjugation in the following work. The conjugates prepared from this polysaccharide may show lower aggregation tendency compared to pullulan. In addition to that, alginate is made up of mannuronic acid and guluronic acid residues, each repeating unit has acid functional groups and curcumin can be directly conjugated to it, without modification.

Dey et al have developed alginate-curcumin conjugate for enhancing solubility and stability of curcumin (Dey & Sreenivasan 2014). The conjugate is found to be cytotoxic towards L-929 cells. The aim of the present work is to check the suitability of the alginate-curcumin conjugate for the targeted delivery of curcumin to hepatocytes by attaching a galactose moiety to alginate ($LANH_2$-Alg Ald-Cur).

Attachment of galactose moiety to alginate is achieved by conjugation with modified lactobionic acid (LA). This method is similar to the strategy adopted in the previous section for the preparation of galactosylated pullulan conjugate. Non galactosylated conjugate (Alg-Cur) is also prepared to compare the targeting efficiency towards hepatocarcinoma cells.

3.3.1 Results and discussions

3.3.1.1 Preparation and characterization of galactosylated and nongalactosylated alginate-curcumin conjugates

The aim of this study is to develop galactosylated alginate-curcumin conjugate to overcome the problems of curcumin such as poor solubility and rapid metabolism. The conjugates possess unique features e.g. 1) they can be easily dispersed in aqueous medium 2) sufficiently stable in physiological pH and 3) provide selective and efficient intracellular uptake and antitumor activity.

Sreenivasan and coworkers prepared alginate-curcumin conjugate to enhance the solubility and stability of curcumin in aqueous medium (Dey & Sreenivasan 2014). The prepared conjugate shows toxicity to L-929 mouse fibroblast cells. In the present study, targeting group is attached to alginate and the suitability of the conjugate for targeted delivery of curcumin to HepG2 cells is analyzed. Physicochemical properties of $LANH_2$-Alg Ald-Cur and Alg-Cur conjugate are compared. Synthetic procedure adopted for the preparation of $LANH_2$-Alg Ald-Cur conjugate is similar to that adopted for $LANH_2$-Pu Ald-Cur SA conjugate. Initially, alginate is oxidized to alginate aldehyde (Alg Ald) by periodate oxidation to introduce aldehyde functionality (Scheme 3.7).

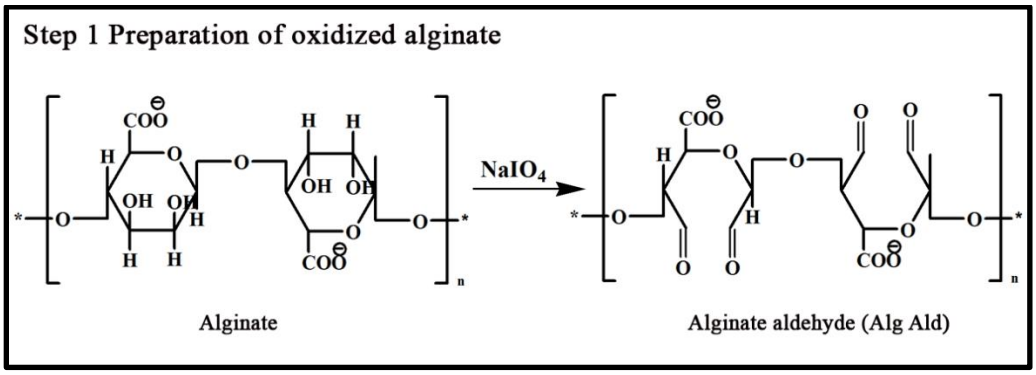

Scheme 3.7 Preparation of alginate aldehyde by the oxidation of alginate using sodium periodate

Oxidized Alg is characterized by FT-IR spectroscopy. In the spectrum of Alg Ald (Figure 3.15b) characteristic aldehyde carbonyl peak is seen at 1746 cm^{-1} which is absent in the spectrum of alginate (Figure 3.15a), indicating the oxidation. The aldehyde content in 50 % oxidized alginate is estimated to be 4.8×10^{-3} mol/g by tirtimetry. In order to get maximum number of available aldehyde groups for conjugation with modified LA ($LANH_2$), 50 % oxidized alginate is selected.

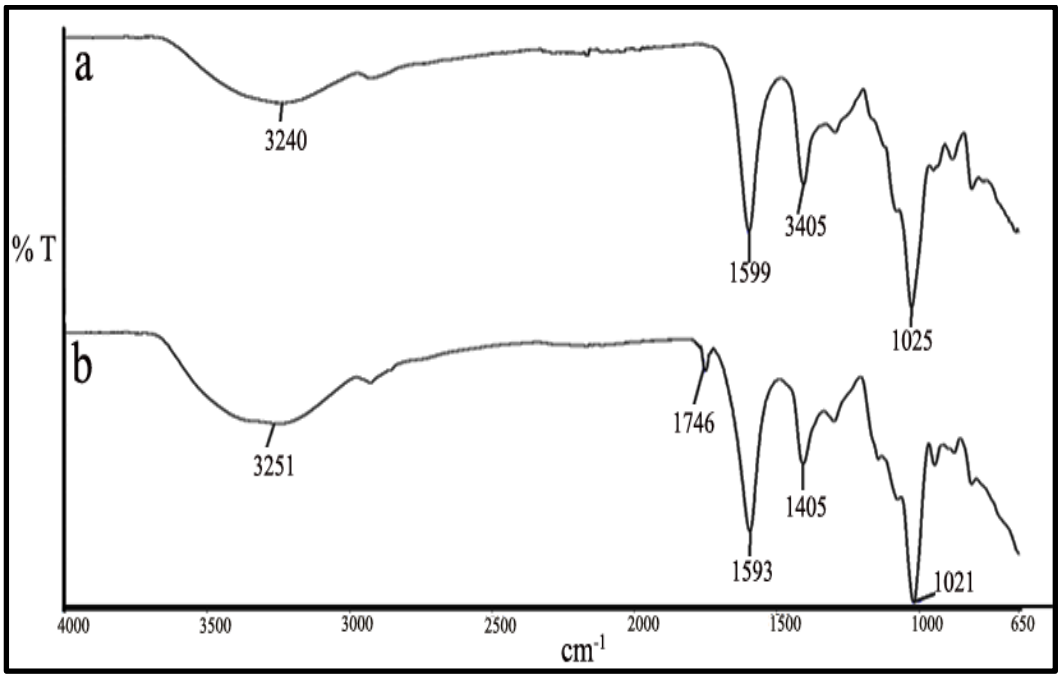

Figure 3.15 FT-IR spectra of alginate (a) alginate aldehyde (b)

For obtaining hepatocyte targeted conjugate, galactose ligand is attached covalently to Alg Ald by Schiff's base reaction between the aldehyde groups of Alg Ald and amino groups of $LANH_2$ (Scheme 3.8). ASGPR present on the sinusoidal surface of the hepatocytes can recognize galactose-terminal molecules and transport them to lysosomes inside liver cells (Yan Li et al. 2008).

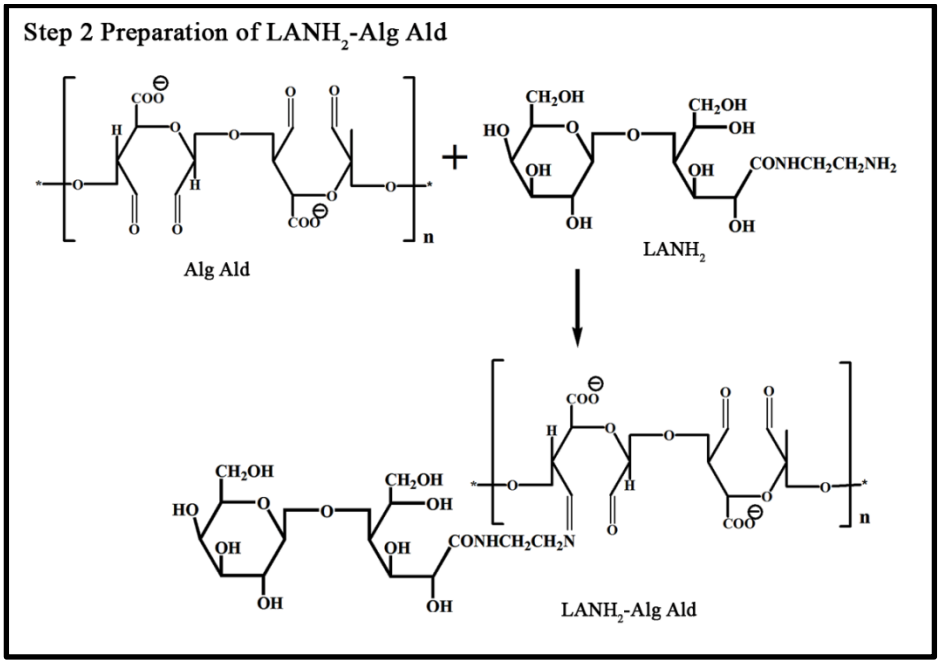

Scheme 3.8 Conjugation of $LANH_2$ to Alg Ald

Elemental (CHN) analysis is used to confirm the conjugation of $LANH_2$ to Alg Ald. Percentage of nitrogen in Alg is nil which shows a value of 7.8 % after $LANH_2$ conjugation. FT-IR spectroscopy is also performed to confirm the successful conjugation of $LANH_2$ to Alg Ald. Aldehyde peak at 1746 cm^{-1} of Alg is not seen in the IR spectrum of $LANH_2$-Alg Ald (Figure 3.16a), indicating the reaction between Alg Ald and $LANH_2$. The peak corresponding to the -C=N group (Schiff's base) (Issa, Khedr, & Rizk 2008, Ye, Xiong, & Sun 2012) formed between aldehyde group of Alg Ald and amino group of $LANH_2$ might have overlapped with amide I band of $LANH_2$. Peaks seen at 1633 cm^{-1} correspond to the overlapped vibrations of amide I band of $LANH_2$ and -C=N vibrations of $LANH_2$-Alg Ald. Amide II band at 1576 cm^{-1} of $LANH_2$ is shifted to 1596 cm^{-1} in $LANH_2$-Alg Ald.

The aldehyde groups present in $LANH_2$-Alg Ald is calculated by titrimetry and found that 70 % of the aldehyde groups are reacted with $LANH_2$. The reaction between $LANH_2$ and Alg Ald is highly feasible under suitable pH conditions. The stability of the Schiff's base reaction depends on the pH of the aqueous solution (Xin & Yuan 2012). Schiff's base is reported as a stimuli-responsive linker. It is unstable at acidic pH (below pH 6.5) and at alkaline pH (above 7.4). Hence the $LANH_2$-Alg Ald conjugate is expected to stable at neutral conditions.

In the final step, curcumin is conjugated to the carboxylic acid group of $LANH_2$-Alg Ald by DCC/DMAP coupling reaction.

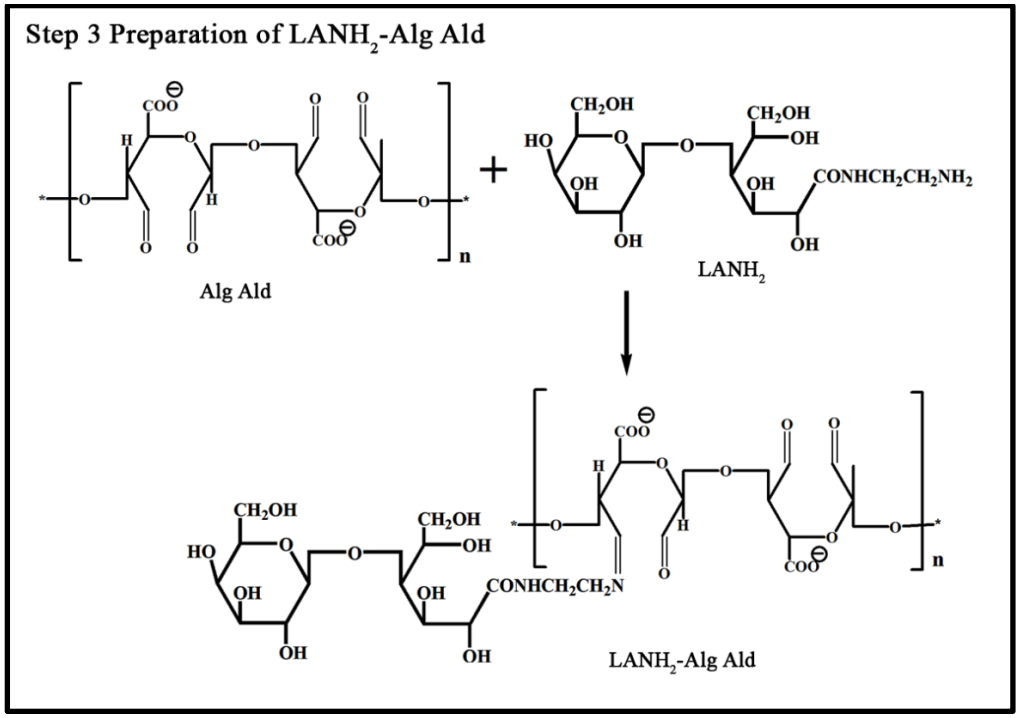

Scheme 3.9 Preparation of $LANH_2$-Alg Ald-Cur

Figure 3.16b represents IR spectrum of $LANH_2$-Alg Ald-Cur and the peak at 1623 cm^{-1} might have resulted from the overlap of –C=O stretching of keto groups in curcumin (Figure 3.16c) and amide I group of $LANH_2$-Alg Ald. Peak at 1588 cm^{-1} may correspond to amide II band of $LANH_2$-Alg Ald or -C=C stretching of the aromatic ring of curcumin. Curcumin conjugation is again indicated by the presence

of C-C stretching of aromatic ring at 1509 cm^{-1}. This peak is not seen in the spectrum of $LANH_2$-Alg Ald (Figure 3.16a).

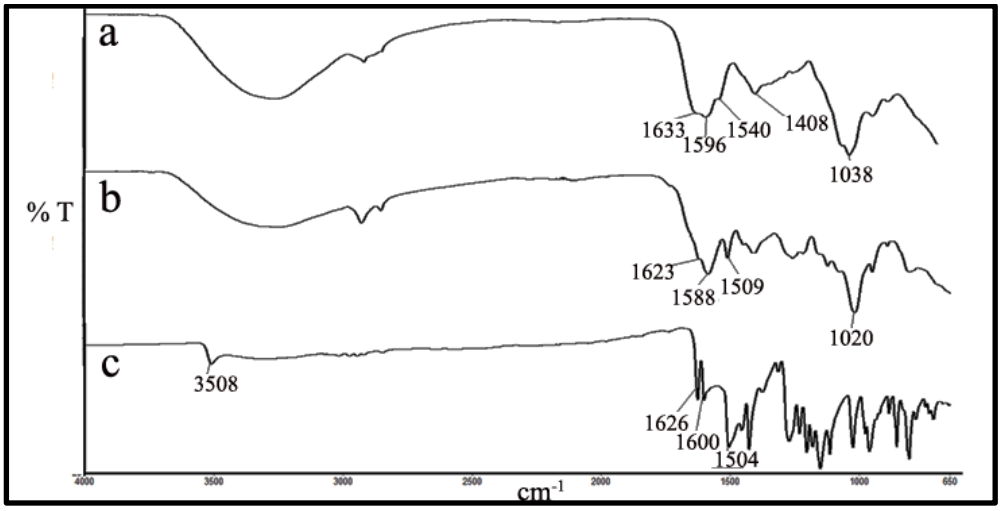

Figure 3.16 FT-IR spectra of $LANH_2$-Alg Ald (a), $LANH_2$-Alg Ald-Cur (b) and curcumin (c)

Alg-Cur conjugate is prepared by the direct conjugation of hydroxyl groups of curcumin to acid groups of alginate (Dey & Sreenivasan 2014). Preparation of Alg-Cur conjugate is shown in scheme 3.10.

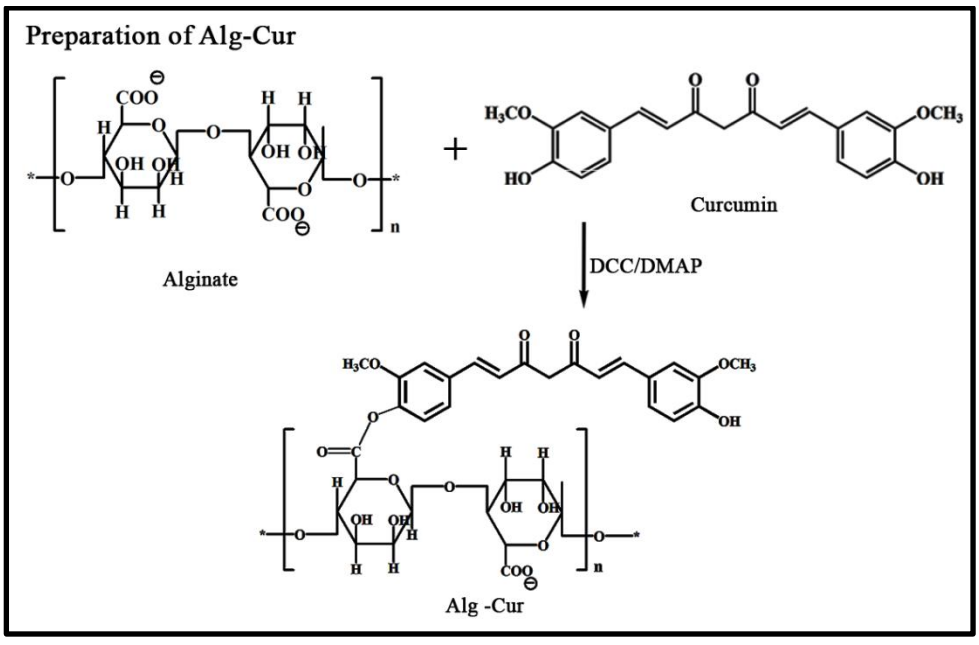

Scheme 3.10 Preparation of Alg-Cur

^{1}H NMR spectra of curcumin, Alg-Cur and $LANH_2$-Alg Ald-Cur are shown in Figure 3.17.

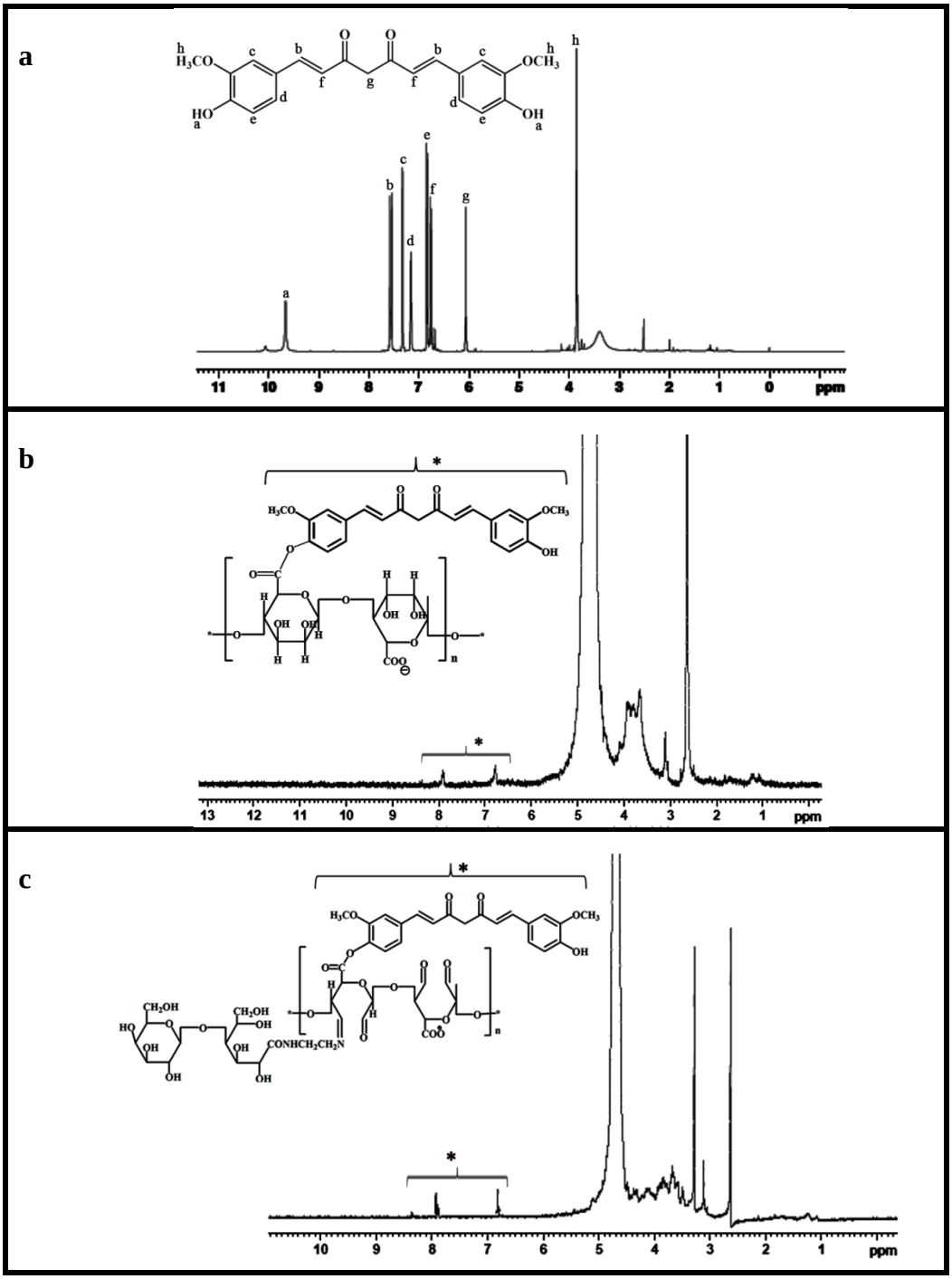

Figure 3.17 ^{1}H NMR spectra of curcumin (a), Alg-Cur (b) and $LANH_2$-Alg Ald-Cur (c)

Curcumin is present in the inner core of the conjugate $LANH_2$-Alg Ald-Cur (Figure 3.17c), hence the intensity of curcumin peak is less in the conjugate compared to free curcumin (Figure 3.17a) and it is seen in the region between 6.5–8 ppm. In addition to this, distinctive singlet $–OCH_3$ proton peak of curcumin is seen at 3.28 ppm. In the ^1H NMR spectrum of Alg-Cur (Figure 3.17b) conjugate also characteristic curcumin peaks are seen.

Alginate has a number average molecular weight (Mn) of 494134 Da and after curcumin conjugation (Alg-Cur) it is reduced to 483000 Da. Molecular weight is expected to increase after galactosylation and conjugation with curcumin. However, the molecular weight of $LANH_2$-Alg Ald-Cur is found to decrease drastically to 11436 Da. The large decrease can be the result of chain cleavages that might have occurred during the reactions required for modification.

$LANH_2$-Alg Ald-Cur and Alg-Cur conjugate contain both hydrophobic and hydrophilic entities arising respectively from curcumin and $LANH_2$-Alg Ald or alginate. Therefore, the polymer-drug conjugates can easily self assemble into micelles in aqueous environment with hydrophobic core arising from the organization of the hydrophobic curcumin moieties and a hydrophilic shell of galactosylated alginate or alginate. The conjugate ($LANH_2$-Alg Ald-Cur) exhibits hydrodynamic diameter in the range of 235 ± 6 nm. Dey et al prepared Alg-Cur conjugate with hydrodynamic diameter of 459 nm (Dey & Sreenivasan 2014). Alg-Cur conjugate, prepared in the present work also exhibits a similar hydrodynamic diameter (500 ± 10 nm). Introduction of $LANH_2$ onto alginate results in significant decrease in the hydrodynamic diameter of $LANH_2$-Alg Ald-Cur. Alg-cur micelle shows a zeta potential of -69 mV while $LANH_2$-Alg Ald-Cur has a zeta potential of -29 mV, much less than that of Alg-Cur. This difference in size and zeta potential after galactosylation is owing to the difference in the nature of self assembly in Alg-cur and $LANH_2$-Alg Ald-Cur. Alginate is considered to be a linear polymer and attaching $LANH_2$ results in a polymer chain with short branches. Alginate is an anionic

polysaccharide with acid groups in each repeating unit. In Alg-Cur conjugate, the high zeta potential is due to the presence of large number of the exposed $–COO^-$ groups and these groups may repel each other leading to high hydrodynamic radius. The drastic decrease in zeta potential obtained after galactosylation can be due to the structural rearrangement consequent to the galactosylation. The exposed acid groups may rearrange and the repulsion between them would have reduced, resulting in smaller size and diminished zeta potential value. This structural change would have affected the hydrophilic hydrophobic interaction, leading to a more compact structure in $LANH_2$-Alg Ald-Cur. However, the detailed structural investigation of the micelle is not discernible at this juncture. Smaller size of the $LANH_2$-Alg Ald-Cur conjugate can lead to enhanced permeability through cell membrane. $LANH_2$-Alg Ald-Cur conjugate micelle prepared in the present work is in the size range suitable for nanoparticles for drug delivery.

High zeta potential of the conjugate indicates stability of the nanoparticles in aqueous medium (Hans & Lowman 2002). Negative surface charge is preferable for drug conjugates because positively charged particles can bind proteins and a large number of cells in the body, before reaching to the target tumor cells (Acharya & Sahoo 2011). Hence it is essential to have negative surface zeta potential for enhanced circulation time with increased EPR effect.

Scanning electron microscopy is used to confirm the nano size and morphology of the conjugate (Figure 3.18). Size of the $LANH_2$-Alg Ald-Cur (Figure 3.18b) conjugate measured from SEM image is 220 ± 10 nm and Alg-Cur (Figure 3.18a) conjugate is shown to be much bigger in size (450 ± 8 nm).

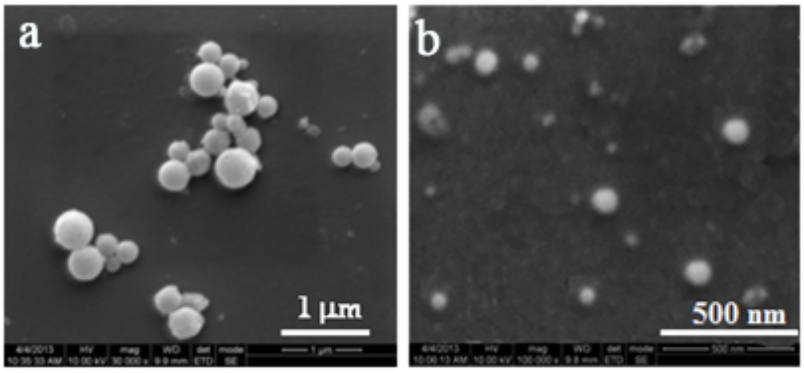

Figure 3.18 SEM images of Alg-Cur (a) and $LANH_2$-Alg Ald-Cur (b) conjugates. Both conjugates show spherical morphology

Self assembly of the conjugate is analyzed by measuring critical micelle concentration of $LANH_2$-Alg Ald-Cur (Figure 3.19) and Alg-Cur (Figure 3.20). From the plot of intensity ratios (I_{373}/ I_{384}), the CMC value of $LANH_2$-Alg Ald-Cur (Figure 3.19) and Alg-Cur (Figure 3.20) is estimated to be 0.044 and 0.014 mg/mL respectively.

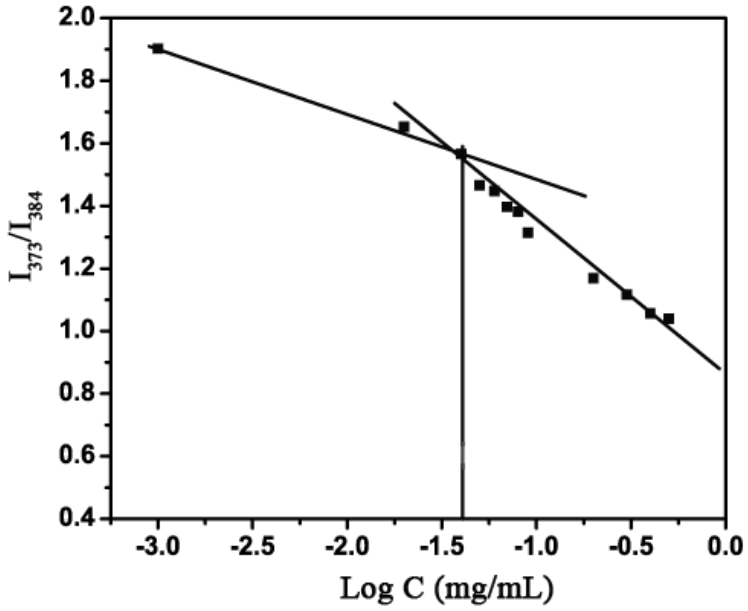

Figure 3.19 Plot of intensity ratio I_{373}/I_{384} of pyrene as a function of logarithm of concentration of Alg-Cur conjugate

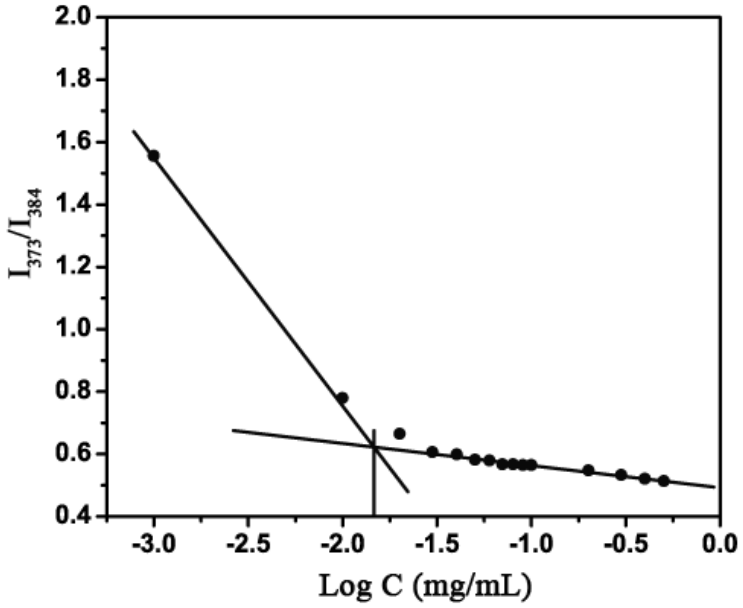

Figure 3.20 Plot of intensity ratio I_{373}/I_{384} of pyrene as a function of logarithm of concentration of $LANH_2$-Alg Ald-Cur conjugate

Thermodynamic stability of the conjugate with lower CMC value will be better and beneficial for prolonged circulation time and tumor targeting (C. Yu et al. 2013). The difference in CMC value of $LANH_2$-Alg Ald-Cur and Alg-Cur also supports the drastic changes in size and zeta potential after galactosylation.

Fluorescence spectra of free curcumin, Alg-Cur and $LANH_2$-Alg Ald-Cur are recorded to understand the changes occurred in curcumin after conjugation to the polysaccharide (Figure 3.21). Curcumin (Figure 3.21b) does not show any change in fluorescence after conjugation to alginate (Alg-Cur, Figure 3.21c) while it shows a blue shift in $LANH_2$-Alg Ald-Cur (Figure 3.21a). Structural changes occurred during the formation of $LANH_2$-Alg Ald-Cur is responsible for the blue shift.

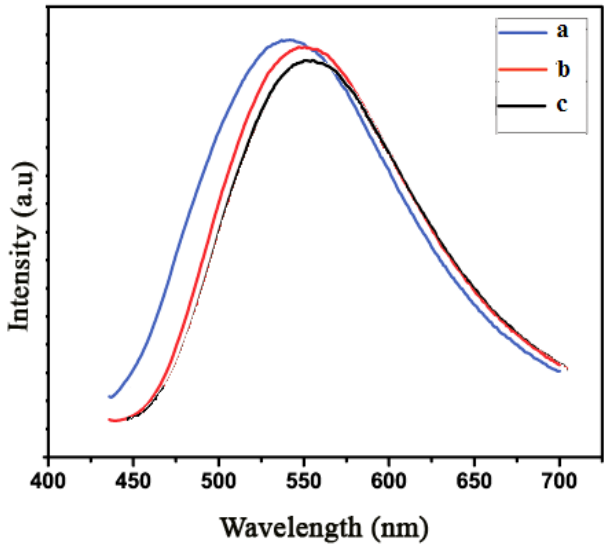

Figure 3.21 Emission spectra of $LANH_2$-Alg Ald-Cur (a), curcumin (b) and Alg-Cur (c)

The principal aim of grafting curcumin to a hydrophilic polysaccharide is to magnify its solubility in aqueous medium. Amount of curcumin conjugated to $LANH_2$-Alg Ald-Cur is evaluated from the standard curcumin curve and it is found that 1 mg of the conjugate contains 30 μg of curcumin. It is reported that Alg-Cur conjugate could solubilize 109 μg of curcumin in 1 mL of aqueous solution (Dey & Sreenivasan 2014). In this study, greater extent of conjugation is achieved leading to increased solubility of curcumin. More than 50 mg of the $LANH_2$-Alg Ald-Cur conjugate can be dissolved in 1 mL of water corresponding to 1.5 mg/mL of curcumin, significantly higher than the solubility of bare curcumin. A 540-fold increase in the solubility of curcumin is achieved after conjugation with galactosylated alginate which is considerably higher than the solubility of the nongalactosylated alginate-curcumin conjugate (70-fold increase). Solubility of alginate in aqueous medium is less compared to other polysaccharides. Galactosylation increases the solubility of alginate to a greater extent resulting in enhanced curcumin conjugation. Hence, $LANH_2$-Alg Ald-Cur conjugate exhibits

higher aqueous solubility. Thus by employing $LANH_2$-Alg Ald-Cur, emancipated solubility of curcumin can be achieved.

3.3.1.2 Stability studies of $LANH_2$-Alg Ald-Cur and Alg-Cur conjugates

For analyzing the improvement in stability after conjugation, $LANH_2$-Alg Ald-Cur (Figure 3.22c) and Alg-Cur (Figure 3.22b) conjugates are dissolved in PBS buffer and the change in absorbance are monitored with time. Curcumin degrades first by hydrolysis, followed by complete molecular fragmentation within 30 min to various degradation products at pH above neutral. Hence drastic decrease in the absorption intensity would be observed. Only a slight change in the absorbance is observed even after 5 h of incubation at 37 °C in PBS (pH 7.4) in the case of the conjugates, whereas curcumin degraded completely within 30 min (Figure 3.22a). Micelle formation of the conjugates protects curcumin from deprotonation and degradation in the alkaline medium increasing its aqueous stability.

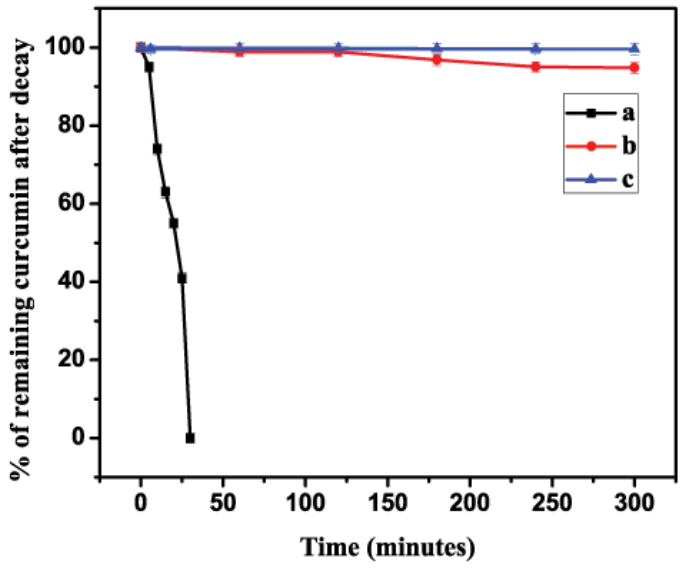

Figure 3.22 Stability studies of free curcumin (a), Alg-Cur (b) and $LANH_2$-Alg Ald-Cur (c) conjugate in PBS at 37 °C. Data shown are mean value ± standard deviation (SD) (n=3, $*p<0.05$). There is no statistically significant difference between the absorbance obtained over the entire time period

3.3.1.3 *In vitro* curcumin release studies

In vitro release of curcumin from $LANH_2$-Alg Ald-Cur SA and Alg-Cur SA is examined at two different pH for 48 h and the release patterns are shown in Figure 3.23. In both conjugates, the release of curcumin is higher at acidic pH and is relatively slower at pH 7.4. The faster release of curcumin at acidic pH is attributed to the easy breakage of the ester linkages at this pH. In $LANH_2$-Alg Ald-Cur SA conjugate, the Schiff's base formed between $LANH_2$ and Alg Ald also breaks at acidic pH (Xin & Yuan 2012) leading to higher release compared to Alg-Cur. It can also be seen that at both pH, compared to the release of Alg-Cur, $LANH_2$-Alg Ald-Cur shows higher curcumin release.

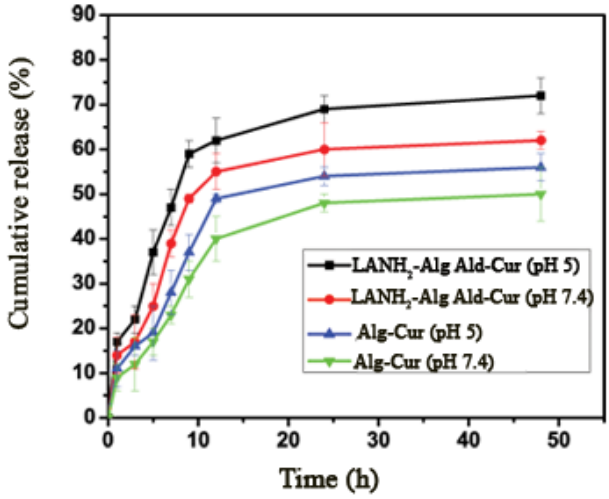

Figure 3.23 *In vitro* curcumin release patterns of $LANH_2$-Alg Ald-Cur and Alg-Cur at pH 5 and 7.4

3.3.1.4 Cytotoxicity studies

The cytotoxic ability of $LANH_2$-Alg Ald-Cur, Alg-cur and free curcumin is examined in HepG2 cells. The cells are incubated with various concentrations of the conjugates (containing 1.5 to 25 μg/mL of curcumin) and free curcumin (1.5 to 25 μg/mL) for 24 h and cell activity is evaluated by MTT assay (Figure 3.24). Alg-Cur conjugate shows 50 % cell death in HepG2 cells at a curcumin equivalent

concentration of 11 µg/mL. The percentage activity of the cells is decreased from 75 ± 1 % to 12 ± 2 % when treated with $LANH_2$-Alg Ald-Cur containing equivalent curcumin concentration of 1.5 µg/mL and 25 µg/mL respectively. On the other hand, percentage activity of Alg-cur (Figure 3.24) treated HepG2 cells is diminished from 97 ± 3 % to 30 ± 6 % in the same concentration range. IC_{50} values of free curcumin, $LANH_2$-Alg Ald-Cur and Alg-cur with HepG2 cells are in the order 5.6 µg/mL, 3.9 µg/mLand 11 µg/mL respectively. The lowest IC_{50} value at a same equivalent curcumin dose range, demonstrates that $LANH_2$-Alg Ald-Cur conjugate has remarkably enhanced ability to specifically target HepG2 cells and induce cytotoxicity compared to Alg-Cur conjugate (Figure 3.24). In all the tested concentrations, $LANH_2$-Alg Ald-Cur conjugate exhibits statistically significant cytotoxicity difference (*$p<0.005$) than Alg-Cur towards HepG2 cells. The improvement in cytotoxic effect is presumably due to the presence of galactose moiety in the $LANH_2$-Alg Ald-Cur conjugate and confirms the target specific toxicity of $LANH_2$-Alg Ald-Cur.

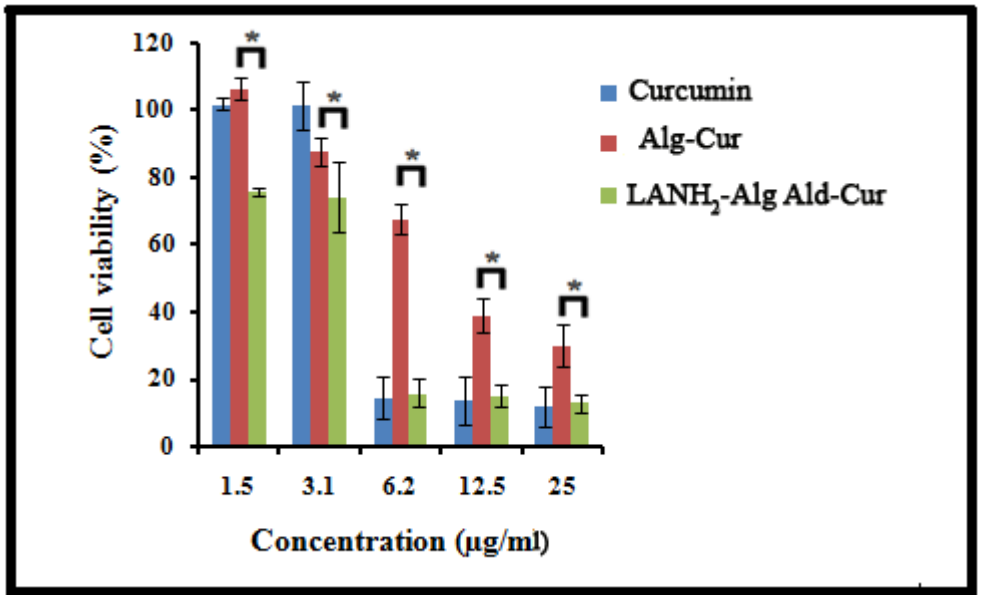

Figure 3.24 Cytotoxicity analysis of Alg-Cur, $LANH_2$-Alg Ald-Cur and free curcumin. $LANH_2$-Alg Ald-Cur conjugate shows enhanced toxicity to HepG2 cells than Alg-Cur. Data shown are mean value ± SD (n =3, ∗$p < 0.05$)

3.3.1.5 *In vitro* cellular uptake studies

The confocal microscopy analysis of cellular uptake of the conjugates and free curcumin by HepG2 cells shows that $LANH_2$-Alg Ald-Cur conjugate is internalized more compared to free curcumin and Alg-Cur (Figure 3.25). Diminished fluorescence intensity of free curcumin in the cells is due to lower internalization due to the lack of galactose moiety. Also, the free curcumin undergoes faster metabolism and elimination compared to the curcumin conjugate. $LANH_2$-Alg Ald-Cur conjugate exhibits higher fluorescence intensity in the cytoplasm of HepG2 cells compared to Alg-Cur, which can be attributed to the enhanced cell internalization capability provided by the galactose moiety.

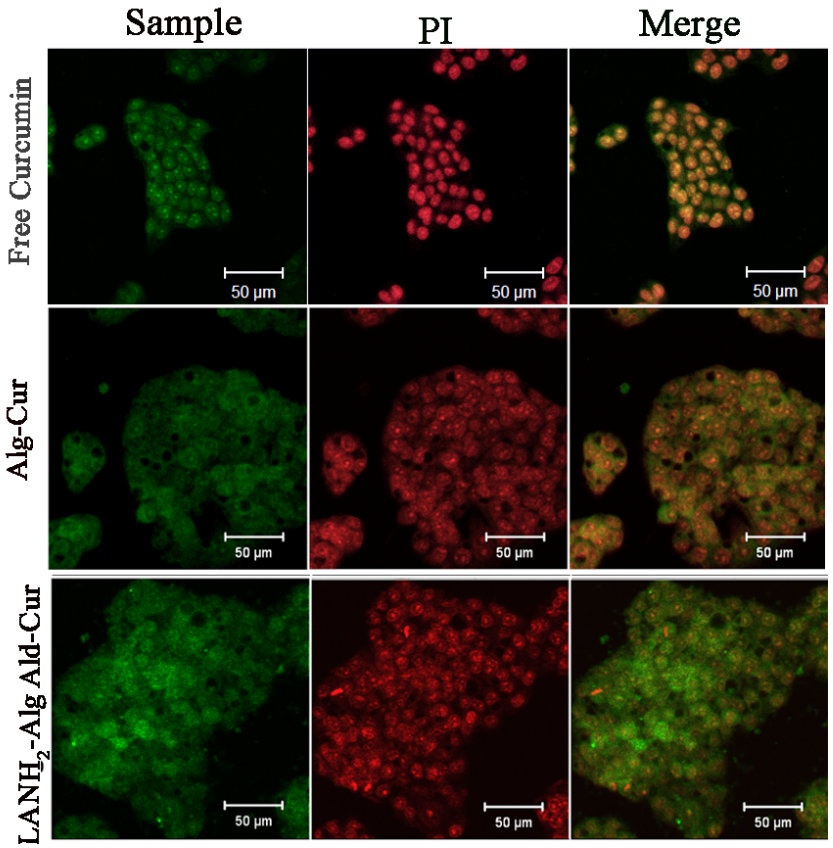

Figure 3.25 Intracellular uptake of free curcumin (row 1), Alg-Cur (row 2) and $LANH_2$-Alg Ald-Cur (row 3) by HepG2 cells observed under CLSM. Signals from curcumin (column 1) and PI (column 2) were separately obtained and merged (column 3). $LANH_2$-Alg Ald-Cur shows higher intensity as a result of increased level of particle internalization compared to Alg-Cur and free curcumin.

It is clear that galactosylation results in enhanced toxicity of the conjugate towards HepG2 cells. Galactosylation is found to increase the solubility and cellular uptake ability.

3.4 Gum arabic-curcumin conjugate

Gum arabic (GA) is a branched, complex polysaccharide containing arabinose, rhamnose, galactose and glucuronic acid residues with backbone consisting of 1,3 linked β-D-galactopyranosyl units. Gum arabic contains galactose units in its complex structure; hence the malignant liver cells may exhibit enhanced binding and uptake of GA.

Gum arabic-drug conjugates have been investigated for controlled drug delivery applications (Nishi, Antony, & Jayakrishnan 2007, Nishi, Antony, Mohanan, et al. 2007). Gum arabic contains 39-42 % galactose, 24-27 % arabinose and 12-16 % rhamnose (Verbeken et al. 2003) in its structure. The designed gum arabic-curcumin conjugate is aimed to have application in curcumin delivery in liver cancer cells. The main motive for selecting gum arabic for conjugate synthesis is its structural peculiarity i.e the presence of galactose moiety on the structure itself.

To the best of our knowledge this is the first report on gum arabic-curcumin conjugate for target specific drug delivery of curcumin to HepG2 cells exploiting the galactose unit on gum arabic as a targeting ligand. Curcumin (Cur) is attached to the polysaccharide by a DCC/DMAP coupling reaction. Physicochemical properties of the gum arabic-curcumin conjugate (GA-Cur) are evaluated. *In vitro* anticancer activity of GA-Cur conjugate in HepG2 and MCF-7 cells are examined by MTT assay. All the results demonstrated that the new GA-Cur conjugate system can be employed to increase solubility and stability of curcumin with target specific delivery to hepatocarcinoma cells.

3.4.1. Results and discussions

3.4.1.1. Preparation and characterization of GA-Cur conjugate

Gum arabic is selected for curcumin conjugation considering its high water solubility (can prepare solutions up to 50 %, w/v), low cost, easy availability and the presence of galactose groups. Since it contains glucuronic acid units, curcumin can be directly conjugated to it. Galactose is already identified as a targeting ligand for HepG2 cells since it can facilitate ASGPR mediated endocytosis in HepG2 cells. Procedure for GA-Cur conjugate preparation is given below (Scheme 3.11). Hydroxyl group of curcumin is conjugated to the acid groups of GA by DCC/DMAP coupling reaction through an ester linkage.

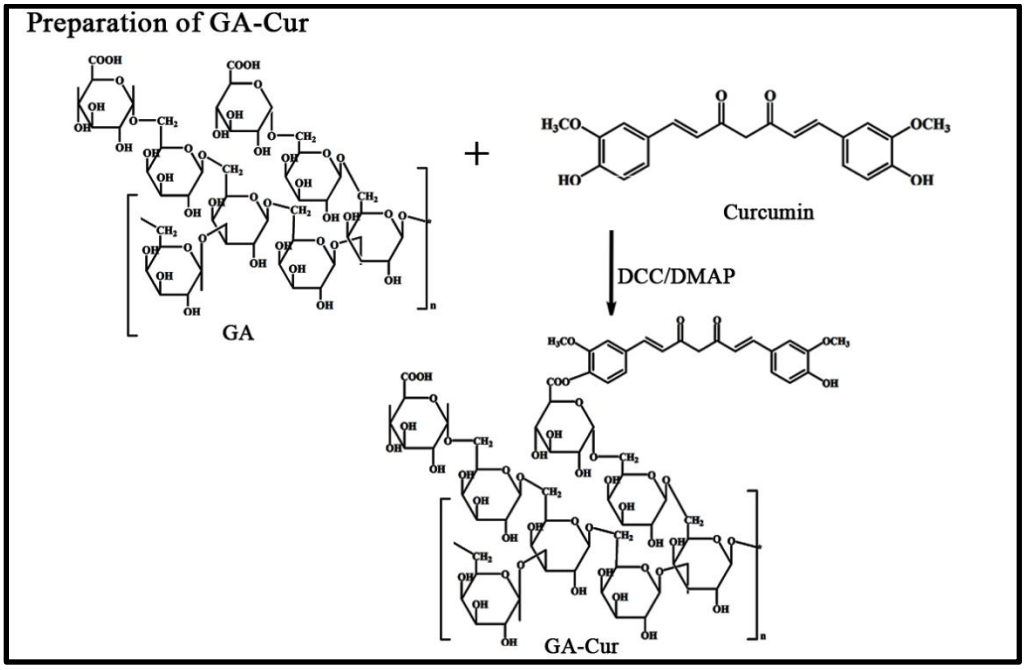

Scheme 3.11 Conjugation of curcumin to gum arabic by DCC/DMAP coupling reaction

Conjugation of curcumin to GA is confirmed by ^{1}H NMR spectroscopy (Figure 3.26). ^{1}H NMR spectrum of the resultant conjugate (GA-Cur) (Figure 3.26b)

contains multiple proton resonance peaks of curcumin in the region between 6–8 ppm (Figure 3.26b, b-g in the spectrum) together with the distinctive singlet $–OCH_3$ proton peak at 3.84 ppm (Figure 3.26b, h). The spectrum also contains characteristic GA proton peaks at 1.27 ppm and characteristic envelope around 3.9 ppm (Figure 3.26b) (Weinbreck, Rollema, Tromp, & de Kruif 2004).

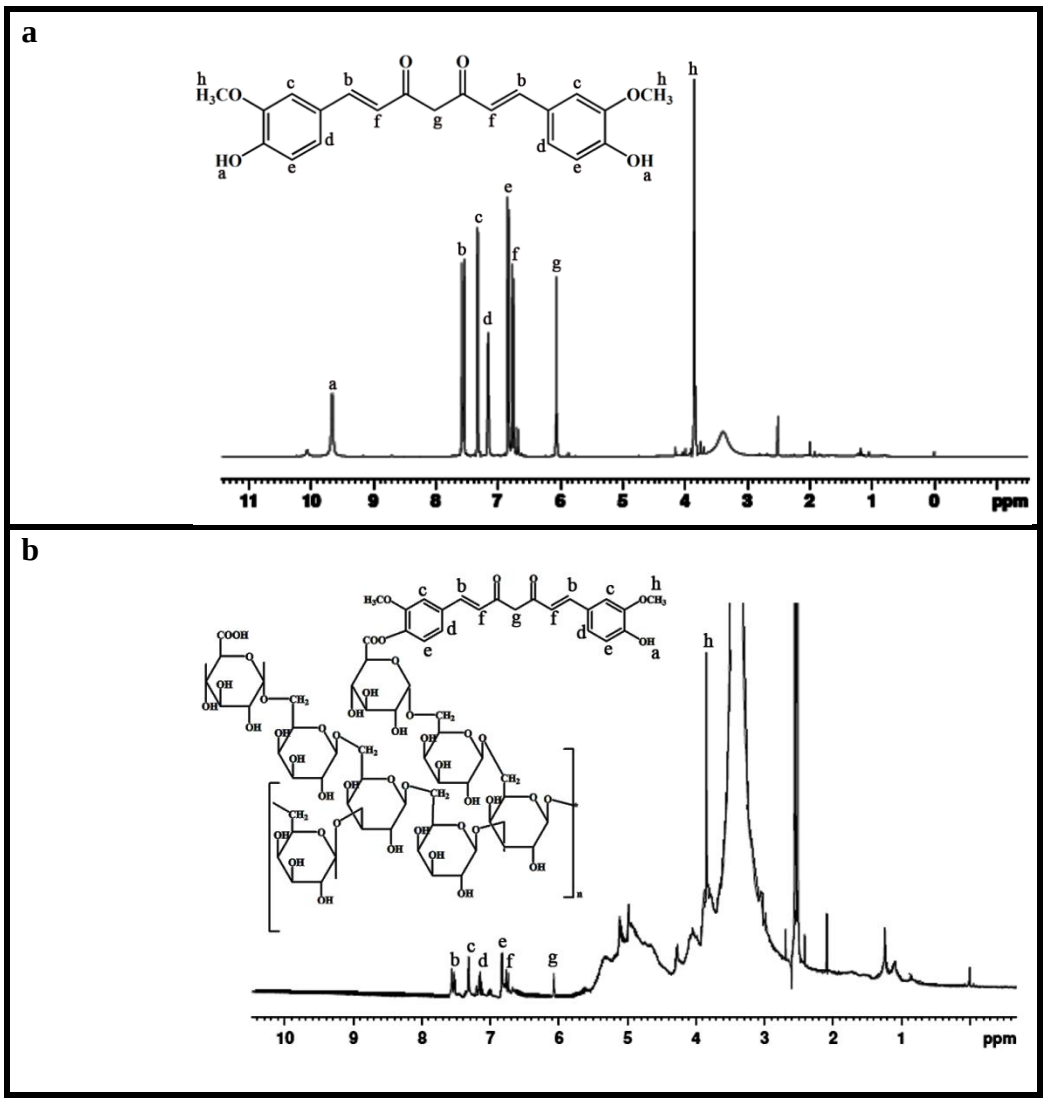

Figure 3.26 ^{1}H NMR spectra of curcumin (a) and GA-Cur conjugate (b). GA-Cur shows peaks of curcumin in the region between 6.5–8 ppm together with the distinctive singlet $–OCH_3$ proton peak at 3.84 ppm

Gum arabic has a number average molecular weight (Mn) of 383903 Da and after curcumin conjugation it is reduced to 367953 Da. Conjugation of curcumin molecules to gum arabic is expected to increase the molecular weight. Gum arabic is a branched polysaccharide and under the reaction conditions for curcumin conjugation, side chain cleavage might have occurred leading to the slight reduction in the molecular weight.

Self assembly of biopolymers in aqueous medium depends upon its amphiphilicity (K Akiyoshi & Sunamoto 1996). The amphiphilic GA-Cur conjugate can be easily dispersed in aqueous medium which self assembles to micelles with hydrophobic curcumin core and hydrophilic GA shell. Self assembly of the conjugate is governed by minimization of the interfacial energy governed by the balance between the hydrophilic-hydrophobic interaction of gum arabic and curcumin (del Barrio et al. 2010).

The size of the conjugate by DLS technique is found to be in the range of 270 ± 5 nm. The particle size in this range is ideal for promoting selective accumulation of GA-Cur micelle in cancer tissues by the EPR effect. Nano micelle formation of amphiphilic polymers like galactosylated O-carboxymethyl chitosan-graft-stearic acid conjugates, siRNA–PLGA hybrid conjugates and PEG-PCL-PEI triblock copolymers are reported in the literature (Endres et al. 2011, Guo et al. 2013, S. H. Lee et al. 2011).

As illustrated in Figure 3.27, SEM (Figure 3.27a) and TEM (Figure 3.27b) images show the spherical morphology of the GA-Cur conjugate micelles. Size of the conjugate micelle obtained by SEM is 203 ± 10 nm. Surface morphology of the conjugate micelle is well evident from TEM analysis. TEM image (Figure 3.27b) represents spherical GA-Cur conjugate micelles with an average diameter of 200 ± 10 nm.

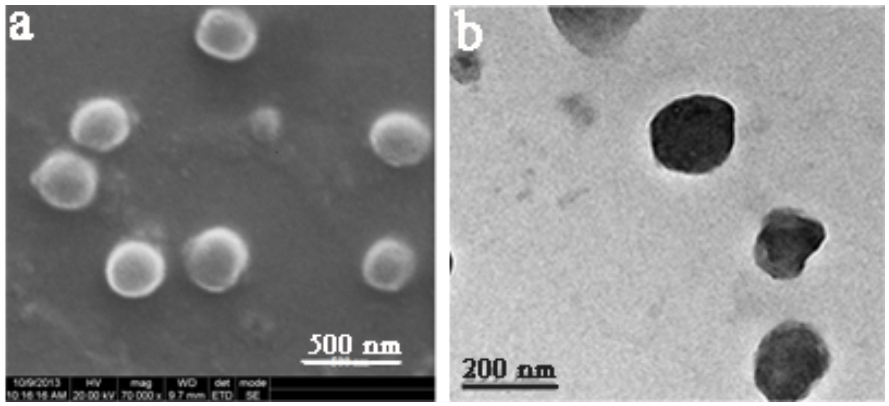

Figure 3.27 SEM (a) and TEM (b) images of GA-Cur conjugate. Spherical morphology of the micelle is evidenced from the image

The zeta potential of GA-Cur is also measured by DLS after dispersing the conjugate in aqueous medium and shows a negative zeta potential of -36.4 mV. The negative charge is due to the carboxylic acid groups of GA and prevents GA-Cur micelles from aggregation. The negatively charged GA-Cur with hydrophilic GA shell would also limit protein adsorption to a greater extent and enhance the circulation time with increased EPR effect leading to high antitumor efficacy.

Self-assembly behavior of GA–Cur conjugate is again investigated by measuring CMC value of GA-Cur conjugate (Figure 3.28). A rapid increase in the fluorescence intensity and a red shift in the absorption of pyrene are observed with increase in the concentration of GA–Cur. From the plot of intensity ratios (I_{373}/ I_{384}), the CMC value is estimated to be 0.023 mg/mL.

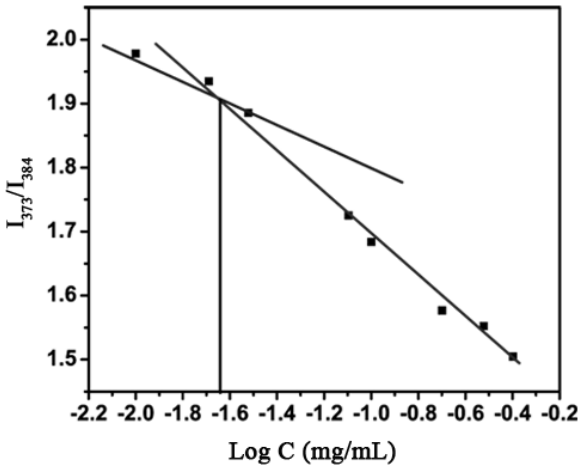

Figure 3.28 Plot of intensity ratio I_{373}/I_{384} of pyrene as a function of logarithm of concentration of GA-Cur

The fluorescence spectrum of GA-Cur recorded in water is shown in Figure 3.29. It also proves the successful formation of the conjugate. Curcumin possesses intrinsic fluorescent properties. Shift in the emission (to higher wavelength, from 547 nm to 568 nm) for the conjugate compared to pure curcumin demonstrates the conjugation between GA and curcumin (S Manju & Sreenivasan 2011a).

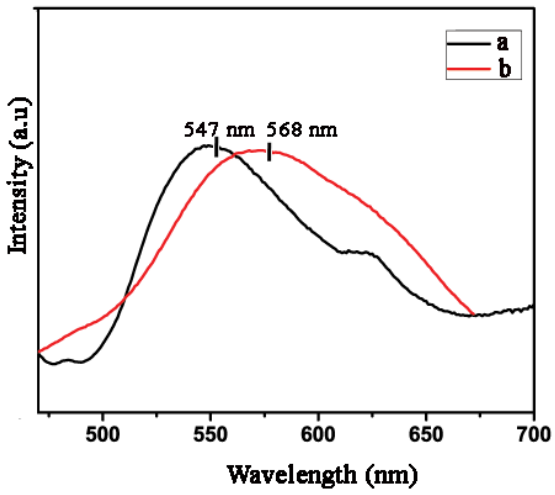

Figure 3.29 Emission spectra of curcumin (a) and GA-Cur conjugate (b). Both the samples were dissolved in water with curcumin equivalent concentration of 5 µg/mL.

It is found that 1 mg of the conjugate contains 13 μg of curcumin. Aqueous solubility of GA-Cur is determined and found that more than 200 mg of the GA-Cur can be solubilised in 1 mL of water which corresponds to 2.6 mg/mL of curcumin. Thus the conjugate tremendously increases the solubility of curcumin, since it is conjugated to a highly hydrophilic polysaccharide. To the best of our knowledge, this is the first report of a polymer-curcumin conjugate which shows 900-fold excess solubility than that of free curcumin. This immense solubility is attributed to the very high aqueous solubility of GA.

3.4.1.2 Stability studies of GA-Cur conjugate

The stability of GA-Cur in PBS buffer (Figure 3.30) at 37 °C is examined to analyze the influence of conjugation on the stability of the conjugated curcumin. Only a slight change in the absorbance is observed even after 5 h of incubation at 37 °C in PBS (pH 7.4), whereas curcumin degraded completely within 30 min (Figure. 3.30a). There is no significant difference in the absorbance of GA-Cur (Figure. 3.30b) even after 5 h (*p=0.65), whereas curcumin shows a significant decrease in the absorbance (*p=0.003) after 5 h. In micelle, curcumin is present in the inner core and is protected from deprotonation and degradation in the physiological pH. The conjugation of curcumin to GA stabilizes curcumin against hydrolysis and increases its aqueous stability.

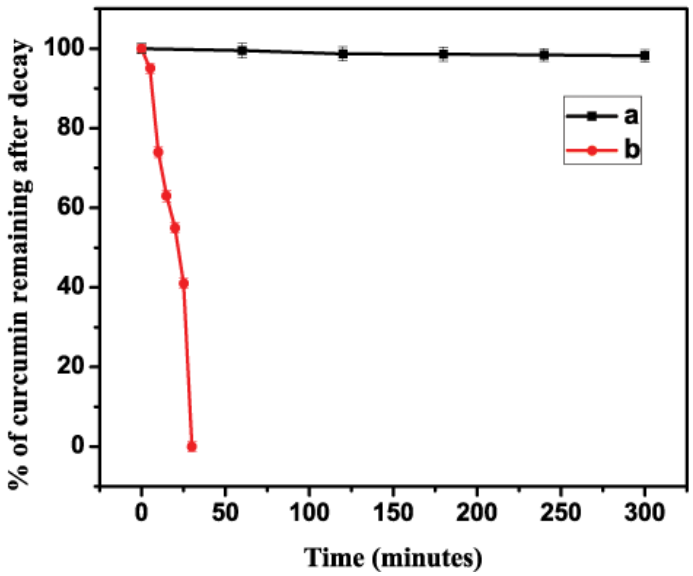

Figure 3.30 Stability studies of free curcumin (a) and GA-Cur (b) in PBS at pH 7.4. After conjugation, stability of curcumin in physiological pH is enhanced. Data shown are mean value ± standard deviation (SD) (n = 3, ∗p < 0.05)

3.4.1.3 *In vitro* curcumin release from GA-Cur conjugate

Curcumin release from GA-Cur conjugate is analyzed at pH 5 and 7.4 and is shown in Figure 3.31. Release of curcumin is higher at acidic pH like that of other two conjugates and it is owing to the destruction of the ester linkages between curcumin and GA. GA-Cur shows 60 % release after 48 h at pH 5, while 40 % curcumin release is observed at pH 7.4 during the same period. The ester linkage between GA and curcumin is comparatively stable at neutral pH, therefore less release was observed. Polysaccharide conjugates of alginate and pullulan show slightly higher release at acidic pH. In galactosylated conjugates ($LANH_2$-Alg Ald-Cur and $LANH_2$-Pu Ald-Cur SA) in addition to the ester linkages, Schiff's base formed between polysaccharide aldehydes and $LANH_2$ also undergoes breakage at acidic pH. In GA-Cur, only ester linkages are broken at acidic pH. This may be the reason for lower curcumin release at acidic pH compared to the conjugates containing galactose moiety.

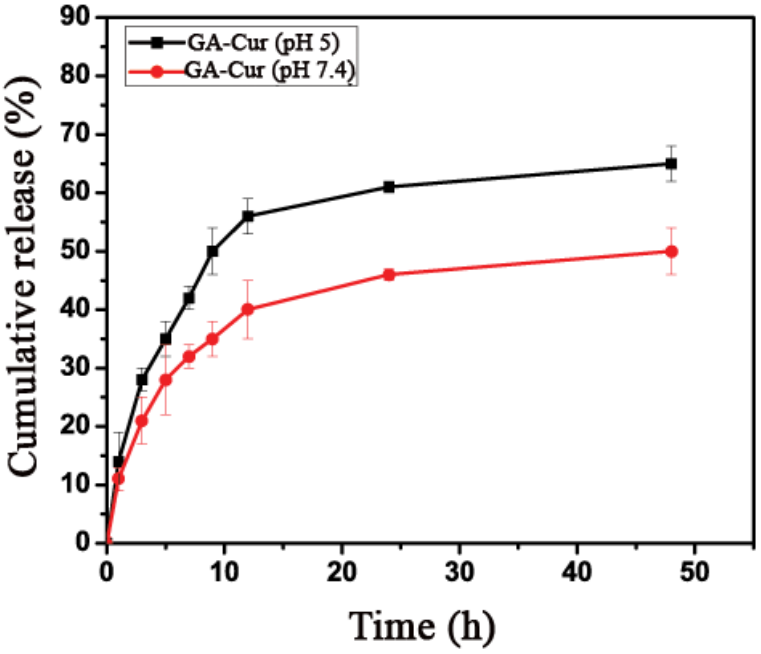

Figure 3.31 *In vitro* curcumin release patterns from GA-Cur conjugate at pH 5 and 7.4

3.4.1.4 Cytotoxicity studies of GA-Cur

The anticancer activity of GA-Cur conjugate is evaluated in HepG2 and MCF-7 cells by MTT assay with free curcumin as assay control. Since GA-Cur conjugate has galactose group in its structure itself, additional galactosylation is not needed for targeted delivery of curcumin to HepG2 cells. In this context, preparation and cytotoxicity analysis of a nongalactosylated GA-Cur conjugate is impossible for the comparison of targeting efficiency. Hence the cytotoxicity studies are performed in HepG2 cells and MCF-7 cells. The cells are exposed to the conjugate in five doses (1.5-25 μg/mL) for 24 h and cell activity is evaluated (Figure 3.32). The results confirm that the doses 25 μg/mL and above show severe cytotoxicity (<20 % metabolic activity) to HepG2 cells. However, the concentration 6.25 μg/mL is noncytotoxic to MCF-7, but cytotoxic to HepG2 cells. IC_{50} values of GA-Cur in HepG2 and MCF-7 cells are 2.29 and 4.07 μg/mL respectively. The cytotoxic

potential of GA-Cur is evident while comparing the cellular activity with the assay control (free curcumin). Curcumin shows IC_{50} values of 3.8 μg/mL and 5.6 μg/mL in MCF-7 and HepG2 cells respectively. Higher toxicity of GA-Cur to HepG2 cells is due to the presence of galactose moiety in the structure of gum arabic which can selectively identify asialoglycoprotein receptor (ASGPR) on the surface of hepatocytes (Rigopoulou et al. 2012). The results demonstrate that the conjugate shows effective anticancer activity towards MCF-7 and HepG2 cells. The cytotoxicity of GA-Cur towards HepG2 cells is higher compared to other conjugates ($LANH_2$-Pu Ald-Cur SA and $LANH_2$-Alg Ald-Cur) studied in the present work. IC_{50} values of $LANH_2$-Pu Ald-Cur SA and $LANH_2$-Alg Ald-Cur are 4.8 μg/mL and 3.9 μg/mL resepectively, whereas GA-Cur has an IC_{50} value of 2.29 μg/mL. GA contains galactose groups in its structure itself and it may give better targeting compared to the conjugated galactose group.

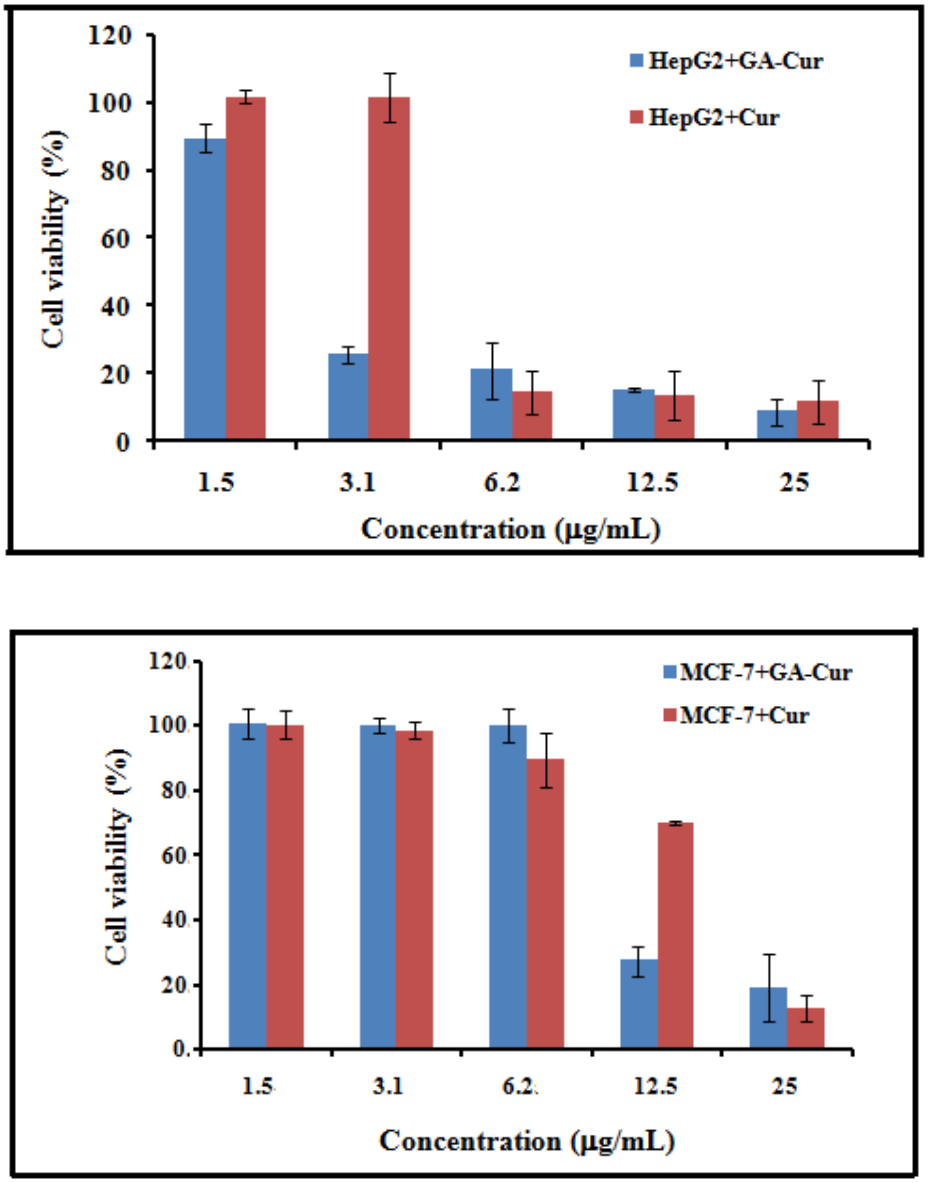

Figure 3.32 Cytotoxicity analysis of GA-Cur and free curcumin in HepG2 (a) and MCF-7 (b) cells. GA-Cur shows selective toxicity towards HepG2 cells. Data shown are mean value ± SD (n = 3)

3.4.1.5 *In vitro* cellular uptake studies of GA-Cur conjugate

The *in vitro* cellular uptake of GA-Cur conjugate by HepG2 and MCF-7 cells for 24 h is analyzed by CLSM. GA-Cur shows cellular uptake in both the cancer cell lines. GA-Cur is internalized in the cytoplasm and nucleus of HepG2 (Figure 3.33)

and MCF-7 cells (Figure 3.34). Free curcumin is located both in the cytoplasm and nucleus of the HepG2 cells (Figure. 3.33) and MCF-7 cells (Figure 3.34) (Saab et al. 2011, R. Yang et al. 2012). Low fluorescence intensity of free curcumin in both the cells (Figure. 3.33 and 3.34) is attributed to its poor uptake and high metabolism. High fluorescence of GA-Cur in HepG2 cells may be explained due to ASGPR mediated increased cellular uptake. The CLSM analysis reveals that the conjugate shows higher fluorescence intensity compared to free curcumin, which is assumed to be the result of enhanced solubility and efficient cell internalization ability. These results indicate that internalization of curcumin is increased after conjugation with GA. Higher solubility and facile passage of the conjugate through the cell membrane provide the cells, efficient drug internalization capability with a longer EET. Better internalization would be favorable to the enhanced cytotoxicity of GA-Cur conjugate.

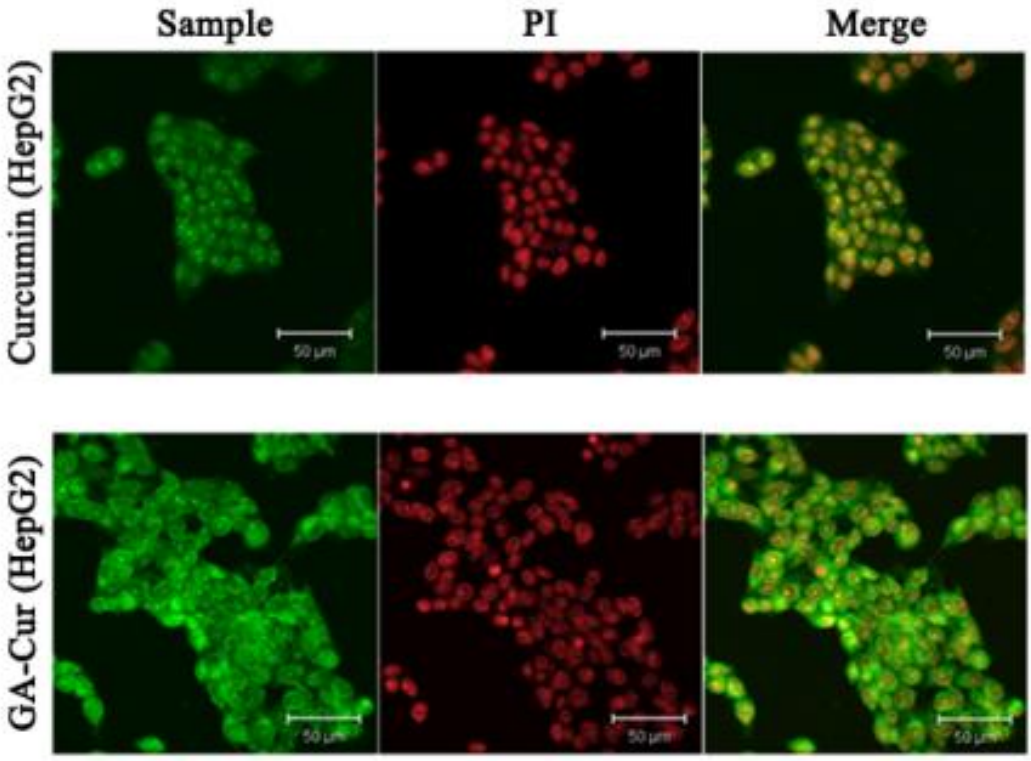

Figure 3.33 Intracellular uptake of free curcumin (row 1) and GA-Cur (row 2) by HepG2 cells observed under CLSM. Signals from curcumin (column 1) and PI (column 2) were separately obtained and merged (column 3). GA-Cur shows higher intensity as a result of increased level of particle internalization compared to free curcumin

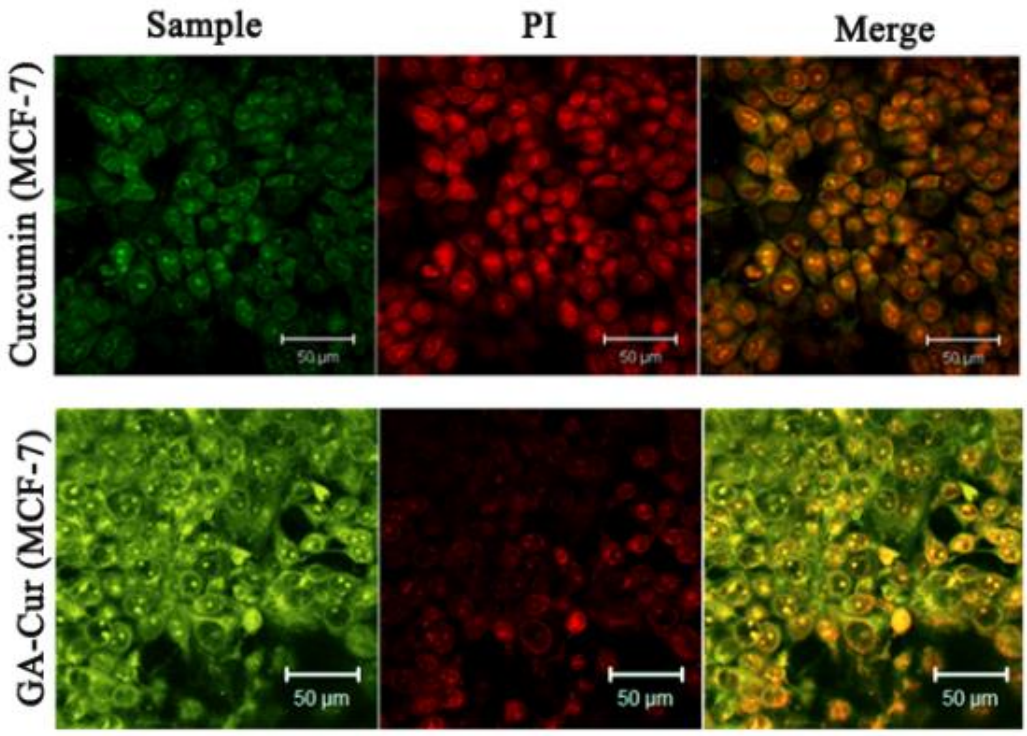

Figure 3. 34 Intracellular uptake of free curcumin (row 1) and GA-Cur (row 2) by MCF-7 cells observed under CLSM. Signals from curcumin (column 1) and PI (column 2) were separately obtained and merged (column 3). GA-Cur shows higher intensity as a result of increased level of particle internalization compared to free curcumin

3.5 Conclusions

This chapter deals with the preparation and characterization of polysaccharide-curcumin conjugates with and without targeting group. In order to improve solubility and stability of curcumin, it is conjugated to three hydrophilic polysaccharides namely pullulan, alginate and gum arabic. The aim of the study is to use these conjugates for targeted delivery of curcumin to hepatocarcinoma cells. Conjugation of targeting ligand namely, galactosyl moiety to pullulan and alginate is achieved by conjugating the polysaccharides with modified lactobionic acid. Drug conjugates without targeting ligand is also prepared with these two polysaccharides.

Introduction of targeting group ($LANH_2$) enhances the toxicity towards the HepG2 cells in conjugates from pullulan and alginate. Curcumin can be conjugated to pullulan after modification, without losing its anticancer activity, while direct conjugation is possible with alginate due to the presence of acid functional groups. Introduction of $LANH_2$ augmented the solubility of alginate leading to higher amount of curcumin being conjugated to alginate. The conjugate shows more toxicity towards HepG2 cells than the conjugate without $LANH_2$. Curcumin could be directly conjugated to gum arabic which contains glucuronic acid groups in the structure. The conjugate also possesses targeting efficiency towards HepG2 cells due to the presence of galactose moiety in the structure. Thus, conjugate for targeted delivery of curcumin to HepG2 cells could be achieved with minimum synthetic steps in the case of gum arabic. The conjugate from gum arabic also shows the highest solubility and toxicity among the three conjugates owing to the very high solubility of the polysaccharide and higher internalization due to the presence of galactose moiety.

CHAPTER 4
NANOGELS

This chapter describes the second class of nanomaterials prepared for the delivery of curcumin. Nanogels are prepared by the cross-linking of polysaccharide and protein by inverse miniemulsion technique. Details of preparation, characterization and drug delivery applications of alginate aldehyde-gelatin and gum arabic aldehyde-gelatin nanogels are described here.

4.1 Introduction

The increasing interest on nanoscale materials with biocompatibility, biodegradability and nontoxicity has accelerated research on development of new nanomaterials and new synthetic routes. Nanogels are one such class of materials which bagged great attention from different areas of biology, chemistry, physics and medicine because of their unique properties offered by its nano size (Oh, Drumright, Siegwart, & Matyjaszewski 2008). Nanogels, formed from physically or chemically cross-linked polymer networks posses unique features such as small size, large surface area, colloidal stability and high drug loading capacity (A. V. Kabanov & S. V. Vinogradov 2009, Raemdonck, Demeester, & De Smedt 2009, Rejinold et al. 2012, Shah, Desai, Patel, & Singh 2012). Because of their potential as versatile carriers for different therapeutic and diagnostic agents, nanogels find applications in biomedical fields, such as gene delivery, drug delivery and bioimaging (Ferreira, Gama, & Vilanova 2013, Alexander V Kabanov & Serguei V Vinogradov 2009, Wu & Zhou 2009).

Nanogel particles have been developed by different approaches such as physical self assembly, homogeneous or heterogeneous polymerization of monomers, cross-linking of preformed polymers, microfluidics, micromolding, photolithography, precipitation polymerization and inverse emulsion polymerization (Alexander V Kabanov & Serguei V Vinogradov 2009, Oh et al. 2008).

Nanogels have been prepared using synthetic as well as natural polymers. Although synthetic polymers like poly(ethylene glycol) (Ding et al. 2011), poly(lactic acid) (W. C. Lee et al. 2006) and poly(ε-caprolactone) (Musyanovych, Schmitz-Wienke, Mailänder, Walther, & Landfester 2008) proved their ability as suitable materials for the development of nanogels, natural polymers like chitosan (Brunel et al. 2009), dextran (Van Thienen et al. 2005) and hyaluronic acid (H. Lee, Mok, Lee, Oh, & Park 2007) received more importance owing to their nontoxicity, biocompatibility and biodegradability. Jayakumar and coworkers developed pH responsive chitin and chitosan nanogels and examined their viability for drug delivery to cancer cells, gene therapy, biosensing and bioimaging (Jayakumar et al. 2010, Jayakumar, Nair, Rejinold, Maya, & Nair 2012, Mangalathillam et al. 2012, Rejinold N, Chennazhi, Tamura, Nair, & Rangasamy 2011) applications.

Self assembled nanogels from hydrophilic biopolymers namely, pullulan, chitosan and dextran were prepared by attaching hydrophobic moieties such as cholesterol, deoxycholic acid and bile acid to the polymer backbone (Hirakura et al. 2004, I. Lee & Akiyoshi 2004, Na, Park, Jo, & Lee 2006). Daoud-Mahammed et al reported nanoassemblies of lauryl-modified dextran and β-cyclodextrin polymers (S Daoud-Mahammed et al. 2007). Pullulan, a highly hydrophilic polysaccharide was hydrophobically modified with cholesterol/spiropyrane and self assembled nanogels were prepared from the resultant amphiphilic polysaccharide (Hirakura et al. 2004, I. Lee & Akiyoshi 2004).

In the present work, nanogels from two polysaccharides namely, gum arabic and alginate by cross-linking with gelatin are developed. The first section deals with the preparation, characterization and application of nanogels from alginate and gelatin. The second section describes the preparation, characterization and applications of nanogels from gum arabic and gelatin.

4.2 Nanogels based on alginate aldehyde and gelatin

Nanogels are developed from alginate aldehyde (Alg Ald) and gelatin (Gel) by an inverse miniemulsion technique. Inverse miniemulsion technique is a less energy intensive method for the formation of nanogels. Nanomaterials such as polymeric nanoparticles, drug nanocrystals, semiconductors and magnetic particles have been prepared by this technique (Munshi, De, & Maitra 1997, Nesamony & Kolling 2005, Sato, Ohtsu, & Komasawa 2000, Sims et al. 2002). Inverse miniemulsion can be obtained very easily by gentle mixing of appropriate amounts of water, oil and surfactant(s). The ease with which miniemulsion can be achieved makes it a preferred technique for nanoparticle synthesis. Spontaneously formed miniemulsions constitute of uniform sized droplets or particles and possess narrow size distribution and spherical or near-spherical shape (Pileni 1997).

Alginate is a polyanionic polysaccharide with β-D-mannuronic acid and α-L-guluronic acid repeating units and is a proven biomedical polymer. Alginate forms gels in the presence of divalent cations, in aqueous medium and these gels are used in drug delivery applications. However, in a recent study, Chan et al report that the Ca^{2+} ions used for cross-linking alginate gels can be immunostimulatory in a dose dependant manner (Chan & Mooney 2013). In order to understand the role of extracellular matrix on adipose tissue formation and vascularization, photo cross-linkable RGD-alginate hydrogels were prepared (Chandler et al. 2011). Alginate aldehyde hydrogels have also been used for adipose tissue engineering (W. S. Kim et

al. 2012). Alginate–chitosan nanoparticles were prepared for the delivery of antimicrobial agents to treat cutaneous pathogens (Friedman et al. 2013).

Gelatin, a protein obtained from collagen has been identified as a biomaterial in various biomedical applications. Even though gelatin nanogels are prepared by the routes mentioned above, researchers are interested to develop methods by which the toxic cross-linking agents can be avoided. The latest development in this direction is the preparation of gelatin nanogels using miniemulsion technique by cross-linking of gelatin by genipin, a naturally occurring cross-linking agent for proteins (Choubey & Bajpai 2010). But, very high cost of genipin may limit the applicability of the process. Even though reports are available on nanoparticles prepared individually from gelatin and alginate, as mentioned above, the possibility of preparing nanogels by self cross-linking of these two biopolymers are yet to be investigated. Hence in the present work, preparation of alginate aldehyde cross-linked gelatin nanogels using inverse miniemulsion technique is attempted. Introduction of aldehyde functionality on alginate and utilization of it for gelatin cross-linking offers a facile route for the preparation of cross-linked Alg Ald-Gel nanogels. Cross-linking leading to nanogel formation can occur between aldehyde groups in Alg Ald and free amino groups in gelatin in presence of borax. Balakrishnan et al have developed injectable *in situ* forming alginate aldehyde–gelatin hydrogel scaffolds for wound dressing applications by avoiding extraneous cross-linking agents (Balakrishnan & Jayakrishnan 2005).

In the present work, stable inverse miniemulsions are prepared by sonication of noncontinuous aqueous phase (mixture of alginate aldehyde and gelatin) in a continuous organic phase (Span 20 dissolved in cyclohexane). Cross-linking occurred between alginate aldehyde (Alg Ald) and gelatin (Gel) in presence of borax by Schiff's base reaction during the formation of inverse miniemulsion. Since the cross-linking takes place in inverse miniemulsion, the process would result in the formation of cross-linked nanogels instead of the macroscopic hydrogels.

The effects of surfactant (Span 20) concentration and volume of the aqueous phase on the size of the alginate aldehyde-gelatin (Alg Ald-Gel) nanoparticles are studied. Nanogels are characterized by DLS, FT-IR spectroscopy, TGA, SEM and TEM. DLS, TEM and SEM studies demonstrated nanosize and spherical morphology of the nanogels. Hemocompatibility and *in vitro* cytocompatibility analysis of the nanogels proved their nontoxicity.

Nanogels are an important class of nanomaterials for the delivery of hydrophobic therapeutic agents (Alexander V Kabanov & Serguei V Vinogradov 2009). Nanogels prepared from biodegradable polymers are excellent candidates for drug delivery applications since they protect the encapsulated drugs from degradation, provide controlled release over extended periods of time and improve the therapeutic index of the loaded drug (Oh et al. 2007). In the present study, Alg Ald-Gel nanogels are prepared for the delivery of the hydrophobic drug, curcumin. Curcumin is encapsulated in Alg Ald-Gel nanogel for improving its therapeutic efficacy to cancer cells. The properties of curcumin loaded nanogels are also analyzed by DLS, SEM, NMR and TGA. Anticancer potential of curcumin loaded nanogels is examined in MCF-7 cells. The results prove the suitability of the curcumin loaded alginate aldehyde-gelatin nanogels for delivery of curcumin to breast cancer cells.

4.2.1 Results and discussions

4.2.1.1 Preparation of bare and curcumin loaded Alg Ald-Gel nanogels

Alginate aldehyde–gelatin hydrogels have been reported in the literature for various biomedical applications. Jayakrishnan and coworkers have reported the efficacy of *in situ* forming alginate aldehyde-gelatin hydrogels for wound healing, as an injectable drug delivery vehicle and as a sealant for polyester vascular graft (Balakrishnan & Jayakrishnan 2005, Balakrishnan et al. 2005, Saraswathy Manju, Muraleedharan, Rajeev, Jayakrishnan, & Joseph 2011). Recently, Sarkar et al

reported the development of alginate aldehyde-gelatin hydrogel microcapsules for tissue engineering (Sarker et al. 2014). The application of alginate aldehyde-gelatin hydrogels for myocardial infarction repair has been demonstrated recently (Bai et al. 2013). Even though alginate aldehyde-gelatin hydrogels have been extensively investigated for various applications; reports are not found on its nanoscopic counterparts.

The main objective of the current study is to prepare nanoscale alginate aldehyde-gelatin hydrogels. An inverse miniemulsion technique is adopted for preparing cross-linked Alg Ald-Gel nanogels. These nanoscopic counter parts are formed by an inverse miniemulsion process involving Schiff's base reaction between aldehyde groups and $-NH_2$ groups. Aldehyde functionality for cross-linking with $-NH_2$ groups of gelatin is introduced on alginate by periodate oxidation. Periodate cleaves the vicinal diols present in the polysaccharide resulting in dialdehyde functionalities. The FT-IR spectra of Alg Ald and alginate are shown in Figure 4.1. In the spectrum of Alg Ald (Figure 4.1b), a characteristic aldehyde peak at 1746 cm^{-1} is seen which is not present in the spectrum of alginate (Figure 4.1a), there by confirming the oxidation. Aldehyde content in 30 % oxidized Alg Ald is estimated by tirtimetry and is found to be 3.5×10^{-3} mol/g. The cross-linking reaction with gelatin (gel formation) becomes too fast if highly oxidized Alg Ald (50 %) is chosen and may result in macroscopic gel. Hence, 30 % oxidized alginate is used for nanogel preparation.

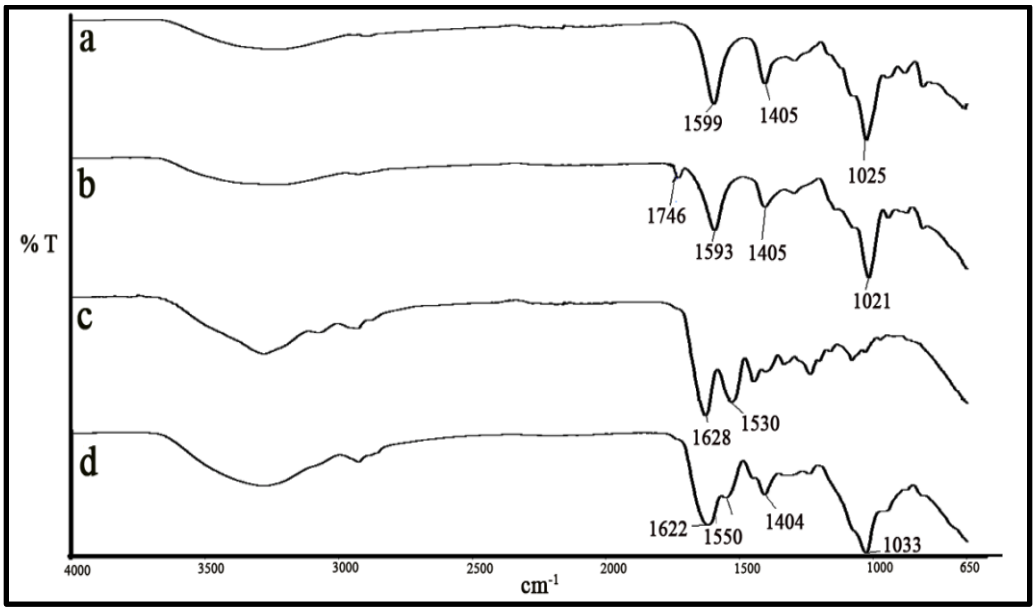

Figure 4.1 FT-IR spectra of alginate (a), 30 % oxidized Alg Ald (b), gelatin (c) and Alg Ald-Gel nanogel (d). In the spectrum of Alg Ald, a new peak at 1746 cm^{-1} corresponds to aldehyde functionality

Scheme 4.1 represents preparation of Alg Ald-Gel nanogels through inverse miniemulsion process. According to Landfester et al, an inverse miniemulsion contains hydrophilic droplets as dispersed phase in hydrocarbon solution of surfactant as the continuous phase (Katharina Landfester, Willert, & Antonietti 2000). In the present work, cyclohexane is used as continuous phase, Span 20 as surfactant and aqueous mixture of Alg Ald and gelatin as non continuous phase. Alg Ald with 30 % oxidation is selected for the reaction, because sufficient aldehyde content is required for cross-linking. Alg Ald solution (10 % solution, (w/v)) is prepared in 0.1 M borax (pH 9.4) which provided alkaline pH. The hydroxyl groups of Alg Ald complexes with borate which is formed by the dissociation of borax in aqueous medium (Strauss & Kral 1982). If gelatin is added to this Alg Ald/borax complex, Schiff's base reaction occurs between aldehyde groups of Alg Ald and amino groups of gelatin and macroscopic hydogel would be formed in less than 1 min (Balakrishnan & Jayakrishnan 2005). Therefore in the present work, the mixture is added to surfactant containing cyclohexane before forming hydrogel and sonicated for 5 min to obtain

inverse miniemulsion. Inverse miniemulsion is formed when the aqueous Alg Ald-Gel mixture is dispersed in continuous cyclohexane phase. Ultrasonication is selected for the dispersion, since it is a very efficient method to reduce the size of the droplets. Initially, polydispersity of the Alg Ald-Gel droplets would be high, later during ultrasonication, polydispersity would decrease due to constant fusion and fission process (K Landfester 2006). Span 20, the surfactant dissolved in cyclohexane stabilizes the resultant Alg Ald-Gel droplets from growth by collision, coalescence and Ostwald ripening. Cross-linked Alg Ald-Gel nanoparticles are formed inside the surfactant micelle.

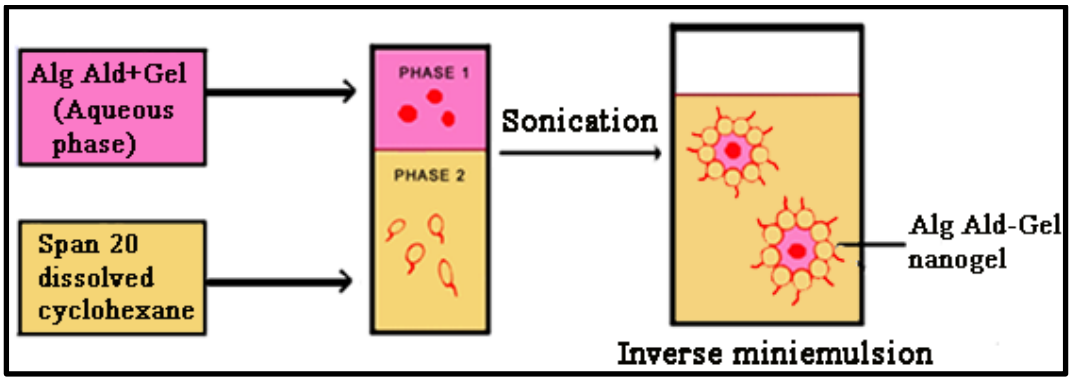

Scheme 4.1 Formation of inverse miniemulsion from Alg Ald and Gel. Cross-linking occurs due to Schiff's base reaction between aldehyde groups of Alg Ald and amino groups of gelatin

The size of the nanogel can be tuned by modulating certain parameters. Landfester et al reported that amount of surfactant determines droplet area and hence the particle size at constant ultrasonication time (Katharina Landfester, Bechthold, Tiarks, & Antonietti 1999). The impact of surfactant/water ratio on particle size by changing the amount of surfactant at constant ultrasonication time and amplitude is investigated. The particle size of the nanogels can be varied over a wide range by changing the amount of the surfactant. From Table 4.1, it is clear that when surfactant concentration is increased, keeping the volume of aqueous phase constant, the size of the nanogel particles decreased. Initially, the surfactant Span 20 dissolved in cyaclohexane, self assembled to micelle and when the aqueous Alg Ald-Gel mixture

is added to cyclohexane and agitated by sonication, droplets of Alg Ald-Gel are formed. Then the nanosized droplets get engulfed by the surfactant micelle and stabilize the nanogel droplets from coalescence and Ostwald ripening. Small droplets undergo very fast collision and if the surfactant amount was less (1 % with respect to the organic phase), the stabilization is decreased and the droplets combined to a big droplet resulting in increased particle size. When the concentration of surfactant increased to 3 %, the particle size is again decreased because more amount of surfactant is available to stabilize the small droplets.

Table 4.1. Effect of volume of aqueous phase and concentration of surfactant on size of the nanogel particles. With increase in concentration of surfactant, particle size decreases and increases with increase in volume of aqueous phase

Amount of surfactant with respect to organic phase (w/v, %)	Total volume of aqueous phase (μL)	Volume of organic phase (mL)	Size (nm) of nanogel in cyclohexane
1	250	10	193 ± 8
1	500	10	240 ± 9
1	750	10	256 ± 7
2	250	10	127 ± 6
2	500	10	168 ± 9
2	750	10	235 ± 5
3	250	10	103 ± 8
3	500	10	172 ± 9
3	750	10	200 ± 7

Parameters such as volume of the aqueous phase also have an impact on the size of Alg Ald-Gel nanogels. Impact of volume of aqueous phase (Alg Ald and gelatin) in the emulsion on the size of the nanogel particles is investigated by maintaining constant surfactant concentration against the aqueous phase to ensure that the same amount of surfactant surrounded the water droplets. Total volume of aqueous phase is varied from 250 μL to 750 μL by keeping the organic phase volume as 10 mL. The size of the nanogel particles is analyzed by DLS and is shown in Table 4.1. From the table, it can be seen that size of the nanogels increased with increase in volume of aqueous phase when surfactant concentration is kept constant.

Even though the combination with surfactant amount 3 % gave nanogels with very small size, the combination which resulted in the smallest nanogels with medium amount of surfactant (surfactant concentration 2 % with total volume of aqueous phase as 500 μL (250 μL of gelatin and 250 μL of Alg Ald) and size 168 ± 9 nm is selected for curcumin loading and further studies.

Nanogel particles are isolated by precipitating the inverse emulsion in acetone, followed by centrifugation. The particles are washed many times with water to remove the impurities and surfactants and finally dried under reduced pressure to obtain nanogel in powder form. Curcumin is encapsulated inside the nanogels by precipitating the nanogels in acetone containing dissolved curcumin.

Intermolecular hydrogen bonding exists between curcumin and Alg Ald-Gel nanogel and drives the encapsulation of curcumin inside the nanogel. Schematic representation of intermolecular hydrogen bond interaction between curcumin and nanogel is shown in Scheme 4.2. Alginate aldehyde contains unreacted –OH functionalities in its structure. These hydroxyl groups interacts with –OH terminal groups of curcumin through end-end hydrogen bonding (Mangalathillam et al. 2012) facilitating encapsulation of curcumin within the nanogel.

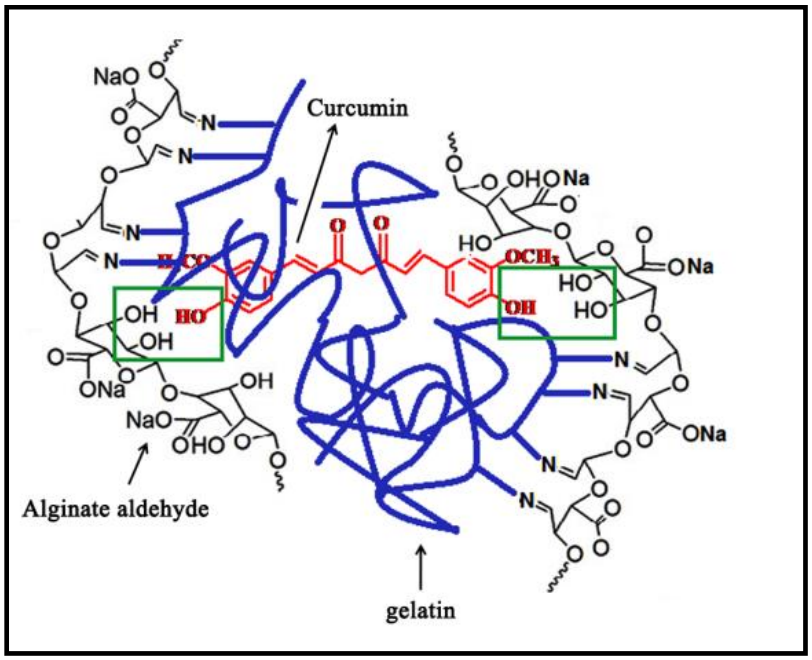

Scheme 4.2 Representation for the possible mechanism of interaction between curcumin and Alg Ald-Gel nanogel

For the successful delivery of the drug, nanoparticles should remain in the blood stream for a considerable duration of time. Size and surface characteristics of the nanoparticles control the fate of the injected nanoparticles. Size should be large enough to avert their diffusion into blood capillaries. Cancer cells demand neovascularization which leads to imbalance of growth factors and matrix metalloproteinase. This make the tumors disorganized and amplified with enormous pores showing expanded gap junctions between endothelial cells and compromised lymphatic drainage. These features constitute enhanced permeability and retention effect which helps to accumulate nanoparticles inside the tumors (Cho, Wang, Nie, & Shin 2008). Many of the solid tumors have enhanced vascular permeability. Vasculature of tumors may vary from 100-600 nm (Cho et al. 2008). Hence the ideal size of the nanopartice designed for drug delivery to tumor cells should be in between 100-600 nm.

4.2.1.2 Characterization of bare and curcumin loaded Alg Ald-Gel nanogels

FT-IR spectra of the dried nanogel (Figure 4.1d) powder samples are recorded in the range of 400–4000 cm^{-1}. Absorption bands from both gelatin and Alg Ald are seen in the spectrum. Aldehyde peak at 1746 cm^{-1} is not seen in the spectrum of nanogel, indicating the cross-linking between Alg Ald and gelatin (Figure 4.1c). In the spectrum of Alg Ald-Gel nanogel (Figure 4.1d), the peak at 1622 cm^{-1} corresponds to the -C=N group (Schiff's base) formed between aldehyde and amino groups (Issa et al. 2008, Ye et al. 2012). This –C=N band is broad due to the overlap of amide I band at 1628 cm^{-1} of gelatin. Amide II band at 1530 cm^{-1} of gelatin is shifted to 1550 cm^{-1} in nanogel and confirms the involvement of amino group in Schiff's base formation (Sarker et al. 2014). The peak observed at 1033 cm^{-1} in the spectrum of nanogel corresponds to Alg Ald. All these observations confirm the formation of cross-linked nanogels.

TGA curves of Alg Ald, gelatin, curcumin and nanogels are shown in Figure 4.2. The first degradation step of Alg Ald (Figure 4.2b) occurs in the range of 50-100 °C, which corresponds to the elimination of absorbed and bound water from Alg Ald. The second degradation step due to the structural degradation of the main chain starts at 250 °C. Gelatin also exhibits three degradation steps (Figure 4.2a). First step corresponds to elimination of water in the region of 50-100 °C and the second and third steps are due to the breakage of protein chain and peptide bond rupture (Cai & Kim 2010). It can be seen from the thermograms that the nanogel (Figure 4.2c) shows a significantly different thermal behavior. Thermal stability of the nanogel is lower than that of Alg Ald, but higher than that of gelatin. Curcumin doesn't show any stage of water loss upto 200 °C owing to its high hydrophobicity. Curcumin (Figure 4.2e) shows a gradual weight loss with first weight loss at 230 °C and second at 381 °C. However, Alg Ald-Gel nanogels (Figure 4.2c) show first degradation at 92 °C indicating the water loss. Curcumin loaded nanogels (Figure 4.2d) and bare nanogels

show almost similar weight loss pattern. Curcumin encapsulation does not alter thermal degradation pattern of the nanogels.

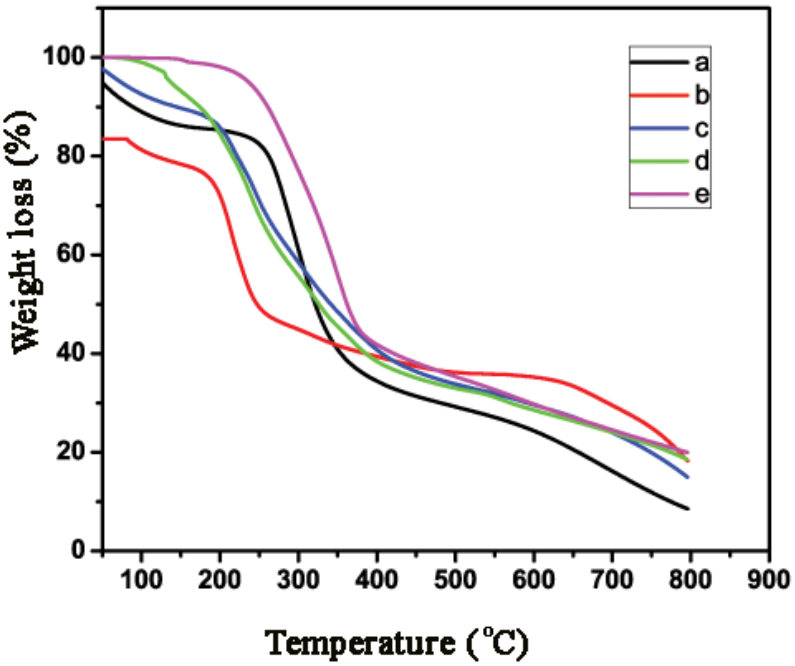

Figure 4.2 TGA curves of gelatin (a), Alg Ald (b), Alg Ald-Gel nanogel (c), curcumin loaded Alg Ald-Gel nanogel (d) and curcumin (e)

Proton nuclear magnetic resonance spectroscopy (^{1}H NMR) is used to obtain the ^{1}H-NMR spectra of curcumin (Figure 4.3a) and curcumin loaded Alg Ald-Gel nanogels (Figure 4.3b). Characteristic peaks of curcumin are seen in the region between 6-8 ppm. Proton peaks from $-CH_3$ groups of curcumin are seen at 3.28 ppm. Thus, curcumin loaded nanogels show peaks characteristic for curcumin. Since curcumin is encapsulated inside the nanogel, the intensity of the peaks corresponding to curcumin is less in the nanogel compared to that observed in the spectrum of free curcumin.

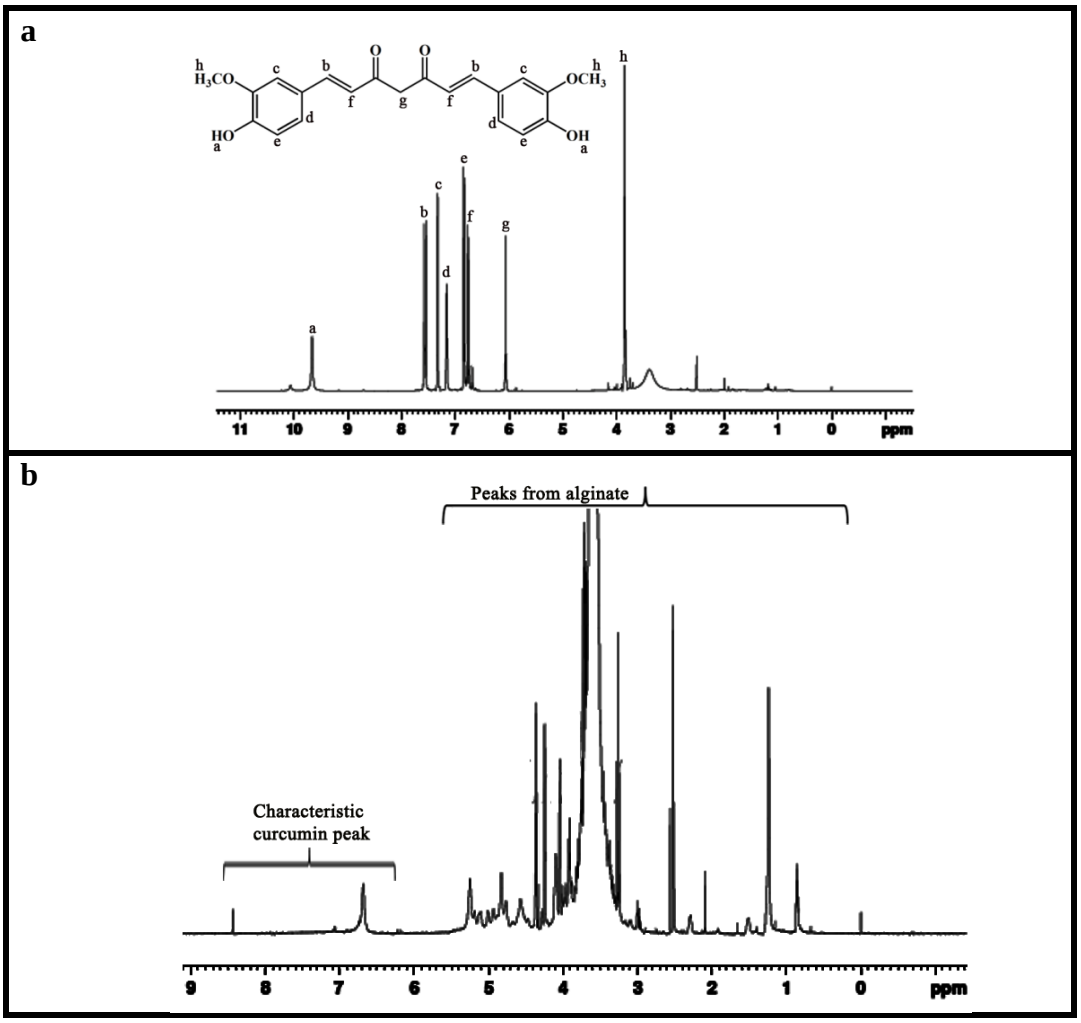

Figure 4.3 ^{1}H NMR spectra of curcumin (a) and curcumin loaded Alg Ald-Gel nanogel (b)

These chemically cross-linked Alg Ald-Gel nanogels and curcumin loaded Alg Ald-Gel nanogels could be redispersed in water without the use of additional surfactant, since Alg Ald contain carboxylic acid groups which provide negative zeta potential to stabilize nanoparticles. Figure 4.4 shows curcumin loaded nanogel (Figure 4.4a) and bare Alg Ald-Gel nanogels (Figure 4.4b) dispersed in water. Particle sizes of the water redispersed nanogels are measured by DLS. Alg Ald-Gel nanogels show hydrodynamic diameter of 297 ± 6 nm. In aqueous medium, the hydrodynamic diameter of Alg Ald-Gel nanogel is much larger than that in organic solvent, as more water can diffuse into the polymer network of both Alg Ald and

gelatin from the dispersion medium to occupy the channels or to the free volume in between the polymer strands until it become fully swollen. Curcumin encapsulation increases the size of the nanogels and it is in the range of 431 ± 3 nm.

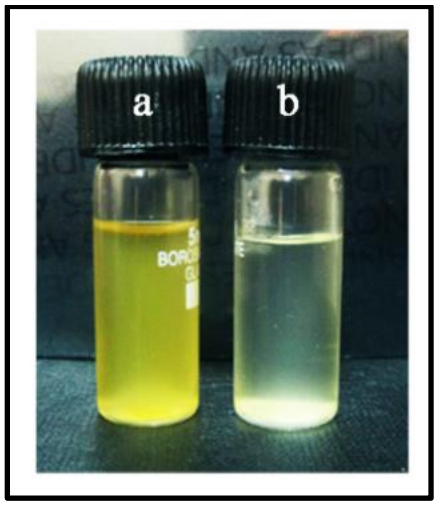

Figure 4.4 Curcumin loaded Alg Ald-Gel nanogel (a) and bare Alg Ald-Gel nanogel (b) redispersed in water

Another important factor that determines the fate and life span of nanoparticles during their circulation in blood stream is their surface characteristics. In order to escape from the macrophages capture, nanoparticle must possess hydrophilic surface (Moghimi & Szebeni 2003). Nanoparticles with positive surface charge and hydrophobic surface promote protein adsorption and *reticuloendothelial clearance* (REF) (Gessner et al. 2000) as already explained in the previous sections. Hence nanoparticles prepared from hydrophilic polymers carrying negative surface charges are considered to be ideal candidates for successful drug delivery to cancer cells. Bare Alg Ald-Gel nanogels showed a zeta potential of -36 ± 3 mV indicating good stability of the nanogels. Curcumin loading does not alter the zeta potential and it also shows zeta potential of -36 ± 5 mV. Negative surface charge of the nanogels is due to the charge density of Alg Ald at neutral pH since at this pH, all the acid groups in Alg Ald remain deprotonated. High negative zeta potential indicates good stability of the nanogels.

4.2.1.3 Morphology analysis of bare and curcumin loaded Alg Ald-Gel nanogels

Morphology of the Alg Ald-Gel nanogels as obtained in inverse miniemulsion and after redispersion in water are analyzed by SEM. Figure 4.5 shows SEM image of as obtained nanogels formed in the miniemulsion. All the particles have spherical morphology with a smooth surface and diameter of about 120-147 nm.

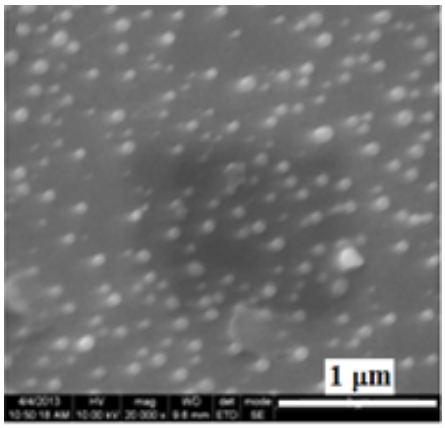

Figure 4.5 SEM image of Alg Ald-Gel nanogels as formed in miniemulsion

Morphology of the redispersed particles is also analyzed by SEM and TEM to investigate the change in size and shape due to redispersion in water. Figure 4.6a and 4.6b show respectively the SEM and TEM images of the redispersed particles after drying. Redispersed nanogels show an average size of 200 nm in SEM.

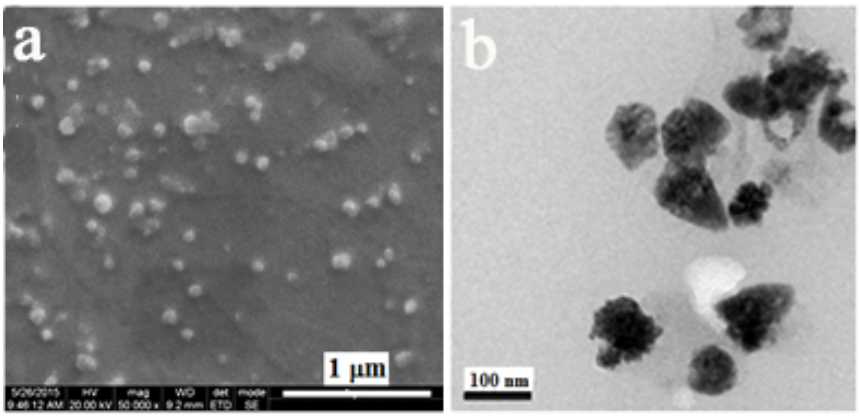

Figure 4.6 SEM (a) and TEM (b) images of the Alg Ald-Gel nanogels, after redispersion in aqueous medium

On redispersion in water, slight increase in size was observed due to the swelling of the nanogels and was found to be 297 nm by DLS measurement. Curcumin loading doesn't alter the morphology of Alg Ald-Gel nanogels and it also shows spherical morphology. The size of the curcumin loaded Alg Ald-Gel nanogels (Figure 4.7) obtained from SEM is in the range of 320-390 nm.

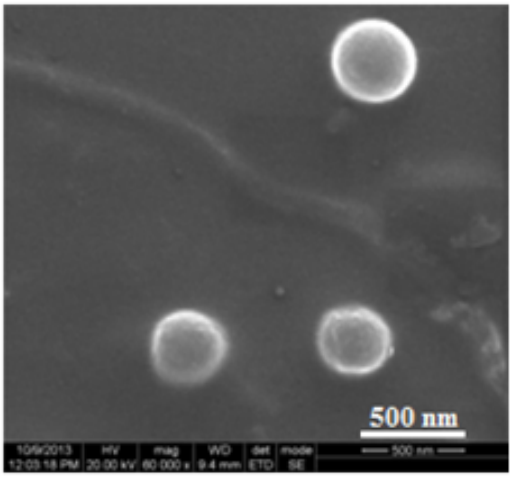

Figure 4.7 Curcumin loaded Alg Ald-Gel nanogels after redispersing in the aqueous medium

4.2.1.4 Encapsulation and loading efficiencies of curcumin loaded Alg Ald-Gel nanogels

The encapsulation and loading efficiencies of curcumin loaded Alg Ald -Gel nanoparticles are calculated by estimating the curcumin present in the supernatant by UV-visible spectrometer at 430 nm. Curcumin encapsulation and loading efficiencies of the nanogels are 72 ± 2 % and 1.4 ± 0.03 % respectively.

4.2.1.5 Curcumin release studies of curcumin loaded Alg Ald-Gel nanogels

In vitro curcumin release from Alg Ald-Gel nanogel is performed in buffer of pH 7.4 and 5 (Anitha, Deepagan, Rani, et al. 2011). The curcumin release profile is shown in Figure 4.8. Initially, a burst release is observed over a period of 5 h followed by a controlled release up to 48 h. The reason for initial burst release may be

the delivery of curcumin adsorbed on to the surface of the nanogel. Almost 70 % of the curcumin is released in this period at acidic pH. Higher curcumin release is observed at acidic pH compared to neutral pH. Hence curcumin loaded Alg Ald-Gel nanogel is suitable for the delivery of the encapsulated drug in tumor cells, since these cells have acidic environment attributed to the accumulation of metabolic products in these cells due to poor blood vessel architecture.

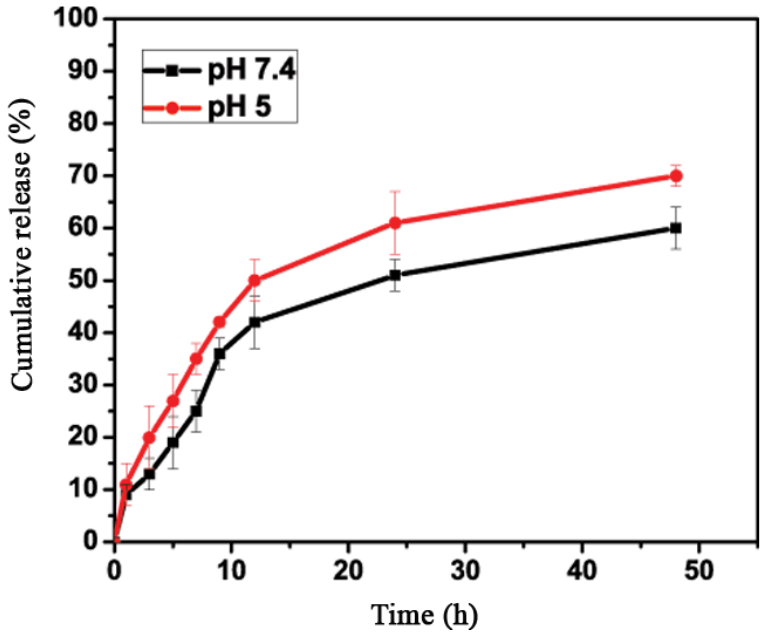

Figure 4.8 *In vitro* curcumin release patterns from Alg Ald-Gel nanogel at pH 5 and 7.4

4.2.1.6 Hemolysis assay of bare and curcumin loaded Alg Ald-Gel nanogels

Since the nanogels are designed for drug delivery applications, hemolysis test is conducted to study the compatibility of the nanogels with blood cells. Initially, nanogels interact with a large fraction of blood cells in the blood, preceding to distribution into tissues. An ideal nanocarrier for drug delivery should possess long-term stability and minimum interaction with blood components in the bloodstream. The results of hemolysis test of curcumin loaded Alg Ald-Gel nanogels with equivalent curcumin concentrations (3.1-50 μg/mL) are shown in Figure 4.9. From the figure, it can be seen that percentage hemolysis of curcumin loaded nanogels is

below 5 %, the critical safe hemolytic ratio for biomaterials according to ISO/TR 7406 (S.-R. Yu, Zhang, He, Liu, & Liu 2004). Percentage hemolysis of curcumin loaded Alg Ald-Gel nanogels is greater than that of the percentage hemolysis of bare Alg Ald-Gel nanogel (Figure 4.9) (Sarika, Kumar, Raj, & James 2015). Curcumin loading induces slight toxicity to the RBC cells but it is far below the critical safe hemolytic ratio for biomaterials.

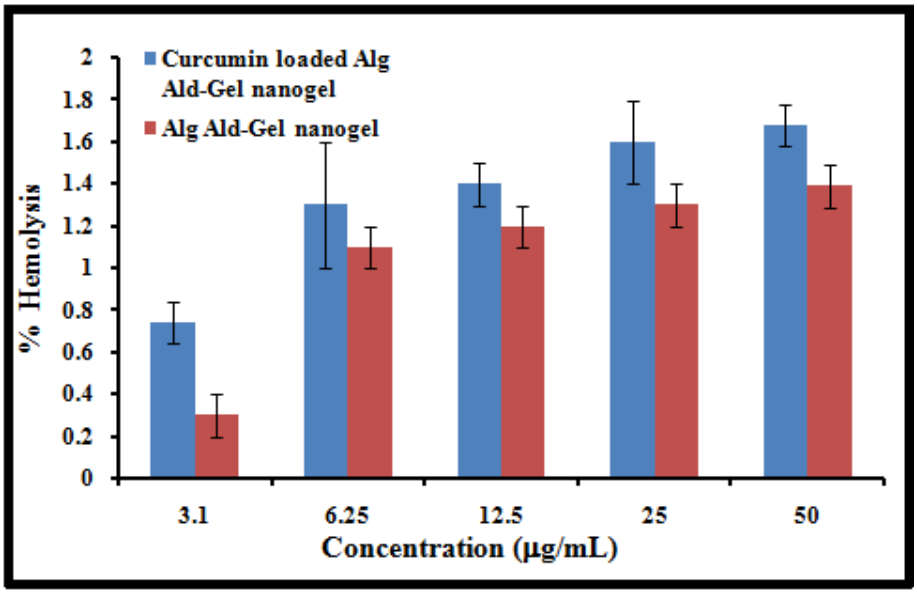

Figure 4.9 Hemolysis assay of bare and curcumin loaded Alg Ald-Gel nanogels with equivalent curcumin concentration of 3.1 to 50 µg/mL in PBS. Positive control, Na_2CO_3 (0.1 %) shows 100 % hemolysis, which is not included in the graph

4.2.1.7 *In vitro* cytotoxicity studies

In vitro anticancer activity of bare and curcumin loaded Alg Ald-Gel nanogels are evaluated by MTT assay in human breast carcinoma cells (MCF-7) and the results are shown in Figure 4.10. The cells are incubated with various concentrations of free curcumin and curcumin loaded nanogels with equivalent curcumin concentrations ranging from 3.1 to 50 to µg/mL for 24 h and cell activity is evaluated by MTT assay. Concentration of bare Alg Ald-Gel nanogels ranged from 3.1-50 mg/mL. From Figure 4.10, it is clear that curcumin shows toxicity to MCF-7 cells from doses 50 to 6.25

μg/mL. Free curcumin is nontoxic to the cells at the lowest dose (3.1 μg/mL). Curcumin loaded nanogels exhibit lower toxicity towards MCF-7 cells in all the concentrations compared to free curcumin. Since free curcumin is dissolved in DMSO it is more available to the cells than that present in the nanogels. Mangalathillam et al also observed similar results that curcumin loaded nanogels are less toxic to the cancer cells than that of free curcumin dissolved in organic solvent at equivalent doses (Mangalathillam et al. 2012). This may be due to the controlled release of curcumin from Alg Ald-Gel nanogels and slow uptake of curcumin loaded Alg Ald-Gel nanogels. Bare Alg Ald-Gel nanogels show nontoxicity towards MCF-7 cells in all the tested concentrations (Sarika et al. 2015). Curcumin loaded nanogels manifested a decrease in cell viability from 77 % to 24 % when the concentration of curcumin was changed from 3.1-50 μg/mL. Whereas percentage cell activity of free curcumin treated MCF-7 cells was diminished from 69 % to 6 %. IC_{50} values of free curcumin and curcumin loaded Alg Ald-Gel nanogels in MCF-7 cells are 3.8 μg/mL and 5.6 μg/mL respectively.

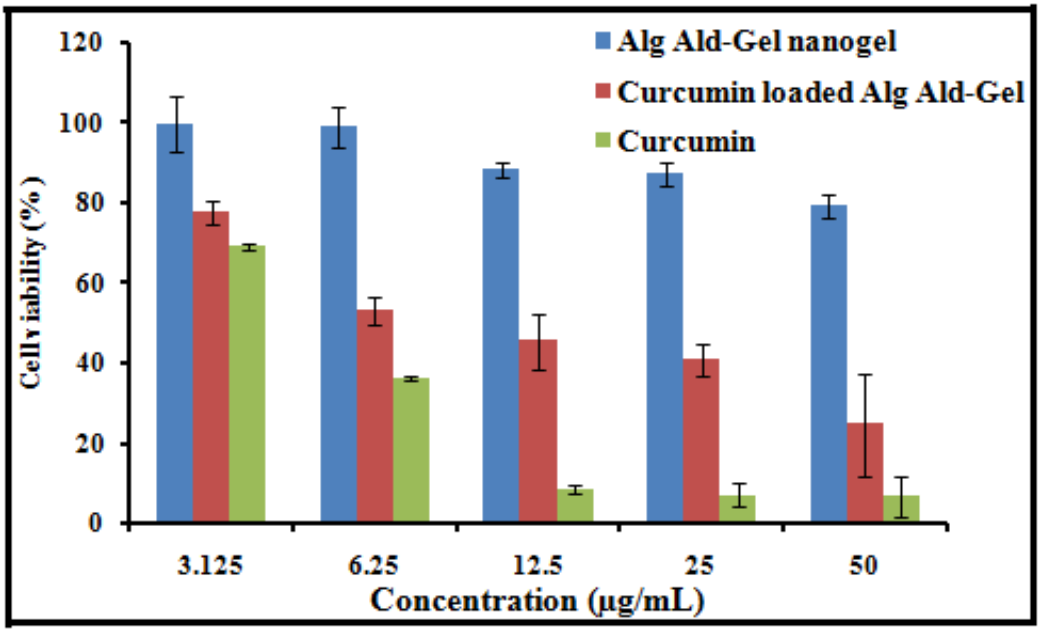

Figure 4.10 *In vitro* cytotoxicity of bare and curcumin loaded Alg Ald-Gel nanogels towards MCF-7 cells

4.2.1.8 Intracellular uptake studies

The intracellular uptake ability of the curcumin loaded Alg Ald-Gel nanogels are performed in MCF-7 cells for 24 h. CLSM images of the intracellular uptake in MCF-7 cells by curcumin and curcumin loaded Alg Ald-Gel nanogels are shown in Figure 4.11. Nucleus of the cells is counter stained with propidium iodide. Both curcumin and curcumin loaded Alg Ald-Gel nanogels show intracellular uptake. Since curcumin is present inside the nanogel it is protected from degradation and hydrolysis in physiological ambience. In addition to that, the nanosize of the nanogel also promotes accumulation in MCF-7 cells by enhanced permeation and retention (EPR) effect.

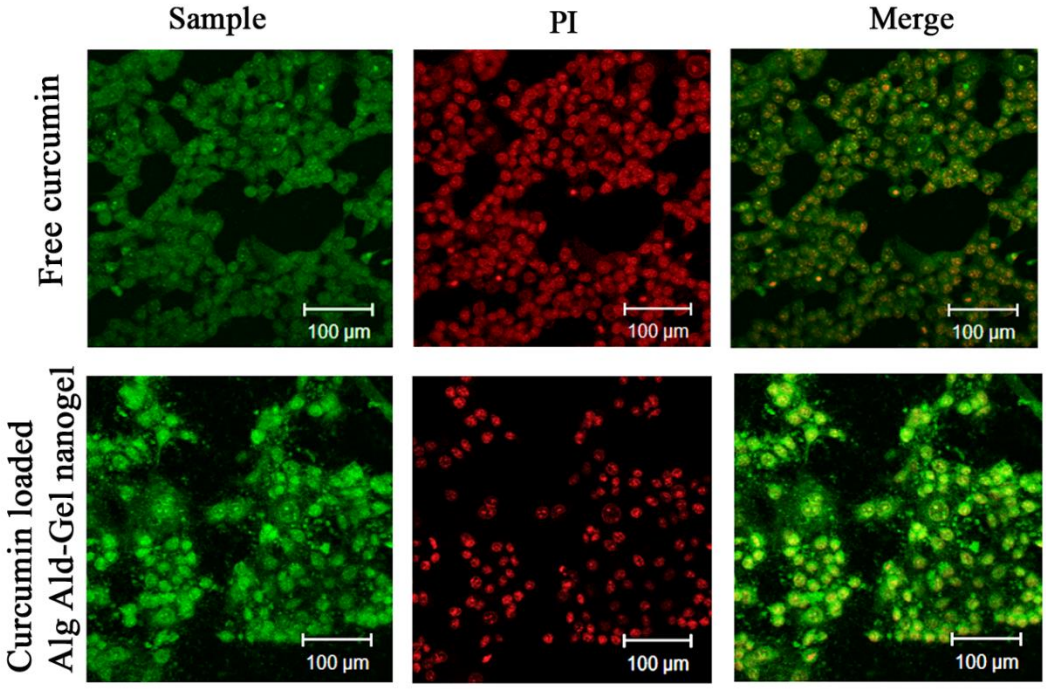

Figure 4.11 Intracellular uptake of curcumin loaded Alg Ald-Gel nanogels (row 1) and curcumin (row 2) by MCF-7 cells observed under CLSM. Signals from curcumin (column 1) and PI (column 2) were separately obtained and merged (column 3)

Thus, curcumin loaded Alg Ald-Gel nanogel should be a promising drug delivery system for the treatment of breast cancer.

4.3 Gum arabic aldehyde-gelatin nanogels

The next category of nanogels is prepared from gum arabic aldehyde (GA Ald) and gelatin (Gel). For this, a plant polysaccharide GA is selected to prepare cross-linked nanogels with gelatin.

Gum arabic (GA) is obtained from the exudates of acacia tree. It has a complex branched structure with rhamnose, galactose and glucuronic acid residues. The back bone and side chains consist of 1,3 linked β-D-galactopyranosyl units with side chain joined to the main chain by 1,6 linkages (Verbeken et al. 2003). High water solubility, biocompatibility and low cost are the main attractions for selecting this polysaccharide for this work. GA is widely used in the food industry as stabilizing, emulsifying and thickening agent. Even though GA was used for the preparation of microparticles and nanoparticles, biomedical applications of this potential polysaccharide were not explored in greater detail. Avadi et al developed gum arabic and chitosan based nanoparticle system for oral delivery of insulin (Avadi et al. 2010). Nishi et al prepared oxidized GA and conjugated it with different drugs and evaluated its application in drug delivery (Nishi, Antony, & Jayakrishnan 2007, Nishi, Antony, Mohanan, et al. 2007, Nishi & Jayakrishnan 2004). However no research effort has been made to prepare GA based nanogels. In this work we have prepared nanogels from oxidized gum arabic (GA Ald) and gelatin by fusion of two separate inverse miniemulsions.

For the preparation of GA Ald-Gel nanogels, we adopted fission and fusion of two separate miniemulsions of GA Ald and gelatin. These two miniemulsions contain individual reactants in aqueous phase and during fusion, inter micellar exchange and cross-linking of individual reactants occur leading to the formation of nanogels. Processing parameters such as concentration of surfactant and aqueous fraction in the inverse miniemulsion are optimized to obtain GA Ald-Gel nanoparticles with smallest size. Physicochemical properties of the nanogels are studied and MTT assay is

performed to assess the cytocompatibility of the nanogels. The suitability of the prepared GA Ald-Gel nanogels for curcumin loading is evaluated and their anticancer activity analyzed in MCF-7 cells. Properties of the curcumin loaded nanogels are also evaluated by SEM, DLS, TGA and blood compatibility studies. MTT assay in MCF-7 cells confirmed the toxicity of curcumin loaded GA Ald-Gel nanogels. Cellular uptake of the curcumin loaded nanogels is analyzed by CLSM and the green fluorescence of curcumin confirmed the successful uptake of the drug loaded nanogels inside the cell. The studies indicate that curcumin loaded GA Ald-Gel nanogels could be a potential candidate for curcumin delivery to cancer cells.

4.3.1 Results and discussions

4.3.1.1 Preparation of bare and curcumin loaded GA Ald-Gel nanogels

Nanogels derived from natural polysaccharides are of great interest for drug delivery and controlled release because of their biodegradability, abundance and biocompatibility. Making use of advantages of the inverse miniemulsion technique, cross-linked GA Ald-Gel nanogel is prepared and curcumin is successfully loaded inside the nanogel particle.

Several techniques such as desolvation method (Balthasar et al. 2005), coacervation (Leo, Angela Vandelli, Cameroni, & Forni 1997) and water-in-oil microemulsion techniques (A. K. Gupta, Gupta, Yarwood, & Curtis 2004) have been used to synthesize gelatin nanoparticles. These methods have advantages as well as disadvantages like less yield of nanoparticles in the case of desolvation method, inhomogeneous cross-linking in coacervation and requirement of excess of surfactant in microemulsion technique. To overcome the aforementioned problems and to prepare highly cross-linked GA Ald-Gel nanogels an inverse miniemulsion technique is adopted with GA Ald as cross-linking agent. For preparing GA Ald-Gel inverse miniemulsion, Span 20 is used as surfactant and cyclohexane as continuous phase. An

inverse miniemulsion contains aqueous droplets as dispersed phase in continuous organic phase containing surfactant (Katharina Landfester et al. 2000). It can be prepared very easily by simple mixing of aqueous non continuous phase with continuous organic phase. Nanoparticles prepared by this method adopt spherical morphology with narrow size distribution (Nesamony, Singh, Nada, Shah, & Kolling 2012).

Gelatin nanoparticles cross-linked by the conventional cross-linking agent, glutaraldehyde is already reported in literature (Ethirajan et al. 2008). Here we report the application of a novel cross-linker, gum arabic aldehyde for the preparation of gelatin nanoparticles. Cross-linking of gelatin with gum arabic aldehyde, resulting in macroscopic hydrogels suitable for tissue engineering applications is recently reported (Sarika, Cinthya, Jayakrishnan, Anilkumar, & James 2014). However, the possibility of using such biopolymer aldehydes for the preparation of gelatin naoparticles by miniemulsion technique is yet to be reported. In the present work, GA Ald-Gel nanoparticles are obtained by the fusion of two separate emulsions. Gum arabic is a natural polysaccharide and contains 90 % of arabinogalactan. It is used in food, pharmaceutical and cosmetic industries (Verbeken et al. 2003). The vicinal diols in GA is subjected to periodate oxidation to introduce aldehyde groups needed for the imine bond formation (cross-linking) with amino groups of gelatin. Oxidized GA (GA Ald) is obtained in high yield of 80-85 %. The aldehyde content in 10 % oxidized GA is estimated by titrimetric method and is found to be 1.125×10^{-3} mol/g.

As a synthetic strategy, inverse miniemulsions containing GA Ald droplets (A) and gelatin droplets (B) are prepared separately (Scheme 4.3). GA Ald-Gel nanoparticles are obtained by the fusion of these two separate emulsions. Instead of using a single emulsion, here fusion of two separate miniemulsions is employed for the preparation of cross-linked GA Ald-Gel nanogels. Since the gelation between GA Ald and gelatin occurs within seconds leading to the macroscopic hydrogel, GA Ald-Gel nanoparticles could not be prepared by single inverse miniemulsion technique.

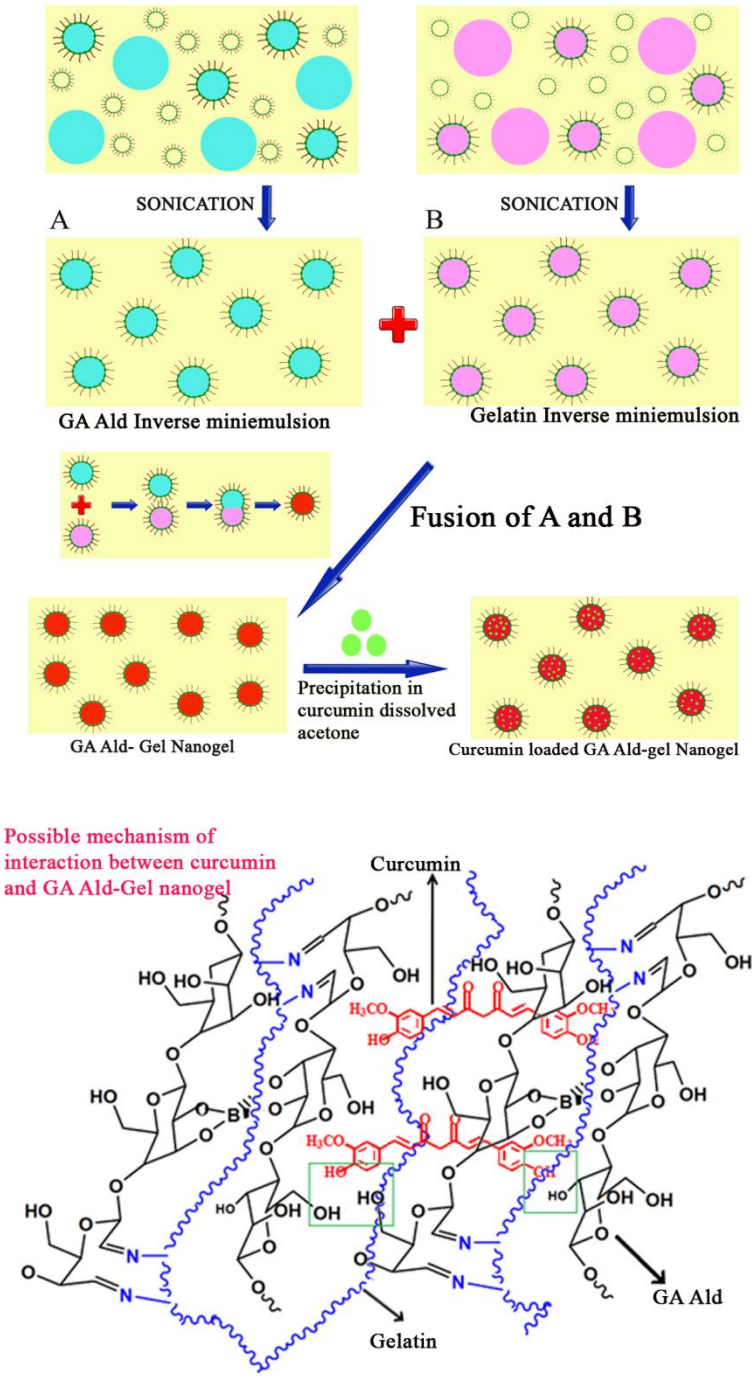

Scheme 4.3 GA Ald-Gel nanogel formation by inverse miniemulsion. Separate miniemulsions are prepared from gelatin (Gel) and gum arabic aldehyde (GA Ald). Later, these emulsions are fused under sonication to obtain cross-linked nanogels. Curcumin is loaded into the nanogels by precipitation. Possible interaction between curcumin and GA Ald-Gel nanogel is also shown in the scheme

For inverse miniemulsion of GA Ald, 10 % solution of gum arabic aldehyde is prepared in 0.1 M borax. Borax provides alkaline pH favorable for the cross-linking between aldehyde groups in GA Ald and amino groups in gelatin. Borax dissociates into borate in aqueous medium as given below:

$$B_4O_7^{2-} + 7\ H_2O \rightleftharpoons 2\ B(OH)_3 + 2\ B(OH)_4^-$$

Borates can complex with the hydroxyl groups present in GA Ald (Strauss & Kral 1982). For the inverse miniemulsion, an organic phase in which surfactant is dissolved is required and here, Span 20 dissolved in cyclohexane acts as the organic phase. Span 20 self assembles to micelles in cyclohexane. When the aqueous solution of GA Ald or gelatin is added to cyclohexane under sonication, droplets of GA Ald or gelatin is formed. Similarly, the miniemulsion of gelatin is prepared and later these two miniemulsions are combined under sonication. When the two emulsions are sonicated, small droplets are formed and they collided with each other with high speed. During this collision, A and B droplets are fused and cross-linking occurred between aldehyde groups of GA Ald and amino groups of gelatin leading to the formation of GA Ald-Gel nanogel.

Effects of parameters such as surfactant concentration and volume of aqueous phase on the size of the nanogels are examined. The impact of surfactant/aqueous phase ratio on particle size of GA Ald-Gel nanogel is also studied by varying the surfactant to water weight percentage at constant ultrasonication time and amplitude. From Table 4.2, it is clear that the hydrodynamic diameter of the nanogel particles decreased with increase in concentration of the surfactant, when the volume of aqueous phase is kept constant.

When the concentration of surfactant is increased to 3 %, the particle size is further decreased because of the availability of increased amount of surfactant to surround and stabilize the small droplets. Volume of the aqueous phase also has an

impact on the size of the gum arabic aldehyde-gelatin (GA Ald-Gel) nanogels. Impact of volume of aqueous phase (GA Ald and gelatin) in the emulsion on the size of the nanogel particles is investigated by maintaining constant surfactant concentration against the aqueous phase. Size of the nanogels increased with increase in volume of aqueous phase with constant surfactant concentration.

Table 4.2 Effect of volume of aqueous phase and concentration of surfactant on size of the GA Ald-gel nanogel particles

Amount of surfactant with respect to organic phase (w/v, %)	Total volume of aqueous phase (μL) (GA Ald+Gel)	Total volume of organic phase (mL)	Size of nanogel (nm)
1	250	10	152 ± 3
1	500	10	160 ± 2
1	750	10	674 ± 5
2	250	10	114 ± 4
2	500	10	151 ± 6
2	750	10	153 ± 5
3	250	10	106 ± 2
3	500	10	147 ± 6
3	750	10	139 ± 3

The combination with surfactant amount 2 % with total volume of aqueous phase as 500 μL (250 μL of gelatin and 250 μL of GA Ald) and size of 151 ± 6 nm is selected for further studies. GA Ald-Gel nanogel particles are separated from the miniemulsion by precipitation of the inverse emulsion in acetone, followed by centrifugation. The particles are washed many times with water to remove the impurities and surfactants and finally dried under reduced pressure to obtain nanogel powder. The prepared nanogels are used for the encapsulation and controlled release of curcumin towards MCF-7 cancer cells.

Curcumin loading is achieved by precipitating GA Ald-Gel nanogel inverse miniemulsion in curcumin dissolved in acetone. Encapsulated curcumin may interact with the nanogel through hydrogen bonding. Hydroxyl group of the curcumin may

form end to end hydrogen bonds with –OH groups and –COOH groups present in GA Ald-Gel nanogel (Mangalathillam et al. 2012). Schematic representation of curcumin loading in GA Ald-Gel nanogels and possible interaction between curcumin and GA Ald-Gel nanogels are shown in Scheme 4.3.

4.3.1.2 Characterization of bare and curcumin loaded GA Ald-Gel nanogels

FT-IR spectra of GA, GA Ald, gelatin and dried GA Ald-Gel nanogel are recorded in the range of 400–4000 cm^{-1} and are shown in Figure 4.12. The spectrum of gum arabic (Figure 4.12a) demonstrates the characteristic absorption bands of its polysaccharide structure, 3278 cm^{-1} (–OH stretching), 1597 cm^{-1}, 1406 cm^{-1} (the characteristic carboxylate asymmetric stretch and symmetric stretch respectively) and 1016 cm^{-1} (C–O–C stretching) (Abu-Dalo, Othman, & Al-Rawashdeh 2012). In the spectrum of GA Ald (Figure 4.12b), the symmetric vibration of aldehyde is seen at 1739 cm^{-1}, thus confirming the oxidation. Absorption bands from both gelatin (Figure 4.12c) and GA Ald are seen in the spectrum of GA Ald-Gel nanogel (Figure 4.12d). The peak corresponding to -C=N- group (Schiff's base) formed between aldehyde and amino groups is overlapped with the amide I band of gelatin. In the spectrum of gelatin, absorption bands at 1632 cm^{-1} and 1533 cm^{-1} correspond to amide I band and amide II bands respectively. In the nanogels, these bands are shifted to 1641 cm^{-1} and to 1550 cm^{-1} and confirm the involvement of amino group of gelatin in Schiff's base formation (Sarker et al. 2014). The peak observed at 1021 cm^{-1} in the spectrum of nanogel is due to GA Ald. All these observations confirm the formation of cross-linked nanogels.

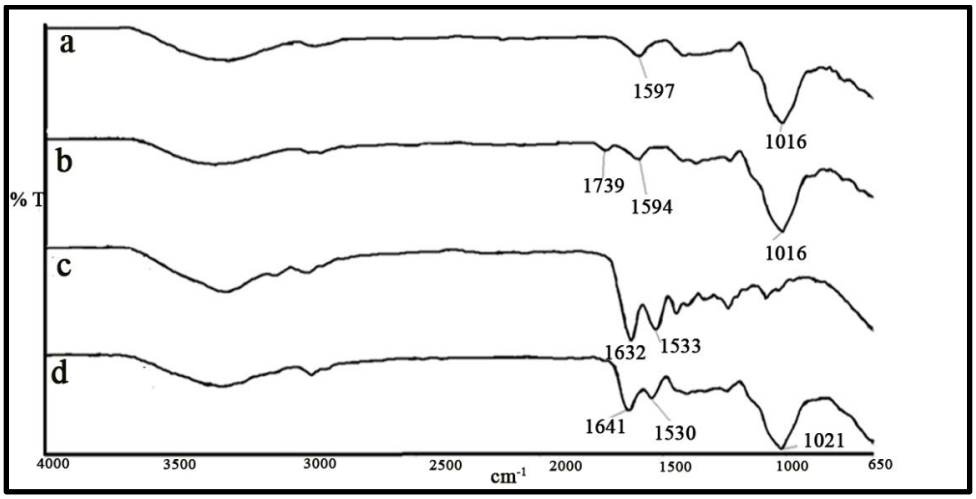

Figure 4.12 FT-IR spectra of GA (a), GA Ald (b), gelatin (c) and GA Ald-Gel nanogel (d)

Thermogravimetric analysis of GA Ald, gelatin, curcumin, GA Ald-Gel and curcumin loaded nanogels are shown in Figure 4.13. In GA Ald, weight loss upto 100 °C is due to the loss of water and the second degradation at 198 °C is owing to the structural degradation. TGA pattern of gelatin (Fig. 4.13c) and curcumin (Fig. 4.13e) is described in section '4.2.1.2. Characterization of bare and curcumin loaded Alg Ald-Gel nanogels'. First stage of weight loss of curcumin loaded nanogels is seen at 146 °C (Fig. 4.13d) while the bare nanogels (Fig. 4.13a) exhibit the same at 196 °C.

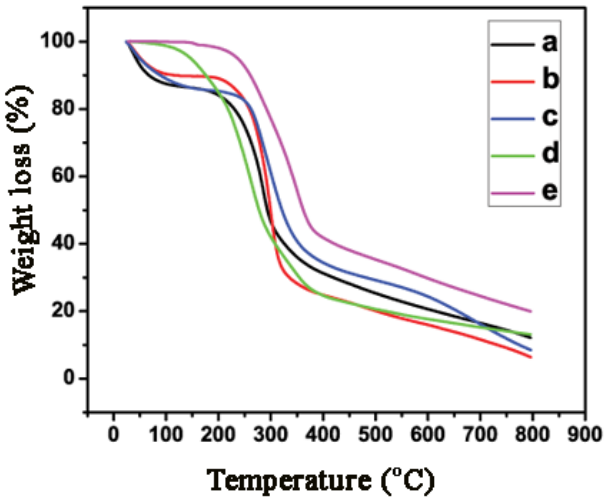

Figure 4.13 TGA curves of GA Ald-gel nanogel (a), GA Ald (b), gelatin (c), curcumin loaded GA Ald-Gel nanogel (d) and curcumin (e)

The presence of curcumin inside the nanogels is further demonstrated by proton nuclear magnetic resonance spectroscopy (^{1}H NMR). Figure 4.14 shows the ^{1}H NMR spectra of curcumin (Figure 4.14a) and curcumin loaded GA Ald-Gel nanogels (Figure 4.14b). Curcumin loaded nanogels show characteristic peaks of curcumin in the region between 6-8 ppm. The intensity of curcumin peak is less in the nanogel, compared to free curcumin, since it is encapsulated inside the nanogel.

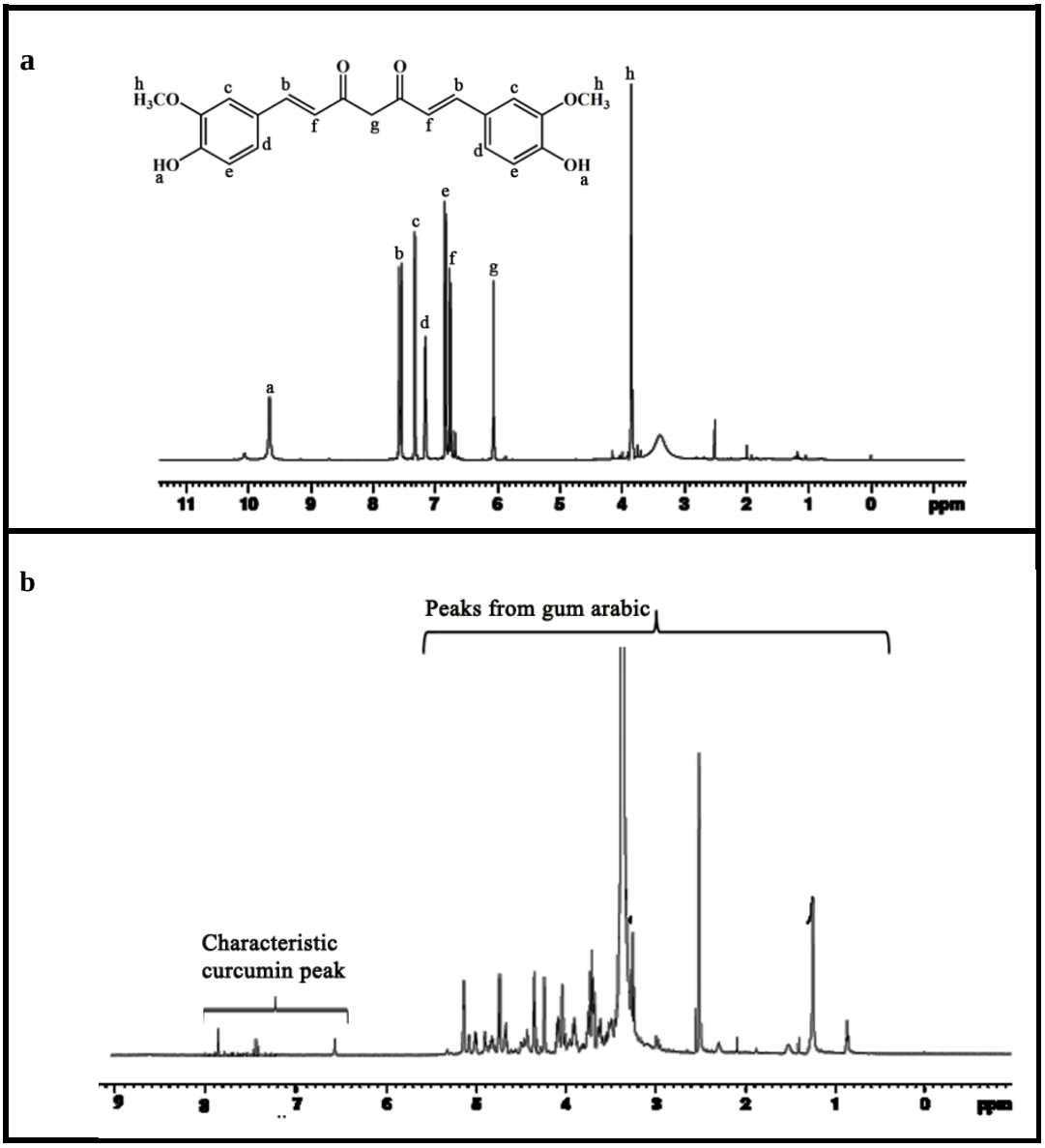

Figure 4.14 ^{1}H NMR spectra of curcumin (a) and curcumin loaded GA Ald-Gel nanogel (b)

Both GA Ald-Gel nanogels (Figure 4.15a) and curcumin loaded GA Ald-Gel nanogels (Figure 4.15b) could be redispersed in water, preserving the identity of the particles, without any additional surfactant.

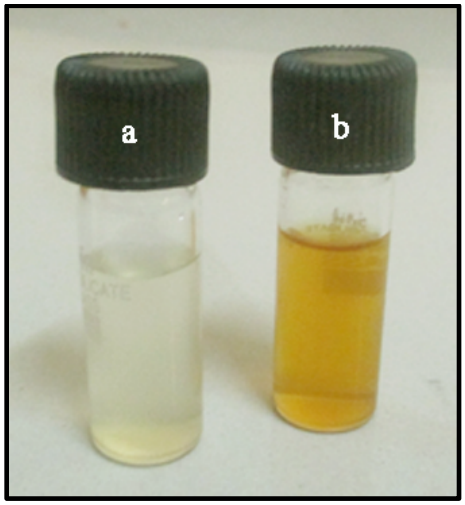

Figure 4.15 Bare GA Ald-Gel nanogel (a) and curcumin loaded GA Ald-Gel nanogel (b) redispersed in water

When the nanogel is redispersed in water, the hydrodynamic diameter is found to be larger, as more water could diffuse into the polymer network of GA Ald and gelatin. Bare GA Ald-Gel nanogels show hydrodynamic diameter of 211 ± 5 nm and a zeta potential of -27 ± 3 mV indicating good stability of the nanogels. GA Ald contains carboxylic acid groups which provide negative zeta potential to stabilize the nanoparticles. Negative surface charge of the GA Ald-Gel nanogels is due to the deprotonation of all the acid groups in GA Ald at neutral pH. Negatively charged GA Ald-Gel nanogels avoid protein adsorption and REF clearance and can provide long circulation time and maximum EPR effect. Curcumin loaded GA Ald-Gel nanogels show a hydrodynamic diameter of 452 ± 8 nm and a zeta potential of -27 ± 4 mV. Curcumin loading does not alter the zeta potential, but increases the hydrodynamic diameter to a great extent. The larger diameter is attributed to the swelling of the nanogels in the aqueous medium. Water is diffused into the cross-linked networks of the drug loaded nanogels and leads to swelling. Presence of curcumin inside the matrix increases the size of the nanogels than the bare nanogel. Even though the

hydrodynamic diameter of the nanogels is higher than bare nanogel, it is still in the size range needed for entry through the vasculature of tumors.

4.3.1.3 Morphology analysis of bare and curcumin loaded GA Ald-Gel nanogels

The morphology of bare GA Ald-Gel nanogels both in inverse miniemulsion and after redispersion in water is analyzed by SEM (Figure 4.16). Figure 4.16a shows the morphology of the nanogels in the miniemulsion. From the SEM image, it is clear that the particles have spherical morphology with a diameter of 80-100 nm. The size obtained from DLS is 151 nm. Figure 4.16b shows the morphology of the particles after redispersion in aqueous medium. After redispersion in water, slight increase in size is observed due to the swelling of nanogels in water. Size of the redispersed nanogels is found to be 211 nm (by DLS). In SEM, redispersed nanogels show an average size of 140 nm**.** Curcumin loaded GA Ald-Gel nanogel (Figure 4.16c) also shows spherical shape. The size of the nanogels obtained from SEM is in the range of 390-410 nm.

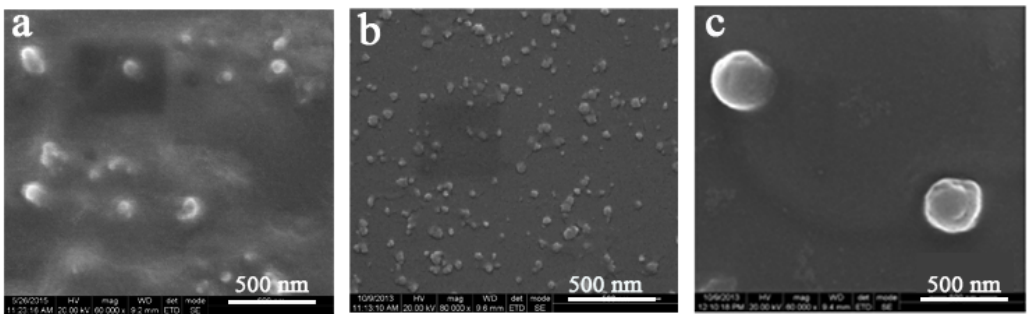

Figure 4.16 GA Ald-Gel nanogel in inverse miniemulsion (a) and GA Ald-Gel nanogel (b) and curcumin loaded GA Ald-Gel nanogels (c) after dispersing in aqueous medium

The encapsulation and loading efficiencies of curcumin loaded GA Ald-Gel nanoparticles are calculated by estimating the curcumin present in the supernatant by UV-Visible spectrometer at 430 nm. GA Ald-Gel nanogel shows an encapsulation efficiency of 65 ± 2 % and loading efficiency of 1.8 ± 0.02 %.

4.3.1.4 Curcumin release studies of GA Ald-Gel nanogel

Curcumin release from GA Ald-Gel nanogel is studied under pH conditions of 5.5 and 7.4 (Anitha, Deepagan, Rani, et al. 2011). Phosphate buffer of pH 7.4 and acetate buffer of pH 5 are used to simulate the physiological condition. The release profile of curcumin from the GA Ald-Gel nanogel is shown in Figure 4.17. In the first 5 h, a burst release is seen due to the release of curcumin adsorbed on the surface of the nanogels. After the burst release, controlled release of curcumin is observed over a period of 48 h. Almost 45 % of curcumin is released after 10 h at acidic pH, while 25 % is released at 7.4. Curcumin release is faster in acidic pH than that at neutral pH (7.4). The Schiff's bond formed between aldehyde groups of GA Ald and amine groups of gelatin undergoes breakage at acidic pH and this leads to the rupture of the nanogel, followed by curcumin release.

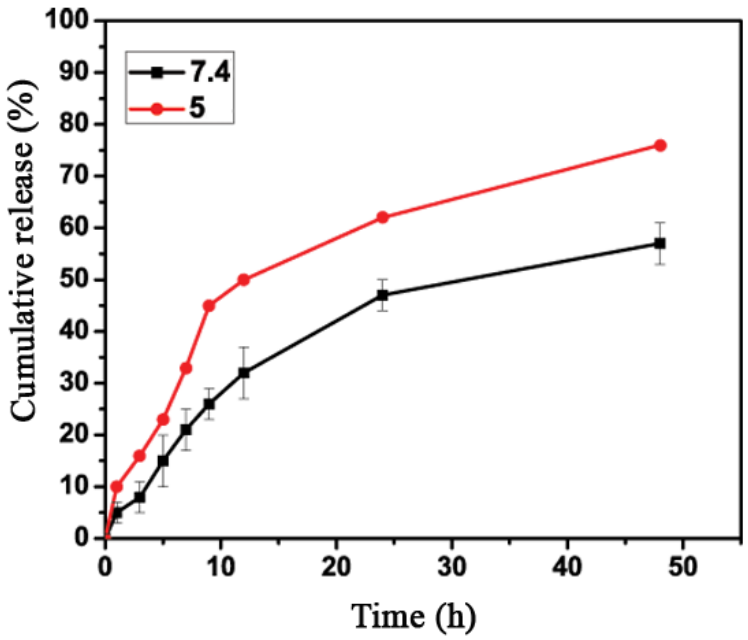

Figure 4.17 *In vitro* curcumin release from curcumin loaded GA Ald-Gel nanogel at pH 5 and 7.4

4.3.1.5 Hemocompatibility studies of bare and curcumin loaded GA Ald-Gel nanogels

Hemolysis assay is performed to assess the ability of curcumin loaded GA Ald-Gel nanogels to induce RBC lysis. Determination of the effect of curcumin loaded GA Ald-Gel nanogels on RBC is important, since the nanomaterials circulate in the blood stream and get exposed to the RBC. Nanocarriers designed for drug delivery applications must show minimum interactions with blood components (S. Kim, Shi, Kim, Park, & Cheng 2010). Hemolysis assay results of curcumin loaded GA Ald-Gel nanogels with equivalent curcumin concentrations (3.1-50 μg/mL) are shown in Figure 4.18. Curcumin loaded nanogels show concentration dependant hemolysis. At the lowest concentration, the hemolysis is minimum, while at higher equivalent curcumin concentrations, hemolysis increases to some extent. From the figure, it can be seen that percentage hemolysis of curcumin loaded nanogels, is below 5 %, the critical safe hemolytic ratio for biomaterials (S.-R. Yu et al. 2004). PBS and Na_2CO_3 exhibit 0 % and 100 % hemolysis respectively (data not included in the graph). Percentage hemolysis of curcumin loaded GA Ald-Gel nanogels is greater than that of the percentage hemolysis of bare GA Ald-Gel nanogels (Sarika & James 2015).

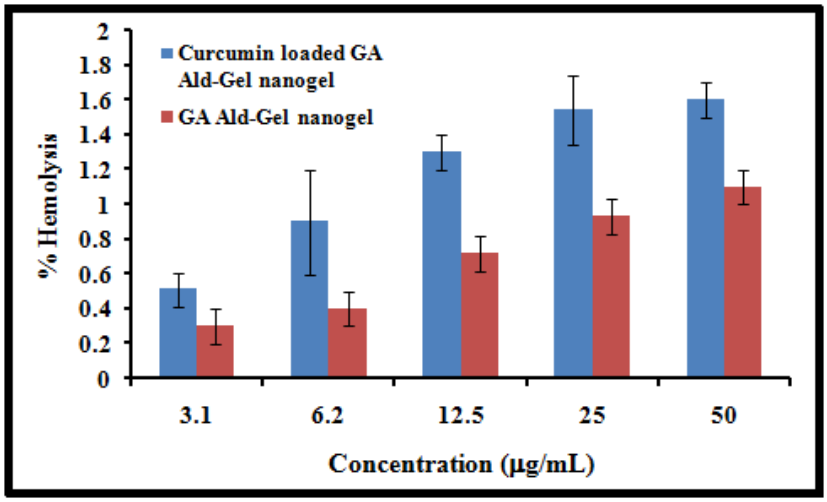

Figure 4.18 Hemolysis assay of bare and curcumin loaded GA Ald-Gel nanogels with equivalent curcumin concentration of 3.1 to 50 μg/mL in PBS. Positive control, Na_2CO_3 (0.1 %) shows 100 % hemolysis, which is not included in the graph

4.3.1.6 *In vitro* cytotoxicity studies

To evaluate the anticancer activity of curcumin loaded nanogels, MTT assay is performed in human breast carcinoma cells (MCF-7) and the results are shown in Figure 4.19. The cells are incubated with various concentrations of free curcumin and curcumin loaded nanogels with equivalent curcumin concentrations ranging from 3.1-50 μg/mL for 24 h and cell activity is evaluated. Bare nanogels do not show any toxicity towards MCF-7 cells and is reported recently (Sarika & James 2015). From Figure 4.19, it is clear that curcumin shows severe toxicity to MCF-7 cells in all the doses. Whereas curcumin loaded GA Ald-Gel nanogels exhibit acute toxicity towards MCF-7 cells at a dose of 50 μg/mL. In other doses toxicity of curcumin loaded nanogels is less than that of curcumin and remains toxic to the cells up to the dose of 12.5 μg/mL. Since aqueous solubility of curcumin is very less, it is dissolved in DMSO for the cytotoxicity analysis. In the previous section, it is already mentioned that in the case of Alg Ald-Gel nanogels also free curcumin showed more toxicity than the curcumin loaded nanogels.

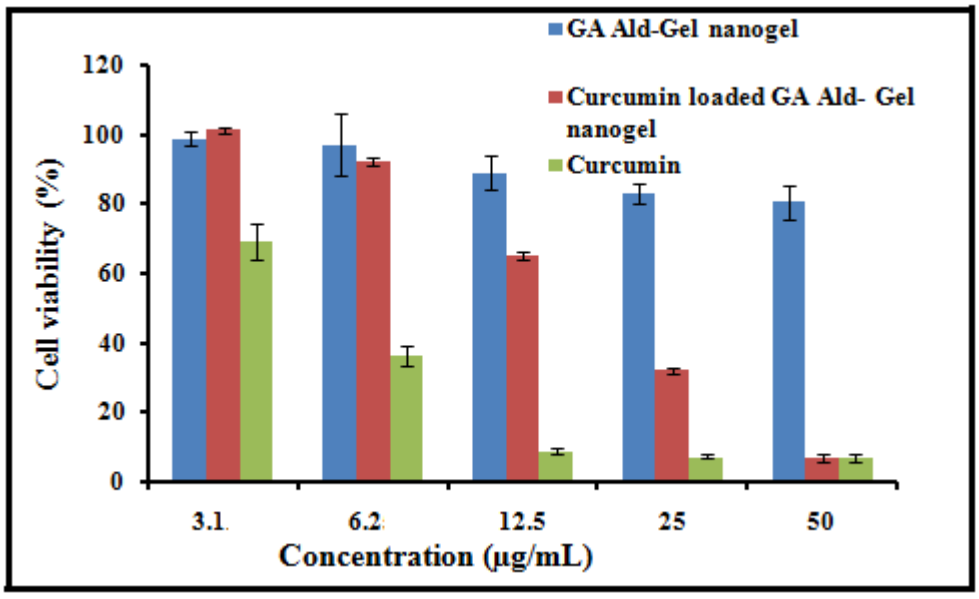

Figure 4.19 *In vitro* cytotoxicity analysis of bare and curcumin loaded GA Ald-Gel nanogels towards MCF-7 cells

4.3.1.7 Intracellular uptake studies

Confocal Laser Scanning Microscopy (CLSM) is utilized to examine the intracellular uptake ability of the curcumin loaded GA Ald-Gel nanogels in MCF-7 cells after incubating for 24 h. Images of the intracellular uptake in MCF-7 cells by curcumin and curcumin loaded GA Ald-Gel nanogels are shown in Figure 4.20. Green fluorescence of curcumin is utilized for imaging. Both curcumin loaded GA Ald-Gel nanogels and curcumin show intracellular uptake. Curcumin undergoes degradation in physiological conditions and hence its fluorescent intensity is less compared to curcumin loaded GA Ald-Gel nanogels. Since curcumin is present inside the nanogel, it is protected from degradation and hydrolysis in physiological ambience and shows high fluorescent intensity. In addition to that, the nanosize of the nanogel also promotes accumulation in MCF-7 cells by enhanced permeation and retention (EPR) effect.

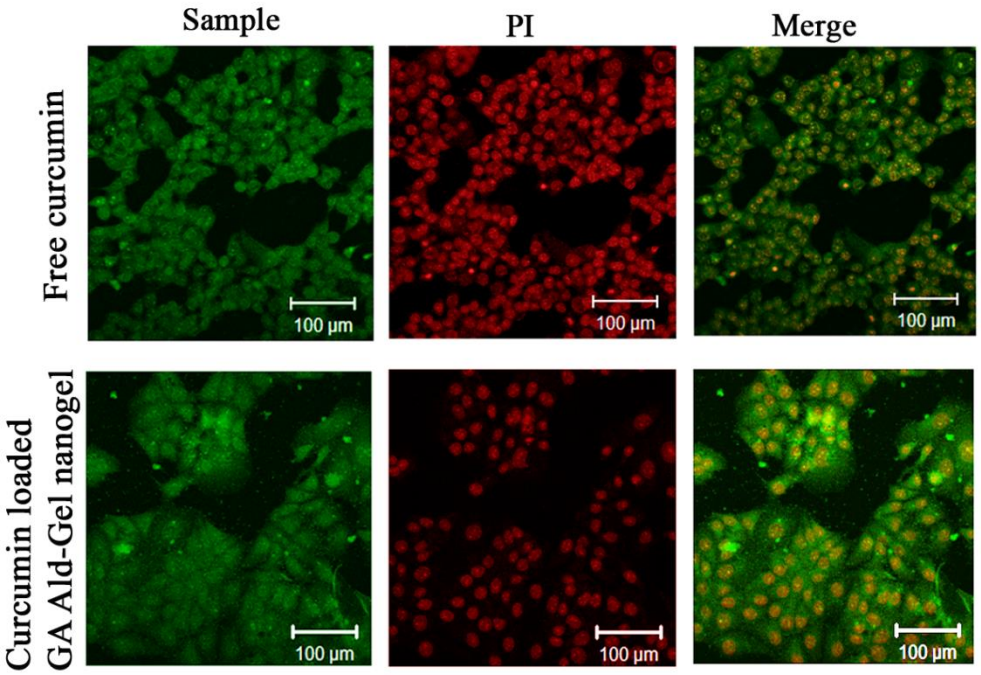

Figure 4.20 Intracellular uptake of curcumin loaded GA Ald-Gel nanogels (row 1) and curcumin (row 2) by MCF-7 cells observed under CLSM. Signals from curcumin (column 1) and PI (column 2) were separately obtained and merged (column 3)

4.4 Conclusions

Nanogels are prepared form alginate aldehyde and gum arabic aldehyde by the cross-linking with gelatin, through inverse emulsion technique. Suitability of both of these nanogels for encapsulation and delivery of curcumin to cancer cells are evaluated. Physical properties of the curcumin loaded nanogels like size; zeta potential and morphology of both nanogels is analyzed. The nanogels exhibit spherical morphology and possess negative zeta potential. Curcumin loaded Alg Ald-Gel and GA Ald-Gel nanogels show higher curcumin release at acidic pH and induce cytotoxicity towards MCF-7 cells. Confocal laser scanning microscopy proves the *in vitro* cellular uptake of curcumin loaded nanogels. Therefore curcumin loaded Alg Ald-Gel and GA Ald-Gel nanogels are promising drug delivery systems for the treatment of breast cancer.

CHAPTER 5
POLYELECTROLYTE COMPLEX NANOPARTICLES

The next class of nanomaterials developed for the encapsulation and delivery of curcumin is polyelectrolyte complex. This chapter deals with the preparation of self assembled hybrid polyelectrolyte complex nanoparticles from cationised gelatin and alginate. Modification and characterization of cationised gelatin is explained in detail. Later, the application of the prepared polyelectrolyte complex for curcumin delivery is explained.

5.1 Introduction

Polyelectrolytes are either polycations or polyanions carrying an electrolyte group in their structure. These polycations or polyanions undergo partial or complete dissociation in aqueous solutions. Neutral polymers adopt random coil conformation in aqueous solutions, while polyelectrolytes stretch out more due to the repulsion from the charges. Polyelectrolyte solutions are viscous since the extended structures take more space and resist the solvent to flow around it. Naturally occurring polyelectrolytes are DNA, polypeptides, chitosan, sodium alginate etc.

Studies on polyelectrolyte complex was started in early 40's and 60's by Fuoss and Sadek and by Michaels and Miekka (Fuoss & Sadek 1949, Michaels & Miekka 1961). Polyelectrolyte complexation occurs when polyelectrolytes of opposite charges are mixed in aqueous solution. Electrostatic interactions are the major force of attraction between the polyelectrolytes. Hydrogen bonding, hydrophobic interactions and *van der* Waal's forces play vital roles in PEC formation. PECs are

divided into water soluble PECs and phase separated or precipitated PECs. Phase separated PECs are again subdivided into stable turbid dispersions, flocculating systems and coacervates. PECs are also classified as stoichiometric or nonstoichiometric. Complexes formed by the mixing of anionic and cationic polyelectrolytes at an equal molar ratio are referred to as "1:1 stoichiometric" PECs. These types of complexes fall into the precipitated or phase-separated types. Non stoichiometric PECs are again divided into two, one with long host polyion and short polyion, the second with excess of either anionic or cationic polyelectrolyte components (Doi & Kokufuta 2010b). Water soluble or dispersible PECs are non stoichiometric and have potential applications in biotechnology and pharmaceutical fields (Doi & Kokufuta 2010b).

The formation and properties of polyelectrolyte complex depend on several factors like pH of the reaction medium, degree of ionization of the polymers, ionic strength, mixing order, mixing ratio, polymer charge density (Berger et al. 2004, Hamman 2010) etc. PECs find applications in tissue engineering (Coimbra et al. 2011), drug delivery (H. Wang & Roman 2011) and wound dressing (H.-J. Kim et al. 1999) .

In this work, formation of hybrid PEC nanoparticles from a polysaccharide and a protein is demonstrated. PEC formation is carried out using alginate which is an anionic polysaccharide and cationically modified gelatin. Gelatin contains carboxyl and amino groups in its structure and gets cationised by protonation of amino groups at pH below its isoelectric point. Modification of gelatin with ethylenediamine or spermine results in cationically modified gelatin which contains excess amino groups and remains protonated even at neutral pH. Cationically modified gelatin is shown to be successful carrier for gene and drug delivery (Matsumoto et al. 2006, Morimoto et al. 2008, X. Xu et al. 2008). In a recent work, Zorzi et al investigated ocular gene delivery using polyelectrolyte nanoparticles prepared from cationised gelatin and anionic polysaccharides dextran sulphate and chondroitin sulfate (Zorzi, Párraga,

Seijo, & Sánchez 2011). Even though, many research articles demonstrate the potential applications of the cationised gelatin (CG) in gene and drug delivery, detailed characterization of this interesting material has not been reported so far. Here, the physicochemical properties of cationically modified gelatin are described in detail which provides information on the structural changes occurred due to the modification.

Cationically modified gelatin is utilized for the polyelectrolyte complex formation with alginate (Alg). Alginate is a polysaccharide with (1-4)-linked β-D-mannuronate (M) and α-L-guluronate (G) residues obtained from sea weeds. It can form complexes with positively charged polymers because of its anionic character. Alginate has been utilized for preparing polyelectrolyte nanoparticles with chitosan (Cafaggi et al. 2007, Sæther, Holme, Maurstad, Smidsrød, & Stokke 2008, Sarmento et al. 2007) and gelatin (Y. Li et al. 2011).

The prepared polyelectrolyte complex from cationised gelatin and alginate (CG/Alg) is utilized for curcumin encapsulation and delivery to breast cancer cells. For overcoming the limitations and improving the properties, curcumin was encapsulated and delivered using different nanoformulations such as polymeric micelles (J. H. Kim et al. 2012), liposomes (Lehtinen et al. 2012), nanogels (Chacko et al. 2012), lipids (Das & Chaudhury 2011), polyelectrolyte complex (Anitha, Deepagan, Rani, et al. 2011) and microspheres (X. Yang et al. 2010).

The polyelectrolyte complexation occurs due to the electrostatic interaction between the negatively charged acid groups of Alg and the positively charged amino groups of CG. The work deals with cationic modification of gelatin, detailed physicochemical characterization of the modified gelatin (CG), self assembled nanoscale polyelectrolyte complex formation of CG with Alg, characterization of the bare and curcumin loaded CG/Alg complex nanoparticles, *in vitro* drug release studies, cytotoxicity evaluation and intracellular uptake studies. This nanosized CG/

Alg polyelectrolyte complex is found to be a suitable carrier for curcumin delivery to cancer cells.

5.2 Results and discussions

5.2.1 Cationic modification of gelatin and characterization

Gelatin is a protein obtained by the denaturation of collagen and contains free amino groups and carboxyl groups in its structure. It is soluble in hot water and during dissolution, the helical structure of gelatin changes to coil structure. Upon cooling, the reverse happens and gelatin forms gel (Djabourov, Leblond, & Papon 1988). Strong hydrogen bonding between carboxyl and amino groups of gelatin is responsible for gelling. Gelatin is a polyampholyte and carries positive charge in aqueous solution of pH below its isoelectric point, pI (pI= 7-9 for Type A gelatin and pI=4.7-5.2 for Type B gelatin) and negative charge at pH above its pI. It can form polyelectrolyte complex with both cationic and anionic polymers depending on the pH of the medium. Yin et al reported PEC formation of gelatin with poly cationic chitosan above pH 4.7 (pH_{iso} of Gel). At pH above 4.7, amino groups in chitosan get protonated and exist as $–NH_3^+$ ions and gelatin contains $–COO^–$ ions. Electrostatic interactions between these oppositely charged polymers result in PEC formation (Yin, Li, Sun, & Yao 2005). Gelatin forms polyelectrolyte complex membrane with anionic alginate in aqueous solution for propylene dehydration and ciprofloxacin hydrochloride drug delivery (Dong, Wang, & Du 2006, Y. Li et al. 2011). Gelatin can also form complex coacervate microcapsules at pH around 3.5–4. There is a strong electrostatic interaction between gelatin and alginate and the electrostatic complexes would be formed in the pH window where gelatin and alginate are oppositely charged (Saravanan & Rao 2010). Another important factor that determines electrostatic complex formation is the ratio between the two biopolymers. Devi et al reported that the ratio between the sodium alginate and gelatin needed for complex coacervation is

1: 3.5 at pH 3 by measuring the turbidity and viscosity of the supernatant (Devi & Kakati 2013).

In the present work, to increase the positive charge on gelatin, it is cationically modified by ethylenediamine, according to the reported procedure (Scheme 5.1).

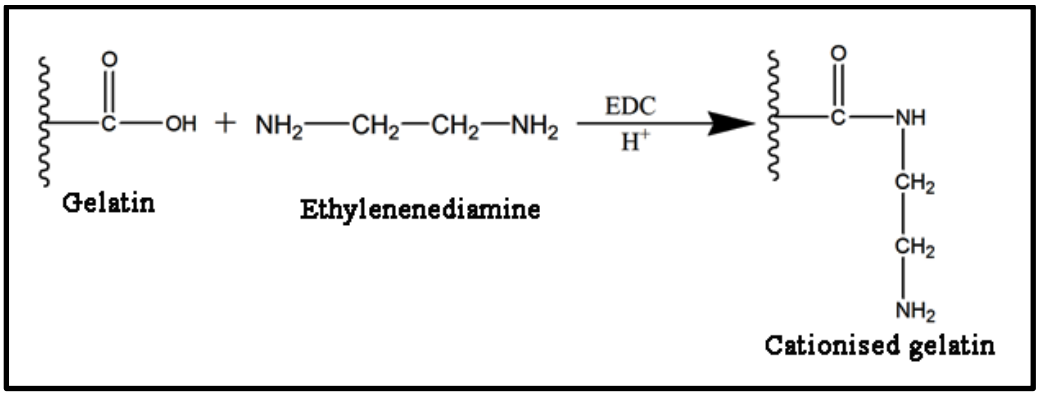

Scheme 5.1 Formation of cationised gelatin by reacting carboxylic acid groups in gelatin with ethylenediamine using EDC

Interestingly, the modified gelatin did not exhibit gelling characteristics of gelatin and is found to be soluble in water at room temperature. After cationisation, zeta potential of 0.1 % solution of gelatin is increased from 2 ± 1 mV to 29 ± 3 mV. Isoelectric point (pI) is the pH at which zeta potential (ζ) becomes zero. The isoelectric point of gelatin is 7.7 (Figure 5.1a), while that of CG (Figure 5.1 b) is 10.5. Modification with ethylenediamine is expected to increase pI due to the increase in number of amino groups (Figure 5.1).

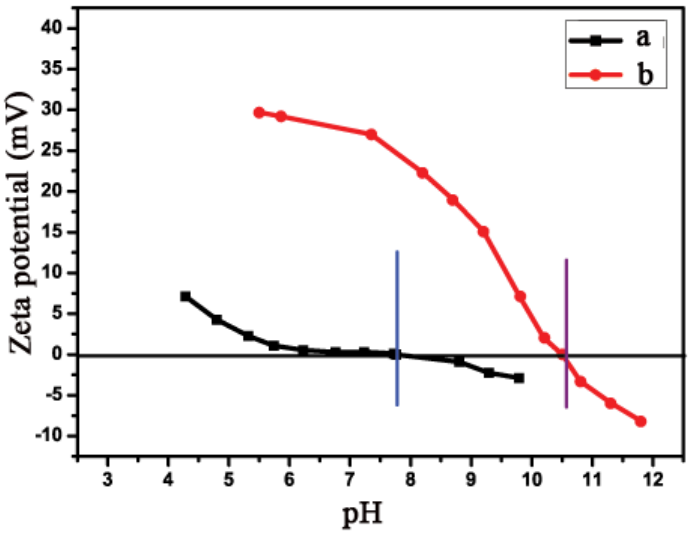

Figure 5.1 Isoelectric point of gelatin (a) and cationised gelatin (b)

Amino groups are introduced on gelatin backbone by the reaction between carboxyl groups of gelatin and ethylenediamine, thereby reducing the number of carboxyl groups available for hydrogen bonding. Amino groups in gelatin are increased after modification and it is analyzed by TNBS assay. Number of amino groups is increased from 18.6×10^{-5} mol/g to 26×10^{-5} mol/g. Cationised gelatin could not undergo gelation consequent to the reduction in the extent of hydrogen bonding. FT-IR spectrum of gelatin (Figure 5.2a) contains a broad band at 3289 cm^{-1} which is due to an overlapped band of –OH stretching and -NH stretching. -CH stretching band is seen at 2951 cm^{-1}. Bands at 1628 cm^{-1} and 1536 $cm^{-1}$are assigned to amide I and amide II stretching respectively. FT-IR spectrum of cationsed gelatin (Figure 5.2b) is very much similar to that of gelatin.

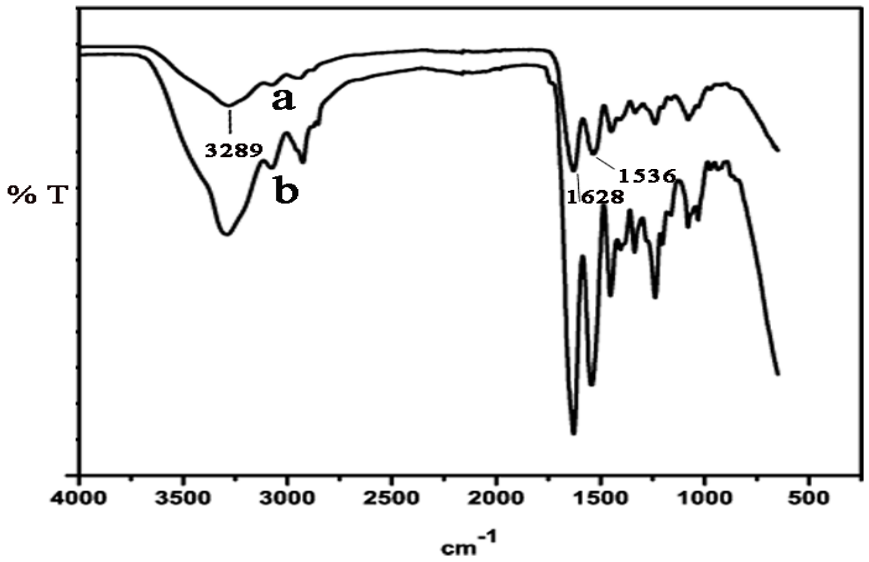

Figure 5.2 FT-IR spectra of gelatin (a) and cationised gelatin (b)

Gelatin shows a wide crystalline XRD peak at 2θ = 20.9 ° due to the triple-helical crystalline structure of collagen renatured in gelatin (Peña, De la Caba, Eceiza, Ruseckaite, & Mondragon 2010). This peak is absent in the pattern of CG (Figure 5.3) indicating the amorphous nature of cationised gelatin. This may be due to the alteration in the helical structure, resulting from the reduced extent of hydrogen bonding in the cationised gelatin.

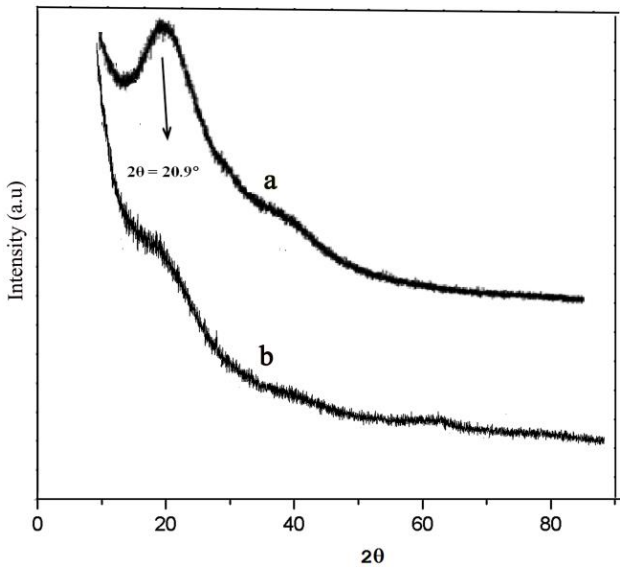

Figure 5.3 XRD pattern of gelatin (a) and cationised gelatin (b)

TGA thermograms of gelatin and cationised gelatin (Figure 5.4) are similar, except for the observation that cationised gelatin shows 3 % increase in char residue compared to gelatin. This can be due to the increased carbon content introduced by the conjugation of ethylenediamine.

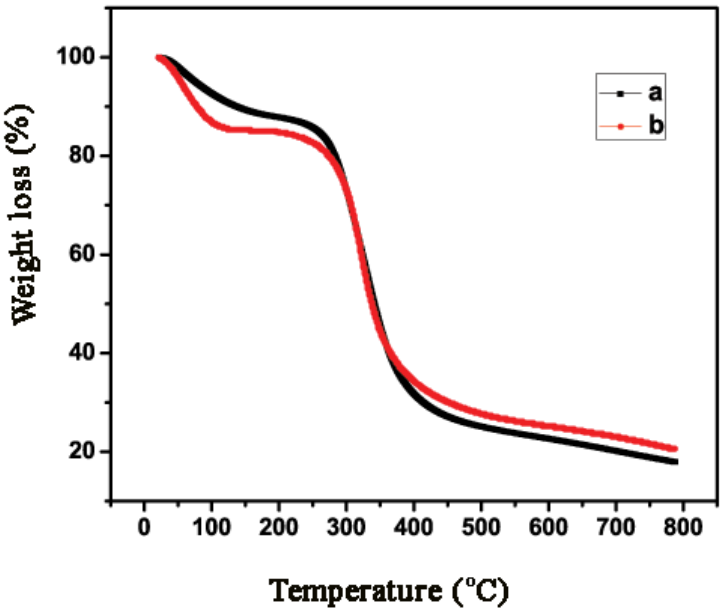

Figure 5.4 TGA thermograms of gelatin (a) and cationised gelatin (b)

Mass spectrometric studies are conducted using a MALDI-TOF-MS. Comparison of mass spectra collected before and after the reaction of ethylenediamine with gelatin is given in Figure 5.5. It is very clear that many main peaks present in gelatin (before reaction with ethylenediamine) are absent in the mass spectrum of cationised gelatin, but appear at higher mass regions. Notable changes in peak positions are given in Table 5.1 and 5.2. The peaks in the highest mass region of m/z 424126 (Figure 5.5a(A)), and 327523 (Figure 5.5a(B)) are now seen at m/z 433276(Figure 5.5 b(A')) and 349754(Figure 5.5b(B')), respectively for gelatin and cationised gelatin. The difference in masses is 9150 and 22231 amu, respectively. This is due to coupling of a high molecular weight amino acid with a smaller amino acid through ethylenediamine. Here one can expect not only coupling reaction but the addition of several ethylenediamine moieties to amino acid residues of gelatin by

forming –NH-CO- bonds. Similar differences in peak positions are observed for m/z 168528 (Figure 5.5a(C)), 98622 (Figure 5.5a(D)), 57275 (Figure 5.5a (E)) etc.

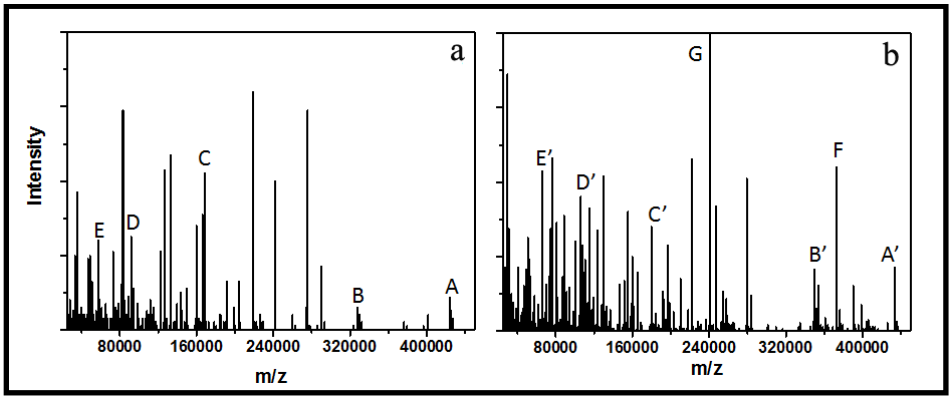

Figure 5.5 MALDI-TOF spectra of gelatin (a) and cationised gelatin (b). CG shows an increase in the molecular weight after modification

It is also interesting to note that the differences in masses are either in 3100 – 3700 range or in 5200–5800 range (Table 5.1). This can be attributed to the addition of a smaller amino acid (of mass m/z 3000 or 5000 range) present originally in gelatin is getting attached to a larger amino acid through coupling reactions of ethylenediamine. Also, smaller peptides could be formed due to degradation of amino acid chains during the reaction. Apart from coupling reaction between a large amino acid and a smaller acid, there could be addition of several ethylenediamine moieties to the various amino acids of gelatin. That is the reason for obtaining the mass difference in a range instead of a constant value.

There are other observations in the given mass spectra. Some of the peaks present in pure gelatin are completely absent or a corresponding peak at higher mass range is appeared. For example, peaks at m/z 168527, 203957, 290167 are not present in the mass spectrum of modified gelatin. Moreover, new peaks are noticed at m/z 240813 (Figure 5.5a(G)) and 372668 (Figure 5.5a(F)) for CG (Table 5.2). The presence of new peaks can be ascribed to the coupling reactions of ethylenediamine with amino acids especially those are absent in the mass spectrum after the reaction. The amino

acids with mass m/z 203957 and 35487 react to give a large single unit at m/z 240813. The difference (203957 + 35487 = 239444) of 1369 is because of the addition of ethylenediamine moieties to the amino acid backbone. Similarly, the amino acid with m/z 372668 is the association of smaller amino acids of mass m/z 203957 and 168527. Here also, the difference (203957 + 168527), 184 amu is due the addition of ethylenediamine species to the amino acid residue.

Table 5.1 Changes in mass observed in gelatin after modification with ethylenediamine

Gelatin (m/z)	Cationised gelatin (m/z)	Difference in mass (amu)
424126	433276	9150
327523	349754	22231
275710	279038	3328
241620	246858	5238
218806	221969	3169
191862	197079	5217
168528	179616	11088
159872	165485	5613
149520	155336	5816
126600	129836	3236
98622	105907	7285
83216	88502	5286
72806	76062	3257
57275	66278	9003
35488	40719	5231

Table 5.2 New peaks observed in cationised gelatin

New peaks in cationised gelatin (m/z)	Expected mass due to coupling reactions of smaller peptides
240813	203957 + 35487 = 239444
372668	203957 + 168527 = 372484

^{1}H NMR spectrum of cationised gelatin and gelatin are shown in Figure 5.6. In the spectrum of gelatin, most of the signals can be assigned to ^{1}H resonances of specific amino acids (Zandi, Mirzadeh, & Mayer 2007). The peak 1 (Figure 5.6b) corresponding to γ- and δ-CH_3 resonance of the amino acids leucine, valine, and

isoleucine is seen at 0.86 ppm. The peak at 1.16 ppm (peak 2, Figure 5.6b) represents γ-CH_3 resonance of threonine. Alanine (-CH_3) is seen at 1.34 ppm (peak 3, Figure 5.6b). The peaks at 1.62 and 1.88 ppm are related to the methyl resonances of lysine (β- and γ- and δ-CH_2) and arginine (β- and γ-CH_2) (peak 4 and 5 respectively, Figure 5.6b). Aspartic acid (peak 6, β-CH_2, Figure 5.6b), lysine (peak 7, ε-CH_2, Figure 5.6b), arginine (peak 8, δ-CH_2, Figure 5.6b) and proline (peak 9, δ-CH_2, Figure 5.6b) are seen at 2.64, 2.93, 3.14, and 3.57 ppm respectively (Rodin & Izmailova 1996). In the spectrum of cationised gelatin, all the above mentioned peaks are seen. Besides that, two additional peaks at 2.9 ppm (Figure 5.6a, 2) and 3.4 ppm (Figure 5.6a, 1) are seen in the spectrum of cationised gelatin. These peaks correspond to the –CH_2 protons introduced by the reaction of amino acids with ethylenediamine.

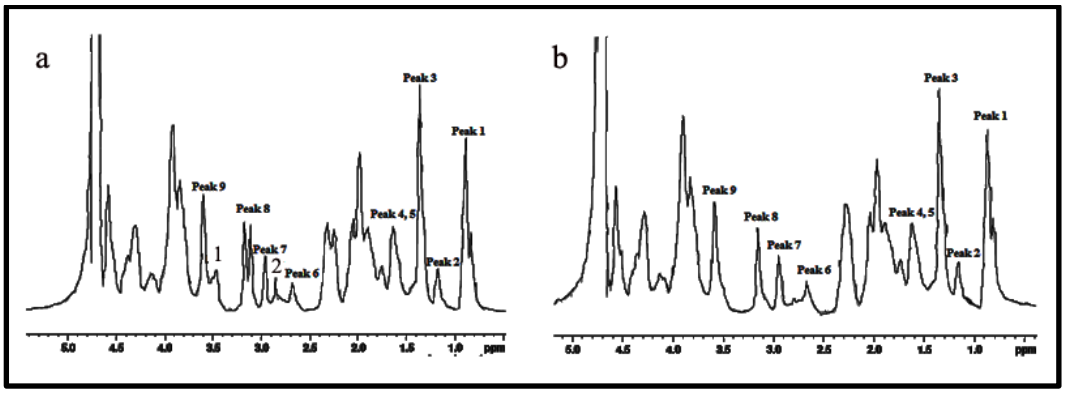

Figure 5.6 ^{1}H NMR spectra of cationised gelatin (a) and gelatin (b). In cationised gelatin two additional peaks at 2.9 ppm (2) and 3.4 ppm (1) are seen, due to the -CH_2 protons of ethylenediamine

Temperature dependant UV Spectroscopy is performed to evaluate the structural changes occurred in gelatin after modification (Figure 5.7). Even though the temperature is increased to 65 °C, the λ_{max} and absorbance value of gelatin (Figure 5.7b) do not change and the spectra are identical. This observation is attributed to the strong intermolecular and intramolecular hydrogen bonding present between amino groups and acid groups of various amino acids in gelatin. The crystalline nature of gelatin originates from the triple helical structure which also contributes to the stability during heating. Upon modification with ethylenediamine,

many of the acid groups are converted into amino groups, thereby decreasing the extent of hydrogen bonding. Noticeable increase in the λ_{max} value is observed in the spectrum of cationised gelatin (Figure 5.7a) recorded at 65 °C. Here, the hydrogen bonding present in the cationised gelatin is presumed to be destroyed or altered due to the high temperature because of the reduced extent of the hydrogen bonding present. All these observations confirm the structural changes occurred in gelatin due to cationisation.

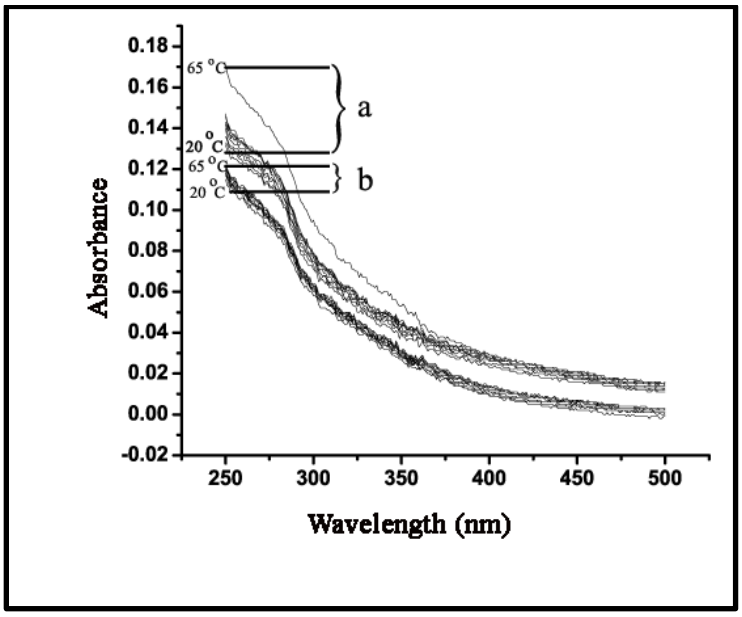

Figure 5.7 Temperature dependant absorbance studies of cationised gelatin (a) and gelatin (b)

5.2.2 Formation of CG/Alg polyelectrolyte complex

Aim of this work is to develop polyelectrolyte complex nanoparticles from alginate and cationised gelatin (CG) for curcumin delivery. For the polyelectrolyte complex formation, both the polymers should possess ionic charges (Samal et al. 2012). In the present work, the cationic charge on gelatin is enhanced by cationisation. PEC formation depends on the composition of the corresponding polymers and pH of the solution. Hybrid polyelectrolyte complex nanoparticles are prepared by simple mixing of CG and Alg solutions in different volume ratios. PEC

formation is clearly evident from the turbid appearance when the two solutions are mixed (Figure 5.8 and Scheme 5.2).

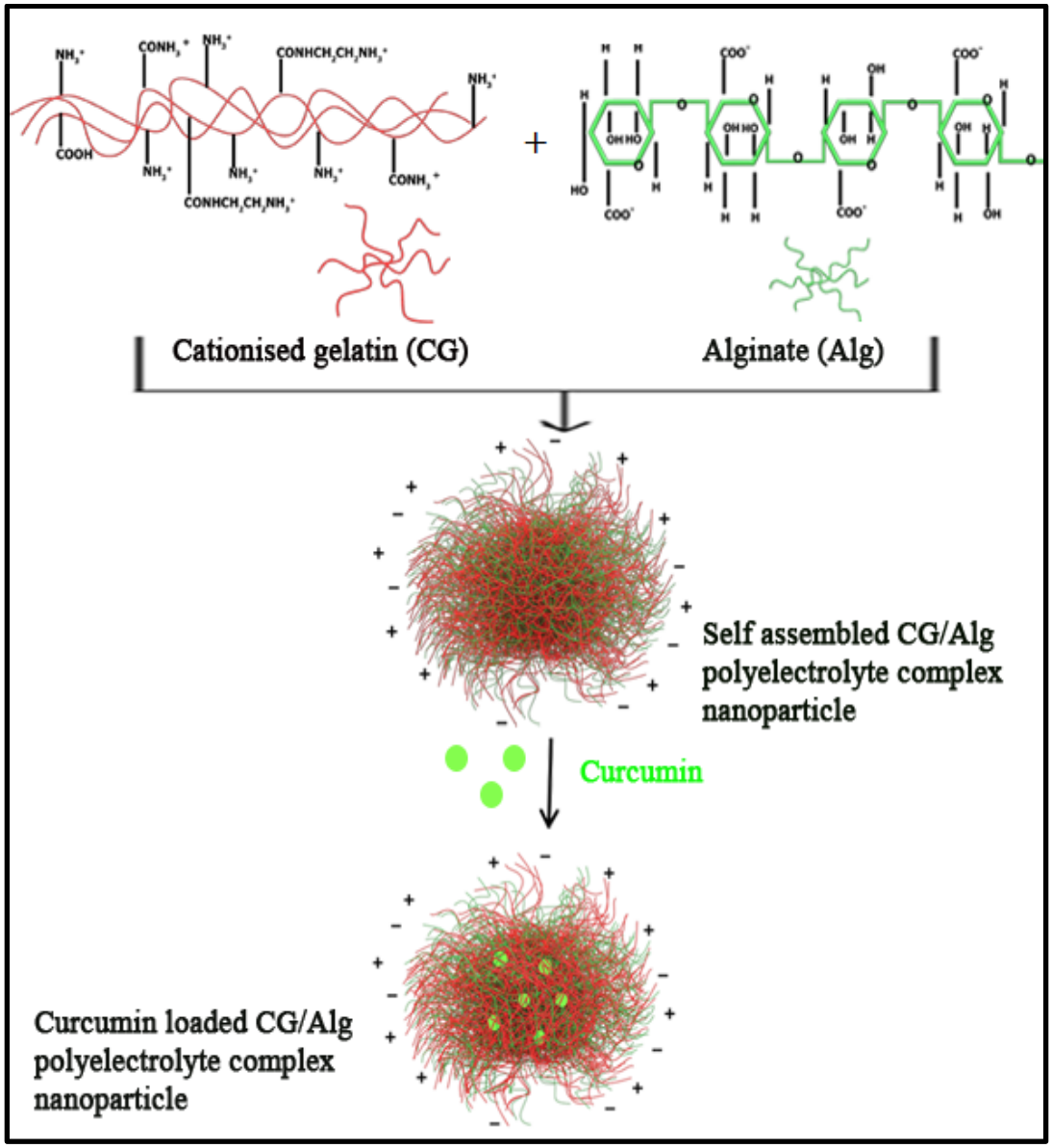

Scheme 5.2 Schematic representation of CG/Alg polyelectrolyte complex nanoparticle formation and encapsulation of curcumin in the complex

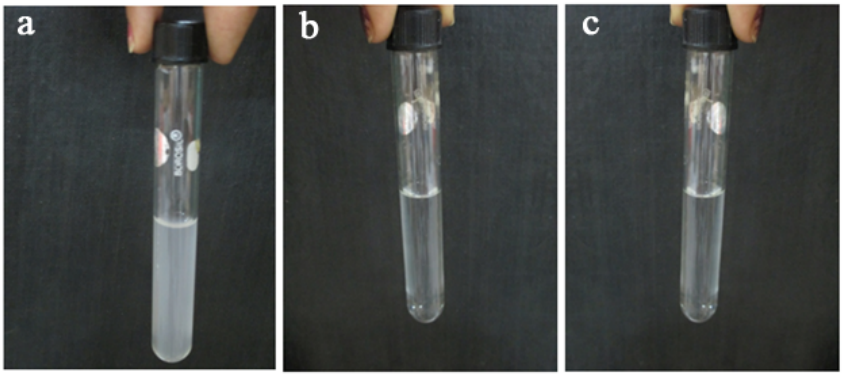

Figure 5.8 Turbid polyelectrolyte complex solution of CG/Alg PEC nanoparticles (a) formed by simple mixing of Alg (b) and CG (c)

Zeta potential of 0.1 % solutions (w/v) of Alg and CG are -69 ± 4 and 29 ± 3 mV respectively. The high negative zeta potential of Alg is due to the complete deprotonation of all the acid groups in Alg. PEC formation occurs for a few combinations of Alg and CG. The possible combinations, zeta potential and their sizes are listed in Table 5.3.

Table 5.3 Size and zeta potential of the complexes formed in aqueous solution

Volume of CG (mL)	Volume of Alg (mL)	Size (nm)	Zeta potential (mV)	% of Alg (w/w) in PEC	% of CG (w/w) in PEC
1	1	533 ± 10	-54 ± 8	50	50
2	1	265 ± 6	-33 ± 9	67	33
3	1	176 ± 7	-24 ± 4	75	25
4	1	232 ± 11	-13 ± 2	80	20
1	4	1308 ± 9	-47 ± 6	20	80
1	3	741 ± 10	-43 ± 5	25	75
1	2	725 ± 13	-40 ± 6	33	67

Complex formation is observed in the above mentioned combinations. However, taking into consideration of the smaller size and ease of formation, PEC formed with CG to Alg with mixing ratio 3:1 (size 176 nm and zeta potential -24 mV) is selected for further characterizations. This particular combination is used for curcumin loading also.

5.2.3 Characterization of bare and curcumin loaded CG/Alg complex

Curcumin loaded CG/Alg complexes are also prepared by the electrostatic interaction between curcumin containing cationised gelatin and alginate. Particle size of bare and curcumin loaded complex particles are analyzed by DLS after dispersing the lyophilized complex in water (1 mg/2mL). Bare complex shows a hydrodynamic radius of 201 ± 10 nm. After drug loading, the hydrodynamic radius is increased to 327 ± 8 nm. The increment in size is due to the presence of curcumin inside the particles. CG/Alg complex nanopartcles do not exhibit any change in the zeta potential (-24 mV) value after drug loading. Negative surface charge of the drug loaded complex is due to the deprotonation of the acid groups present on the alginate. As already mentioned in the previous sections, negative zeta evades RES clearance and provides maximum circulation time to achieve maximum EPR effect. Morphology of both polyelectrolyte complex particles are analyzed by SEM (Figure 5.9 a and b). Analysis shows that both of the complexes are in the form of self assembled spheres when dispersed in water. Drug loading does not alter the morphology and spherical morphology is maintained.

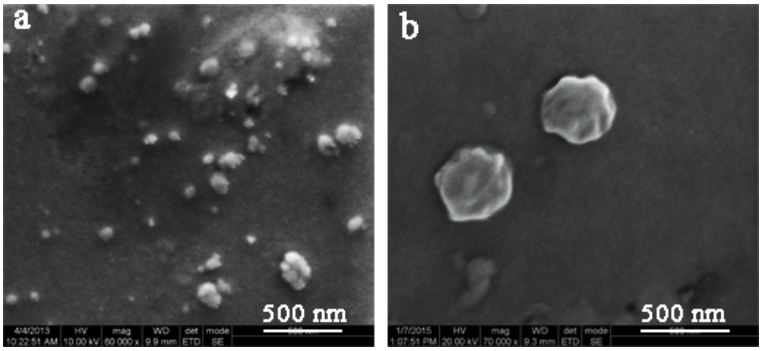

Figure 5.9 SEM images of bare CG/Alg PEC nanoparticles (a) and curcumin loaded CG/ Alg PEC nanoparticles (b) after redispersion in water

The encapsulation and loading efficiencies of curcumin loaded CG/Alg complex nanoparticles are calculated by estimating the curcumin present in the supernatant by UV-Visible spectrometer at 430 nm. Curcumin encapsulation and

loading efficiencies are 69 ± 3 % and 2.3 ± 0.02 % respectively for CG/Alg nanoparticles. Anitha et al reported similar curcumin encapsulation efficiency for dextran sulfate–chitosan nanoparticles (Anitha, Deepagan, Rani, et al. 2011).

5.2.4 *In vitro* curcumin release studies

Release studies of curcumin loaded CG/Alg polyelectrolyte complex is performed in acetate buffer of pH 5 and in phosphate buffer of pH 7.4. The release pattern is shown in Figure 5.10. A burst release is seen in the first 5 h followed by a controlled release of curcumin over a period of 48 h. The reason for initial burst release can be the delivery of curcumin adsorbed on the surface of the nanoparticles. Almost 87 % of the curcumin is released in 48 h at acidic pH. Curcumin release is faster in acidic pH than that in neutral pH owing to the decrease in electrostatic interaction between Alg and CG at acidic pH. The acid groups in Alg get protonated at acidic pH and lead to dwindled electrostatic interaction with cationised gelatin. As a result curcumin release is faster from CG/Alg complex at acidic pH. The acidic pH of the tumor attributing from the accumulation of metabolic products in these cells due to poor blood vessel architecture may favor faster release of curcumin from the nanoparticles.

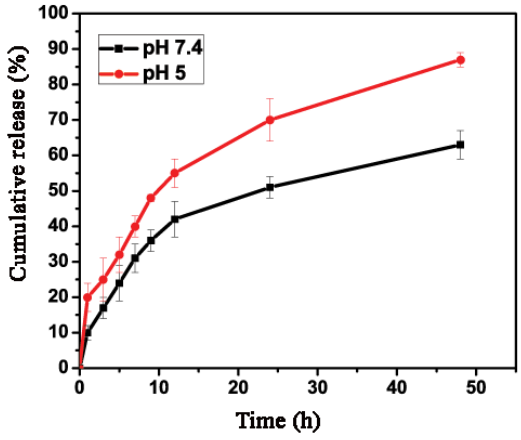

Figure 5.10 *In vitro* curcumin release pattern of CG/Alg PEC nanoparticles at pH 5 and pH 7.4

5.2.5 Hemolysis analysis

Hemolysis test is conducted to study the compatibility of both bare and curcumin loaded PEC nanoparticles with blood cells, since these nanoparticles have been designed for drug delivery application, where it might be exposed in blood environment. Figure 5.11 shows the hemolytic potential of various concentrations of bare and curcumin loaded PEC nanoparticles. Like that of nanogels, PEC nanoparticles also shows higher hemolytic ratio after curcumin loading however, it is in the range of safe hemolytic ratio for biomaterials. This indicates the hemocompatibility of the PEC nanoparticle samples.

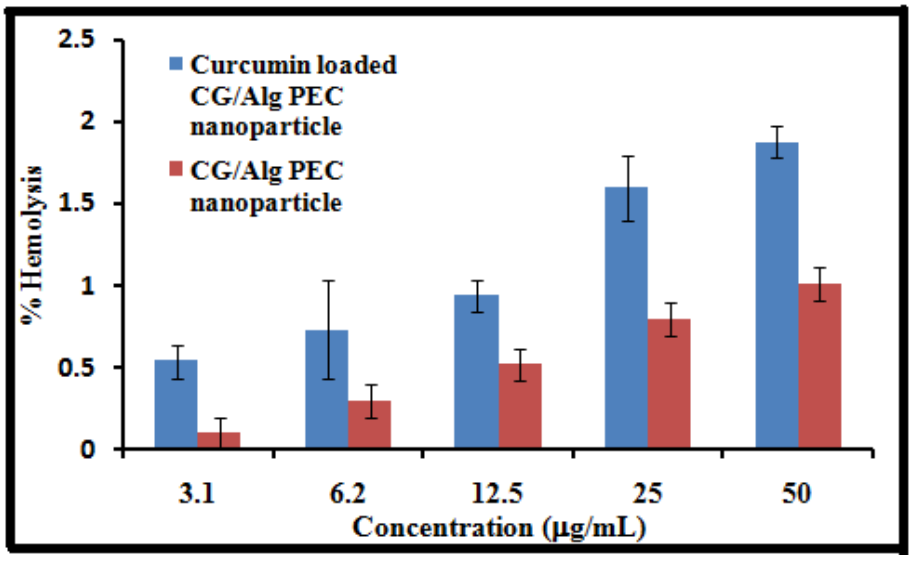

Figure 5.11 Hemolysis assay of bare and curcumin loaded CG/Alg PEC nanoparticles with equivalent curcumin concentration of 3.1 to 50 µg/mL in PBS (b). Positive control, Na_2CO_3 (0.1 %) shows 100 % hemolysis, which is not included in the graph

5.2.6 Cytotoxicity studies

From Figure 5.12, it is evident that both curcumin and drug loaded complex exhibit concentration dependant toxicity towards MCF-7 cells. The toxicity increases with increase in concentration of curcumin. Since curcumin is insoluble in water, curcumin dissolved in DMSO is used. The cells are exposed to curcumin and complex nanoparticles in five doses (equivalent curcumin concentration) ranging from 3.12-50

μg/mL. Drug loaded CG/Alg complex shows comparable toxicity to free curcumin at a dose of 50 μg/mL. In lower doses, toxicity of the drug loaded CG/Alg complex nanoparticles towards MCF-7 cells is lower than that of free curcumin. From Figure 5.12, it is clear that drug loaded CG/Alg complex is toxic to the cells up to a concentration of 12.5 μg/mL and it is nontoxic in the remaining doses. Since curcumin is highly soluble in DMSO, it is fully available to the cells and can show severe toxicity. Bare CG/Alg complex nanoparticles are found to be nontoxic in all the concentrations.

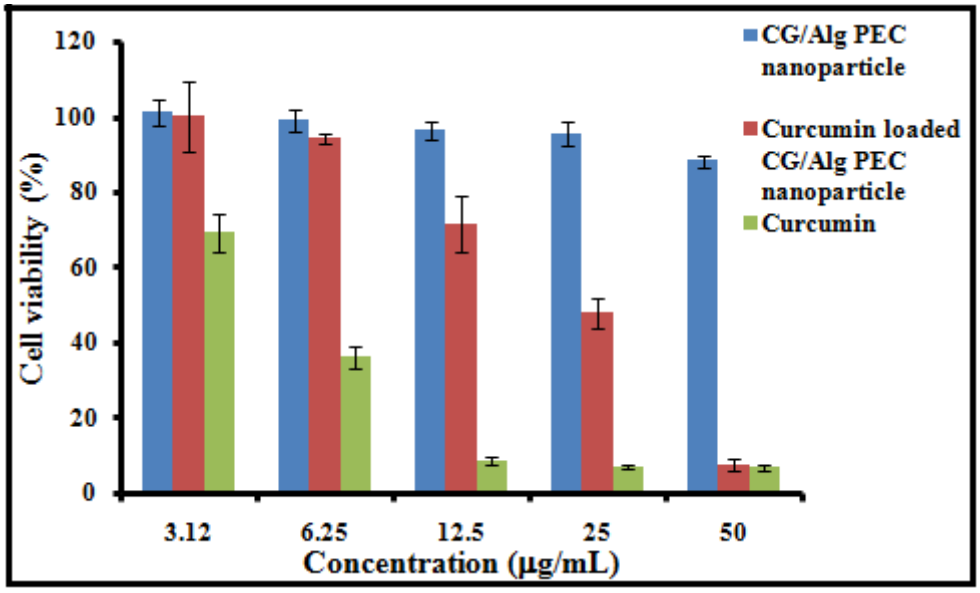

Figure 5.12 *In vitro* cytotoxicity analysis of bare and curcumin loaded CG/Alg PEC nanoparticles towards MCF-7 cells. Drug loaded complex shows toxicity towards cancer cells

5.2.7 Intracellular uptake studies

In vitro cellular uptake studies of curcumin loaded CG/Alg polyelectrolyte complex by MCF-7 cells for 24 h are carried out by fluorescent imaging using confocal laser scanning microscopy (CLSM). Nucleus of the cells is counter stained with propidium iodide. Figure 5.13 shows intracellular uptake studies of free curcumin and curcumin loaded CG/Alg complex in MCF-7 cells. Both curcumin and

curcumin loaded complex show intracellular uptake in MCF-7 cells. Curcumin undergoes rapid metabolism inside the cell, therefore its fluorescence intensity fades during incubation. Since curcumin is present inside the complex it is protected from degradation and hydrolysis in physiological ambience. In addition to that, the nanosize of the complex also promotes accumulation in MCF-7 cells by enhanced permeation and retention (EPR) effect.

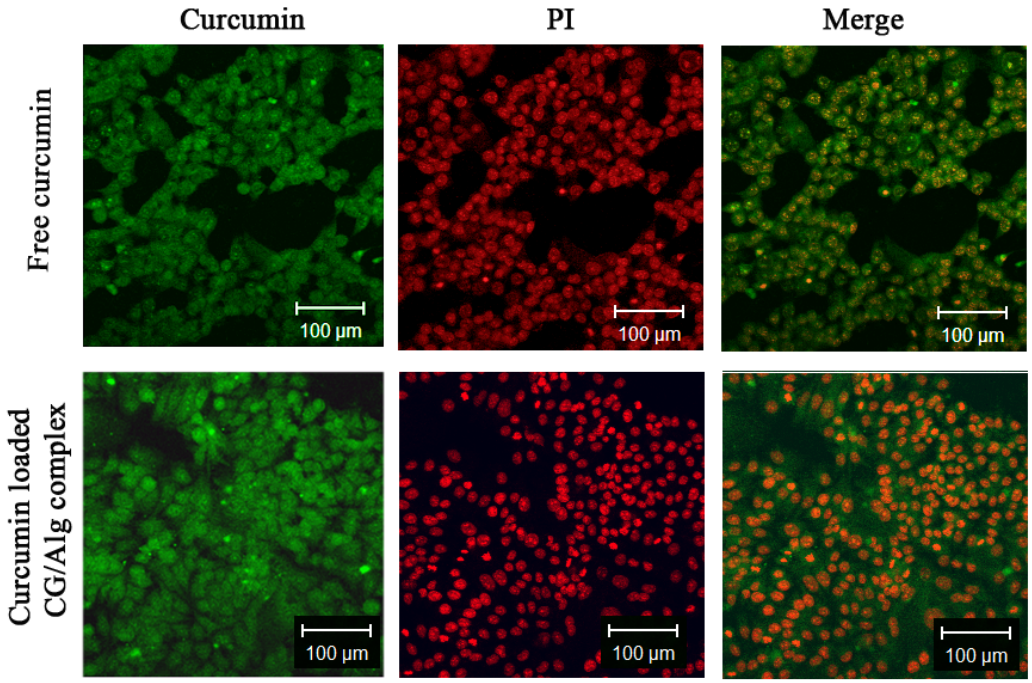

Figure 5.13 Intracellular uptake of curcumin loaded CG/Alg PEC nanoparticles (row 1) and curcumin (row 2) by MCF-7 cells observed under CLSM. Signals from curcumin (column 1) and PI (column 2) were separately obtained and merged (column 3)

5.3 Conclusions

Cationised gelatin (CG) is prepared by modification of gelatin with ethylenediamine. It is found that gelatin when cationically modified; lose its crystalline structure due to the reduced extent of hydrogen bonding between amino groups and carboxylic acid groups compared to the unmodified gelatin. XRD, MALDI-TOF-MS, ^{1}H NMR spectroscopy and temperature dependant UV-

spectroscopy analysis give insights into the structural changes occurred due to the modification. Hybrid polyelectrolyte complex possessing size in nanometer range and spherical morphology is formed by simple mixing of protonated CG and anionic alginate (Alg). These polyelectrolyte complex nanoparticles are found to be suitable matrixes for encapsulation and delivery of curcumin to carcinoma cells. The entrapment efficiency of CG/Alg nanoparticles is 69 % and exhibit sustained release of curcumin *in vitro*. Curcumin loaded CG/Alg nanoparticles show anticancer activity towards MCF-7 cells. CLSM images demonstrate the intracellular uptake of drug encapsulated nanoparticles. All these results indicate that curcumin loaded CG/Alg polyelectrolyte complex nanoparticles could be a promising candidate in cancer therapy.

CHAPTER 6
SUMMARY AND CONCLUSIONS

This chapter presents the summary and conclusions of the work described in the previous chapters. It also depicts future perspectives of the work.

6.1 Summary

This thesis deals with the development of different types of polysaccharide based nanomaterials to overcome the shortcomings of curcumin for its better anticancer potential. The three types of nanomaterials developed for the study are polymer-drug conjugates, nanogels and polyelectrolyte complex. Considering the biocompatibility and biodegradability of polysaccharides, all the three nanomaterials are developed from polysaccharides, namely pullulan, alginate and gum arabic.

Curcumin is covalently conjugated to all the three polysaccharides for the preparation of polymer-curcumin conjugates. Curcumin is directly conjugated to alginate and gum arabic, while modified curcumin is used for pullulan-curcumin conjugate preparation. All the three polymer-curcumin conjugates self assembled to micelle in aqueous medium and enhanced the solubility and stability to a great extent. With pullulan and alginate, conjugates with and without targeting ligand are prepared for the targeted delivery of curcumin to hepatocarcinoma cells. In alginate and pullulan conjugates, targeting ligand is introduced into the polymer chain, while in gum arabic it is already present in the polymer chain itself. Among the three polymer-curcumin conjugates, gum arabic-curcumin conjugate shows the highest toxicity and solubility. The release pattern of curcumin from the conjugates indicated faster release in acidic pH compared to that in neutral pH. The preparation and evaluation of

properties including biological activities of these polysaccharide-curcumin conjugates are presented in Chapter 3.

Chapter 4 is about the development and application of nanogels from alginate and gum arabic. These two nanogls are used for the encapsulation and delivery of curcumin to breast carcinoma cells. Cross-linked nanogels are prepared by inverse miniemulsion technique. By varying the concentration of surfactant and amount of aqueous phase, nanogels with size in the preferred range was prepared. Nanogels maintained spherical morphology after dispersion in aqueous medium and after drug loading. Characterizations of curcumin loaded nanogels were done by NMR spectroscopy, SEM and TGA analysis. Curcumin release profile depicts that cumulated release is faster in acidic pH than that in neutral pH. Anticancer activity of curcumin loaded nanogels is evaluated by MTT assay in human breast carcinoma cells (MCF-7). Curcumin loaded nanogels exhibited lower toxicity towards MCF-7 cells in all the concentrations compared to free curcumin. The intracellular uptake ability of both curcumin loaded nanogels was performed in MCF-7 cells for 24 h. Both curcumin and curcumin loaded nanogels showed intracellular uptake.

The development of polyelectrolyte complex from cationised gelatin and alginate is described in chapter 5. Alginate is a highly anionic polysaccharide. In order to form complex with alginate, gelatin was modified cationically to increase the positive charge needed for complexation. Cationisation reduced the extent of hydrogen bonding in gelatin leading to appreciable solubility in water at room temperature. PEC formation depends on the composition of the corresponding polymers and pH of the solution. Hybrid polyelectrolyte complex nanoparticles were prepared by simple mixing of CG and Alg solutions in different volume ratios. Complexes in different size range could be prepared by varying the volume of CG and Alg. Considering, the smaller size and the ease of formation, PEC formed with CG to Alg mixing ratio 3:1 (size 176 nm and zeta potential -24 mV) was selected for further characterizations and drug loading. Spherical morphology of the nanoparticles did not get affected by drug loading. Curcumin release studies from the

PEC showed faster release in acidic pH than that in neutral pH owing to the decrease in electrostatic interaction between Alg and CG at acidic pH. Both curcumin and drug loaded complex exhibited concentration dependant toxicity towards MCF-7 cells. Curcumin loaded complex show intracellular uptake in MCF-7 cells.

6.2 Conclusions

Conjugation of curcumin to polysaccharides such as pullulan, alginate and gum arabic enhances the solubility and stability of curcumin leading to greater bioavailability and elevated toxicity of the drug. Galctosylated and nongalactosylated conjugate prepared with modified curcumin increased the solubility and stability of curcumin. The conjugates with pullulan exhibits low zeta potential owing to the neutral nature of pullulan. Galactosylation, doesn't have much influence on the hydrodynamic diameter of pullulan-curcumin conjugates. Critical micelle concentrations of the conjugates support these findings. The nongalactosylated pullulan-curcumin conjugate is toxic to HepG2 cells due to the increased solubility. The galactosylated conjugate exhibited increased toxicity to HepG2 cells. In addition to the high solubility, ASGPR mediated endocytosis promoted its toxicity.

Since alginate contains several acid functional groups, curcumin could be conjugated directly to alginate. The acid groups offered high negative zeta potential and higher stability to the conjugate micelles. Introduction of $LANH_2$ resulted in structural reorganisation and augmented the solubility of alginate leading to higher amount of curcumin being conjugated to alginate. It also decreased the hydrodynamic diameter and zeta potential to a significant extent. This observation is supported by the CMC values of the nongalactosylated and galactosylated conjugates. Higher solubility consequent to galactosylation, and the presence of targeting ligand enhanced the toxicity of the conjugate to HepG2 cells compared to the nongalactosylated conjugate. Gum arabic offered the possibility for direct conjugation of curcumin without modification. The presence of galactose moieties in the structure provided targeting efficiency towards hepatocarcinoma cells. These advantages, along

with the very high solubility of gum grabic made the GA-Cur conjugate the best among the conjugates investigated in terms of size, zeta potential, solubility and cytotoxicity.

Nanogels and polyelectrolytes in which curcumin is encapsulated were also studied. Inverse miniemulsion technique endowed preparation of small sized, spherical nanogels. Encapsulation in nanogels increased the solubility of curcumin and reduced the degradation in the physiological conditions. Toxicity towards MCF-7 cells proved the anticancer activity of the loaded curcumin.

Gelatin was modified cationically for complexation with alginate. Due to the reduction in the extent of hydrogen bonding, structural properties of gelatin were altered after modification. The complexation of the modified gelatin with alginate in appropriate compositions yielded stable nanoparticles. Encapsulation of curcumin in the nanoparticles increased the solubility and stability of curcuin. The nanoparticles could act as matrixes for controlled release of curcumin. Cytotoxicity analysis and intracellular uptake studies proved that CG/Alg complex could be a suitable carrier for curcumin delivery.

Future directions

Detailed investigation of biological activities of the prepared polymer-curcumin conjugate will result in better understanding and the application potential of the properties of the conjugates. Incorporation of quantum dots or any other fluorescent nanomaterials inside the micelle of the polymer-drug conjugate may enable simultaneous biomaging and drug delivery. The anticancer activity of curcumin loaded nanogels and polyelectrolyte complex may be analyzed in other cancer cells. These nanoparticles can be explored for the encapsulation and delivery of other hydrophobic drugs. Introduction of targeting group on this nanogels and PEC complex nanoparticles may enhance their toxicity towards cancer cells and will provide targeted drug delivery.

REFERENCES

1. Abu-Dalo, M., Othman, A. and Al-Rawashdeh, N. (2012). Exudate Gum from Acacia Trees as Green Corrosion Inhibitor for Mild Steel in Acidic Media. *International Journal of Electrochemical Science 7*(10).

2. Abu-Rabeah, K., Polyak, B., Ionescu, R. E., Cosnier, S. and Marks, R. S. (2005). Synthesis and characterization of a pyrrole-alginate conjugate and its application in a biosensor construction. *Biomacromolecules 6*(6): 3313-3318.

3. Acharya, S. and Sahoo, S. K. (2011). PLGA nanoparticles containing various anticancer agents and tumour delivery by EPR effect. *Advanced drug delivery reviews 63*(3): 170-183.

4. Aggarwal, B. B. (2008). Prostate cancer and curcumin. *Cancer biology & therapy 7*(9): 1436-1440.

5. Aggarwal, B. B., Kumar, A. and Bharti, A. C. (2003). Anticancer potential of curcumin: preclinical and clinical studies. *Anticancer res 23*(1A): 363-398.

6. Aggarwal, B. B. and Shishodia, S. (2006). Molecular targets of dietary agents for prevention and therapy of cancer. *Biochemical pharmacology 71*(10): 1397-1421.

7. Aggarwal, B. B., Surh, Y.-J. and Shishodia, S. (2007). *The molecular targets and therapeutic uses of curcumin in health and disease*, Springer.

8. Akiyoshi, K., Kobayashi, S., Shichibe, S., Mix, D., Baudys, M., Wan Kim, S. and Sunamoto, J. (1998). Self-assembled hydrogel nanoparticle of cholesterol-bearing pullulan as a carrier of protein drugs: complexation and stabilization of insulin. *Journal of controlled release 54*(3): 313-320.

9. Akiyoshi, K. and Sunamoto, J. (1996). Supramolecular assembly of hydrophobized polysaccharides. *Supramolecular Science 3*(1): 157-163.

10. Al-Shamkhani, A. and Duncan, R. (1995). Synthesis, controlled release properties and antitumour activity of alginate-cis-aconityl-daunomycin conjugates. *International journal of pharmaceutics 122*(1): 107-119.

11. Alam, S., Panda, J. J. and Chauhan, V. S. (2012). Novel dipeptide nanoparticles for effective curcumin delivery. *International journal of nanomedicine 7*: 4207.

12. Aliyar, H. A., Hamilton, P. D., Remsen, E. E. and Ravi, N. (2005). Synthesis of polyacrylamide nanogels by intramolecular disulfide cross-linking. *Journal of bioactive and compatible polymers 20*(2): 169-181.

13. Anand, P., Kunnumakkara, A. B., Newman, R. A. and Aggarwal, B. B. (2007). Bioavailability of curcumin: problems and promises. *Molecular pharmaceutics 4*(6): 807-818.

14. Anitha, A., Deepagan, V., Divya Rani, V., Menon, D., Nair, S. and Jayakumar, R. (2011). Preparation, characterization, in vitro drug release and biological studies of curcumin loaded dextran sulphate–chitosan nanoparticles. *Carbohydrate polymers 84*(3): 1158-1164.

15. Anitha, A., Deepagan, V., Rani, V. D., Menon, D., Nair, S. and Jayakumar, R. (2011). Preparation, characterization, in vitro drug release and biological studies of curcumin loaded dextran sulphate–chitosan nanoparticles. *Carbohydrate polymers 84*(3): 1158-1164.

16. Auzenne, E., Ghosh, S. C., Khodadadian, M., Rivera, B., Farquhar, D., Price, R. E., Ravoori, M., Kundra, V., Freedman, R. S. and Klostergaard, J. (2007). Hyaluronic acid-paclitaxel: antitumor efficacy against CD44 (+) human ovarian carcinoma xenografts. *Neoplasia 9*(6): 479-486.

17. Avadi, M. R., Sadeghi, A. M. M., Mohammadpour, N., Abedin, S., Atyabi, F., Dinarvand, R. and Rafiee-Tehrani, M. (2010). Preparation and characterization of insulin nanoparticles using chitosan and Arabic gum with ionic gelation method. *Nanomedicine: Nanotechnology, Biology and Medicine 6*(1): 58-63.

18. Axiak-Bechtel, S. M., Upendran, A., Lattimer, J. C., Kelsey, J., Cutler, C. S., Selting, K. A., Bryan, J. N., Henry, C. J., Boote, E. and Tate, D. J. (2014). Gum arabic-coated radioactive gold nanoparticles cause no short-term local or systemic toxicity in the clinically relevant canine model of prostate cancer. *International journal of nanomedicine 9*: 5001.

19. Ayame, H., Morimoto, N. and Akiyoshi, K. (2008). Self-assembled cationic nanogels for intracellular protein delivery. *Bioconjugate chemistry 19*(4): 882-890.

20. Bae, B.-c. and Na, K. (2010). Self-quenching polysaccharide-based nanogels of pullulan/folate-photosensitizer conjugates for photodynamic therapy. *Biomaterials 31*(24): 6325-6335.

21. Bai, X., Fang, R., Zhang, S., Shi, X., Wang, Z., Chen, X., Yang, J., Hou, X., Nie, Y. and Li, Y. (2013). Self-cross-linkable hydrogels composed of partially oxidized alginate and gelatin for myocardial infarction repair. *Journal of Bioactive and Compatible Polymers 28*(2): 126-140.

22. Baiguera, S., Del Gaudio, C., Lucatelli, E., Kuevda, E., Boieri, M., Mazzanti, B., Bianco, A. and Macchiarini, P. (2014). Electrospun gelatin scaffolds incorporating rat decellularized brain extracellular matrix for neural tissue engineering. *Biomaterials 35*(4): 1205-1214.

23. Balakrishnan, B. and Jayakrishnan, A. (2005). Self-cross-linking biopolymers as injectable in situ forming biodegradable scaffolds. *Biomaterials 26*(18): 3941-3951.

24. Balakrishnan, B., Joshi, N., Jayakrishnan, A. and Banerjee, R. (2014). Self-crosslinked oxidized alginate/gelatin hydrogel as injectable, adhesive biomimetic scaffolds for cartilage regeneration. *Acta biomaterialia*.

25. Balakrishnan, B., Mohanty, M., Umashankar, P. and Jayakrishnan, A. (2005). Evaluation of an in situ forming hydrogel wound dressing based on oxidized alginate and gelatin. *Biomaterials 26*(32): 6335-6342.

26. Balthasar, S., Michaelis, K., Dinauer, N., von Briesen, H., Kreuter, J. and Langer, K. (2005). Preparation and characterisation of antibody modified gelatin nanoparticles as drug carrier system for uptake in lymphocytes. *Biomaterials 26*(15): 2723-2732.

27. Basnet, P. and Skalko-Basnet, N. (2012). Curcumin: A Challenge in Cancer Treatment. *Journal of Nepal Pharmaceutical Association 26*(1): 19-47.

28. Bencherif, S. A., Gao, H., Srinivasan, A., Siegwart, D. J., Hollinger, J. O., Washburn, N. R. and Matyjaszewski, K. (2009). Cell-adhesive star polymers prepared by ATRP. *Biomacromolecules 10*(7): 1795-1803.

29. Berger, J., Reist, M., Mayer, J., Felt, O. and Gurny, R. (2004). Structure and interactions in chitosan hydrogels formed by complexation or aggregation for biomedical applications. *European Journal of Pharmaceutics and Biopharmaceutics 57*(1): 35-52.

30. Bertolini, A., Siani, A. and Grosso, C. (2001). Stability of monoterpenes encapsulated in gum arabic by spray-drying. *Journal of agricultural and food chemistry 49*(2): 780-785.

31. Boanini, E., Rubini, K., Panzavolta, S. and Bigi, A. (2010). Chemico-physical characterization of gelatin films modified with oxidized alginate. *Acta biomaterialia 6*(2): 383-388.

32. Bouhadir, K. H., Alsberg, E. and Mooney, D. J. (2001). Hydrogels for combination delivery of antineoplastic agents. *Biomaterials 22*(19): 2625-2633.

33. Brannon-Peppas, L. and Blanchette, J. O. (2012). Nanoparticle and targeted systems for cancer therapy. *Advanced drug delivery reviews 64*: 206-212.

34. Bruneel, D. and Schacht, E. (1993). Chemical modification of pullulan: 1. Periodate oxidation. *Polymer 34*(12): 2628-2632.

35. Brunel, F., Véron, L., Ladavière, C., David, L., Domard, A. and Delair, T. (2009). Synthesis and structural characterization of chitosan nanogels. *Langmuir 25*(16): 8935-8943.

36. Bubnis, W. A. and Ofner, C. M. (1992). The determination of ϵ-amino groups in soluble and poorly soluble proteinaceous materials by a spectrophotometrie method using trinitrobenzenesulfonic acid. *Analytical biochemistry 207*(1): 129-133.

37. Cafaggi, S., Russo, E., Stefani, R., Leardi, R., Caviglioli, G., Parodi, B., Bignardi, G., De Totero, D., Aiello, C. and Viale, M. (2007). Preparation and evaluation of nanoparticles made of chitosan or N-trimethyl chitosan and a cisplatin–alginate complex. *Journal of Controlled Release 121*(1): 110-123.

38. Cai, Z. and Kim, J. (2010). Preparation and characterization of novel bacterial cellulose/gelatin scaffold for tissue regeneration using bacterial cellulose hydrogel. *Journal of Nanotechnology in Engineering and Medicine 1*(2): 021002.

39. Caldorera-Moore, M., Guimard, N., Shi, L. and Roy, K. (2010). Designer nanoparticles: incorporating size, shape and triggered release into nanoscale drug carriers. *Expert opinion on drug delivery 7*(4): 479-495.

40. Chacko, R. T., Ventura, J., Zhuang, J. and Thayumanavan, S. (2012). Polymer nanogels: A versatile nanoscopic drug delivery platform. *Advanced drug delivery reviews 64*(9): 836-851.

41. Chainani-Wu, N. (2003). Safety and anti-inflammatory activity of curcumin: a component of tumeric (Curcuma longa). *The Journal of Alternative & Complementary Medicine 9*(1): 161-168.

42. Chan, G. and Mooney, D. J. (2013). Ca $^{2+}$ released from calcium alginate gels can promote inflammatory responses in vitro and in vivo. *Acta biomaterialia 9*(12): 9281-9291.

43. Chandler, E. M., Berglund, C. M., Lee, J. S., Polacheck, W. J., Gleghorn, J. P., Kirby, B. J. and Fischbach, C. (2011). Stiffness of photocrosslinked RGD-alginate gels regulates adipose progenitor cell behavior. *Biotechnology and bioengineering 108*(7): 1683-1692.

44. Chang, C.-P., Leung, T.-K., Lin, S.-M. and Hsu, C.-C. (2006). Release properties on gelatin-gum arabic microcapsules containing camphor oil with added polystyrene. *Colloids and Surfaces B: Biointerfaces 50*(2): 136-140.

45. Chau, Y., Dang, N. M., Tan, F. E. and Langer, R. (2006). Investigation of targeting mechanism of new dextran-peptide-methotrexate conjugates using biodistribution study in matrix-metalloproteinase-overexpressing tumor xenograft model. *Journal of pharmaceutical sciences 95*(3): 542-551.

46. Chau, Y., Tan, F. E. and Langer, R. (2004). Synthesis and characterization of dextran-peptide-methotrexate conjugates for tumor targeting via mediation by matrix metalloproteinase II and matrix metalloproteinase IX. *Bioconjugate chemistry 15*(4): 931-941.

47. Cheng, A. L., Hsu, C. H., Lin, J. K., Hsu, M. M., Ho, Y. F., Shen, T. S. and Hsieh, C. Y. (2001). Phase I clinical trial of curcumin, a chemopreventive agent, in patients with high-risk or pre-malignant lesions. *Anticancer research 21*: 2895-2900.

48. Chetouani, A., Elkolli, M., Bounekhel, M. and Benachour, D. (2014). Characterization and Bioevaluation of New Class of Hydrogels Based on Oxidized Pectin Crosslinked to Gelatin. *Journal of Biomaterials and Tissue Engineering 4*(6): 465-470.

49. Cho, K., Wang, X., Nie, S. and Shin, D. M. (2008). Therapeutic nanoparticles for drug delivery in cancer. *Clinical cancer research 14*(5): 1310-1316.

50. Choubey, J. and Bajpai, A. (2010). Investigation on magnetically controlled delivery of doxorubicin from superparamagnetic nanocarriers of gelatin crosslinked with genipin. *Journal of Materials Science: Materials in Medicine 21*(5): 1573-1586.

51. Coimbra, P., Ferreira, P., De Sousa, H., Batista, P., Rodrigues, M., Correia, I. and Gil, M. (2011). Preparation and chemical and biological characterization of a pectin/chitosan polyelectrolyte complex scaffold for possible bone tissue engineering applications. *International journal of biological macromolecules 48*(1): 112-118.

52. Connolly, S., Fenyo, J.-C. and Vandevelde, M.-C. (1988). Effect of a proteinase on the macromolecular distribution of Acacia senegal gum. *Carbohydrate polymers 8*(1): 23-32.

53. Craparo, E. F., Triolo, D., Pitarresi, G., Giammona, G. and Cavallaro, G. (2013). Galactosylated Micelles for a Ribavirin Prodrug Targeting to Hepatocytes. *Biomacromolecules 14*(6): 1838-1849.

54. Crescenzi, V., Dentini, M., Bontempo, D. and Masci, G. (2002). Hydrogels based on pullulan derivatives crosslinked via a "living" free-radical process. *Macromolecular Chemistry and Physics 203*(10-11): 1285-1291.

55. Daoud-Mahammed, S., Couvreur, P., Bouchemal, K., Chéron, M., Lebas, G., Amiel, C. and Gref, R. (2009). Cyclodextrin and polysaccharide-based nanogels: entrapment of two hydrophobic molecules, benzophenone and tamoxifen. *Biomacromolecules 10*(3): 547-554.

56. Daoud-Mahammed, S., Ringard-Lefebvre, C., Razzouq, N., Rosilio, V., Gillet, B., Couvreur, P., Amiel, C. and Gref, R. (2007). Spontaneous association of hydrophobized dextran and poly-β-cyclodextrin into nanoassemblies.: Formation and interaction with a hydrophobic drug. *Journal of colloid and interface science 307*(1): 83-93.

57. Das, S. and Chaudhury, A. (2011). Recent advances in lipid nanoparticle formulations with solid matrix for oral drug delivery. *AAPS PharmSciTech 12*(1): 62-76.

58. De Santis, S., Diociaiuti, M., Cametti, C. and Masci, G. (2014). Hyaluronic acid and alginate covalent nanogels by template cross-linking in polyion complex micelle nanoreactors. *Carbohydrate polymers 101*: 96-103.

59. del Barrio, J., Oriol, L., Sánchez, C., Serrano, J. L., Di Cicco, A., Keller, P. and Li, M.-H. (2010). Self-assembly of linear− dendritic diblock copolymers: from nanofibers to polymersomes. *Journal of the American Chemical Society 132*(11): 3762-3769.

60. Devi, N. and Kakati, D. K. (2013). Smart porous microparticles based on gelatin/sodium alginate polyelectrolyte complex. *Journal of Food Engineering 117*(2): 193-204.

61. Dey, S. and Sreenivasan, K. (2014). Conjugation of curcumin onto alginate enhances aqueous solubility and stability of curcumin. *Carbohydrate polymers 99*: 499-507.

62. Dhule, S. S., Penfornis, P., Frazier, T., Walker, R., Feldman, J., Tan, G., He, J., Alb, A., John, V. and Pochampally, R. (2012). Curcumin-loaded γ-cyclodextrin liposomal nanoparticles as delivery vehicles for osteosarcoma. *Nanomedicine: Nanotechnology, Biology and Medicine 8*(4): 440-451.

63. Ding, J., Shi, F., Xiao, C., Lin, L., Chen, L., He, C., Zhuang, X. and Chen, X. (2011). One-step preparation of reduction-responsive poly (ethylene glycol)-poly (amino acid) s nanogels as efficient intracellular drug delivery platforms. *Polymer Chemistry 2*(12): 2857-2864.

64. Djabourov, M., Leblond, J. and Papon, P. (1988). Gelation of aqueous gelatin solutions. I. Structural investigation. *Journal de physique 49*(2): 319-332.

65. Doi, R. and Kokufuta, E. (2010a). Conductometric and Light Scattering Studies on the Complexation between Cationic Polyelectrolyte Nanogel and Anionic Polyion. *Langmuir 27*(1): 392-398.

66. Doi, R. and Kokufuta, E. (2010b). On the water dispersibility of a 1: 1 stoichiometric complex between a cationic nanogel and linear polyanion. *Langmuir 26*(16): 13579-13589.

67. Dong, Z., Wang, Q. and Du, Y. (2006). Alginate/gelatin blend films and their properties for drug controlled release. *Journal of Membrane Science 280*(1): 37-44.

68. Douglas, K. L. & Tabrizian, M. (2005) Effect of experimental parameters on the formation of alginate–chitosan nanoparticles and evaluation of their potential application as DNA carrier. *Journal of Biomaterials Science, Polymer Edition 16*(1): 43-56.

69. Duan, C., Gao, J., Zhang, D., Jia, L., Liu, Y., Zheng, D., Liu, G., Tian, X., Wang, F. and Zhang, Q. (2011). Galactose-decorated pH-responsive nanogels for hepatoma-targeted delivery of oridonin. *Biomacromolecules 12*(12): 4335-4343.

70. Duncan, R. (2006). Polymer conjugates as anticancer nanomedicines. *Nature Reviews Cancer 6*(9): 688-701.

71. Elvira, C., Mano, J., San Roman, J. and Reis, R. (2002). Starch-based biodegradable hydrogels with potential biomedical applications as drug delivery systems. *Biomaterials 23*(9): 1955-1966.

72. Endres, T. K., Beck-Broichsitter, M., Samsonova, O., Renette, T. and Kissel, T. H. (2011). Self-assembled biodegradable amphiphilic PEG–PCL–lPEI triblock copolymers at the borderline between micelles and nanoparticles designed for drug and gene delivery. *Biomaterials 32*(30): 7721-7731.

73. Ethirajan, A., Schoeller, K., Musyanovych, A., Ziener, U. and Landfester, K. (2008). Synthesis and optimization of gelatin nanoparticles using the miniemulsion process. *Biomacromolecules 9*(9): 2383-2389.

74. Fajardo, A. R., Lopes, L. C., Pereira, A. G., Rubira, A. F. and Muniz, E. C. (2012). Polyelectrolyte complexes based on pectin–NH_2 and chondroitin sulfate. *Carbohydrate polymers 87*(3): 1950-1955.

75. Ferreira, S. A., Coutinho, P. J. and Gama, F. M. (2011). Synthesis and characterization of self-assembled nanogels made of pullulan. *Materials 4*(4): 601-620.

76. Ferreira, S. A., Gama, F. M. and Vilanova, M. (2013). Polymeric nanogels as vaccine delivery systems.

77. Fischbach, C., Kong, H. J., Hsiong, S. X., Evangelista, M. B., Yuen, W. and Mooney, D. J. (2009). Cancer cell angiogenic capability is regulated by 3D culture and integrin engagement. *Proceedings of the National Academy of Sciences 106*(2): 399-404.

78. Friedman, A. J., Phan, J., Schairer, D. O., Champer, J., Qin, M., Pirouz, A., Blecher-Paz, K., Oren, A., Liu, P. T. and Modlin, R. L. (2013). Antimicrobial and anti-inflammatory activity of chitosan–alginate nanoparticles: a targeted therapy for cutaneous pathogens. *Journal of investigative Dermatology 133*(5): 1231-1239.

79. Fundueanu, G., Constantin, M. and Ascenzi, P. (2008). Preparation and characterization of pH-and temperature-sensitive pullulan microspheres for controlled release of drugs. *Biomaterials 29*(18): 2767-2775.

80. Fuoss, R. M. and Sadek, H. (1949). Mutual interaction of polyelectrolytes. *Science 110*(2865): 552-554.

81. Gamal-Eldeen, A., Moustafa, D., El-Daly, S. and Katti, K. (2014). P0131 Efficacy of gum arabic-conjugated gold nanoparticles as a photothermal therapy for lung cancer: In vitro and in vivo approaches. *European journal of cancer 50*: e46.

82. Garcea, G., Jones, D., Singh, R., Dennison, A., Farmer, P., Sharma, R., Steward, W., Gescher, A. and Berry, D. (2004). Detection of curcumin and its metabolites in hepatic tissue and portal blood of patients following oral administration. *British journal of cancer 90*(5): 1011-1015.

83. Gessner, A., Waicz, R., Lieske, A., Paulke, B.-R., Mäder, K. and Müller, R. (2000). Nanoparticles with decreasing surface hydrophobicities: influence on plasma protein adsorption. *International journal of pharmaceutics 196*(2): 245-249.

84. Givetal, N.I., Ushakov, S.N., Panarin, E.F. and Popova, G.O. (1965). Experimental studies on penicillin polymer derivatives. Antibiotiki, 10(4): 701–706.

85. Goel, A., Boland, C. R. and Chauhan, D. P. (2001). Specific inhibition of cyclooxygenase-2 (COX-2) expression by dietary curcumin in HT-29 human colon cancer cells. *Cancer letters 172*(2): 111-118.

86. Gomes, J. F., Rocha, S., Pereira, M. d. C., Peres, I., Moreno, S., Toca-Herrera, J. and Coelho, M. A. (2010). Lipid/particle assemblies based on maltodextrin–gum arabic core as bio-carriers. *Colloids and Surfaces B: Biointerfaces 76*(2): 449-455.

87. Gonçalves, C., Pereira, P., Schellenberg, P., Coutinho, P. J. and Gama, F. M. (2012). Self-assembled dextrin nanogel as curcumin delivery system. *Journal of Biomaterials and Nanobiotechnology 3*: 178.

88. Goodarzi, N., Varshochian, R., Kamalinia, G., Atyabi, F. and Dinarvand, R. (2013). A review of polysaccharide cytotoxic drug conjugates for cancer therapy. *Carbohydrate polymers 92*(2): 1280-1293.

89. Gou, M., Men, K., Shi, H., Xiang, M., Zhang, J., Song, J., Long, J., Wan, Y., Luo, F. and Zhao, X. (2011). Curcumin-loaded biodegradable polymeric micelles for colon cancer therapy in vitro and in vivo. *Nanoscale 3*(4): 1558-1567.

90. Grenha, A., Gomes, M. E., Rodrigues, M., Santo, V. E., Mano, J. F., Neves, N. M. and Reis, R. L. (2010). Development of new chitosan/carrageenan nanoparticles for drug delivery applications. *Journal of Biomedical Materials Research Part A 92*(4): 1265-1272.

91. Guo, H., Zhang, D., Li, C., Jia, L., Liu, G., Hao, L., Zheng, D., Shen, J., Li, T. and Guo, Y. (2013). Self-assembled nanoparticles based on galactosylated O-carboxymethyl chitosan-graft-stearic acid conjugates for delivery of doxorubicin. *International journal of Pharmaceutics 458*(1): 31-38.

92. Gupta, A. K., Gupta, M., Yarwood, S. J. and Curtis, A. S. (2004). Effect of cellular uptake of gelatin nanoparticles on adhesion, morphology and cytoskeleton organisation of human fibroblasts. *Journal of controlled release 95*(2): 197-207.

93. Gupta, M. and Gupta, A. K. (2004). Hydrogel pullulan nanoparticles encapsulating pBUDLacZ plasmid as an efficient gene delivery carrier. *Journal of Controlled Release 99*(1): 157-166.

94. Haensler, J. and Schuber, F. (1988). Preparation of neo-galactosylated liposomes and their interaction with mouse peritoneal macrophages. *Biochimica et Biophysica Acta (BBA)-Biomembranes 946*(1): 95-105.

95. Hamman, J. H. (2010). Chitosan based polyelectrolyte complexes as potential carrier materials in drug delivery systems. *Marine Drugs 8*(4): 1305-1322.

96. Hans, M. and Lowman, A. (2002). Biodegradable nanoparticles for drug delivery and targeting. *Current Opinion in Solid State and Materials Science 6*(4): 319-327.

97. Hasegawa, U., Nomura, S.-i. M., Kaul, S. C., Hirano, T. and Akiyoshi, K. (2005). Nanogel-quantum dot hybrid nanoparticles for live cell imaging. *Biochemical and biophysical research communications 331*(4): 917-921.

98. Hasuda, H., Kwon, O. H., Kang, I.-K. and Ito, Y. (2005). Synthesis of photoreactive pullulan for surface modification. *Biomaterials 26*(15): 2401-2406.

99. Haug, I. J., Draget, K. I. and Smidsrød, O. (2004). Physical behaviour of fish gelatin-κ-carrageenan mixtures. *Carbohydrate polymers 56*(1): 11-19.

100. Hayashi, Y., Mori, Y., Yamashita, S., Motoyama, K., Higashi, T., Jono, H., Ando, Y. and Arima, H. (2012). Potential use of lactosylated dendrimer (G3)/α-cyclodextrin conjugates as hepatocyte-specific sirna carriers for the treatment of familial amyloidotic polyneuropathy. *Molecular pharmaceutics 9*(6): 1645-1653.

101. Hirakura, T., Nomura, Y., Aoyama, Y. and Akiyoshi, K. (2004). Photoresponsive nanogels formed by the self-assembly of spiropyrane-bearing pullulan that act as artificial molecular chaperones. *Biomacromolecules 5*(5): 1804-1809.

102. Hoehle, S. I., Pfeiffer, E., Sólyom, A. M. and Metzler, M. (2006). Metabolism of curcuminoids in tissue slices and subcellular fractions from rat liver. *Journal of agricultural and food chemistry 54*(3): 756-764.

103. Hu, F.-Q., Liu, L.-N., Du, Y.-Z. and Yuan, H. (2009). Synthesis and antitumor activity of doxorubicin conjugated stearic acid- g-chitosan oligosaccharide polymeric micelles. *Biomaterials 30*(36): 6955-6963.

104. Huang, Y., Onyeri, S., Siewe, M., Moshfeghian, A. and Madihally, S. V. (2005). In vitro characterization of chitosan–gelatin scaffolds for tissue engineering. *Biomaterials 26*(36): 7616-7627.

105. Ibrahim, H., Bindschaedler, C., Doelker, E., Buri, P. and Gurny, R. (1992). Aqueous nanodispersions prepared by a salting-out process. *International journal of pharmaceutics 87*(1): 239-246.

106. Imani, R., Rafienia, M. and Hojjati Emami, S. (2013). Synthesis and characterization of glutaraldehyde-based crosslinked gelatin as a local hemostat sponge in surgery: An in vitro study. *Bio-medical materials and engineering 23*(3): 211-224.

107. Inci, I., Kirsebom, H., Galaev, I. Y., Mattiasson, B. and Piskin, E. (2013). Gelatin cryogels crosslinked with oxidized dextran and containing freshly formed hydroxyapatite as potential bone tissue-engineering scaffolds. *Journal of tissue engineering and regenerative medicine 7*(7): 584-588.

108. Inoue, K., Yoshimura, Y. and Nakazawa, H. (2001). Evaluation of the turmeric (Curcuma longa L.) based on the flow-injection analysis with ultraviolet and fluorometric detections. *Analytical letters 34*(10): 1711-1718.

109. Ireson, C., Orr, S., Jones, D. J., Verschoyle, R., Lim, C.-K., Luo, J.-L., Howells, L., Plummer, S., Jukes, R. and Williams, M. (2001). Characterization of metabolites of the chemopreventive agent curcumin in human and rat hepatocytes and in the rat in vivo, and evaluation of their ability to inhibit phorbol ester-induced prostaglandin E2 production. *Cancer Research 61*(3): 1058-1064.

110. Ireson, C. R., Jones, D. J., Orr, S., Coughtrie, M. W., Boocock, D. J., Williams, M. L., Farmer, P. B., Steward, W. P. and Gescher, A. J. (2002). Metabolism of the cancer chemopreventive agent curcumin in human and rat intestine. *Cancer Epidemiology Biomarkers & Prevention 11*(1): 105-111.

111. Issa, R. M., Khedr, A. M. and Rizk, H. (2008). 1H NMR, IR and UV/VIS Spectroscopic Studies of Some Schiff Bases Derived from 2-Aminobenzothiazole and 2-Amino-3-Hydroxypyridine. *Journal of the Chinese Chemical Society 55*(4): 875-884.

112. Jagatha, B., Mythri, R. B., Vali, S. and Bharath, M. S. (2008). Curcumin treatment alleviates the effects of glutathione depletion in vitro and in vivo: therapeutic implications for Parkinson's disease explained via in silico studies. *Free Radical Biology and Medicine 44*(5): 907-917.

113. Jayakumar, R., Chennazhi, K., Muzzarelli, R., Tamura, H., Nair, S. and Selvamurugan, N. (2010). Chitosan conjugated DNA nanoparticles in gene therapy. *Carbohydrate polymers 79*(1): 1-8.

114. Jayakumar, R., Nair, A., Rejinold, N. S., Maya, S. and Nair, S. (2012). Doxorubicin-loaded pH-responsive chitin nanogels for drug delivery to cancer cells. *Carbohydrate polymers 87*(3): 2352-2356.

115. Jiang, L., Zhou, Q., Mu, K., Xie, H., Zhu, Y., Zhu, W., Zhao, Y., Xu, H. and Yang, X. (2013). pH/temperature sensitive magnetic nanogels conjugated with Cy5. 5-labled lactoferrin for MR and fluorescence imaging of glioma in rats. *Biomaterials 34*(30): 7418-7428.

116. Jintapattanakit, A., Junyaprasert, V. B. and Kissel, T. (2009). The role of mucoadhesion of trimethyl chitosan and PEGylated trimethyl chitosan nanocomplexes in insulin uptake. *Journal of pharmaceutical sciences 98*(12): 4818-4830.

117. Joe, B., Vijaykumar, M. and Lokesh, B. (2004). Biological properties of curcumin-cellular and molecular mechanisms of action. *Critical Reviews in Food Science and Nutrition 44*(2): 97-111.

118. Jovanovic, S. V., Steenken, S., Boone, C. W. and Simic, M. G. (1999). H-atom transfer is a preferred antioxidant mechanism of curcumin. *Journal of the American Chemical Society 121*(41): 9677-9681.

119. Kabanov, A. V. and Vinogradov, S. V. (2009). Nanogels as pharmaceutical carriers: finite networks of infinite capabilities. *Angewandte Chemie International Edition 48*(30): 5418-5429.

120. Kang, H.-W., Tabata, Y. and Ikada, Y. (1999). Fabrication of porous gelatin scaffolds for tissue engineering. *Biomaterials 20*(14): 1339-1344.

121. Kanokpanont, S., Damrongsakkul, S., Ratanavaraporn, J. and Aramwit, P. (2012). An innovative bi-layered wound dressing made of silk and gelatin for accelerated wound healing. *International journal of pharmaceutics 436*(1): 141-153.

122. Kattumuri, V., Katti, K., Bhaskaran, S., Boote, E. J., Casteel, S. W., Fent, G. M., Robertson, D. J., Chandrasekhar, M., Kannan, R. and Katti, K. V. (2007). Gum Arabic as a Phytochemical Construct for the Stabilization of Gold Nanoparticles: In Vivo Pharmacokinetics and X-ray-Contrast-Imaging Studies. *Small 3*(2): 333-341.

123. Kaul, G. and Amiji, M. (2002). Long-circulating poly (ethylene glycol)-modified gelatin nanoparticles for intracellular delivery. *Pharmaceutical research 19*(7): 1061-1067.

124. Khopde, S. M., Indira Priyadarsini, K. and Mukherjee, T. (2000). Effect of Solvent on the Excited-state Photophysical Properties of Curcumin. *Photochemistry and photobiology 72*(5): 625-631.

125. Kim, H.-J., Lee, H.-C., Oh, J.-S., Shin, B.-A., Oh, C.-S., Park, R.-D., Yang, K.-S. and Cho, C.-S. (1999). Polyelectrolyte complex composed of chitosan and sodium alginate for wound dressing application. *Journal of Biomaterials Science, Polymer Edition 10*(5): 543-556.

126. Kim, J. H., Li, Y., Kim, M. S., Kang, S. W., Jeong, J. H. and Lee, D. S. (2012). Synthesis and evaluation of biotin-conjugated pH-responsive polymeric micelles as drug carriers. *International journal of Pharmaceutics 427*(2): 435-442.

127. Kim, M. S., Jun, I., Shin, Y. M., Jang, W., Kim, S. I. and Shin, H. (2010). The Development of Genipin-Crosslinked Poly (caprolactone)(PCL)/Gelatin Nanofibers for Tissue Engineering Applications. *Macromolecular bioscience 10*(1): 91-100.

128. Kim, S., Shi, Y., Kim, J. Y., Park, K. and Cheng, J.-X. (2010). Overcoming the barriers in micellar drug delivery: loading efficiency, in vivo stability, and micelle-cell interaction. *Expert opinion on drug delivery 7*(1): 49-62.

129. Kim, T. H., Jiang, H. H., Youn, Y. S., Park, C. W., Tak, K. K., Lee, S., Kim, H., Jon, S., Chen, X. and Lee, K. C. (2011). Preparation and characterization of water-soluble albumin-bound curcumin nanoparticles with improved antitumor activity. *International journal of Pharmaceutics 403*(1): 285-291.

130. Kim, W. S., Mooney, D. J., Arany, P. R., Lee, K., Huebsch, N. and Kim, J. (2012). Adipose tissue engineering using injectable, oxidized alginate hydrogels. *Tissue Engineering Part A 18*(7-8): 737-743.

131. Kim, Y. D. and Morr, C. V. (1996). Microencapsulation properties of gum arabic and several food proteins: spray-dried orange oil emulsion particles. *Journal of agricultural and food chemistry 44*(5): 1314-1320.

132. Kołodziejska, I., Piotrowska, B., Bulge, M. and Tylingo, R. (2006). Effect of transglutaminase and 1-ethyl-3-(3-dimethylaminopropyl) carbodiimide on the solubility of fish gelatin–chitosan films. *Carbohydrate polymers 65*(4): 404-409.

133. Kuckling, D., Vo, C. D., Adler, H.-J., Völkel, A. and Cölfen, H. (2006). Preparation and characterization of photo-cross-linked thermosensitive PNIPAAm nanogels. *Macromolecules 39*(4): 1585-1591.

134. Kudlay, A. and de la Cruz, M. O. (2004). Precipitation of oppositely charged polyelectrolytes in salt solutions. *The Journal of chemical physics 120*(1): 404-412.

135. Kumar, D., Saini, N., Pandit, V. and Ali, S. (2012). An insight to pullulan: a biopolymer in pharmaceutical approaches. *International Journal of Basic and Applied Sciences 1*(3): 202-219.

136. Landfester, K. (2006). Synthesis of colloidal particles in miniemulsions. *Annu. Rev. Mater. Res. 36*: 231-279.

137. Landfester, K., Bechthold, N., Tiarks, F. and Antonietti, M. (1999). Formulation and stability mechanisms of polymerizable miniemulsions. *Macromolecules 32*(16): 5222-5228.

138. Landfester, K., Willert, M. and Antonietti, M. (2000). Preparation of polymer particles in nonaqueous direct and inverse miniemulsions. *Macromolecules 33*(7): 2370-2376.

139. Lankalapalli, S. and Kolapalli, V. (2009). Polyelectrolyte complexes: A review of their applicability in drug delivery technology. *Indian journal of pharmaceutical sciences 71*(5): 481.

140. Lao, C. D., Ruffin, M. T., Normolle, D., Heath, D. D., Murray, S. I., Bailey, J. M., Boggs, M. E., Crowell, J., Rock, C. L. and Brenner, D. E. (2006). Dose escalation of a curcuminoid formulation. *BMC complementary and alternative medicine 6*(1): 10.

141. Lavergne, M., Derkaoui, M., Delmau, C., Letourneur, D., Uzan, G. and Le Visage, C. (2012). Porous Polysaccharide-Based Scaffolds for Human Endothelial Progenitor Cells. *Macromolecular bioscience 12*(7): 901-910.

142. Leathers, T. D. (2003). Biotechnological production and applications of pullulan. *Applied Microbiology and Biotechnology 62*(5-6): 468-473.

143. Lee, G.-S., Park, J.-H., Shin, U. S. and Kim, H.-W. (2011). Direct deposited porous scaffolds of calcium phosphate cement with alginate for drug delivery and bone tissue engineering. *Acta biomaterialia 7*(8): 3178-3186.

144. Lee, H., Mok, H., Lee, S., Oh, Y.-K. and Park, T. G. (2007). Target-specific intracellular delivery of siRNA using degradable hyaluronic acid nanogels. *Journal of Controlled Release 119*(2): 245-252.

145. Lee, I. and Akiyoshi, K. (2004). Single molecular mechanics of a cholesterol-bearing pullulan nanogel at the hydrophobic interfaces. *Biomaterials 25*(15): 2911-2918.

146. Lee, K. Y. and Mooney, D. J. (2001). Hydrogels for tissue engineering. *Chemical reviews 101*(7): 1869-1880.

147. Lee, K. Y. and Mooney, D. J. (2012). Alginate: properties and biomedical applications. *Progress in polymer science 37*(1): 106-126.

148. Lee, S. H., Mok, H., Lee, Y. and Park, T. G. (2011). Self-assembled siRNA–PLGA conjugate micelles for gene silencing. *Journal of controlled release 152*(1): 152-158.

149. Lee, S. J., Yhee, J. Y., Kim, S. H., Kwon, I. C. and Kim, K. (2013). Biocompatible gelatin nanoparticles for tumor-targeted delivery of polymerized siRNA in tumor-bearing mice. *Journal of controlled release 172*(1): 358-366.

150. Lee, W. C., Li, Y. C. and Chu, I. (2006). Amphiphilic Poly (D, L-lactic acid)/Poly (ethylene glycol)/Poly (D, L-lactic acid) Nanogels for Controlled Release of Hydrophobic Drugs. *Macromolecular bioscience 6*(10): 846-854.

151. Lehtinen, J., Raki, M., Bergström, K. A., Uutela, P., Lehtinen, K., Hiltunen, A., Pikkarainen, J., Liang, H., Pitkänen, S. and Määttä, A.-M. (2012). Pre-targeting and direct immunotargeting of liposomal drug carriers to ovarian carcinoma. *PloS one 7*(7): e41410.

152. Lemarchand, C., Gref, R., Lesieur, S., Hommel, H., Vacher, B., Besheer, A., Maeder, K. and Couvreur, P. (2005). Physico-chemical characterization of polysaccharide-coated nanoparticles. *Journal of Controlled Release 108*(1): 97-111.

153. Leo, E., Angela Vandelli, M., Cameroni, R. and Forni, F. (1997). Doxorubicin-loaded gelatin nanoparticles stabilized by glutaraldehyde: involvement of the drug in the cross-linking process. *International journal of Pharmaceutics 155*(1): 75-82.

154. Li, H., Chen, C., Zhang, S., Jiang, J., Tao, H., Xu, J., Sun, J., Zhong, W. and Chen, S. (2012). The use of layer by layer self-assembled coatings of hyaluronic acid and cationized gelatin to improve the biocompatibility of poly (ethylene terephthalate) artificial ligaments for reconstruction of the anterior cruciate ligament. *Acta biomaterialia 8*(11): 4007-4019.

155. Li, H., Yang, J., Hu, X., Liang, J., Fan, Y. and Zhang, X. (2011). Superabsorbent polysaccharide hydrogels based on pullulan derivate as antibacterial release wound dressing. *Journal of Biomedical Materials Research Part A 98*(1): 31-39.

156. Li, J. K., Wang, N. and Wu, X. S. (1997). A novel biodegradable system based on gelatin nanoparticles and poly (lactic-co-glycolic acid) microspheres for protein and peptide drug delivery. *Journal of pharmaceutical sciences 86*(8): 891-895.

157. Li, P., Luo, Z., Liu, P., Gao, N., Zhang, Y., Pan, H., Liu, L., Wang, C., Cai, L. and Ma, Y. (2013). Bioreducible alginate-poly (ethylenimine) nanogels as an antigen-delivery system robustly enhance vaccine-elicited humoral and cellular immune responses. *Journal of controlled release 168*(3): 271-279.

158. Li, T., Shi, X. W., Du, Y. M. and Tang, Y. F. (2007). Quaternized chitosan/alginate nanoparticles for protein delivery. *Journal of Biomedical Materials Research Part A 83*(2): 383-390.

159. Li, Y., Huang, G., Diakur, J. and Wiebe, L. I. (2008). Targeted delivery of macromolecular drugs: asialoglycoprotein receptor (ASGPR) expression by selected hepatoma cell lines used in antiviral drug development. *Current drug delivery 5*(4): 299-302.

160. Li, Y., Jia, H., Cheng, Q., Pan, F. and Jiang, Z. (2011). Sodium alginate–gelatin polyelectrolyte complex membranes with both high water vapor permeance and high permselectivity. *Journal of Membrane Science 375*(1): 304-312.

161. Liang, H.-F., Chen, C.-T., Chen, S.-C., Kulkarni, A. R., Chiu, Y.-L., Chen, M.-C. and Sung, H.-W. (2006). Paclitaxel-loaded poly (gamma-glutamic acid)-poly (lactide) nanoparticles as a targeted drug delivery system for the treatment of liver cancer. *Biomaterials 27*(9): 2051-2059.

162. Lim, Y. C., Johnson, J., Fei, Z., Wu, Y., Farson, D. F., Lannutti, J. J., Choi, H. W. and Lee, L. J. (2011). Micropatterning and characterization of electrospun poly (ε-caprolactone)/gelatin nanofiber tissue scaffolds by femtosecond laser ablation for tissue engineering applications. *Biotechnology and bioengineering 108*(1): 116-126.

163. Liu, L., Liu, C.-K., Fishman, M. L. and Hicks, K. B. (2007). Composite films from pectin and fish skin gelatin or soybean flour protein. *Journal of agricultural and food chemistry 55*(6): 2349-2355.

164. Liu, Q., Loo, W. T., Sze, S. and Tong, Y. (2009). Curcumin inhibits cell proliferation of MDA-MB-231 and BT-483 breast cancer cells mediated by down-regulation of NFκB, cyclinD and MMP-1 transcription. *Phytomedicine 16*(10): 916-922.

165. Liu, X., Smith, L. A., Hu, J. and Ma, P. X. (2009). Biomimetic nanofibrous gelatin/apatite composite scaffolds for bone tissue engineering. *Biomaterials 30*(12): 2252-2258.

166. Liu, Z., Jiao, Y., Wang, Y., Zhou, C. and Zhang, Z. (2008). Polysaccharides-based nanoparticles as drug delivery systems. *Advanced drug delivery reviews 60*(15): 1650-1662.

167. López-Lázaro, M., Willmore, E., Jobson, A., Gilroy, K. L., Curtis, H., Padget, K. and Austin, C. A. (2007). Curcumin Induces High Levels of Topoisomerase I− and II− DNA Complexes in K562 Leukemia Cells. *Journal of natural products 70*(12): 1884-1888.

168. López-Lázaro, M. (2008). Anticancer and carcinogenic properties of curcumin: considerations for its clinical development as a cancer chemopreventive and chemotherapeutic agent. *Molecular nutrition & food research 52*(S1): S103-S127.

169. Lu, D., Wen, X., Liang, J., Gu, Z., Zhang, X. and Fan, Y. (2009). A pH-sensitive nano drug delivery system derived from pullulan/doxorubicin conjugate. *Journal of Biomedical Materials Research Part B: Applied Biomaterials 89*(1): 177-183.

170. Ma, Z., Haddadi, A., Molavi, O., Lavasanifar, A., Lai, R. and Samuel, J. (2008). Micelles of poly (ethylene oxide)-b-poly (ε-caprolactone) as vehicles for the solubilization, stabilization, and controlled delivery of curcumin. *Journal of Biomedical Materials Research Part A 86*(2): 300-310.

171. Maeda, H., Seymour, L. W. and Miyamoto, Y. (1992). Conjugates of anticancer agents and polymers: advantages of macromolecular therapeutics in vivo. *Bioconjugate chemistry 3*(5): 351-362.

172. Maheshwari, R. K., Singh, A. K., Gaddipati, J. and Srimal, R. C. (2006). Multiple biological activities of curcumin: a short review. *Life sciences 78*(18): 2081-2087.

173. Mandeville, J.-S., Froehlich, E. and Tajmir-Riahi, H. (2009). Study of curcumin and genistein interactions with human serum albumin. *Journal of pharmaceutical and biomedical analysis 49*(2): 468-474.

174. Mangalathillam, S., Rejinold, N. S., Nair, A., Lakshmanan, V.-K., Nair, S. V. and Jayakumar, R. (2012). Curcumin loaded chitin nanogels for skin cancer treatment via the transdermal route. *Nanoscale 4*(1): 239-250.

175. Manju, S., Muraleedharan, C. V., Rajeev, A., Jayakrishnan, A. and Joseph, R. (2011). Evaluation of alginate dialdehyde cross-linked gelatin hydrogel as a biodegradable sealant for polyester vascular graft. *Journal of Biomedical Materials Research Part B: Applied Biomaterials 98*(1): 139-149.

176. Manju, S. and Sreenivasan, K. (2011a). Conjugation of curcumin onto hyaluronic acid enhances its aqueous solubility and stability. *Journal of colloid and interface science 359*(1): 318-325.

177. Manju, S. and Sreenivasan, K. (2011b). Synthesis and characterization of a cytotoxic cationic polyvinylpyrrolidone–curcumin conjugate. *Journal of pharmaceutical sciences 100*(2): 504-511.

178. Matsumoto, G., Kushibiki, T., Kinoshita, Y., Lee, U., Omi, Y., Kubota, E. and Tabata, Y. (2006). Cationized gelatin delivery of a plasmid DNA expressing small interference RNA for VEGF inhibits murine squamous cell carcinoma. *Cancer science 97*(4): 313-321.

179. Mehvar, R. (2003). Recent trends in the use of polysaccharides for improved delivery of therapeutic agents: pharmacokinetic and pharmacodynamic perspectives. *Current pharmaceutical biotechnology 4*(5): 283-302.

180. Michaels, A. S. and Miekka, R. G. (1961). Polycation-polyanion complexes: Preparation and properties of poly-(vinylbenzyltrimethylammonium) poly-(styrenesulfonate). *The Journal of Physical Chemistry 65*(10): 1765-1773.

181. Mimi, H., Ho, K. M., Siu, Y. S., Wu, A. and Li, P. (2012). Polyethyleneimine-based core-shell nanogels: a promising siRNA carrier for argininosuccinate synthetase mRNA knockdown in HeLa cells. *Journal of Controlled Release 158*(1): 123-130.

182. Moghimi, S. and Szebeni, J. (2003). Stealth liposomes and long circulating nanoparticles: critical issues in pharmacokinetics, opsonization and protein-binding properties. *Progress in lipid research 42*(6): 463-478.

183. Morimoto, K., Chono, S., Kosai, T., Seki, T. and Tabata, Y. (2008). Design of cationic microspheres based on aminated gelatin for controlled release of peptide and protein drugs. *Drug delivery 15*(2): 113-117.

184. Morris, V. B. and Sharma, C. P. (2010). Folate mediated in vitro targeting of depolymerised trimethylated chitosan having arginine functionality. *Journal of colloid and interface science 348*(2): 360-368.

185. Mourtas, S., Lazar, A. N., Markoutsa, E., Duyckaerts, C. and Antimisiaris, S. G. (2014). Multifunctional nanoliposomes with curcumin–lipid derivative and brain targeting functionality with potential applications for Alzheimer disease. *European journal of medicinal chemistry 80*: 175-183.

186. Mukerjee, A. and Vishwanatha, J. K. (2009). Formulation, characterization and evaluation of curcumin-loaded PLGA nanospheres for cancer therapy. *Anticancer research 29*(10): 3867-3875.

187. Munshi, N., De, T. K. and Maitra, A. (1997). Size modulation of polymeric nanoparticles under controlled dynamics of microemulsion droplets. *Journal of colloid and interface science 190*(2): 387-391.

188. Musyanovych, A., Schmitz-Wienke, J., Mailänder, V., Walther, P. and Landfester, K. (2008). Preparation of biodegradable polymer nanoparticles by miniemulsion technique and their cell interactions. *Macromolecular bioscience 8*(2): 127-139.

189. Na, K. and Bae, Y. H. (2002). Self-assembled hydrogel nanoparticles responsive to tumor extracellular pH from pullulan derivative/sulfonamide conjugate: characterization, aggregation, and adriamycin release in vitro. *Pharmaceutical research 19*(5): 681-688.

190. Na, K., Lee, K. H. and Bae, Y. H. (2004). pH-sensitivity and pH-dependent interior structural change of self-assembled hydrogel nanoparticles of pullulan acetate/oligo-sulfonamide conjugate. *Journal of controlled release 97*(3): 513-525.

191. Na, K., Park, K. M., Jo, E. A. and Lee, K. S. (2006). Self-organized pullulan/deoxycholic acid nanogels: Physicochemical characterization and anti-cancer drug-releasing behavior. *Biotechnology and Bioprocess Engineering 11*(3): 262-267.

192. Na, K., Seong Lee, E. and Bae, Y. H. (2003). Adriamycin loaded pullulan acetate/sulfonamide conjugate nanoparticles responding to tumor pH: pH-dependent cell interaction, internalization and cytotoxicity in vitro. *Journal of Controlled Release 87*(1): 3-13.

193. Nesamony, J. and Kolling, W. M. (2005). IPM/DOSS/water microemulsions as reactors for silver sulfadiazine nanocrystal synthesis. *Journal of pharmaceutical sciences 94*(6): 1310-1320.

194. Nesamony, J., Singh, P. R., Nada, S. E., Shah, Z. A. and Kolling, W. M. (2012). Calcium alginate nanoparticles synthesized through a novel interfacial cross-linking method as a potential protein drug delivery system. *Journal of pharmaceutical sciences 101*(6): 2177-2184.

195. Nielsen, U. B., Kirpotin, D. B., Pickering, E. M., Hong, K., Park, J. W., Shalaby, M. R., Shao, Y., Benz, C. C. and Marks, J. D. (2002). Therapeutic efficacy of anti-ErbB2 immunoliposomes targeted by a phage antibody selected for cellular endocytosis. *Biochimica et Biophysica Acta (BBA)-Molecular Cell Research 1591*(1): 109-118.

196. Nishi, K., Antony, M. and Jayakrishnan, A. (2007). Synthesis and evaluation of ampicillin-conjugated gum arabic microspheres for sustained release. *Journal of pharmacy and pharmacology 59*(4): 485-493.

197. Nishi, K., Antony, M., Mohanan, P., Anilkumar, T., Loiseau, P. and Jayakrishnan, A. (2007). Amphotericin B-gum arabic conjugates: synthesis, toxicity, bioavailability, and activities against Leishmania and fungi. *Pharmaceutical research 24*(5): 971-980.

198. Nishi, K. and Jayakrishnan, A. (2004). Preparation and in vitro evaluation of primaquine-conjugated gum arabic microspheres. *Biomacromolecules 5*(4): 1489-1495.

199. Ofokansi, K., Winter, G., Fricker, G. and Coester, C. (2010). Matrix-loaded biodegradable gelatin nanoparticles as new approach to improve drug loading and delivery. *European journal of pharmaceutics and biopharmaceutics 76*(1): 1-9.

200. Oh, J. K., Drumright, R., Siegwart, D. J. and Matyjaszewski, K. (2008). The development of microgels/nanogels for drug delivery applications. *Progress in Polymer Science 33*(4): 448-477.

201. Oh, J. K., Siegwart, D. J., Lee, H.-i., Sherwood, G., Peteanu, L., Hollinger, J. O., Kataoka, K. and Matyjaszewski, K. (2007). Biodegradable nanogels prepared by atom transfer radical polymerization as potential drug delivery carriers: synthesis, biodegradation, in vitro release, and bioconjugation. *Journal of the American Chemical Society 129*(18): 5939-5945.

202. Orive, G., Hernández, R. M., Gascón, A. R. and Pedraz, J. L. (2005). Micro and nano drug delivery systems in cancer therapy. *Cancer Therapy 3*: 131-138.

203. Park, I.-K., Kim, Y. J., Tran, T. H., Huh, K. M. and Lee, Y.-k. (2010). Water-soluble heparin–PTX conjugates for cancer targeting. *Polymer 51*(15): 3387-3393.

204. Park, K. M., Lee, Y., Son, J. Y., Oh, D. H., Lee, J. S. and Park, K. D. (2012). Synthesis and characterizations of in situ cross-linkable gelatin and 4-arm-PPO-PEO hybrid hydrogels via enzymatic reaction for tissue regenerative medicine. *Biomacromolecules 13*(3): 604-611.

205. Patel, R., Singh, S., Singh, S., Sheth, N. and Gendle, R. (2009). Development and characterization of curcumin loaded transfersome for transdermal delivery. *J Pharm Sci Res 1*(4): 71-80.

206. Peña, C., De la Caba, K., Eceiza, A., Ruseckaite, R. and Mondragon, I. (2010). Enhancing water repellence and mechanical properties of gelatin films by tannin addition. *Bioresource technology 101*(17): 6836-6842.

207. Perevyazko, I. Y., Bauer, M., Pavlov, G. M., Hoeppener, S., Schubert, S., Fischer, D. and Schubert, U. S. (2012). Polyelectrolyte complexes of DNA and linear PEI: formation, composition and properties. *Langmuir 28*(46): 16167-16176.

208. Picone, C. S. F. and Cunha, R. L. (2013). Chitosan–gellan electrostatic complexes: Influence of preparation conditions and surfactant presence. *Carbohydrate polymers 94*(1): 695-703.

209. Pileni, M. (1997). Nanosized particles made in colloidal assemblies. *Langmuir 13*(13): 3266-3276.

210. Prajapati, V. D., Jani, G. K. and Khanda, S. M. (2013). Pullulan: An exopolysaccharide and its various applications. *Carbohydrate polymers 95*(1): 540-549.

211. Prata, A. S., Zanin, M. H., Ré, M. I. and Grosso, C. R. (2008). Release properties of chemical and enzymatic crosslinked gelatin-gum Arabic microparticles containing a fluorescent probe plus vetiver essential oil. *Colloids and Surfaces B: Biointerfaces 67*(2): 171-178.

212. Priyadarsini, K. I. (2009). Photophysics, photochemistry and photobiology of curcumin: Studies from organic solutions, bio-mimetics and living cells. *Journal of Photochemistry and Photobiology C: Photochemistry Reviews 10*(2): 81-95.

213. Qi, C., Chen, Y., Huang, J. H., Jin, Q. Z. and Wang, X. G. (2012). Preparation and characterization of catalase-loaded solid lipid nanoparticles based on soybean phosphatidylcholine. *Journal of the Science of Food and Agriculture 92*(4): 787-793.

214. Raemdonck, K., Demeester, J. and De Smedt, S. (2009). Advanced nanogel engineering for drug delivery. *Soft Matter 5*(4): 707-715.

215. Ramachandran, C., Fonseca, H. B., Jhabvala, P., Escalon, E. A. and Melnick, S. J. (2002). Curcumin inhibits telomerase activity through human telomerase reverse transcritpase in MCF-7 breast cancer cell line. *Cancer letters 184*(1): 1-6.

216. Randall, R., Phillips, G. and Williams, P. (1989). Fractionation and characterization of gum from Acacia senegal. *Food Hydrocolloids 3*(1): 65-75.

217. Ray, A. K., Bird, P. B., Iacobucci, G. A. and Clark Jr, B. C. (1995). Functionality of gum arabic. Fractionation, characterization and evaluation of gum fractions in citrus oil emulsions and model beverages. *Food Hydrocolloids 9*(2): 123-131.

218. Reis, A. V., Guilherme, M. R., Cavalcanti, O. A., Rubira, A. F. and Muniz, E. C. (2006). Synthesis and characterization of pH-responsive hydrogels based on chemically modified Arabic gum polysaccharide. *Polymer 47*(6): 2023-2029.

219. Rejinold N, S., Chennazhi, K. P., Tamura, H., Nair, S. V. and Rangasamy, J. (2011). Multifunctional chitin nanogels for simultaneous drug delivery, bioimaging, and biosensing. *ACS applied materials & interfaces 3*(9): 3654-3665.

220. Rejinold, N. S., Nair, A., Sabitha, M., Chennazhi, K., Tamura, H., Nair, S. V. and Jayakumar, R. (2012). Synthesis, characterization and in vitro cytocompatibility studies of chitin nanogels for biomedical applications. *Carbohydrate Polymers 87*(1): 943-949.

221. Rekha, M. and Sharma, C. P. (2007). Pullulan as a promising biomaterial for biomedical applications: a perspective. *Trends in Biomaterials and Artificial Organs 20*(2): 116-121.

222. Rekha, M. and Sharma, C. P. (2009). Blood compatibility and in vitro transfection studies on cationically modified pullulan for liver cell targeted gene delivery. *Biomaterials 30*(34): 6655-6664.

223. Rekha, M. and Sharma, C. P. (2011). Hemocompatible pullulan–polyethyleneimine conjugates for liver cell gene delivery: In vitro evaluation of cellular uptake, intracellular trafficking and transfection efficiency. *Acta biomaterialia 7*(1): 370-379.

224. Rigopoulou, E. I., Roggenbuck, D., Smyk, D. S., Liaskos, C., Mytilinaiou, M. G., Feist, E., Conrad, K. and Bogdanos, D. P. (2012). Asialoglycoprotein receptor (ASGPR) as target autoantigen in liver autoimmunity: lost and found. *Autoimmunity reviews 12*(2): 260-269.

225. Rinaudo, M. (2008). Main properties and current applications of some polysaccharides as biomaterials. *Polymer International 57*(3): 397-430.

226. Ringsdorf, H. (1975). *Structure and properties of pharmacologically active polymers.* Paper presented at the Journal of Polymer Science: Polymer Symposia.

227. Rodin, V. and Izmailova, V. (1996). NMR method in the study of the interfacial adsorption layer of gelatin. *Colloids and Surfaces A: Physicochemical and Engineering Aspects 106*(2): 95-102.

228. Rowley, J. A., Madlambayan, G. and Mooney, D. J. (1999). Alginate hydrogels as synthetic extracellular matrix materials. *Biomaterials 20*(1): 45-53.

229. Sa, G. and Das, T. (2008). Anti cancer effects of curcumin: cycle of life and death. *Cell Division 3*(1): 14.

230. Saab, M. b., Estephan, E., Bec, N., Larroque, M., Aulombard, R., Cloitre, T. and Gergely, C. (2011). Multimicroscopic study of curcumin effect on fixed nonmalignant and cancerous mammalian epithelial cells. *Journal of biophotonics 4*(7-8): 533-543.

231. Sæther, H. V., Holme, H. K., Maurstad, G., Smidsrød, O. and Stokke, B. T. (2008). Polyelectrolyte complex formation using alginate and chitosan. *Carbohydrate polymers 74*(4): 813-821.

232. Safavy, A., Raisch, K. P., Mantena, S., Sanford, L. L., Sham, S. W., Krishna, N. R. and Bonner, J. A. (2007). Design and Development of Water-Soluble Curcumin Conjugates as Potential Anticancer Agents. *Journal of medicinal chemistry 50*(24): 6284-6288.

233. Sahu, A., Bora, U., Kasoju, N. and Goswami, P. (2008). Synthesis of novel biodegradable and self-assembling methoxy poly (ethylene glycol)–palmitate nanocarrier for curcumin delivery to cancer cells. *Acta biomaterialia 4*(6): 1752-1761.

234. Samal, S. K., Dash, M., Van Vlierberghe, S., Kaplan, D. L., Chiellini, E., Van Blitterswijk, C., Moroni, L. and Dubruel, P. (2012). Cationic polymers and their therapeutic potential. *Chemical Society Reviews 41*(21): 7147-7194.

235. San Juan, A., Hlawaty, H., Chaubet, F., Letourneur, D. and Feldman, L. J. (2007). Cationized pullulan 3D matrices as new materials for gene transfer. *Journal of Biomedical Materials Research Part A 82*(2): 354-362.

236. Sanoj Rejinold, N., Muthunarayanan, M., Divyarani, V., Sreerekha, P., Chennazhi, K., Nair, S., Tamura, H. and Jayakumar, R. (2011). Curcumin-loaded biocompatible thermoresponsive polymeric nanoparticles for cancer drug delivery. *Journal of colloid and interface science 360*(1): 39-51.

237. Saravanan, M. and Rao, K. P. (2010). Pectin–gelatin and alginate–gelatin complex coacervation for controlled drug delivery: Influence of anionic polysaccharides and drugs being encapsulated on physicochemical properties of microcapsules. *Carbohydrate polymers 80*(3): 808-816.

238. Sarika, P., Cinthya, K., Jayakrishnan, A., Anilkumar, P. and James, N. R. (2014). Modified gum arabic cross-linked gelatin scaffold for biomedical applications. *Materials Science and Engineering: C 43*: 272-279.

239. Sarika, P. and James, N. R. (2015). Preparation and characterisation of gelatin–gum arabic aldehyde nanogels via inverse miniemulsion technique. *International journal of biological macromolecules 76*: 181-187.

240. Sarika, P., Kumar, P. A., Raj, D. K. and James, N. R. (2015). Nanogels based on alginic aldehyde and gelatin by inverse miniemulsion technique: synthesis and characterization. *Carbohydrate polymers 119*: 118-125.

241. Sarker, B., Papageorgiou, D. G., Silva, R., Zehnder, T., Gul-E-Noor, F., Bertmer, M., Kaschta, J., Chrissafis, K., Detsch, R. and Boccaccini, A. R. (2014). Fabrication of alginate–gelatin crosslinked hydrogel microcapsules and evaluation of the microstructure and physico-chemical properties. *Journal of Materials Chemistry B*.

242. Sarmento, B., Ribeiro, A., Veiga, F., Sampaio, P., Neufeld, R. and Ferreira, D. (2007). Alginate/chitosan nanoparticles are effective for oral insulin delivery. *Pharmaceutical research 24*(12): 2198-2206.

243. Sato, H., Ohtsu, T. and Komasawa, I. (2000). Atomic force microscopy study of ultrafine particles prepared in reverse micelles. *Journal of colloid and interface science 230*(1): 200-204.

244. Schmitt, C., Sanchez, C., Desobry-Banon, S. and Hardy, J. (1998). Structure and technofunctional properties of protein-polysaccharide complexes: a review. *Critical Reviews in Food Science and Nutrition 38*(8): 689-753.

245. Scomparin, A., Salmaso, S., Bersani, S., Satchi-Fainaro, R. and Caliceti, P. (2011). Novel folated and non-folated pullulan bioconjugates for anticancer drug delivery. *European Journal of Pharmaceutical Sciences 42*(5): 547-558.

246. Seo, S., Lee, C.-S., Jung, Y.-S. and Na, K. (2012). Thermo-sensitivity and triggered drug release of polysaccharide nanogels derived from pullulan-g-poly (l-lactide) copolymers. *Carbohydrate polymers 87*(2): 1105-1111.

247. Shah, P. P., Desai, P. R., Patel, A. R. and Singh, M. S. (2012). Skin permeating nanogel for the cutaneous co-delivery of two anti-inflammatory drugs. *Biomaterials 33*(5): 1607-1617.

248. Shaikh, J., Ankola, D., Beniwal, V., Singh, D. and Kumar, M. (2009). Nanoparticle encapsulation improves oral bioavailability of curcumin by at least 9-fold when compared to curcumin administered with piperine as absorption enhancer. *European Journal of Pharmaceutical Sciences 37*(3): 223-230.

249. Shakibaei, M., Mobasheri, A., Lueders, C., Busch, F., Shayan, P. and Goel, A. (2013). Curcumin enhances the effect of chemotherapy against colorectal cancer cells by inhibition of NF-κB and Src protein kinase signaling pathways. *PloS one 8*(2): e57218.

250. Sharma, R., Gescher, A. and Steward, W. (2005). Curcumin: the story so far. *European journal of cancer 41*(13): 1955-1968.

251. Sharma, R. A., Euden, S. A., Platton, S. L., Cooke, D. N., Shafayat, A., Hewitt, H. R., Marczylo, T. H., Morgan, B., Hemingway, D. and Plummer, S. M. (2004). Phase I clinical trial of oral curcumin biomarkers of systemic activity and compliance. *Clinical cancer research 10*(20): 6847-6854.

252. Shen, L. and Ji, H.-F. (2012). The pharmacology of curcumin: is it the degradation products? *Trends in molecular medicine 18*(3): 138-144.

253. Shi, L., Khondee, S., Linz, T. H. and Berkland, C. (2008). Poly (N-vinylformamide) nanogels capable of pH-sensitive protein release. *Macromolecules 41*(17): 6546-6554.

254. Shumikina, K.I., Panarin, E.F.and Ushakov, S.N. (1966). Experimental study ofpolymer salts of penicillins (in Russian). *Antibiotiki* 11: 767–770.

255. Shoba, G., Joy, D., Joseph, T., Majeed, M., Rajendran, R. and Srinivas, P. (1998). Influence of piperine on the pharmacokinetics of curcumin in animals and human volunteers. *Planta medica 64*(04): 353-356.

256. Sims, J., Kumbhar, A., Lin, J., Agnoli, F., Carpenter, E., Sangregorio, C., Frommen, C., Kolesnichenko, V. and O'CONNOR, C. (2002). Synthesis and manipulation of nanophase magnetic materials. *Molecular Crystals and Liquid Crystals 379*(1): 113-120.

257. Smitha, B., Sridhar, S. and Khan, A. (2004). Polyelectrolyte complexes of chitosan and poly (acrylic acid) as proton exchange membranes for fuel cells. *Macromolecules 37*(6): 2233-2239.

258. Strauss, G. and Kral, F. (1982). Borate complexes of amphotericin B: polymeric species and aggregates in aqueous solutions. *Biopolymers 21*(2): 459-470.

259. Sudimack, J. and Lee, R. J. (2000). Targeted drug delivery via the folate receptor. *Advanced drug delivery reviews 41*(2): 147-162.

260. Syng-ai, C., Kumari, A. L. and Khar, A. (2004). Effect of curcumin on normal and tumor cells: role of glutathione and bcl-2. *Molecular Cancer Therapeutics 3*(9): 1101-1108.

261. Tang, H., Murphy, C. J., Zhang, B., Shen, Y., Sui, M., Van Kirk, E. A., Feng, X. and Murdoch, W. J. (2010). Amphiphilic curcumin conjugate-forming nanoparticles as anticancer prodrug and drug carriers: in vitro and in vivo effects. *Nanomedicine 5*(6): 855-865.

262. Thakor, D. K., Teng, Y. D. and Tabata, Y. (2009). Neuronal gene delivery by negatively charged pullulan–spermine/DNA anioplexes. *Biomaterials 30*(9): 1815-1826.

263. Thomsen, L. B., Lichota, J., Kim, K. S. and Moos, T. (2011). Gene delivery by pullulan derivatives in brain capillary endothelial cells for protein secretion. *Journal of Controlled Release 151*(1): 45-50.

264. Tian, B., Wang, Z., Zhao, Y., Wang, D., Li, Y., Ma, L., Li, X., Li, J., Xiao, N. and Tian, J. (2008). Effects of curcumin on bladder cancer cells and development of urothelial tumors in a rat bladder carcinogenesis model. *Cancer letters 264*(2): 299-308.

265. Tiwari, S. K., Agarwal, S., Seth, B., Yadav, A., Nair, S., Bhatnagar, P., Karmakar, M., Kumari, M., Chauhan, L. K. S. and Patel, D. K. (2014). Curcumin Loaded Nanoparticles Potently Induce Adult Neurogenesis and Reverse Cognitive Deficits in Alzheimer's Disease Model via Canonical Wnt/β-catenin Pathway. *ACS nano*.

266. Tomita, M., Kawakami, H., Uchihara, J. n., Okudaira, T., Masuda, M., Takasu, N., Matsuda, T., Ohta, T., Tanaka, Y. and Ohshiro, K. (2006). Retracted: Curcumin (diferuloylmethane) inhibits constitutive active NF-κB, leading to suppression of cell growth of human T-cell leukemia virus type I-infected T-cell lines and primary adult T-cell leukemia cells. *International journal of cancer 118*(3): 765-772.

267. Tseng, C.-L., Su, W.-Y., Yen, K.-C., Yang, K.-C. and Lin, F.-H. (2009). The use of biotinylated-EGF-modified gelatin nanoparticle carrier to enhance cisplatin accumulation in cancerous lungs via inhalation. *Biomaterials 30*(20): 3476-3485.

268. Tseng, C.-L., Wu, S. Y.-H., Wang, W.-H., Peng, C.-L., Lin, F.-H., Lin, C.-C., Young, T.-H. and Shieh, M.-J. (2008). Targeting efficiency and biodistribution of biotinylated-EGF-conjugated gelatin nanoparticles administered via aerosol delivery in nude mice with lung cancer. *Biomaterials 29*(20): 3014-3022.

269. Van Thienen, T., Lucas, B., Flesch, F., Van Nostrum, C., Demeester, J. and De Smedt, S. (2005). On the synthesis and characterization of biodegradable dextran nanogels with tunable degradation properties. *Macromolecules 38*(20): 8503-8511.

270. Van Vlierberghe, S., Dubruel, P. and Schacht, E. (2011). Biopolymer-based hydrogels as scaffolds for tissue engineering applications: a review. *Biomacromolecules 12*(5): 1387-1408.

271. Verbeken, D., Dierckx, S. and Dewettinck, K. (2003). Exudate gums: occurrence, production, and applications. *Applied Microbiology and Biotechnology 63*(1): 10-21.

272. Villa, R., Cerroni, B., Viganò, L., Margheritelli, S., Abolafio, G., Oddo, L., Paradossi, G. and Zaffaroni, N. (2013). Targeted doxorubicin delivery by chitosan-galactosylated modified polymer microbubbles to hepatocarcinoma cells. *Colloids and Surfaces B: Biointerfaces 110*: 434-442.

273. Vinogradov, S. V., Bronich, T. K. and Kabanov, A. V. (2002). Nanosized cationic hydrogels for drug delivery: preparation, properties and interactions with cells. *Advanced drug delivery reviews 54*(1): 135-147.

274. Wahlström, B. and Blennow, G. (1978). A study on the fate of curcumin in the rat. *Acta pharmacologica et toxicologica 43*(2): 86-92.

275. Wang, H. and Roman, M. (2011). Formation and properties of chitosan−cellulose nanocrystal polyelectrolyte− macroion complexes for drug delivery applications. *Biomacromolecules 12*(5): 1585-1593.

276. Wang, Y.-J., Pan, M.-H., Cheng, A.-L., Lin, L.-I., Ho, Y.-S., Hsieh, C.-Y. and Lin, J.-K. (1997). Stability of curcumin in buffer solutions and characterization of its degradation products. *Journal of pharmaceutical and biomedical analysis 15*(12): 1867-1876.

277. Wei, X., Senanayake, T. H., Bohling, A. and Vinogradov, S. V. (2014). Targeted Nanogel Conjugate for Improved Stability and Cellular Permeability of Curcumin: Synthesis, Pharmacokinetics, and Tumor Growth Inhibition. *Molecular pharmaceutics 11*(9): 3112-3122.

278. Weinbreck, F., Rollema, H. S., Tromp, R. H. and de Kruif, C. G. (2004). Diffusivity of whey protein and gum arabic in their coacervates. *Langmuir 20*(15): 6389-6395.

279. Wells, L. and Sheardown, H. (2007). Extended release of high pI proteins from alginate microspheres via a novel encapsulation technique. *European journal of pharmaceutics and biopharmaceutics 65*(3): 329-335.

280. Wichitnithad, W., Nimmannit, U., Callery, P. S. and Rojsitthisak, P. (2011). Effects of different carboxylic ester spacers on chemical stability, release characteristics, and anticancer activity of mono-PEGylated curcumin conjugates. *Journal of pharmaceutical sciences 100*(12): 5206-5218.

281. Wilson Jr, O. C., Blair, E., Kennedy, S., Rivera, G. and Mehl, P. (2008). Surface modification of magnetic nanoparticles with oleylamine and gum Arabic. *Materials Science and Engineering: C 28*(3): 438-442.

282. Wong, V. W., Rustad, K. C., Glotzbach, J. P., Sorkin, M., Inayathullah, M., Major, M. R., Longaker, M. T., Rajadas, J. and Gurtner, G. C. (2011). Pullulan Hydrogels Improve Mesenchymal Stem Cell Delivery into High-Oxidative-Stress Wounds. *Macromolecular bioscience 11*(11): 1458-1466.

283. Wu, W., Shen, J., Banerjee, P. and Zhou, S. (2010). Core–shell hybrid nanogels for integration of optical temperature-sensing, targeted tumor cell imaging, and combined chemo-photothermal treatment. *Biomaterials 31*(29): 7555-7566.

284. Wu, W. and Zhou, S. (2009). Hybrid micro-/nanogels for optical sensing and intracellular imaging. *Nano reviews 1*: 341-343.

285. Xi, J., Zhou, L. and Dai, H. (2012). Drug-loaded chondroitin sulfate-based nanogels: Preparation and characterization. *Colloids and Surfaces B: Biointerfaces 100*: 107-115.

286. Xiao, H., Qi, R., Liu, S., Hu, X., Duan, T., Zheng, Y., Huang, Y. and Jing, X. (2011). Biodegradable polymer− cisplatin (IV) conjugate as a pro-drug of cisplatin (II). *Biomaterials 32*(30): 7732-7739.

287. Xin, Y. and Yuan, J. (2012). Schiff's base as a stimuli-responsive linker in polymer chemistry. *Polymer Chemistry 3*(11): 3045-3055.

288. Xu, J., Gattacceca, F. and Amiji, M. (2013). Biodistribution and pharmacokinetics of EGFR-targeted thiolated gelatin nanoparticles following systemic administration in pancreatic tumor-bearing mice. *Molecular pharmaceutics 10*(5): 2031-2044.

289. Xu, X., Capito, R. M. and Spector, M. (2008). Delivery of plasmid IGF-1 to chondrocytes via cationized gelatin nanoparticles. *Journal of Biomedical Materials Research Part A 84*(1): 73-83.

290. Yallapu, M. M., Gupta, B. K., Jaggi, M. and Chauhan, S. C. (2010). Fabrication of curcumin encapsulated PLGA nanoparticles for improved therapeutic effects in metastatic cancer cells. *Journal of colloid and interface science 351*(1): 19-29.

291. Yallapu, M. M., Jaggi, M. and Chauhan, S. C. (2012). Curcumin nanoformulations: a future nanomedicine for cancer. *Drug discovery today 17*(1): 71-80.

292. Yang, F., Lim, G. P., Begum, A. N., Ubeda, O. J., Simmons, M. R., Ambegaokar, S. S., Chen, P. P., Kayed, R., Glabe, C. G. and Frautschy, S. A. (2005). Curcumin inhibits formation of amyloid β oligomers and fibrils, binds plaques, and reduces amyloid in vivo. *Journal of Biological Chemistry 280*(7): 5892-5901.

293. Yang, L., Zhang, B., Wen, L., Liang, Q. and Zhang, L.-M. (2007). Amphiphilic cholesteryl grafted sodium alginate derivative: Synthesis and self-assembly in aqueous solution. *Carbohydrate polymers 68*(2): 218-225.

294. Yang, R., Meng, F., Ma, S., Huang, F., Liu, H. and Zhong, Z. (2011). Galactose-decorated cross-linked biodegradable poly (ethylene glycol)-b-poly (ε-caprolactone) block copolymer micelles for enhanced hepatoma-targeting delivery of paclitaxel. *Biomacromolecules 12*(8): 3047-3055.

295. Yang, R., Zhang, S., Kong, D., Gao, X., Zhao, Y. and Wang, Z. (2012). Biodegradable polymer-curcumin conjugate micelles enhance the loading and delivery of low-potency curcumin. *Pharmaceutical research 29*(12): 3512-3525.

296. Yang, W.-z., Chen, H.-l., Gao, F.-p., Chen, M.-m., Li, X.-m., Zhang, M.-m., Zhang, Q.-q., Liu, L.-r., Jiang, Q. and Wang, Y.-s. (2010). Self-aggregated nanoparticles of cholesterol-modified pullulan conjugate as a novel carrier of mitoxantronep. *Current Nanoscience 6*(3): 298-306.

297. Yang, X., Chen, L., Han, B., Yang, X. and Duan, H. (2010). Preparation of magnetite and tumor dual-targeting hollow polymer microspheres with pH-sensitivity for anticancer drug-carriers. *Polymer 51*(12): 2533-2539.

298. Yang, Y., Anvari, M., Pan, C.-H. and Chung, D. (2012). Characterisation of interactions between fish gelatin and gum arabic in aqueous solutions. *Food Chemistry 135*(2): 555-561.

299. Yao, B., Ni, C., Xiong, C., Zhu, C. and Huang, B. (2010). Hydrophobic modification of sodium alginate and its application in drug controlled release. *Bioprocess and biosystems engineering 33*(4): 457-463.

300. Ye, J., Xiong, J. and Sun, R. (2012). The fluorescence property of Schiff's bases of carboxymethyl cellulose. *Carbohydrate polymers 88*(4): 1420-1424.

301. Yin, Y., Li, Z., Sun, Y. and Yao, K. (2005). A preliminary study on chitosan/gelatin polyelectrolyte complex formation. *Journal of materials science 40*(17): 4649-4652.

302. Yinsong, W., Lingrong, L., Jian, W. and Zhang, Q. (2007). Preparation and characterization of self-aggregated nanoparticles of cholesterol-modified O-carboxymethyl chitosan conjugates. *Carbohydrate polymers 69*(3): 597-606.

303. Yoon, I.-S., Park, J.-H., Kang, H. J., Choe, J. H., Goh, M. S., Kim, D.-D. and Cho, H.-J. (2015). Poly (d, l-lactic acid)-glycerol-based nanoparticles for curcumin delivery. *International journal of pharmaceutics 488*(1): 70-77.

304. Yu, C., Gao, C., Lü, S., Chen, C., Huang, Y. and Liu, M. (2013). Redox-responsive shell-sheddable micelles self-assembled from amphiphilic chondroitin sulfate-cholesterol conjugates for triggered intracellular drug release. *Chemical Engineering Journal 228*: 290-299.

305. Yu, S.-R., Zhang, X.-P., He, Z.-M., Liu, Y.-H. and Liu, Z.-H. (2004). Effects of Ce on the short-term biocompatibility of Ti–Fe–Mo–Mn–Nb–Zr alloy for dental materials. *Journal of Materials Science: Materials in Medicine 15*(6): 687-691.

306. Zandi, M., Mirzadeh, H. and Mayer, C. (2007). Early stages of gelation in gelatin solution detected by dynamic oscillating rheology and nuclear magnetic spectroscopy. *European polymer journal 43*(4): 1480-1486.

307. Zern, T. L. and Fernandez, M. L. (2005). Cardioprotective effects of dietary polyphenols. *The Journal of nutrition 135*(10): 2291-2294.

308. Zhan, F., Chen, W., Wang, Z., Lu, W., Cheng, R., Deng, C., Meng, F., Liu, H. and Zhong, Z. (2011). Acid-activatable prodrug nanogels for efficient intracellular doxorubicin release. *Biomacromolecules 12*(10): 3612-3620.

309. Zhang, H.-z., Gao, F.-p., Liu, L.-r., Li, X.-m., Zhou, Z.-m., Yang, X.-d. and Zhang, Q.-q. (2009). Pullulan acetate nanoparticles prepared by solvent diffusion method for epirubicin chemotherapy. *Colloids and Surfaces B: Biointerfaces 71*(1): 19-26.

310. Zhang, H., Li, F., Yi, J., Gu, C., Fan, L., Qiao, Y., Tao, Y., Cheng, C. and Wu, H. (2011). Folate-decorated maleilated pullulan–doxorubicin conjugate for active tumor-targeted drug delivery. *European Journal of Pharmaceutical Sciences 42*(5): 517-526.

311. Zhang, M., Zhou, X., Wang, B., Yung, B. C., Lee, L. J., Ghoshal, K. and Lee, R. J. (2013). Lactosylated gramicidin-based lipid nanoparticles (Lac-GLN) for targeted delivery of anti-miR-155 to hepatocellular carcinoma. *Journal of controlled release 168*(3): 251-261.

312. Zhang, Z.-Q., Pan, C.-H. and Chung, D. (2011). Tannic acid cross-linked gelatin–gum arabic coacervate microspheres for sustained release of allyl isothiocyanate: Characterization and in vitro release study. *Food Research International 44*(4): 1000-1007.

313. Zheng, D., Duan, C., Zhang, D., Jia, L., Liu, G., Liu, Y., Wang, F., Li, C., Guo, H. and Zhang, Q. (2012). Galactosylated chitosan nanoparticles for hepatocyte-targeted delivery of oridonin. *International journal of pharmaceutics 436*(1): 379-386.

314. Zhou, N., Zan, X., Wang, Z., Wu, H., Yin, D., Liao, C. and Wan, Y. (2013).Galactosylated chitosan–polycaprolactone nanoparticles for hepatocyte-targeted delivery of curcumin. *Carbohydrate polymers 94*(1): 420-429.

315. Zorzi, G. K., Párraga, J. E., Seijo, B. and Sánchez, A. (2011). Hybrid nanoparticle design based on cationized gelatin and the polyanions dextran sulfate and chondroitin sulfate for ocular gene therapy. *Macromolecular bioscience 11*(7): 905-913.

LIST OF PUBLICATIONS BASED ON THE THESIS

PUBLISHED

(Based on the thesis)

1. Sarika, P. R., and James, N. R. (2015). Preparation and characterization of gelatin–gum arabic aldehyde nanogels via inverse miniemulsion technique. *International Journal of Biological Macromolecules 76*: 181-187.

2. Sarika, P. R, Kumar, P. A., Raj, D. K. and James, N. R. (2015). Nanogels based on alginic aldehyde and gelatin by inverse miniemulsion technique: synthesis and characterization. *Carbohydrate Polymers 119*: 118-125.

3. Sarika, P. R., James, N. R., Nishna, N., Kumar, P. A. and Raj, D. K. (2015). Galactosylated pullulan–curcumin conjugate micelles for site specific anticancer activity to hepatocarcinoma cells. *Colloids and Surfaces B: Biointerfaces, 133*: 347-355.

4. Sarika, P. R., James, N. R., Kumar, P. A., Raj, D. K. and Kumary, T.V. (2015). Gum arabic-curcumin conjugate micelles with enhanced loading for curcumin delivery to hepatocarcinoma cells. *Carbohydrate Polymers,134:167-174).*

PUBLISHED

(Not included in the thesis)

1. Sarika, P. R., Cinthya, K., A. Jayakrishnan, Kumar, P. A. and James, N. R. Modified gum arabic cross-linked gelatin scaffold for biomedical applications. *Materials Science and Engineering C 43 (2014) 272–279.*

2. Sarika, P. R., Sidhy Viha, C.V., Sajin Raj, R.G., James, N. R. and Kumar, P. A. A non-adhesive hybrid scaffold from gelatin and gum Arabic as packed bed matrix for hepatocyte perfusion culture. *Materials Science and Engineering C 46 (2015) 341–347.*

3. Sarika P.R, Anupama, P. and James, N. R. Cationised gelatin/gum arabic polyelectrolyte complex: study of electrostatic interactions. *Food Hydrocolloids 49(2015) 176-182.*

COMMUNICATED

1. Sarika, P. R. and James, N. R. Preparation, characterization and biological studies of curcumin loaded alginic aldehyde and gelatin nanogels. *Carbohydrate Polymers (Under revision).*

2. Sarika, P. R., James, N. R., Kumar, P. A. and Raj, D. K. Galactosylated alginate - curcumin micelles for hepatocyte targeted delivery of curcumin. *International Journal of Biological Macromolecules (Under review).*

3. Sarika, P. R. and James, N. R. Self assembled hybrid polyelectrolyte complex nanoparticles from cationised gelatin and alginic acid for curcumin delivery. *Material Science and Engineering C (Under review).*

4. Sarika, P. R., James, N. R., Raj, D. K., Kumary, T.V. and Kumar P.A. Microgravity as a Means to Incorporate HepG2 Aggregates in Polysaccharide – Protein Hybrid Scaffold. *Journal of Material Science: Materials in Medicine (Under revision).*

5. Sarika, P. R. and James, N. R. Curcumin loaded gelatin-gum arabic aldehyde nanogels for breast cancer therapy. *International Journal of Biological Macromolecules (Under review).*

PRESENTAIONS IN CONFERENCES/SEMINARS

Oral presentations

1. Sarika, P.R. and James, N. R. Self assembled pullulan - curcumin conjugate micelles as efficient drug delivery platform to for cancer therapy. Indo-Australian Conference on Biomaterials, Tissue Engineering, Drug delivery system & Regenerative medicine (BiTERM 2015), 5-7 February, 2015, Anna University, Chennai, India.

2. Sarika, P.R. and James, N. R. Polysaccharide based nano materials for drug delivery applications. National Conference on Recent Trends in Materials Science and Technology, 3-5 July 2013**,** IIST, Trivandrum, India.

3. Sarika, P.R. and James, N. R. **S**ynthesis and characterization of alginic aldehyde – gelatin nanogels. 25th Kerala Science Congress. 29-1 January, 2013, Technopark, Trivandrum, India.

Poster presentaions

1. Sarika, P.R. and James, N. R. Nanogel based on gelatin and gumarabic aldehyde using miniemulsion process**.** Nanobio 2012: Second International Conference on Nanotechnology at the Medical Interface. 21-23 February, 2012, Amrita Centre for Nanosciences and molecular medicine, Kochi, India.

2. Sarika, P.R. and James, N. R. Design and development of gumarabic - curcumin conjuate for cancer therapy. Research Scholars day-2013, 16-17 December, 2013, IIST, Trivandrum, India.

3. Sarika, P.R. and James, N. R. Self assembled galactosylated gumarabic-curcumin conjuate for cancer therapy. International Conference on Materials and Charecterisation Techniques**,** 10-12 March, 2014, VIT University, Vellore, India.

4. Sarika, P. R., James, N. R., Kumar, P. A. and Raj D. K. Targeted delivery of curcumin to hepatocyte using galactosylated alginate-curcumin conjugate. 7th Bangalore India Nano, 5-7 December, 2014, Hotel Lalit Ashok Bangalore, India.

5. Sarika, P. R., James, N. R., Kumar, P. A. And Raj D. K. Galactosylated pullulan-curcumin conjugate for site specific anticancer activity to hepatocarcinoma cells. 27th Kerala Science Congress, 27-29 January, 2015, Vijaya Camelot Convention Centre, Alappuzha, Trivandrum , India (**Best poster award)**.

6. Sarika P R and Nirmala Rachel James. Dextran aldehyde-gelatin nanoparticles for efficient delivery of curcumin via a green process. International Symposium on Photonics Applications and Nanomaterials, 28-30 October, 2015, Thiruvananthapuram, India